Advanced Series in Agricultural Sciences 13

A. J. Koolen H. Kuipers

Agricultural Soil Mechanics

With 128 Figures

Springer-Verlag
Berlin Heidelberg New York Tokyo
1983

Dr. Ir. ADRIANUS JOZEF KOOLEN
Professor Ir. HENDERIKUS KUIPERS
Tillage Laboratory, Diedenweg 20
Wageningen/The Netherlands

ISBN-13:978-3-642-69012-9 e-ISBN-13:978-3-642-69010-5
DOI: 10.1007/978-3-642-69010-5

Library of Congress Cataloging in Publication Data. Koolen, A. J. (Adrianus Jozef), 1944– Agricultural soil mechanics. (Advanced series in agricultural sciences; 13) Bibliography: p. Includes index. 1. Soil mechanics. 2. Tillage. I. Kuipers, H. (Henderikus), 1926–. II. Title. III. Series, TA710.K653 1983 631.4'3 83-4646

Typesetting: K + V Fotosatz, Beerfelden

2131/3130-543210

Preface

Compared with forces occurring in soil mechanics problems in civil engineering, the forces that are applied to soil in farming operations generally have a short duration, less than a few seconds, a small loaded area, no more than a few square decimeters, and small intensities, 10 bar being a high value. On the other hand, soil properties vary widely between those of a weak mud and a stone-like dry soil. Tillage and related applications of force to soil are practiced worldwide in farming. Tillage operations are performed on one hectare of land for every three human beings. This means that for the food production for each individual daily, something like one cubic meter of soil is stirred, or about 20 times his body weight. Theoretical knowledge of this most common human activity, which largely determines the surface shape of the fertile part of the earth, is still very limited. In this book the authors have tried to give an outline of the present state of the art. One of the starting points was a course in soil dynamics taught by the authors at the Agricultural University at Wageningen, The Netherlands. We hope to reach interested readers who have no more theoretical knowledge than high school level, as well as readers who want to go beyond the level of a third year university student.

For the chapter on wheels and tires we received substantial support from F. G. J. Tijink of the Tillage Laboratory at Wageningen. Much care was given to the illustrations, because an instructive drawing may explain much more than many written sentences. The authors are greatly indebted to Mr. B. W. Peelen of the Tillage Laboratory at Wageningen, for preparing with great skill the large number of figures. A second aspect that received special attention was the selection of suitable references. Scientists all over the world, although small in number compared to the immense field of knowledge involved, contributed to the present state of the art. We tried to select those references which should provide for interested readers an easy entry to the literature. Finally, we would like to mention that Dr. C. Dirksen of the Department of Soils and Fertilizers of the Agricultural University read and corrected the manuscript in a very constructive way, and that Miss H. A. van den Dikkenberg was a real support to us in preparing the manuscript for the printer.

The authors hope that this book will encourage interest in the field of agricultural soil mechanics. Suggestions to improve the book will be most welcome.

Wageningen, April 1983

A. J. KOOLEN
H. KUIPERS

Contents

Part 3 Load Bearing and Soil Loosening Processes

Introduction

This book, Agricultural Soil Mechanics, deals with the knowledge of forces and movements in soil caused by tillage operations and field traffic. In *farming* the knowledge contained in this book may be applied when choosing implements, tires, size of machinery, etc. In *research,* especially in the field of agronomy or soil science, this knowledge will facilitate the evaluation of the role of tillage and traffic with respect to production systems and soil conditions. This may be of special importance for the lay-out and interpretation of field experiments. In *industry* this knowledge may be applied in designing field equipment.

Successively, two viewpoints will be presented.

1. Study of the mechanical behavior of soil elements: This is focused on the relationship between the geometrical change and the state of stress of a soil volume element under the condition that both the stress and the soil are uniform throughout the element. The geometrical change will be divided into the following reactions:

- compaction,
- deformation (apart from volume change),
- break (failure),
- displacement (as a rigid body).

2. Study of the load bearing and soil loosening processes. In soils, stresses and geometrical changes during the action of tillage tools and field traffic usually vary strongly from place to place and with time. In the process approach attention is paid to these variations. The presentation uses a division of the tillage tools and wheels into the following groups of soil engaging bodies:

- rollers, wheels, and tires,
- penetrating bodies,
- sliding and shearing bodies,
- tracks and cages,
- tines,
- plow bodies.

Groups 1 to 4 induce so-called load bearing processes, and groups 5 and 6 loosening processes.

Within each of these two viewpoints we distinguish between three categories of knowledge.

1. Occurrence of soil reactions and processes under practical conditions; for instance, occurrence of soil compaction or occurrence of a certain tool. Which particular phenomena will occur may depend on factors outside the field of agricultural soil mechanics. For instance, the degree of fragmentation required for a seedbed in a given field depends on the crop to be grown. From the viewpoint of agricultural soil mechanics such a requirement has an incidental character that needs no explanation. These requirements will change continuously with progress in agricultural practices.

2. Fundamentals of elemental mechanical behavior and processes. This type of knowledge is very coherent and logical, has a high degree of exactness, and is not likely to change considerably. Fundamentals of the soil reactions are as much as possible presented according to the following scheme:

- measures of the behavior,
- important models which enable clear insight as to the relationship between soil reaction and stress,
- loading rate and repeated loading effects,
- soil physical aspects that explain soil reaction from soil texture, moisture content, porosity, etc.

For each group of soil engaging bodies, process fundamentals are presented in the following order:

Kinematic aspects:
- kinematics of the tool or wheel itself (if its movement can be complex),
- movement at the tool (wheel)-soil interface,
- movement of the soil.

Dynamic aspects:
- forces on tool or wheel,
- forces in the interface,
- forces within the soil.

The description of large strains, being mathematically difficult, is presented as an appendix.

3. Applications. They concern predictions of quantities desired to be known in tillage and field traffic. Such predictions are usually complicated and simplifying assumptions are, therefore, very common. Solutions will have more an approximative than an exact character and will be abandoned as soon as a more accurate or more convenient method is available.

It should be obvious that the boundary between these three types of knowledge often is not very sharp.

The forces and movements induced by tillage and traffic will be analysed primarily from a macroscopic point of view, which means that soil bodies are assumed to be continuous rather than composed of individual material parts. Soil mechanics, being one of the soil physical sciences, touches the other parts in important areas:

1. for a particular soil, reactions to stress depend on, and influence, porosity, particle arrangement, moisture content, moisture distribution, number of bonds not arising from the soil water, and distribution of these bonds,
2. soil reactions change soil physical quantities like capacities and conductivities of soil water, gas, and heat.

Only soil physical factors that directly relate to soil strength will be discussed.

The book starts with a chapter on the different conditions in which soil can appear.

Part 1 Soil Conditions

1.1 Strength-Determining Factors

In agricultural soil mechanics the most relevant soil properties are the reactions of soils to applied forces. For simplicity these properties are called strength properties. For a given soil they will change with time under influence of climate, soil management, and plant growth. The strength properties, of that given soil, and their change with time are determined by the following factors:

1. Number of particles per unit of volume, that is, the complement of pore volume: If a certain force is acting on a volume of soil, the forces in the contact points between the particles will be smaller if there are more particles. Moreover, the number of particles will determine how far the particles can move.
2. Spatial distribution of particles, is comparable to pore-size distribution. Particles can be distributed evenly in space but there may also be spots with closely packed particles alternating with very loosely packed areas. Stresses will then concentrate on the dense and therefore stronger parts. Loosely packed areas make the soil weaker because they give little support to the denser parts. This complicates the effect of particle distribution on strength properties. Another complication is that soil particles do not always have a random orientation, especially in dense parts there may be a clear, parallel orientation of plate-like particles in clusters and the degree of parallel orientation may be an important strength factor. Pore-size distribution, which is to a large extent determined by particle-size distribution, will affect soil strength properties indirectly by influencing water suction at a given water content. This is mentioned under 4).
3. Moisture content as a percentage of total volume. Soil moisture in the upper soil layers is mostly under a negative pressure with respect to atmospheric pressure. Soil particles are pulled together by the resulting suction force and at a given porosity the volume of water present will determine the area over which this binding force is acting.
4. Moisture distribution: Many differing soil moisture distributions may occur with one and the same system of pores. Water contained in a certain pore may be connected to water in other pores or may be isolated. Also empty pores may be present. Moisture distribution and pore-size distribution together largely determine moisture suction. This suction may well vary from place to place, so that this will result in a tendency towards a more uniform moisture distribution by water movement in the liquid or vapor phase.
5. Bonds between particles: Soil particles may be held together by forces between mineral particles (edge to face binding forces and Madelung forces), mineral and organic particles, mineral and oxide or hydroxide particles, and between organic

and oxide or hydroxide particles. On the other hand there may be repulsive forces between mineral particles with an electrical charge. There may be a difference between actual and potential binding forces. These potential binding forces depend on the possibilities for edge to face contacts and Madelung forces. In the case of parallel plates these bonds are mainly Madelung forces. Parallel plates with terrassed surfaces may also involve edge to face bonds.
6. Distribution of bonds. Bonds may exist in a more or less high percentage of contact points. Especially after loosening tillage operations, there may be a relatively large number of contact points with no, or very low, binding forces.

1.2 Variation of Strength-Determining Factors in the Course of Time

Precompaction. To demonstrate the time dependency of strenght-determining factors, consider a loose soil, e.g. a plowed soil, just before a seedbed is made. During seedbed preparation this soil will be compacted by the traffic involved and sometimes by the implements used. This first compaction is called precompaction. It has the following effects on the strength determining factors:

1. due to this precompaction the number of particles per unit volume will increase. The degree to which the initially loose soil is compacted depends on the moisture content at the time compaction takes place. At a given stress there will be an optimum moisture content for this compaction. A drier soil will show less compaction because of a higher resistance to compaction. A wetter soil will also give low compaction because the soil may move aside or may become saturated and therefore incompressible;
2. the distribution of soil particles will become more uniform. Dense clods may be crushed, loose pockets will be compacted. Moreover, at higher moisture contents clay platelets may be forced to reorient themselves into a more parallel arrangement, and soil particles may be moved under influence of pressure induced water and air movement;
3. the volumetric moisture content will increase. In general, stresses will last only for very short time intervals, which will strongly restrict water movement. The main effect will be a reduction of the total soil volume and, therefore, an increase of volumetric water content;
4. the moisture distribution will be changed. Because of the uneven stress distribution on a microscopic scale and the resulting irregular moving pattern of the soil particles, soil moisture suction will change irregularily from place to place. This will result in subsequent moisture movements. These effects will be more pronounced in wet soils and are known to be negligible if the soil is drier than pF 3.7;
5. bonds will be established and disrupted. This will be a selective process. All kinds of bonds may be disrupted but only bonds between mineral particles will be newly established. At higher moisture contents this rearragement of bonds will be more likely,

6. the distribution of bonds will become more homogeneous. This effect will also increase with moisture content.

Growing Season. After seedbed preparation and sowing, the strength properties of the soil may be influenced by further compaction as a result of crop management and harvest operations. The compaction processes will be more or less identical to those discussed under precompaction. During the growing season the soil strength will also be influenced strongly by changes in water content under the influence of climatic conditions and by root action either by water extraction and by mechanical bonding. The following processes may be observed:

- suction equilibration: compaction may have resulted in an uneven suction distribution. Equilibration of the pressure distribution by water movement may take rather long, especially if vapor movement through empty pores is involved,
- suction-thixotropy: suction equilibration after compaction may result in a change of the average suction with time, even if the total amount of water in the soil under consideration does not change,
- drying: near the contact points of larger particles the concentration of colloidal particles may increase considerably on drying, and this will result in stronger bonds. Drying may also result in stronger edge to face and Madelung bonds. If soil bulk movement is restricted during shrinkage, cracks will be formed. The same process, but on a micro-scale, also may occur when larger particles, e.g. sand grains, act as rigid framework. In that case microcracks develop in the pores,
- wetting: wetting and consequential swelling may disrupt bonds, but confinement of swelling soil may establish better edge to face and Madelung bonds. Increasing air pressure in entrapped air pockets may lead to micro-explosions of soil aggregates, disrupting bonds and rearranging particles into a more homogeneous situation.

Suction equilibration and suction-thixotropy, as well as wetting and drying influence moisture distribution. All moisture movement may cause local swelling or shrinkage and is, therefore, likely to influence particle distribution, strength of bonds, and bond distribution.

Tillage Effects. In between growing seasons precompacted soils are reloosened by tillage operations that strongly influence all strength determining factors. During the period after the tillage operations the influence of the weather on the strength-determining factors is often very pronounced. This depends, of course, largely on the climate. In principle the same phenomena will occur as described above, sometimes supplemented by frost action. All these actions together will result in a still relatively loose soil, and this condition was chosen as a starting point for this description.

From this description of possible processes it is clear that a particular soil does not have a specific strength. Its strength varies strongly with the various events that take place during the course of time. As a first approximation, a distinction can be made between the stages of loose soil, precompacted soil, and precompacted soil with a changed moisture content.

1.3 Influences of Soil Type on Strength-Determining Factors

Strength-determining factors depend on soil type. However, in general, strength variations in time are more spectacular than between soil types. Extreme values of strength properties will be more frequent in problem soils, such as blowing sands, weak peat soils, or sticky clay soils. For a farmer, soil type is a given factor which he cannot change, whereas he is able to control his soils strength variations with time to a certain extent. Therefore, the change of soil properties under the influence of, or in relation to, mechanical handling may deserve more attention than strength variations with soil type, although in agricultural and especially soil science the emphasis is commonly reversed.

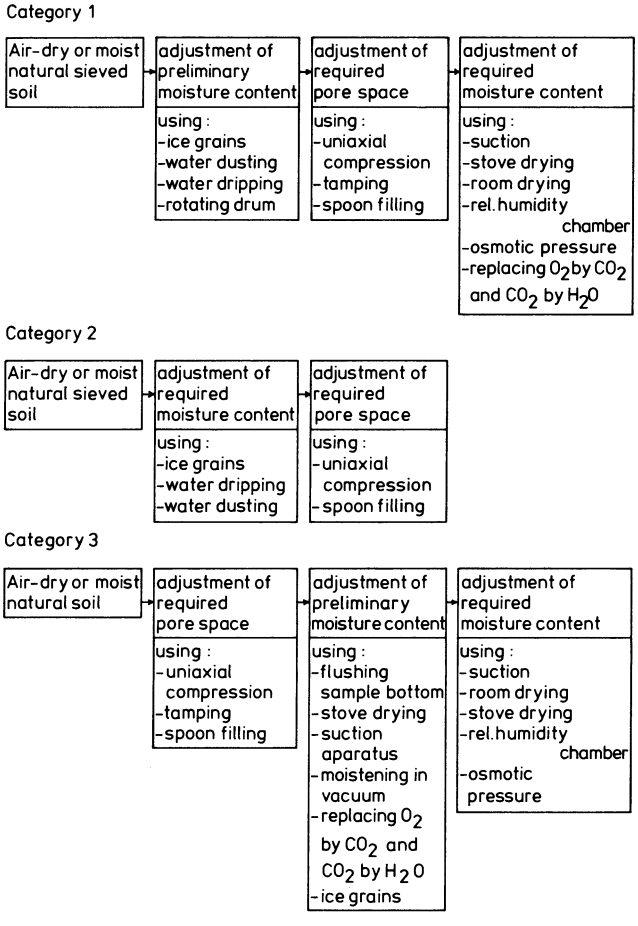

Fig. 1.1. Main procedures to prepare soil for laboratory experiments

1.4 Soil Prepared for Laboratory Experiments

For laboratory experiments uniform and highly reproducible soil conditions are needed. It is common to use special procedures of soil preparation to obtain such conditions. Nearly all published preparation methods belong to one of the three following categories:

1. Compaction in a rather wet condition
2. Compaction at the moisture content at testing
3. Compaction at a relatively low moisture content.

In each group there are variations in degree of clod prevention, prevention of air explosion, and moisture homogenization. Figure 1.1 indicates the main procedures. Categories 1 and 3 result in precompacted soil with changed water content. On most occasions the same holds for category 2 because, before testing, the soils are normally left to equilibrate by means of movement of water and spotwise changes of moisture content. The average moisture content remains unchanged in this case.

For puddled soils other preparation methods are required. A few methods mentioned in the literature are:

a) prepare a paste from moist field soil using distilled water ; push paste through a fine mesh sieve; stir the soil thoroughly;
b) add air-dried soil to devaporized water; boil under vacuum;
c) pulverize air-dried soil, pushing it through a 0.3 mm screen; compress with 3.5 bar pressure; push the soil through a 5 mm screen;
d) knead the soil material at a moisture suction of pF 1.5; dry to an intermediate moisture content; sieve to obtain aggregates of $1-2$ mm.

Part 2 Mechanical Behavior of Soil Elements

2.1 General Aspects of the Mechanical Behavior of Soil Elements

2.1.1 Small Volume Elements Instead of Large Soil Bodies

In general, tillage means that forces are applied to the soil by a tool surface. Applied forces can be great or small and surfaces large or small. For the reaction of the soil the absolute value of force or surface will not be predominant, rather the force per unit area, or *force-intensity* will be. A high intensity will cause strong compaction, high strains and/or intensive crumbling.

Figure 2.1 demonstrates the definition of force-intensity. The tine is moving through the soil and, therefore, exerts forces on the soil. To define force-intensity in a point D a small area dA around point D is considered and we calculate the quotient

$$\frac{\sum \text{forces on } dA}{dA}.$$

This quotient will depend on position and size of dA: If e.g. we choose dA somewhat higher or lower along the tine, the quotient will be different. To avoid this ambiguity we let dA shrink to a point. Then force-intensity on tine surface in point D is defined by and is

$$\lim_{dA \to 0} \frac{\sum \text{forces on } dA}{dA} = p.$$

This is called the *stress* on the tool surface in point D. Using this limit implicitly means, that we assume that the soil is a *continuum*; that is, we assume that there are no voids and that the soil substance is uniformly distributed around point D. Such an assumption will be sufficiently valid as long as voids are small and irreg-

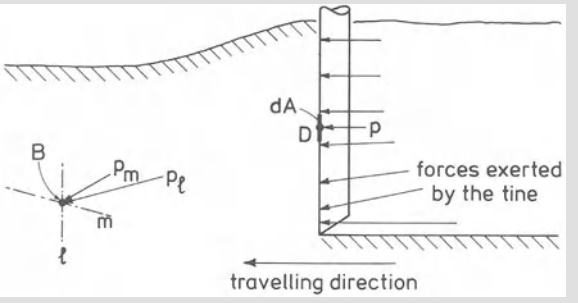

Fig. 2.1. Force-intensity in soil-tool interface and within the soil

ularities are present only on a scale small in comparison to the size of the tool under consideration.

Stresses along the tine surface will induce stresses within the soil, because the load is spreading out into the soil from the tool-soil contact surface. Suppose that in point B stress p_l is acting on the small plane l. The magnitude of p_l will depend on the direction of plane l. If e.g. we choose plane m instead of l, we may find that the stress acting on this plane is p_m and in the situation of Fig. 2.1 it is clear that $p_l \gg p_m$. This demonstrates a difficulty faced with this concept of stress in a point. We can get a more convenient description of the state of stress in the point if we consider a very small elemental cube instead of a small plane. On all faces of such a cube there will be stresses. This approach yields a theory called *stress theory,* the subject discussed in 2.1.2. Stresses acting on the cube will yield reactions; the cube may be compacted, deformed, broken, or displaced as a rigid body. Compaction and deformation of such cubes can be described in terms comparable to stress theory. This approach is called *strain theory* (2.1.3). For the elemental cube there will be a certain relation between stress and strain, which is characteristic for the soil considered. Such relations are known as *stress-strain relations.* This relation is in fact decisive for the level and distribution of stresses in the soil body as well as for the accompanying magnitude and distribution of strains. In 2.1.4 general aspects of stress-strain relations will be discussed.

2.1.2 Stress Theory

Short treatises of stress theory can be found in various textbooks (Timoshenko and Goodier 1951, Stippes et al. 1961, Harr 1966, Drucker 1967). The first two books use no matrix notation. A more extensive treatise is given by (Ford 1963). In this chapter only a few aspects of stress theory are given without proofs.

2.1.2.1 Stress Tensor

We will first describe the state of stress in a point. In Fig. 2.2 the broken line represents the boundary of a loaded soil body and we want to describe the resulting

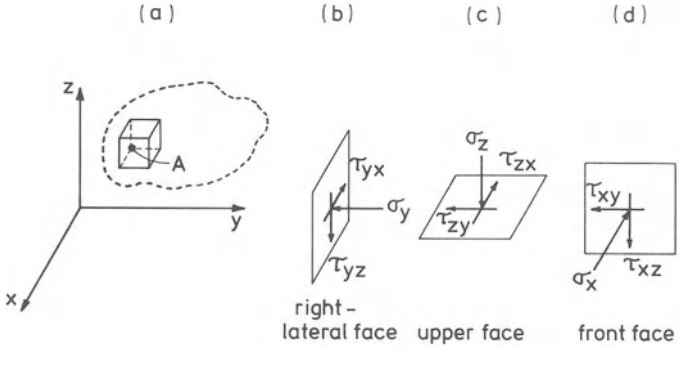

Fig. 2.2a – d. Stress tensor components

stress in point A. For this we must first select an xyz co-ordinate system. Then we consider an infinitely small cube in point A with sides parallel to the co-ordinate planes. Figure 2.2b is an enlarged picture of the right-hand face of the cube. The stress on this face can be resolved into one component perpendicular to the plane and two components tangential to the plane, parallel to the co-ordinate axes. The perpendicular component is called *normal stress*, denoted by σ_y. (Subscript y is used because this normal stress is parallel to the y axis.) The tangential components are called *shear stresses* and are denoted by τ_{yz} and τ_{yx}. (For each τ the first subscript is the same as the subscript of the normal stress on the same plane and the second subscript denotes the coordinate axis parallel to the shear stress considered.) Figures 2.2c and d describe the situation for the top and front planes, respectively. The resulting nine components of Figs. 2.2b, c, and d are combined in a matrix,

$$\begin{pmatrix} \sigma_x & \tau_{xy} & \tau_{xz} \\ \tau_{yx} & \sigma_y & \tau_{yz} \\ \tau_{zx} & \tau_{zy} & \sigma_z \end{pmatrix}.$$

Each component has its own fixed place in the matrix. Normal stresses are on the diagonal from the top left to the bottom, and shear stresses are on the other positions. The matrix is a complete description of the state of stress in point A. One could argue that we used only three faces of the cube, but this remark is not relevant because our cube was assumed to be infinitely small and then stresses at opposite cube faces can only differ by an infinitely small amount. The given matrix is called the matrix of the stress tensor in A. We shall discuss a few properties of this matrix.

In the first place one should be aware that the numerical values of the components of the matrix depend on the choice of the co-ordinate system. If, e.g., the co-ordinate system of Fig. 2.3 had been chosen, with axes $x'y'z'$, the cube would have had an inclined position and the matrix (at the right side in this figure) would have different component values than the one belonging to the xyz system. However, both matrices describe the same state of stress. Therefore, a matrix always belongs to a certain co-ordinate system.

A second property is that the matrix of a stress tensor is always symmetrical, implying

$$\tau_{xy} = \tau_{yx}, \quad \tau_{yz} = \tau_{zy} \quad \text{and} \quad \tau_{zx} = \tau_{xz}.$$

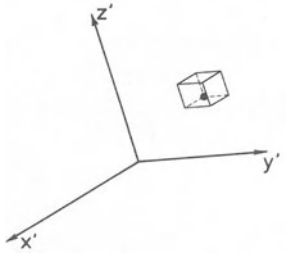

$$\begin{pmatrix} \sigma_{x'} & \tau_{x'y'} & \sigma_{x'z'} \\ \tau_{y'x'} & \sigma_{y'} & \tau_{y'z'} \\ \tau_{z'x'} & \tau_{z'y'} & \sigma_{z'} \end{pmatrix}$$

Fig. 2.3. Stress tensor relative to $x'y'z'$ system

This can be proven by considering the equilibrium of forces on the infinitely small cube.

A third, very important property is that there are always positions of the co-ordinate system that simplify the numbers in the stress tensor. For a given state of stress it is e.g. always possible to choose the co-ordinate system in such a way that all τ's are zero at the same time. Let this system be the $x''y''z''$ system. Then the corresponding matrix is

$$\begin{pmatrix} \sigma_{x''} & 0 & 0 \\ 0 & \sigma_{y''} & 0 \\ 0 & 0 & \sigma_{z''} \end{pmatrix}.$$

If one of the three stresses $\sigma_{x''}$, $\sigma_{y''}$, $\sigma_{z''}$ is larger than the other two, then this stress is also the highest normal stress occurring in that point. In all other directions only lower normal stresses will be found. We call this highest stress the first (or major) principal stress σ_1 and its direction the first principal direction, i.e. the direction of the first principal axis. If one of the three stresses $\sigma_{x''}$, $\sigma_{y''}$, $\sigma_{z''}$ is smaller than the other two, then this stress is the smallest stress occurring in that point. It is called the third (or minor) principal stress σ_3 occurring in the third principal direction along the third principal axis. The remaining intermediate value of the stresses $\sigma_{z''}$, $\sigma_{y''}$, $\sigma_{z''}$ is the second (or intermediate) principal stress σ_2. If there are equal principal stresses then the state of stress is very simple. For instance, if $\sigma_2 = \sigma_3$, then any plane parallel to σ_1 is acted upon by a normal stress equal to $\sigma_2 = \sigma_3$ and is free from shear stress. When $\sigma_1 = \sigma_2 = \sigma_3$, all normal stresses are equal and the stress state does not have any shear stress components. The matrix belonging to the principal axes is

$$\begin{pmatrix} \sigma_1 & 0 & 0 \\ 0 & \sigma_2 & 0 \\ 0 & 0 & \sigma_3 \end{pmatrix}.$$

This is the most common way to describe stresses in a point but, of course, the directions of principal stresses should be known. For a point under the center of a driven, but not pulling tire, principal directions are vertical, horizontal forward in the direction of travel, and horizontal sideways perpendicular to the direction of travel. Principal stresses in this case could be $\sigma_1 = 3$ bar, $\sigma_2 = 1.5$ bar and $\sigma_3 = 1$ bar. Then the matrix is

$$\begin{pmatrix} 3 & 0 & 0 \\ 0 & 1.5 & 0 \\ 0 & 0 & 1 \end{pmatrix}.$$

Another special position of the coordinate system is indicated in Fig. 2.4 as $x'''y'''z'''$, which has the following characteristics. The y''' direction is the direction of σ_2 and the x''' and z''' directions are at 45° with the σ_1 and σ_3 directions. In this position the highest shear stress in the point considered appear in the stress tensor, that is

$$\tau_{x'''z'''} = \tau_{z'''x'''} = \tfrac{1}{2}(\sigma_1 - \sigma_3).$$

As a fourth property of stress tensors the existence of *invariants* is mentioned. If we calculated the sum $\sigma_x + \sigma_y + \sigma_z$ for the xyz system, the sum $\sigma_{x''} + \sigma_{y''} + \sigma_{z''}$

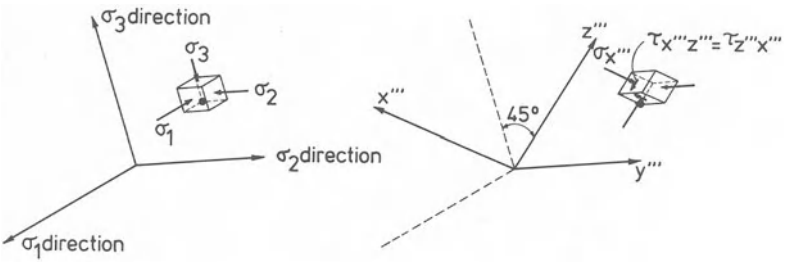

Fig. 2.4. Principal stresses and maximum shear stress

for the $x''y''z''$ system, etc., we would find that these sums are equal. Thus, the sum of normal stresses in any matrix of a given stress tensor does not depend on the position of the co-ordinate system. This sum is called the first invariant, I_1, normally expressed as the sum of principal stresses

$$I_1 = \sigma_1 + \sigma_2 + \sigma_3 .$$

Of course, the mean normal stress $\sigma_m = (\sigma_1 + \sigma_2 + \sigma_3)/3$ is also invariant. Other invariants are

$$I_2 = \sigma_x\sigma_y + \sigma_x\sigma_z + \sigma_y\sigma_z - \tau_{xy}^2 - \tau_{xz}^2 - \tau_{yz}^2 = \sigma_1\sigma_2 + \sigma_1\sigma_3 + \sigma_2\sigma_3$$

$$I_3 = \sigma_x\sigma_y\sigma_z + 2\tau_{xy}\tau_{xz}\tau_{yz} - \sigma_x\tau_{yz}^2 - \sigma_y\tau_{xz}^2 - \sigma_z\tau_{xy}^2 = \sigma_1\sigma_2\sigma_3 .$$

Suppose that the xyz directions are principal directions and that the stress on a plane perpendicular to a space diagonal (octahedral plane) is decomposed into one normal and one tangential component. These components are known as the octahedral normal stress σ_{oct} and the octahedral shear stress τ_{oct}. Both components can be expressed in terms of invariants,

$$\sigma_{oct} = \tfrac{1}{3}(\sigma_1 + \sigma_2 + \sigma_3) = \tfrac{1}{3}I_1$$

$$\tau_{oct} = \tfrac{1}{3}\sqrt{(\sigma_1 - \sigma_2)^2 + (\sigma_2 - \sigma_3)^2 + (\sigma_1 - \sigma_3)^2} = \sqrt{\tfrac{2}{9}(I_1^2 - 3I_2)} .$$

A fifth property of stress tensors is that they can be added or subtracted by adding or subtracting corresponding stress components. A common treatment is to suppose that the stress tensor is composed of a mean stress part and a deviatoric part,

$$\begin{bmatrix} \sigma_x & \tau_{xy} & \tau_{xz} \\ \tau_{yx} & \sigma_y & \tau_{yz} \\ \tau_{zx} & \tau_{zy} & \sigma_z \end{bmatrix} = \begin{bmatrix} \sigma_m & 0 & 0 \\ 0 & \sigma_m & 0 \\ 0 & 0 & \sigma_m \end{bmatrix} + \begin{bmatrix} \sigma_x - \sigma_m & \tau_{xy} & \tau_{xz} \\ \tau_{yx} & \sigma_y - \sigma_m & \tau_{yz} \\ \tau_{zx} & \tau_{zy} & \sigma_z - \sigma_m \end{bmatrix} .$$

The second matrix can be considered as a hydrostatic pressure acting uniformly from all directions.

The sixth and last property of stress tensors that will be discussed is that the matrix of stress components relative to a known co-ordinate system is a complete description of the state of stress in the point considered. This means that the stresses in any direction can be calculated. This is demonstrated for a matrix belonging to the principal directions in point A of Fig. 2.5a. The second principal

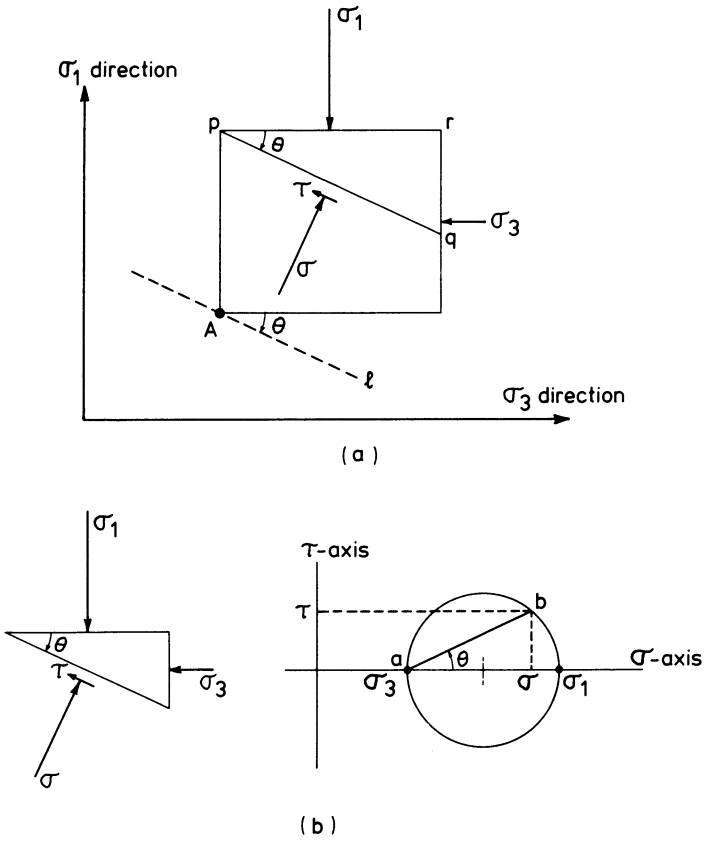

Fig. 2.5a, b. Determination of the stress on an arbitrary plane l when major and minor principal stresses are known

stress is perpendicular to the plane of the drawing. The stress on plane l at angle θ with the horizontal is to be calculated. We notice that the stress on l will be equal to the stress on plane pq parallel to l, because an infinitely small parallel displacement does not change the stress. In fact, we have to calculate σ and τ on this plane and, therefore, we consider the equilibrium of forces on body pqr. For convenience, we suppose that this body has a width equal to unity in the direction perpendicular to the drawing. Length pq is called L and represents also the area of the inclined side of the body pqr. The other sides have areas $rq = L\sin\theta$ and $pr = L\cos\theta$. Multiplication of the areas with corresponding stress components yields force components. Equating each of the sum of horizontal and vertical force components to zero, gives the equations describing equilibrium:

$$L\sigma\sin\theta - L\tau\cos\theta - \sigma_3 L\sin\theta = 0$$

$$L\sigma\cos\theta + L\tau\sin\theta - \sigma_1 L\cos\theta = 0.$$

Solving for σ and τ yields

$$\sigma = \sigma_1 \cos^2\theta + \sigma_3 \sin^2\theta \tag{1}$$

$$\tau = (\sigma_1 - \sigma_3) \sin\theta \cos\theta. \tag{2}$$

2.1.2.2 Mohr's Graphical Representation

Mohr introduced a method for visual representation of stresses for any plane through a point. The method, known as "Mohr's diagram" or "Mohr's circle", is demonstrated here for a simple situation: the graphical representation of σ and τ from Fig. 2.5a for given σ_1 and σ_3, but a variable direction θ. The quantities involved are shown in the left part of Fig. 2.5b, the solution in the right part. The construction is as follows:

1. draw a rectangular σ, τ coordinate system,
2. plot σ_1 and σ_3 on the σ-axis,
3. draw a circle through σ_1 and σ_3, with its center on the σ-axis,
4. draw line ab, from σ_3, at an angle θ to the horizontal. The line intersects the circle in b,
5. determine the coordinates of point b. These coordinates represent σ and τ, respectively.

In this way we can find σ and τ for any θ, if σ_1 and σ_3 are known. This construction is based on the fact that the circle of Fig. 2.5b represents the locus of the formulas (1) and (2) at the end of the previous section.

2.1.2.3 Uniform Stress Distribution in Finite Soil Bodies

The stress theory for infinitely small cubes can be extended to finite soil bodies provided the stress distribution is uniform. This extension is important with devices that measure geometrical changes of a soil volume due to loading. In such devices soil samples are finite bodies rather than infinitely small cubes. This extension will be discussed for the following sample shapes: a finite cube, a finite cylinder, and a finite sphere. The cube in Fig. 2.6a is assumed to be composed of small cubes like the one in Fig. 2.6b and all small cubes are loaded by σ_1, σ_2, σ_3. It is obvious that the large cube will have the following stresses: on the top and bottom faces a normal stress σ_1, on the left and right faces a normal stress σ_3, and on the front and back faces a normal stress σ_2. Therefore, if a large cube is loaded by σ_1, σ_2, and σ_3, the stress in each point will be given by the matrix

$$\begin{pmatrix} \sigma_1 & 0 & 0 \\ 0 & \sigma_2 & 0 \\ 0 & 0 & \sigma_3 \end{pmatrix}$$

with axes parallel to the sides of the cube.

The cylinder of Fig. 2.6c is assumed to consist of small cubes like Fig. 2.6d and at the cylinder wall small prisms like Fig. 2.6e. For the small cubes it is supposed that $\sigma_2 = \sigma_3$. For the top and bottom of the cylinder the stress will be σ_1 and for the stress on the wall we may use the formulas (1) and (2) in section 2.1.2.1, or Mohr's circle (Fig. 2.5b), and we will find that in Fig. 2.6e σ has to be

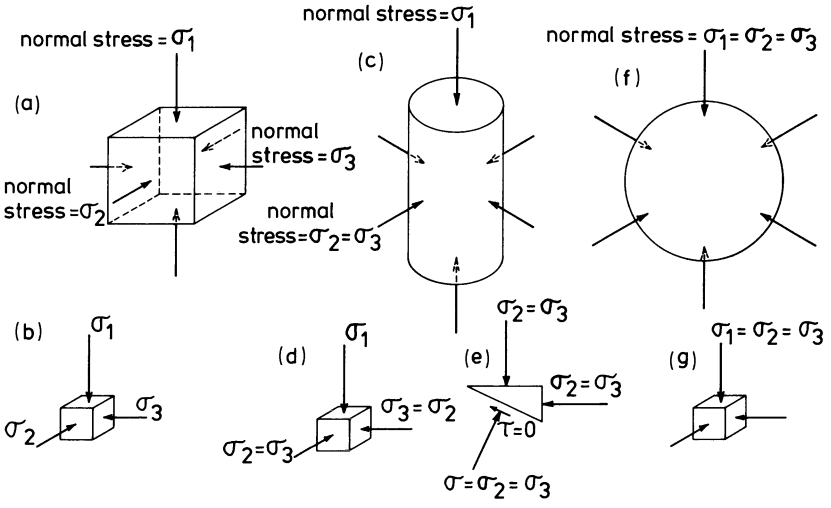

Fig. 2.6a – g. Uniform stress distribution in a finite cube, a finite cylinder, and a finite sphere

equal to $\sigma_2 = \sigma_3$ and τ has to be equal to 0. Therefore, if a large cylinder is loaded with σ_1 on top and bottom and σ_m on the wall, then the stress in each point is given by the matrix

$$\begin{pmatrix} \sigma_1 & 0 & 0 \\ 0 & \sigma_2 = \sigma_m & 0 \\ 0 & 0 & \sigma_3 = \sigma_m \end{pmatrix}$$

with the σ_1 acting in the direction along the cylinder axis.

In the same way it can be shown that for a sphere loaded by a σ_h in all directions (Fig. 2.6f), the state of stress in any point is given by the matrix

$$\begin{pmatrix} \sigma_1 = \sigma_h & 0 & 0 \\ 0 & \sigma_2 = \sigma_h & 0 \\ 0 & 0 & \sigma_3 = \sigma_h \end{pmatrix}.$$

2.1.3 Strain Theory

The theory of the state of deformation in a point is named strain theory. This theory is discussed in the same books mentioned in part II. This chapter as chapter 2.1.2 only presents a few aspects of strain theory and is confined to small deformations. Proofs are omitted. A mathematical treatise of large and small homogeneous strains in two dimensions is given in the appendix.

In each point of a loaded soil body there is a state of stress and a state of strain. Strain can be described in a way comparable to the description of stress. Where the state of stress was described by normal stresses and shear stresses, the components of deformation are *normal strains* and *shear strains.* A normal strain is defined as follows: If an infinitely small line segment has a length l

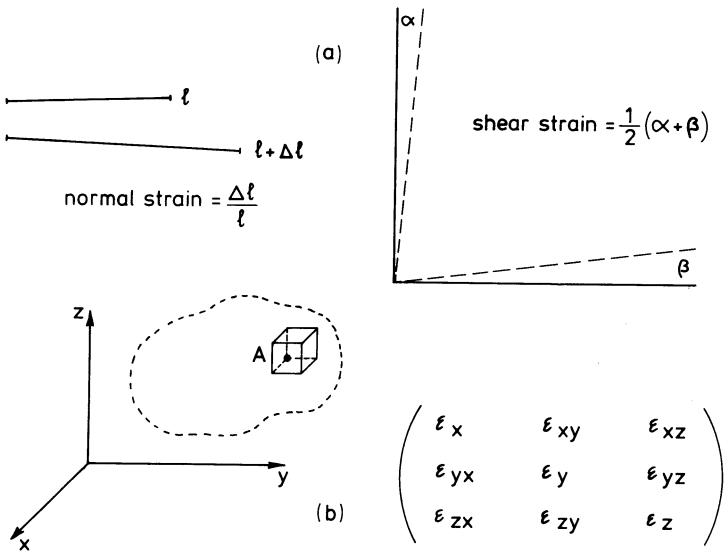

Fig. 2.7a, b. Definition of strain components (a) and the strain tensor (b)

before deformation (Fig. 2.7a left) and a length ($l + \Delta l$) after deformation, then the normal strain of that line element is $\frac{\Delta l}{l}$. A shear strain is defined on the basis of an angle that is right before deformation (Fig. 2.7a, right), with infinitely small sides. If the vertical side is rotated clockwise over the small angle α and the horizontal side counterclockwise over the small angle β (both expressed as radials) then the shear strain of the initially right angle is $\frac{1}{2}(\alpha + \beta)$. (On many occasions, shear strain is more directly expressed as $\alpha + \beta$, and denoted by γ, but this quantity is not suitable for matrix calculus). Now, the state of strain in a point can be described as follows: In Fig. 2.7b the broken line indicates an unloaded soil body with point A. We choose a co-ordinate system xyz and suppose an infinitely small soil cube in point A with sides parallel to the three coordinate axes. If the soil is loaded and deformed, the cube will also be deformed. In general, the cube will become a parallellepiped, because the cube is so small that parallel sides remain parallel. The sides will change in length:

Normal strain in the x-direction is denoted by ε_x
Normal strain in the y-direction is denoted by ε_y
Normal strain in the z-direction is denoted by ε_z.

The unloaded cube has right angles but, due to the loading, these angles will change:

Shear strain between the x and y directions is denoted by ε_{xy}
Shear strain between the x and z directions is denoted by ε_{xz}
Shear strain between the y and z directions is denoted by ε_{yz}

These six quantities are gathered in a symmetrical matrix as shown in Fig. 2.7. This matrix together with the co-ordinate system describes the state of strain in a point completely. According to the mathematical background of strain (see Appendix), the strain components defined in Fig. 2.7 should be taken as positive. However, on many occasions in soil mechanics practice they are considered negative. Therefore, it is not useful to adopt a stringent sign convention. Of course, in a different coordinate system the matrix will have different numerical values. The matrix is called the matrix of the strain tensor or deformation tensor. Its properties are much the same as those of the stress tensor. The symmetry is alike and there are again special positions of the co-ordinate system. This system can always be chosen in such a way that all shear strains are zero. The normal strains are then referred to as principal strains ε_1, ε_2, and ε_3, and the coordinate directions as principal directions. In this case the matrix is

$$\begin{bmatrix} \varepsilon_1 & 0 & 0 \\ 0 & \varepsilon_2 & 0 \\ 0 & 0 & \varepsilon_3 \end{bmatrix}.$$

There is also a position where the shear strain has a maximum value $\frac{1}{2}(\varepsilon_1 - \varepsilon_3)$, or $\gamma_{max} = \varepsilon_1 - \varepsilon_3$. The first invariant of the deformation tensor is

$$J_1 = \varepsilon_x + \varepsilon_y + \varepsilon_z = \varepsilon_1 + \varepsilon_2 + \varepsilon_3.$$

J_1 equals the fractional volume change of the cube. The octahedral normal strain and octahedral shear strain are, respectively,

$$\varepsilon_{oct} = \tfrac{1}{3}(\varepsilon_1 + \varepsilon_2 + \varepsilon_3)$$

$$\gamma_{oct} = \tfrac{2}{3}\sqrt{(\varepsilon_1 - \varepsilon_2)^2 + (\varepsilon_2 - \varepsilon_3)^2 + (\varepsilon_1 - \varepsilon_3)^2}.$$

Matrices of strain tensors can be added or decomposed as wanted. A common way of decomposition uses $\varepsilon_m = \frac{1}{3}(\varepsilon_x + \varepsilon_y + \varepsilon_z)$ and gives the following result:

$$\begin{bmatrix} \varepsilon_x & \varepsilon_{xy} & \varepsilon_{xz} \\ \varepsilon_{yx} & \varepsilon_y & \varepsilon_{yz} \\ \varepsilon_{zx} & \varepsilon_{zy} & \varepsilon_z \end{bmatrix} = \begin{bmatrix} \varepsilon_m & 0 & 0 \\ 0 & \varepsilon_m & 0 \\ 0 & 0 & \varepsilon_m \end{bmatrix} + \begin{bmatrix} \varepsilon_x - \varepsilon_m & \varepsilon_{xy} & \varepsilon_{xz} \\ \varepsilon_{yx} & \varepsilon_y - \varepsilon_m & \varepsilon_{yz} \\ \varepsilon_{zx} & \varepsilon_{zy} & \varepsilon_z - \varepsilon_m \end{bmatrix}.$$

The second matrix shows the volume change and the third matrix the distortion (= deformation without volume change) of the cube. The state of strain can also be represented graphically by Mohr's circle. Finally, it also holds true that these theories for infinitely small cubes can be extended to a finite soil body if the strain is the same throughout the soil body.

2.1.4 Stress-Strain Relations

Consider, at an arbitrary point in a soil, an infinitely small soil cube with respect to a certain co-ordinate system. When the soil is loaded the state of stress and the state of strain at that point can be described using this single cube. In general, stresses and strains will be time dependent. So we have

$$\begin{bmatrix} \sigma_x(t) & \tau_{xy}(t) & \tau_{xz}(t) \\ \tau_{yx}(t) & \sigma_y(t) & \tau_{yz}(t) \\ \tau_{zx}(t) & \tau_{zy}(t) & \sigma_z(t) \end{bmatrix} \quad \text{and} \quad \begin{bmatrix} \varepsilon_x(t) & \varepsilon_{xy}(t) & \varepsilon_{xz}(t) \\ \varepsilon_{yx}(t) & \varepsilon_y(t) & \varepsilon_{yz}(t) \\ \varepsilon_{zx}(t) & \varepsilon_{zy}(t) & \varepsilon_z(t) \end{bmatrix}.$$

In high-strength soils large stresses are accompanied by small strains and in weak soils large strains result from small stresses. The relation between stress and strain is specific for a certain soil. This can be expressed by the general formula

$$\begin{bmatrix} \sigma_x(t) & \tau_{xy}(t) & \tau_{xz}(t) \\ \tau_{yx}(t) & \sigma_y(t) & \tau_{yz}(t) \\ \tau_{zx}(t) & \tau_{zy}(t) & \sigma_z(t) \end{bmatrix} = f\left(\begin{bmatrix} \varepsilon_x(t) & \varepsilon_{xy}(t) & \varepsilon_{xz}(t) \\ \varepsilon_{yx}(t) & \varepsilon_y(t) & \varepsilon_{yz}(t) \\ \varepsilon_{zx}(t) & \varepsilon_{zy}(t) & \varepsilon_z(t) \end{bmatrix} \right).$$

Note that this linking of the two matrices is only possible for small deformations. If the deformations are large the position of the faces of the parallelepiped will be too different from the position of the faces used to describe the stresses. The function f is specific for a certain soil and must be determined experimentally. This can be done by subjecting a soil cube, cylinder, or sphere to a uniform stress, or a uniform strain and to measure the resulting strain or stress. This measured function f can vary widely. The following simple example applies when soil behaves as a linearly elastic material

$$\varepsilon_x = \frac{1}{E}(\sigma_x - \nu(\sigma_y + \sigma_z))$$

$$\varepsilon_y = \frac{1}{E}(\sigma_y - \nu(\sigma_x + \sigma_z))$$

$$\varepsilon_z = \frac{1}{E}(\sigma_z - \nu(\sigma_x + \sigma_y))$$

$$\varepsilon_{xy} = \frac{(1 + \nu)}{E}\tau_{xy}$$

$$\varepsilon_{yz} = \frac{(1 + \nu)}{E}\tau_{yz}$$

$$\varepsilon_{xz} = \frac{(1 + \nu)}{E}\tau_{xz}$$

or, using matrix notation,

$$\begin{bmatrix} \sigma_x & \tau_{xy} & \tau_{xz} \\ \tau_{yx} & \sigma_y & \tau_{yz} \\ \tau_{zx} & \tau_{zy} & \sigma_z \end{bmatrix} = \frac{E}{(1 + \nu)} \begin{bmatrix} \varepsilon_x - \varepsilon_m & \varepsilon_{xy} & \varepsilon_{xz} \\ \varepsilon_{yx} & \varepsilon_y - \varepsilon_m & \varepsilon_{yz} \\ \varepsilon_{zx} & \varepsilon_{zy} & \varepsilon_z - \varepsilon_m \end{bmatrix} + \frac{E}{3(1 - 2\nu)} \begin{bmatrix} \varepsilon_m & 0 & 0 \\ 0 & \varepsilon_m & 0 \\ 0 & 0 & \varepsilon_m \end{bmatrix}.$$

In this formula E (modulus of elasticity) and ν (Poisson's ratio) are constants describing the mechanical behavior of linearly elastic material (Drucker 1967). On most occasions the function f is more complicated. A number of ideal forms of

function f have been developed for soil and other materials and in general a certain material will strongly resemble one of these theoretical approaches. This field of knowledge is known as *rheology* (Drucker 1967, Reiner 1960). It is not true that we can load or deform the little soil cube to any extent. At a certain stress or strain the cube will break or start to flow. A state of stress or strain at which breaking or flowing starts is named a *yield condition.* A simple yield condition sometimes occurring in wet, dense clay soils is

$$\sigma_1 - \sigma_3 = \text{constant}.$$

This means that the difference between σ_1 and σ_3 cannot exceed a certain value. This example demonstrates that the same material can yield under different stress states. Each material has its own yield conditions, which may be idealized again. Such ideal yield conditions are called *yield criteria.* Yield conditions are expressed in formulas using components of the stress tensor and/or components of the strain tensor. A very common yield condition for soil is

$$\sigma_1 - A\sigma_3 = B$$

where the constants A and B are unique for a given soil under given conditions, with $A \geqslant 1$. This means that $\sigma_1 - \sigma_3$ can be greater if the mean stress on the cube is higher. Yield conditions of a soil also must be determined experimentally.

Function f and yield conditions constitute the so-called *mechanical properties* of soil. Soil mechanical properties have a number of general characteristics.

Thixotropy. In general, mechanical properties of soil change with aging. Such changes are the greatest shortly after events like loading or moistening. This phenomenon is known as thixotropy. It is caused by micro-processes in the soil (see part 1) and it usually implies that soil strength increases with time.

Anisotropy. A certain mechanical soil property may well depend on the direction considered. Stress to reach tensile failure along a horizontal plane, for instance, may differ from that for a vertical plane. This direction-dependency of a given soil mechanical property is called anisotropy. It may be caused by a preferential orientation of the soil particles, or by micro-cracks dominating in a certain direction.

Temperature Influence. Soil mechanical properties normally depend on temperature. An important cause is that surface tension and viscosity of soil moisture decrease with increasing temperature. On most occasions soil strength decreases with increasing temperature (NN 1969). Freezing and thawing have their own specific influences.

Hardening and Softening as a result of deformation. In some soils strength properties change very much on deformation. If this change weakens the soil it is said to be a sensitive soil.

Stress Relaxation. When soil is deformed to a certain extent, stresses in the soil will rise to a certain value. As soon as deformation is stopped, the stresses will

start to diminish at an ever decreasing rate (which is called stress relaxation). The state of zero stress will never be reached unless the soil is allowed to a full rebound after deformation.

Creep. If a soil is loaded to a certain stress, deformation will take place during the loading process and will continue at a very low rate, if the load is kept constant. This ever increasing deformation at constant load is called creep.

In general, function f and yield conditions can be determined on soil samples when a known, uniform state of stress or deformation is induced throughout the sample. However, there are also *indirect tests* that are often quicker and simpler. In these tests soil is loaded in a simple non-uniform way and calculations are carried out to estimate the stress distribution in the soil. Comparison of the soil reaction with the estimated stress distribution yields an estimate of the desired mechanical property. Such estimates may give less accurate results than methods with uniform stress and strain distributions.

2.2 Elemental Treatment of Compaction

2.2.1 Occurrence of Compaction

In the field, soil compaction depends largely on the agricultural system. In primitive agriculture a relatively large number of trips with small loads will be carried out, whereas in a highly mechanized system a few trips with large loads will be the normal practice. In most systems a soil profile consists of an arable layer, and a subsoil. The arable layer, which is loosened periodically, overlays a subsoil which is not loosened at all, or far less frequently. A change in this composition will have consequences for the bulk density profile of the soil. Examples are compaction of previously loosened layers after a reduction in plowing depth, and still more after introduction of direct drilling. Another important change can arise from a reduction of wheel tracks, especially when they are restricted to special strips instead of being distributed at random over the entire surface. This is the case when systems such as traffic lane-systems and bed-systems are introduced.

In general, compaction of soil in the field will be accompanied by soil deformation.

Top Layer. Seedbeds and the loose layer in dry farming are well-known top layers. The top layer is strongly influenced by the weather, which often leads to compaction due to slaking and crust formation. Moreover, the top layer is compacted mechanically. This may be an accidental effect, as in field traffic, or an intended action, for instance to control the seedbed moisture regime.

Arable Layer. The bulk density of the cultivated layer will change in the course of the year. Consider, for instance, the culture of a summer crop in the temporate regions for which the soil is plowed before the winter. The general pattern is a considerable upheaval at plowing, a consolidation starting immediately there-

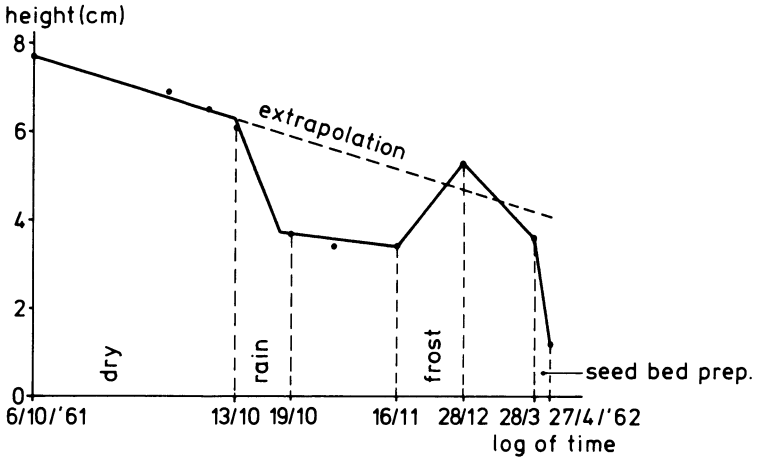

Fig. 2.8. Mean surface height of Wageningen clay soil in relation to log of time after plowing

after, and a considerable compaction at seedbed preparation. Obviously, this results in a fairly constant, small pore space during the growing season. Figure 2.8 refers to a part of this period, i.e. the period between plowing and sowing (Kuipers and Van Ouwerkerk 1963.) Upheaval at fall plowing is about 7 cm. After one month this was reduced by consolidation to only 4 cm, while in spring still 3.5 cm is left. This remaining upheaval disappears almost entirely on field preparation in spring. The graph demonstrates clearly the important influence of rainfall on the consolidation process. (See also section 2.2.3.5). In contrast, frost can result in a slight increase in pore space.

Subsoil. During field operations on farms the subsoil will be loaded. At low mechanization levels this may not result in significant compaction, but in modern agriculture subsoil compaction is likely to occur. Because the induced stresses decrease with depth, the risk will be greater at smaller depths. Indeed, subsoil top layers often have relatively high densities. Such layers are called plow-pans, be it that the plow is not to be blamed in the first place but the practice of driving through the open furrow when plowing. Moreover, soil particles of the plowed layer may be washed into the subsoil and contribute to the high density. On sandy soil, plow pans are massive, with little or no voids visible to the naked eye. Slightly heavier soils may have a clear tendency to pan formation. If the clay content is higher than about 20%, plow pans are influenced by processes like freezing, swelling and shrinking which makes them in general less pronounced. The still increasing weight of agricultural vehicles tends to increase the depth of compaction. Research in this field is in progress (Boels et al. 1982).

Combined Compaction and Deformation. A soil volume element subjected to compaction, for instance by a tractor tyre, is likely to shorten in the vertical direction and to elongate horizontally. Soil compaction in agriculture is almost always accompanied by deformation.

2.2.2 Fundamentals

2.2.2.1 Measures of Compaction

The degree of soil compaction can be expressed by one of the following quantities.

Pore space (P) of a soil volume element is the volume of pores (water + air) divided by the total volume of the element. It is expressed as a percentage or as a fraction.

Void ratio (e) is total volume of pores divided by total volume of solids.

Dry volume weight (γ_d) is weight of solids in a unit of volume (g/cm^3). For a given pore space γ_d depends on specific density of the solids.

Bulk weight volume (BWV) is $1/\gamma_d$ (cm^3/g).

The relationships between these quantities are given Fig. 2.9 where ρ = specific density of solids in g/cm^3. The accuracy that should be obtained for the different values can be estimated from the following: for a pore space of 45% a pore space increment ΔP of 0.10% corresponds to

$$\Delta e = 0.0033$$
$$\Delta \gamma_d = -0.0026 \text{ g/cm}^3$$
$$\Delta BWV = 0.0013 \text{ cm}^3/\text{g}.$$

2.2.2.2 General Model for Rapid Soil Compaction

Consider a point in a loaded soil. Its state of stress and state of strain are linked together by the so-called stress-strain relation,

state of strain = f (state of stress).

The function f is rather complicated and must be determined experimentally. The right hand side of the equation contains the state of stress as the variable

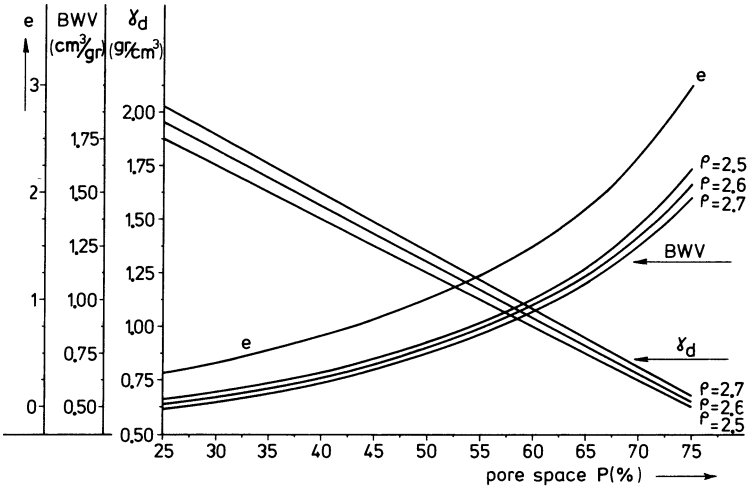

Fig. 2.9. Interrelationships between pore space (P), void ratio (e), bulk weight volume (BWV) and dry volume weight (γ_d)

quantity, which implies that the stress quantities σ_1, σ_2 and σ_3 and their directions are all variables. These stresses and directions change during loading. Hence, they are time-dependent and we may write

$$\text{state of strain} = f(\vec{\sigma}_1(t), \vec{\sigma}_2(t), \vec{\sigma}_3(t)) .$$

This function will be discussed after the following simplifications:

- of the strain, only volume changes will be considered. Volume will be expressed as bulk weight volume (BWV),
- loading is started in a very loose soil, e.g. a freshly rotavated soil,
- loading is carried out in such a way that during the loading process no increase in BWV occurs from elastic recovery (the model will be extended to include unloading and reloading in Section 2.2.2.2),
- σ_2 is chosen equal to σ_3. Calculations made on experimental results of Dunlap and Weber (1971) showed that the σ_1-pore space relationship is about one percent pore space lower when $\sigma_1 = \sigma_2$ than when $\sigma_2 = \sigma_3$,
- loading is quick enough to prevent water movement over macroscopic distances,
- principal directions are kept constant. Principal stresses are then scalars and vector notation is not necessary. (If principal directions change during loading, the process will be referred to as kneading. Söhne (1952) showed that, in general, kneading has only a minor influence on compaction).

These simplifications reduce the above formula to

$$(BWV)_t = f(\sigma_1(t), \sigma_3(t)) .$$

This function can be determined experimentally on a cylindrical sample that is loaded with an axial stress σ_1 and a radial stress σ_3, by continuously measuring BWV.

Such measurements can be carried out in a so-called tri-axial apparatus (Fig. 2.10). In this apparatus a cylindrical sample of loose soil is enclosed by rigid top and bottom plates and a cylindrical rubber membrane. σ_1 is applied through a

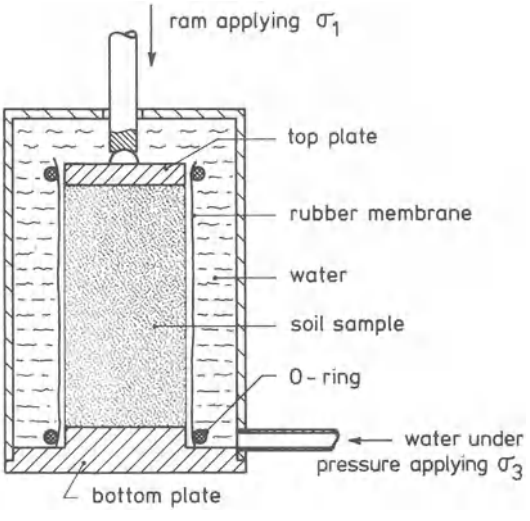

Fig. 2.10. Tri-axial apparatus for measuring soil compactibility

loading ram to the top plate. The enclosed sample is surrounded by water in a rigid transparant cylinder. σ_3 is varied by applying pressure to this water. (This water pressure is also acting on the top plate and must also be added to the value of σ_1). BWV can be calculated from the size of the sample or from the volume of water that flows to the cylinder during the test. The test starts with $\sigma_1 = \sigma_3 = 0$. Both σ_1 and σ_3 are changed gradually under continuous registration of their values and of the quantity needed to calculate BWV. Any pattern of σ_1- and σ_3-changes may be followed as long as only the volume of the sample decreases, because this was one of the simplifications introduced.

Such tests show that at any moment BWV is determined only by the values of σ_1 and σ_3, and not by the path followed to attain these values. This means that in the formula the index t is superfluous, so that we may write

$$BWV = f(\sigma_1, \sigma_3).$$

For many materials density is fully determined by σ_m. Therefore, it is often suggested that substituting σ_1 and σ_3 by σ_m and τ_{max} leads to further simplification. This substitution is not complicated because

$$\left.\begin{aligned} \sigma_m &= \tfrac{1}{3}(\sigma_1 + 2\sigma_3) \\ \tau_{max} &= \tfrac{1}{2}(\sigma_1 - \sigma_3) \end{aligned}\right\} \rightarrow \begin{cases} \sigma_1 = \sigma_m + \tfrac{4}{3}\tau_{max} \\ \sigma_3 = \sigma_m - \tfrac{2}{3}\tau_{max}. \end{cases}$$

The substitution gives a new function, F,

$$BWV = F(\sigma_m, \tau_{max}).$$

From a series of tests with different σ_1 and σ_3 paths the function f, as well as F, can be derived. So, two points of view are possible: the one considers BWV a function of σ_m and τ_{max}, the other a function of σ_1 and σ_3.

The Function $BWV = F(\sigma_m, \tau_{max})$

For a particular soil the function F can be determined from a series of tri-axial tests with different paths of σ_1 and σ_3. In a three dimensional, orthogonal co-ordinate system with axes BWV, σ_m, and τ_{max}, F represents a surface. In Fig. 2.11a the BWV axis is in the horizontal plane pointing left forward; the σ_m axis is in the same plane pointing left backward. The τ_{max} axis is pointing upwards. F is the surface between AB and CD. The curves connecting AB and CD are contour-lines of this surface. It appears that BWV decreases in the direction of σ_m as well as in the direction of τ_{max}.

An important aspect is that the surface F is bounded upward by CD. This can be understood by considering a special tri-axial test, in which at first σ_1 is kept equal to σ_3. This means that $\tau_{max} = 0$, and thus we follow curve AB in Fig. 2.11a, e.g. up to point E. Thereafter, we let σ_1 increase further and σ_3 decrease in such a way that σ_m stays constant. This means that τ_{max} is increasing and we follow curve EF in Fig. 2.11a. Along path EF the ram of the tri-axial apparatus will move further downwards. When we reach point F it appears that σ_1 does not increase any further with further ram movement, and at the same time the sample volume and BWV do not change any more; distortion continues with constant σ_m, τ_{max}, and BWV. This situation is called "critical state". Curve CD represents

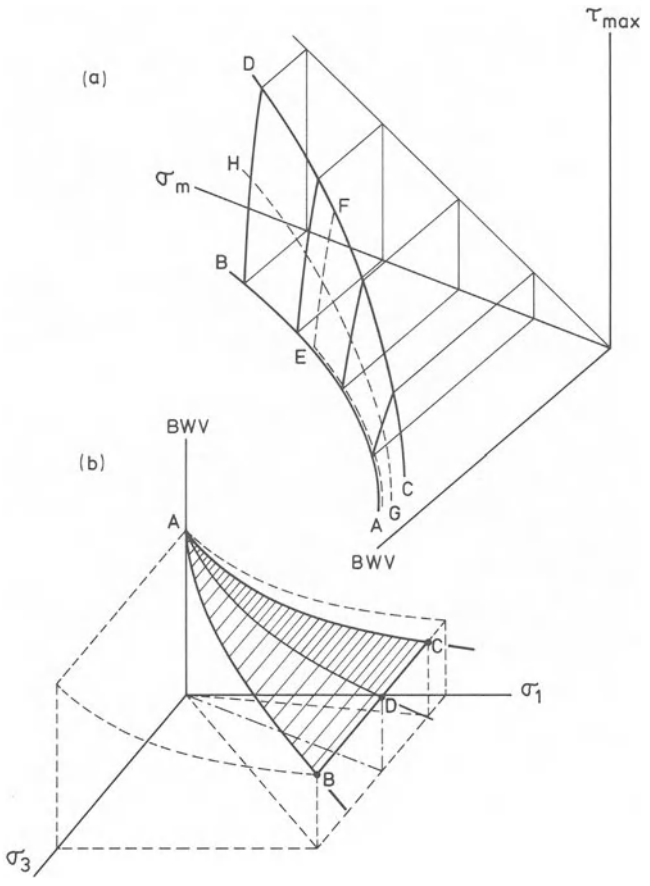

Fig. 2.11 a, b. Compaction surfaces in a (σ_m, τ_{max}, BWV) space (a) and in a (σ_1, σ_3, BWV) space (b)

all possible critical states of the particular soil. Along this curve, τ_{max}/σ_m is constant. Bailey and VandenBerg found for this ratio for Lloyd clay a value of 1.1. This soil behavior model is called "critical state soil mechanics" (CSSM). Literature on CSSM and critical states is found in Bailey and VandenBerg (1968), Chancellor and Korayem (1965), Dunlap and Weber (1971), and Kurtay and Reece (1970).

As to the distortion of the sample, along line AB, $\sigma_1 = \sigma_3$ and thus the sample is compressed equally from all directions and becomes shorter and thinner. For a point on CD the sample will shorten at constant volume and thus the sample will become thicker. Somewhere in between these two curves there must be a boundary curve on surface F, at which the sample diameter does not change (e.g. curve GH). During agricultural activities generally the soil is loaded from one direction and the compaction path will be somewhere on surface F between curves GH and CD.

The Function $BWV = f(\sigma_1, \sigma_3)$

The tri-axial tests that we considered to determine function F are also suitable to determine function f in the (BWV, σ_1, σ_3) space. In Fig. 2.11b surface f is between curves AC and AB. Co-ordinate space left of AB is not part of f, because then $\sigma_1 < \sigma_3$. Curve AB represents equal compression from all directions ($\sigma_1 = \sigma_3$), and thus changes in vertical and radial sample dimensions are procentually the same. Curve AC represents critical states. In a test that follows AC, the sample will become denser and shorter on increases of σ_1 and σ_3. If the state represented by a point of AC is maintained, the sample will continue to distort in such a way that vertical shortening and radial thickening compensate each other, leaving the sample volume unchanged. On curve AC, σ_3/σ_1 is constant. For cylindrical samples it is easy to calculate that at the critical state (cs)

$$\left(\frac{\sigma_3}{\sigma_1}\right)_{cs} = \frac{3 - 2\left(\frac{\tau_{max}}{\sigma_m}\right)_{cs}}{3 + 4\left(\frac{\tau_{max}}{\sigma_m}\right)_{cs}}.$$

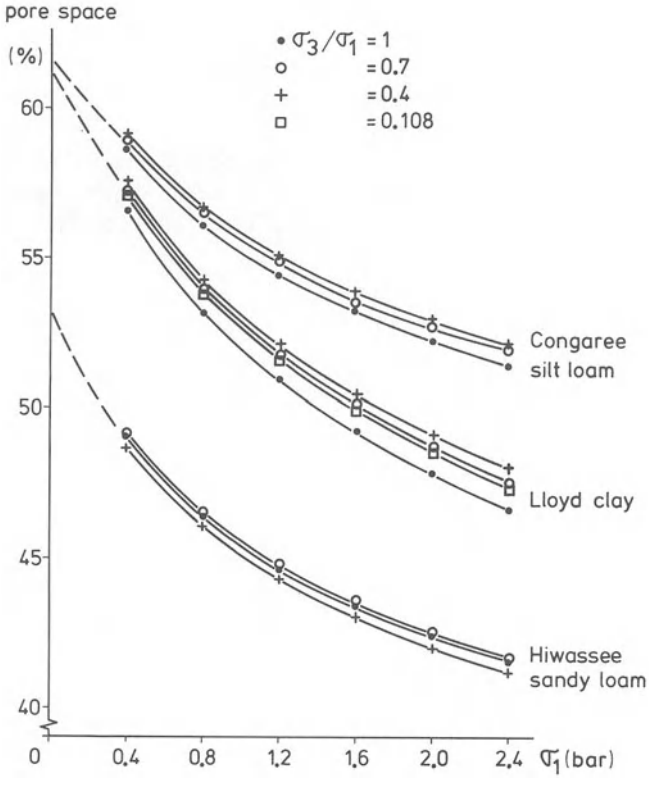

Fig. 2.12. σ_1-pore space relationships as affected by σ_3/σ_1 ratio

Substituting the results of Bailey and VandenBerg (1968) for Lloyd clay yields $\sigma_3/\sigma_1 = 0.11$. For compaction at constant diameter of the sample an approximate relation is $\sigma_3 = 0.5\,\sigma_1$ (Tschebotarioff 1951). This condition is represented by curve AD. Compaction as a result of agricultural activities will be along surface f between curves AD and AC. Figure 2.11b assumes that BWV varies mainly with σ_1 and only little with σ_3. Calculations on results of tri-axial tests by Bailey and VandenBerg (1968) confirm this (Fig. 2.12). Calculations applied to the results of Dunlap and Weber (1971) also show that σ_3 has only a slight influence. This means that soil compactibility could be represented by a still simpler function than F or f, namely a relation between degree of compaction and σ_1. Such a relationship can be determined in a simple way. No tri-axial apparatus is needed; compaction of loose soil in a rigid cylinder by a piston is sufficient. In such tests the sample diameter is constant and, in fact, curve AD in Fig. 2.11b is followed. This test will be referred to as uni-axial compression test.

The Uni-Axial Compression Test

In uni-axial compression tests soil is compacted in a rigid cylinder by a downward moving piston. Stress on the piston and volume of the sample are recorded continually (see Fig. 2.13). The piston can be loaded in different ways: stepwise by placing weights on a lever, increasing linearly with time as obtained easily with a constant flow of water into a container placed on the lever, or at constant piston speed using a hand-operated or powered screw press. The way of loading is not very important, in contrast with the time involved in the loading. Most common is a constant speed of the piston.

If we start with a loose sample, the height will decrease considerably during the test. At all stages the height-to-diameter ratio should not be too high, otherwise the friction between the cylinder wall and the soil makes the stress measured

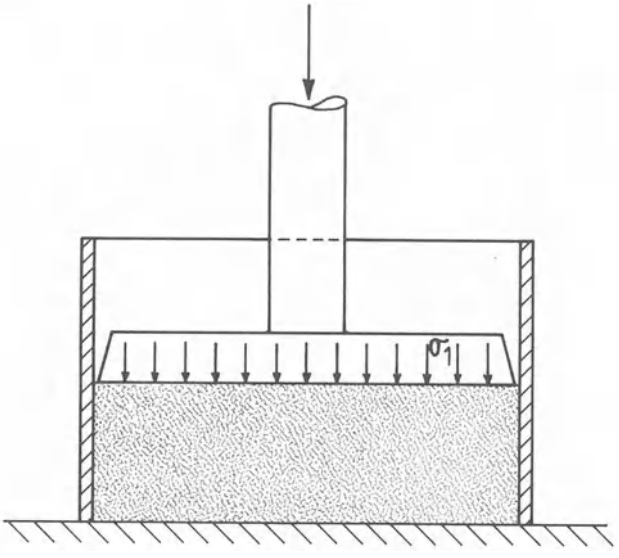

Fig. 2.13. Uni-axial compression test

on the piston much higher than the effective compactive stress. A suitable ratio can be found from the formula (Koolen 1974)

$$\frac{\sigma_b}{\sigma_t} = \frac{(D/h) - 2K\tan\delta}{(D/h) + 2K\tan\delta}$$

where: σ_t = mean normal stress on top of the sample,
σ_b = mean normal stress at the bottom of the sample,
D = inner diameter of the cylinder,
h = actual height of the sample,
$\tan\delta$ = coefficient of friction between cylinder wall and soil,
K = σ_3/σ_1 in "ideal" uni-axial compression, without wall friction. In general $K = 0.5$ (Tschebotarioff 1951).

When $K = 0.5$ and $\delta = 25°$, the formula predicts that $\sigma_b/\sigma_t = 0.7$ at $D/h = 3$ and 0.5 at $D/h = 1.5$.

Extension of the Model to Include Unloading and Reloading

If, after compaction to a certain volume, the sample is unloaded, the sample will rebound. The simplest model for this recovery is obtained by assuming elasticity. Strain on recovery is generally small in comparison to strain on compression of a loose soil. Therefore, soil obtained after initial compaction is called precompacted soil. If precompacted soil is loaded again, the simplest model is obtained by assuming that:

- compaction and distortion of the soil are elastic, with the same values of the modulus of elasticity E and Poisson's ratio ν as during recovery after the first compaction,
- after compaction to the same volume as that attained in the first compaction process, the sample behaves in the same way as it would have if the first compaction were continued without unloading.

In the stages where elasticity is assumed compressibility is defined as the proportionality coefficient κ according to

$$\varepsilon_m = \kappa\sigma_m$$

where $\varepsilon_m = (\varepsilon_1 + \varepsilon_2 + \varepsilon_3)/3$ and $\sigma_m = (\sigma_1 + \sigma_2 + \sigma_3)/3$. The compressibility κ is related to E and ν. From the matrix equation of elasticity in section 2.1.4 it can easily be derived that

$$\kappa = \frac{3(1 - 2\nu)}{E}.$$

Comparing elastic (recoverable) and plastic (non recoverable) deformation, it is obvious that elasticity will be relatively more important after stronger precompaction.

Although this elastic model is attractive for its simplicity, it is insufficient for many practical problems as will be discussed below.

2.2.2.3 Effects of Loading Rate, Repeated Loading, and Vibrations

A higher loading rate requires a higher stress to attain a certain bulk density. In uni-axial compression tests, Söhne (1953a) found a 0.5% higher pore space during compression of a sandy loam at a six times higher loading rate. This effect was measured on samples and is relatively small compared to the effect of tractor velocity on compaction under tractor tires (see Sect. 2.2.2.4).

Figure 2.14 shows the results of uni-axial compression with repeated loading and unloading (Söhne 1952). This figure shows that the simple elasticity model is not quite correct because there is a hysteresis effect. Moreover, the process is obviously time-dependent. Each vertical part of the curve corresponds to a period of 3 min during which the pressure was kept constant. During each of these time periods further compaction is observed. The additional compaction due to repeated loading to the same maximum stress has not been investigated extensively. Probably the length of the period between two loadings plays a role. There are at least two aspects involved in this time-dependency. Firstly, there is a rate effect in loading and unloading and, secondly, micro-processes such as soil water suction equilibration may occur in the period between two loadings. The effect of repeated loading of a sample in a tri-axial apparatus may be characterized by an additional decrease in height (ε_1) and an additional increase in diameter (ε_3). These strains are for a small part a volume change, but mainly a deformation (Wu 1971). This is in agreement with the observation that upheaval beside a wheel track increases with repeated passages. Interesting phenomena with uni-axial compression tests are that σ_3/σ_1 is higher on unloading than on loading, and that after unloading σ_3 still may have a certain value.

Compaction can also be caused by vibrations. In this one should distinguish between (Wu 1971):

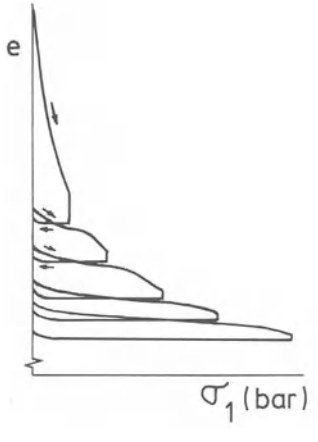

Fig. 2.14. Void ratio (e) – σ_1 relationship in an uni-axial compression test with repeated loading and unloading

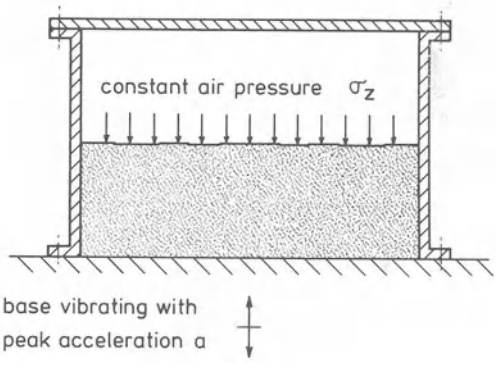

Fig. 2.15. Apparatus for investigating the compacting effect of soil acceleration and deceleration

1. compaction caused by stress changes, which can be explained from the process of repeated loading. In vibration tests with tri-axial cells it is observed that strain increments decrease with increasing number of cycles, if σ_3/σ_1 is large, and that these increments increase if σ_3/σ_1 is small. In the last case fatigue failure will occur.
2. compaction caused by acceleration effects. This acceleration effect can be examined with the aid of the apparatus shown in Fig. 2.15. If σ_z is small enough, and the peak acceleration a is high enough, soil particles have the opportunity to fall freely for a very short time and become very densely packed. At zero σ_z, free fall will occur if the peak acceleration exceeds the acceleration of gravity. At higher σ_z the peak acceleration that allows free fall is also higher. Acceleration effects will occur only in soils where cohesion is negligible, as in dry or saturated sands.

2.2.2.4 Soil Physical Aspects

Texture. Pore space ranges between about 40% and 50% in sand, and between about 45% and 60% in clay. Thus,

- the highest level of pore space is higher in clay than in sand,
- the lowest level of pore space is slightly higher in clay than in sand,
- the range of pore spaces is smaller in sand than in clay.

These facts are caused mainly by the stronger tendency of clay to form aggregates. This can be illustrated as follows. Pore space depends on the relative particle-size distribution and particle arrangement, but not on the absolute size of the particles. A certain arrangement of particles having a certain size distribution, has a certain pore space. Now suppose that each particle is composed of a number of smaller particles. Voids will be present between these smaller particles and this additional pore space adds to the total pore space. If the smaller particles, in turn, are composed of still smaller particles, pore space will increase once more. During compaction soil aggregates will be destroyed more and more and the soil will tend to become more homogeneous. Therefore, aggregation is likely to be less important at low pore space levels.

If soil is compacted with a kneading action, this may result in an additional compaction. This influence is relatively strong for "a soil with moderate quantities of particles of a very broad range of sizes" (Chancellor 1976). Repeated loading and vibrations are especially effective in compaction of soils without cohesion (sand). Because clay platelets are very elastic in bending, recovery after loading generally increases with increasing clay content.

Water Content. Figure 2.16a shows results of six uni-axial compression tests (Söhne 1958). Each test was carried out at a different moisture content. It shows that compactibility increases very strongly with moisture content. The curves for the moisture contents of 20.9% and 24.1% show a special phenomenon, namely that compaction is limited by a large amount of water. This is demonstrated in Fig. 2.16b. From the curves in Fig. 2.16a, pore spaces at 1, 2, 5 and 10 bar were determined for the different moisture contents and plotted in Fig. 2.16b. For ex-

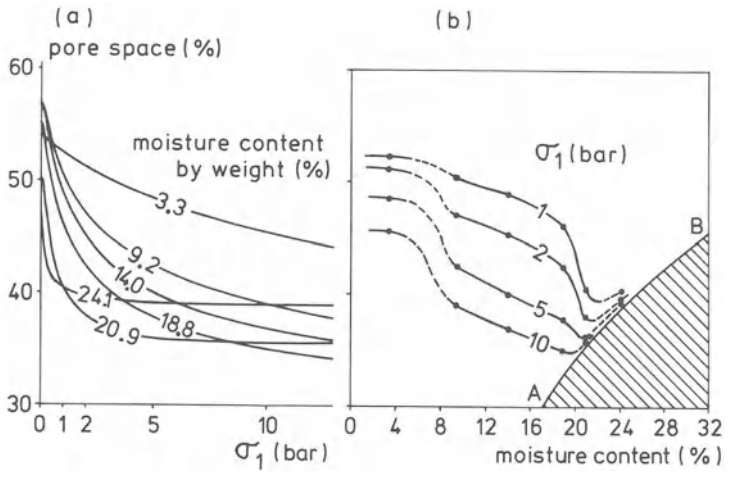

Fig. 2.16a, b. Soil compactibility as affected by moisture content (Söhne 1958)

ample, the top curve relates pore space obtained at a stress of 1 bar to moisture content. These curves consist of two parts. At the left, the pore space decreases with increasing moisture content. In this range compactibility increases with increasing moisture content. At the right, pore space increases with increasing moisture content. In fact, the curves in this part follow the boundary AB of the shaded area. This boundary represents the relation between pore space and moisture content at saturation, or zero air content. This curve can be calculated easily if the specific weight of the solids is known. Compaction can never result in a condition represented by a point in the shaded area, because then the soil would hold more water than can be stored in the pore space. Whether saturation will be reached under field conditions depends on the moisture content of the soil; in sand it does not occur often, but in clay soils it is common. When the moisture content is continuously high, as in the heavier unripened soils in new polders, the soil is prevented from being compacted to a normal porosity level.

Moisture content influences the sensitivity of sandy soils for vibration. Unless sands are completely dry or completely saturated, the capillary attractive force between the particles makes them less susceptible for compaction by vibration.

Soil Air. Decrease of pore space on compaction has to be accompanied by outflow of air. In general, not all air can escape freely; a certain amount will be entrapped. On heavier soils this may amount to 5 volume percent. If, during compaction, the entrapped air is compressed to significant pressures, and if the amount is high, the soil may rebound considerably when the stress is released. The outflow of air requires a pressure gradient. The gradient will have to be built up by the external compactive force. The force required for building up this gradient may be strongly dependent on loading rate because of the air viscosity. This aspect of compaction has not had much attention in research, but the following hypothesis seems justified: "external stress required for compaction to a certain pore space, and the rate dependency of this stress, are greater for larger

soil bodies". This is so because in large soil bodies the air has to travel over long distances, which requires relatively high air pressures. The hypothesis gives a reasonable explanation of the difference in speed effects measured under tires in the field (Baganz 1963/64) and in tests on soil samples in the laboratory (Söhne 1952).

Organic Matter. Under wet conditions, soils with a high content of organic matter are more resistant to compaction than soils low in organic matter; under dry conditions, the reverse holds true. This means that during drying the soil resistance to compaction increases most in soils low in organic matter (Kuipers 1959a).

Temperature. Temperature influences compactibility of soil, but the effect is insufficiently investigated (NN 1969).

The Influence of Water Movement in Soil. Water movement in precompacted soils influences compactibility in further compaction. Two situations may occur.

1. Total moisture content does not change, but thixotropic effects occur. This was measured by Söhne (1955) in uni-axial compression tests. Thixotropy is discussed in more detail by Seed and Chan (1957).
2. Change in total moisture content. Resistance against further compaction depends on actual moisture content, moisture content at precompaction, and on the path along which the actual moisture content was reached. Measurements on the effect of moisture content at precompaction on compactibility were presented by Koolen (1976). These results showed that resistance against further compaction decreases with increasing moisture content at precompaction. Also, further compaction due to drying (shrinkage) increases with increasing moisture content at precompaction. Whether there is still a unique compaction surface (as in Figs. 2.11a or b) after moisture changes has not yet been investigated. Under field conditions precompacted soils with changed moisture contents are the normal situation.

2.2.2.5 Slow Compression

Whether volume reduction is called slow or quick does not depend on the absolute value of the rate of reduction, but on the character of the process. Characteristics for slow compression are

- compression is slow enough for the air to escape without significant pressure build-up in non-entrapped air,
- if positive water pressures exist and outflow of water is possible water transport occurs over macro-distances,
- on a micro-scale, water distribution does not become chaotic and water pressures remain at equilibrium,
- acceleration forces do not play a role in the strain field; the application of stresses does not have the character of a stress wave. A stress wave cannot produce a uniform compaction. A consequence of this is that large soil samples cannot be compacted quickly in a uniform way.

An example of a slow compression experiment is the consolidation test used in civil engineering. This is a uni-axial compression test on saturated soil with an escape for soil water. A certain load is applied instantly and kept constant for a certain period, e.g. a number of days. The test is used for predicting consolidation under structures. Because small compressions are involved the test is carried out at constant temperature. In the moment that the load is applied, water in the sample can be regarded as immobile. Since in the saturated samples the contact area between the soil water and the loading plate is much larger than between the plate and the soil particles, the total load applied will initially be supported by the water and the initial water pressure will equal the applied stress. The sample rests on a porous plate that allows drainage of water. The more water escapes, the more the load will be transferred to the soil particles. The soil particles will be rearranged till a stable final state is reached. Final consolidation z is linearly related to the logarithm of the applied stress p,

$$z = a + b \log p$$

where a and b are constants. Rates of consolidation of clay and peat soils are inversely proportional with time t,

$$\frac{dz}{dt} = \frac{c}{t} \quad \text{or} \quad z = d + e \log t$$

where c, d, and e are constants. Slow compression is probably important with respect to consolidation of plowed layers, consolidation due to irrigation, and consolidation under "parked" vehicles.

2.2.3 Applications

2.2.3.1 Estimation of Soil Compaction by Means of Estimated Stress Distributions

If bulk density is determined by σ_1 and the relation between σ_1 and bulk density is known, a compaction (volume strain) distribution can be calculated from any known σ_1 distribution. Several methods, all based on the assumption of *elastic soil behavior*, are available to estimate σ_1 distributions under surface loads.

Vertical Point-Load Method. It is assumed that a tire-soil system can be approximated by a vertical point-load resting on a semi-infinite elastic medium. Boussinesq (Söhne 1953a) described principal stresses for this case (Fig. 2.17a). Consider a small cube in such a position that radius vector r is perpendicular to one of the sides. Calculations of Boussinesq show that in this case there are no stresses on all the sides except on the sides perpendicular to the radius. On these two faces there is only a normal stress which, therefore, is a principal stress. This stress is given by

$$\sigma_r = \sigma_1 = \frac{3P}{2\pi r^2} \cos\theta .$$

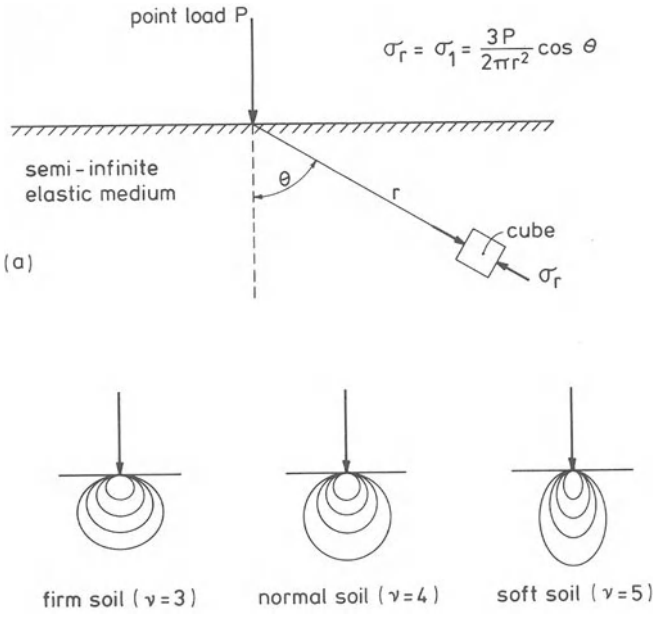

Fig. 2.17a, b. Soil stresses due to a vertical point-load (a) and modification to match agricultural conditions (b)

With the aid of this formula σ_1 can be calculated in any point of the medium and the direction of σ_1 is given by the radius vector r. Of special interest is the relation between depth and principal stress in a vertical line under the point load. In this case $\theta = 0$, or $\cos\theta = 1$.

Modified Vertical Point Load Method. Because of the assumption of elastic soil behavior, the vertical point load method predicts the same stress distribution for all soils. It is known, however, that soil behaves far from always as an elastic material and that, consequently, soil strength influences stress distribution. To account for this, Fröhlich (Söhne 1953a) modified the above formula in the following way

$$\sigma_r = \frac{\nu P}{2\pi r^2} \cos^{\nu-2}\theta.$$

ν is called *concentration factor.* This factor increases as soils become softer. Accepted values are

hard soil: $\nu = 3$
normal soil: $\nu = 4$
soft soil: $\nu = 5$.

Why this factor is called concentration factor can be seen in Fig. 2.17b which shows isobars, curves of constant stress. It is clear that stresses are more concentrated under the load and reach deeper in the soil as ν is greater.

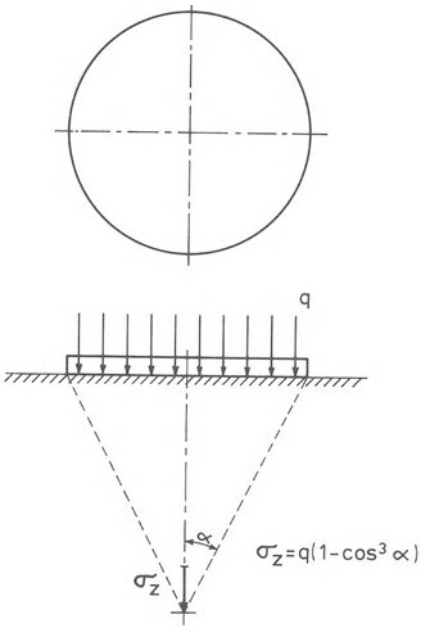

Fig. 2.18. Soil stresses below the center of a uniformly loaded circular area

In a third method the tire-soil system is described by a *circular area* that is loaded by a uniformly distributed normal load. The area of the circle is chosen equal to the area of the soil-tire contact surface and the stress q on the circular area is taken equal to the mean normal stress in the soil-tire interface (Fig. 2.18). Consider a small horizontal plane below the center of the circular area. Angle α characterizes the depth of the plane under consideration. If $\alpha = 90°$, the plane is at the surface; if $\alpha = 0°$, the plane is infinitely deep. Because of q, there is a normal stress σ_z on the plane. This σ_z is a principal stress and for the depth considered also the greatest stress. According to Söhne (1953a) this stress is given by

$$\sigma_z = q(1 - \cos^3\alpha).$$

If $\alpha = 90°$, $\sigma_z = q$, and if $\alpha = 0$, $\sigma_z = 0$.

Modified Circular Area Method. The method based on an evenly loaded circular area can, according to Fröhlich, be adjusted for differences in soil strength by introducing the concentration factor ν,

$$\sigma_z = q(1 - \cos^\nu\alpha)$$

where $\nu = 3$, 4 or 5 in case of hard, normal or soft soil, respectively.

Strip Load Method. A fifth method describes the tire-soil system as an evenly loaded infinite strip (strip load). In that case the width of the strip is taken equal to the tire width and the normal stress on the strip is chosen equal to the mean normal stress in the soil-tire interface (Fig. 2.19). With this method the first principal stress can be calculated in each point of the semi-infinite medium. In point A this stress is found as follows,

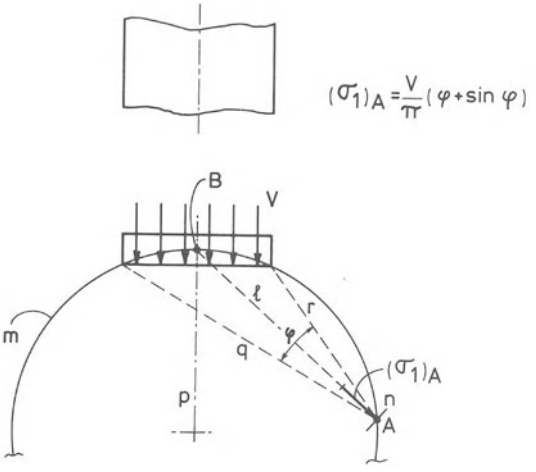

Fig. 2.19. Major principal stresses in the soil due to a strip load

- draw circle m (through A and the sides of the soil-strip interface),
- draw line p perpendicular to the strip, through the middle of the strip, to find B on the circle, and draw line l connecting A and B,
- draw lines q and r through A and the sides of the soil-strip interface to find angle ϕ enclosed by q and r.

Now, the value of the first principal stress in A is given by

$$(\sigma_1)_A = \frac{V}{\pi}(\phi + \sin\phi)$$

and its direction by line l. In Fig. 2.19 this σ_1 is shown by an arrow acting on a small plane in A perpendicular to l. It stands to reason that in the given formula the numerical value of ϕ is in radians. From the given solution Bekker (1956) derived the following rule of thumb; "at a depth equal to the width of the strip load, the stress under the center of the load is about half the surface stress".

Söhne's Summation Procedure (Söhne 1953a). This is a numerical procedure, yielding a specific solution for a certain tire, a certain inflation pressure, a certain tire load and a certain soil. For such a specific case, shape and size of the contact area and the pressure distribution in this contact area must first be determined by whatever method is most suitable. Then the contact area is divided into surface elements as shown in Fig. 2.20. The shaded element, indicated as element i, with an area A_i and a normal stress p_i, carries a total force $P_i = p_i \times A_i$, and this force is treated as a point load. Now consider a point B in the soil, under the center of the tire and a small horizontal plane in that point. The point load P_i will induce a vertical stress $(\sigma_z)_i$ on that plane which can be calculated from σ_1 predicted by the modified vertical point load method and the stress transformation procedure demonstrated in Fig. 2.5

$$(\sigma_z)_i = \frac{\nu P_i}{2\pi r^2}\cos^{\nu}\theta\,.$$

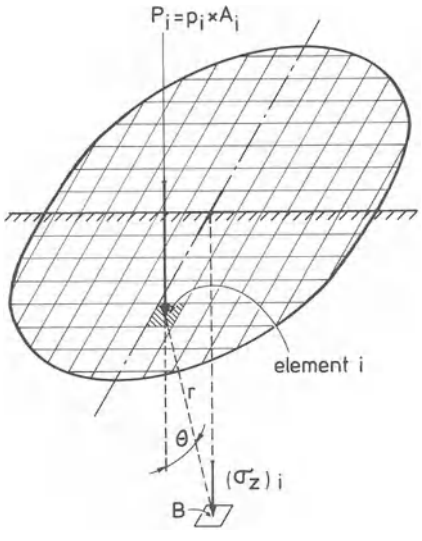

Fig. 2.20. Refers to Söhne's summation procedure

Each element of the contact area supports a load and all these loads contribute to the normal stress on the small plane in B. Total normal stress on that small plane can be obtained by adding all contributions

$$(\sigma_z)_{tot} = \sigma_z \text{ due to } P_1 + \sigma_z \text{ due to } P_2 + \ldots .$$

Because B is on a vertical axis of symmetry, total σ_z in B is the first principal stress in B. In this way it is possible to calculate the first principal stress for each point under the center of a tire.

Comparison of Methods. Consider a tire on a certain soil, with load G, contact area A, width b and mean normal stress in the contact area p. To calculate stresses in the soil under the center of the tire, we can use the approximation of a point load G (Fig. 2.21a), and evenly loaded circular area of size A with stress p (Fig. 2.21b), a strip load having a width of b with stress p (Fig. 2.21c), or we may use Söhne's summation procedure for load G, contact area A, width b and stress p (Fig. 2.21d). Söhne's procedure is the most detailed and it is likely to give the most realistic result for stresses under the center of the tire. However, it appears that the much simpler calculations for the circular area give about the same values. At greater depths the point load gives the same values as Söhne's approximation, but at small depths the point load gives too high values because the assumed load is more concentrated than the real load exerted by the tire. The strip load gives too high values at any depth, because the strip is assumed to be infinitely long, which means that the assumed total load is higher than the real one.

Rules of Thumb. In addition to the rule of Bekker the calculation methods discussed lead to the following statements:

- If the surface stresses are multiplied by a factor b, the stress in any point of the soil is multiplied by b,

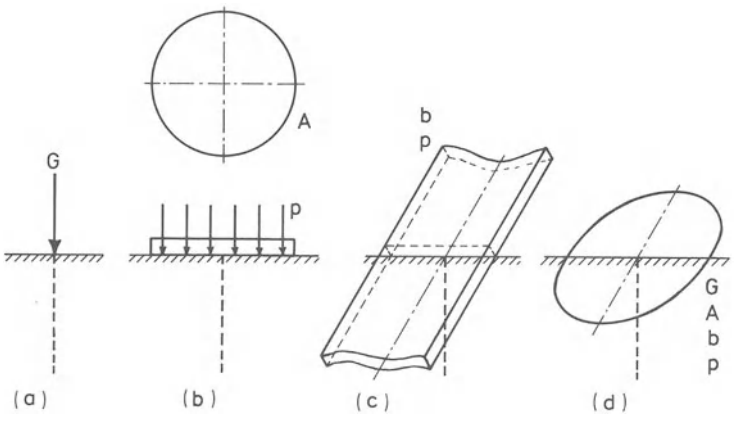

Fig. 2.21 a – d. Comparison of methods to simulate the tire-soil system

- maximum normal stresses occur at the contact area,
- for points at greater depths tires may be assumed to be point loads,
- if the normal stresses on the surface elements of the contact area remain unchanged and all linear dimensions of each surface element (and, therefore, all linear dimensions of the contact area) are multiplied by b, stresses will reach b times deeper into the soil.

2.2.3.2 Curve Fitting Formulas for Compression Tests

Degree of Compaction – σ_1 Relations

Quick compaction tests, like e.g. quick uni-axial compression tests, yield measuring curves relating sample degree of compaction to σ_1. Such curves can be described mathematically by different formulas. Best known are the logarithmic, hyperbolic and exponential relations.

Logarithmic Relation. In use are e.g. for pore space, $P = -A \log \sigma_1 + B$ (Söhne 1952), and for bulk density $\gamma = c \log \sigma_1 + k$ (Bertilsson 1971). Constants A, B, c and k can be found easily by making a semi-logarithmic plot of the measuring curve.

Hyperbolic Relation. Kuipers (1959b) used a hyperbolic curve that gave a close fit. Koolen (1974) transformed the formula to a more universal form. Figure 2.22 gives an experimental curve representing the result of a uni-axial compression test on "Wageningen" soil at a moisture content of 23.7%. As Kuipers showed a great part of such a line is hyperbolic. In Fig. 2.22, the broken curve represents the hyperbola that fits the experimental curve best. The experimental curve at low stresses is not hyperbolic. This is due to the method used for filling the cylinder. In general, the effect of the way of filling overwhelms the "true" soil behavior in compaction in that stage of the test. At high pressures the experimental curve is also not hyperbolic, because at higher values of σ_1 the stress dis-

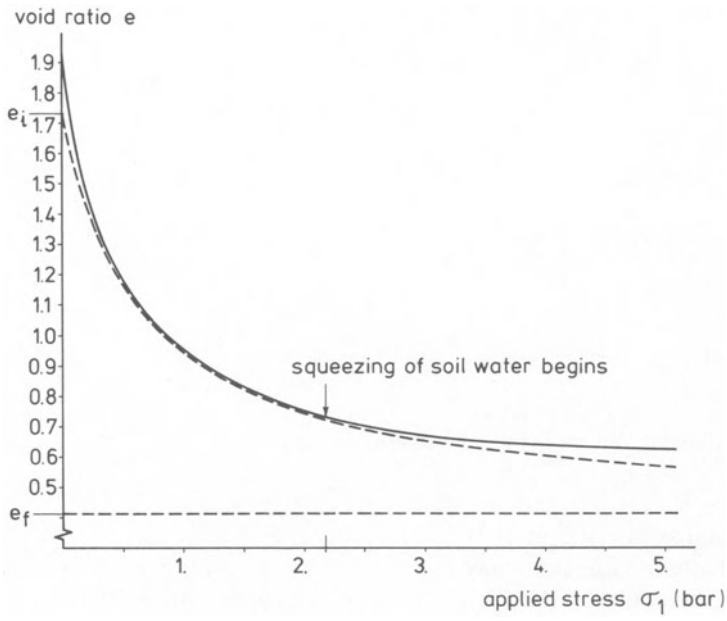

Fig. 2.22. Fitting a compaction curve by a hyperbolic relation (Koolen 1974)

tribution within the soil becomes uneven as a result of water being forced out of the sample. The hyperbola represented by the broken line satisfies the equation

$$\frac{e - e_f}{e_i - e_f} = \frac{1}{1 + \frac{p}{c}}$$

where $p = \sigma_1$. For $p = 0$ this hyperbola predicts the value e_i (e_i is called theoretical initial void ratio). As $p \to \infty$ the hyperbola approaches the asymptote $e = e_f$ (e_f is called theoretical final void ratio). c is the stress that gives a value of e which lies half-way between e_i and e_f. c can be called "median stress". Values for e_i, e_f and c can be derived from experimentally obtained compression data as follows:

1. determine n (for instance 20) experimental points (p_j, e_j), $j = 1, \ldots n$, which should be evenly spread along the experimental curve,
2. from these, select one experimental point (p_k, e_k) that approximately lies in the middle of the expected hyperbolic part of the experimental curve,
3. compute $B_j = \frac{p_j - p_k}{e_k - e_j}$ for each experimental point (p_j, e_j),
4. plot B_j against p_j. A great part of this curve is a straight line, $B_j = mp_j + q$,
5. determine m and q graphically.

It can be shown that $c = (q/m)$ and $e_i - e_f = (1 + (p_k/c))/m$. These expressions, together with the equation obtained by substituting the numerical values of p_k and e_k into the hyperbolic equation, are sufficient to compute e_i, e_f and c. This

method of curve-fitting should be preferred over statistical methods because it gives a result that is not affected by the deviating initial and final parts of the experimental curves.

Exponential Relation. Exponential fitting curves were presented by Dexter and Tanner (1973) and Kermis (1968).

Fitting Formulas with More than one Stress Component

Bailey and VandenBerg (1968), Kumar and Weber (1974), and Dunlap and Weber (1971) describe formulas for the compaction surface in a (BWV, σ_m, τ_{max}) co-ordinate system. Formulas using spherical and deviatoric stresses are used by Kurtay and Reece (1970). VandenBerg (1966) applied a formula containing σ_m and a deformation characteristic (γ_{max}).

2.2.3.3 Håkansson's Compaction Test

Håkansson (1973) expressed the state of compaction by the "degree of compactness", D, defined as $D = 100\ \gamma_t/\gamma_{t,p}$, where γ_t is the actual bulk density and $\gamma_{t,p}$ is the bulk density of the soil in a standard compacted state. This standard state is obtained by exposing a large (12 dm^3) sample of loose soil (which passed a 25 mm sieve), after thoroughly wetting, to a pressure of 2.0 kp/cm^2 (=196 kPa) under free drainage until equilibrium is reached. This roughly gives the highest bulk density obtainable with the pressure used.

2.2.3.4 Simulating Tire Effect by a Uni-Axial Compression Test

To predict compaction under a tire the following empirical-analytical method can be used. For a given tire on a given soil and for a known load, compaction of a soil volume element as shown in Fig. 2.23 can be predicted by compacting a sample of the soil in a uni-axial compression test. In this test the maximum stress on the loading plate should equal the tire inflation pressure increased or decreased with certain corrections. Provided the corrections are well chosen, the test sample will reach the same density as the soil element under the tire. Sample size in this case should not be too small, e.g. 10 cm diameter cylinders may be used.

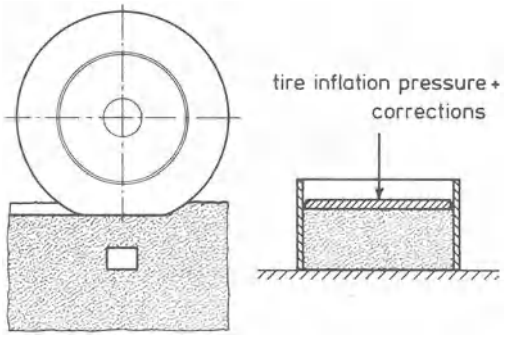

Fig. 2.23. Simulating tire effect by a uni-axial compression test

In this method the corrections play a decisive role. They should be made to counteract the following phenomena:

Stiffness of the Tire Carcass. A certain force is required to deflect an unmounted, uninflated tire, because of its stiffness. Therefore, the contact area of a deflected, operating tire carries a load due to the inflation pressure, plus a load required to deflect the tire. To find the mean normal stress in the contact area, this stiffness factor, e.g. 0.25 bar as a first correction, must be added to the inflation pressure.

Uneven Stress Distribution in the Contact Area. From measurements it is well known that stresses on the outer parts of the contact surface are much higher than on the center part. Maximum stresses may well be 1.5 to 2 times the mean contact stress. Because the maximum stress that ever acted on a soil volume element is decisive for its density, this uneven distribution asks for a considerable correction.

Shear Stresses in the Contact Area. Tangential stresses may well exist in the soil-tire interface due to the rubbing movement of the tire, especially when the tire is slipping. Even without slip, such a rubbing movement may be caused by a flattening of the tire, which changes the radius and, therefore, also the circumferential speed. Such shear forces increase compaction stresses by about 50%.

Stress Reduction with Depth. Stresses decrease with increasing depth. The correction required for this increases with soil strength.

Size of Contact Area. Stress reduction with depth decreases with increasing loaded area.

Lateral Movement of the Soil. In the field, a soil volume element under a tire will not only flatten, but also broaden (σ_3/σ_1 being smaller than 0.5). This is not the case in compaction tests in rigid cylinders (σ_3/σ_1 is about 0.5). For substances like metals, plastics, and liquids, such broadening reduces "compaction" at a given σ_1-value. For soils often the reverse is true: broadening increases compaction at a given σ_1 value. This phenomenon is then due to moving soil particles filling up existing pores. This may result in a correction of e.g. 25%.

Wall Friction in the Uni-Axial Compression Test. This last correction is necessary because of friction between soil particles and cylinder wall during the compaction test. A higher wall friction results in a higher force required to obtain a certain density. This correction may be 10% (see Sect. 2.2.2.2).

How great the sum of corrections should be can be determined experimentally by comparing compaction under a tire with a uni-axial compression test in which the compaction $-\sigma_1$ relation is measured continuously. In general, it is assumed that a "normal" tractor tire can be simulated by a uni-axial compaction test with a maximum stress of 4 bar.

2.2.3.5 Predicting Soil Density Following Irrigation

Ghavami et al. (1974) reasoned that, in a relatively dry, loose bed of aggregates, bulk density may be increased by overhead irrigation not only because the weight of the soil increases, but especially because soil strength decreases with water suction. In this case, the increase in bulk density is due to decreasing pore space between aggregates rather than within aggregates.

For a very thin horizontal soil layer,

$$e = f(\sigma, u)$$

where e = void ratio in the irrigated layer, σ = normal stress on that layer arising from the weight of the overlaying soil mass, calculated for the period of maximum water content in that mass, and u = water suction (negative pressure) in the thin layer when its water content is highest. (σ and u will have their extreme values at the same time, i.e. the time of maximum water content.) This relationship can be determined from consolidometer-tests. In such a test the soil is loaded by a "dead weight" for a certain period. The sample rests on a porous plate in which a certain suction (u) is maintained by a vacuum-drainage system. To find f, tests with different loads and different suctions are needed. Such tests showed that at a certain irrigation intensity and after equilibration, there is no great influence of depth in the soil profile on moisture content and suction. When intensity increases, moisture content and water pressure increase leading to more compaction. If f and the relationship between irrigation intensity and soil water suction are known, compaction can be calculated for different layers. Because u is nearly constant in the profile, and σ is increasing with depth, compaction will also increase with depth. In the article mentioned above figures are given for Melville silt loam.

2.2.3.6 Complexity of Compactibility Concept

Soil compactibility cannot be described adequately by a single compaction curve (σ_1-degree of compaction relationship), determined at a certain moisture content. Information is needed on

1. influence of moisture content on the compaction curve,
2. the range of moisture contents that will be relevant for field conditions (e.g. the pF-curve),
3. amount of air in the soil,
4. influence of aggregation on the compaction curve.

A still incomplete example is given in Fig. 2.24 for "Wageningen" silt loam (Koolen 1974). Curve e_i refers to (estimated) void ratio under very loose conditions, curve e_f to the estimated void ratio at very high stress. On the horizontal scale the moisture content at the beginning of the compaction tests is indicated. Curve 1 is the theoretical saturation line and curve 2 shows void ratios obtained at a stress of 5.2 bar. At void ratios smaller than indicated by curve 3, water was squeezed out of the sample. The top curve shows the stress needed to reach a void ratio half way e_i and e_f.

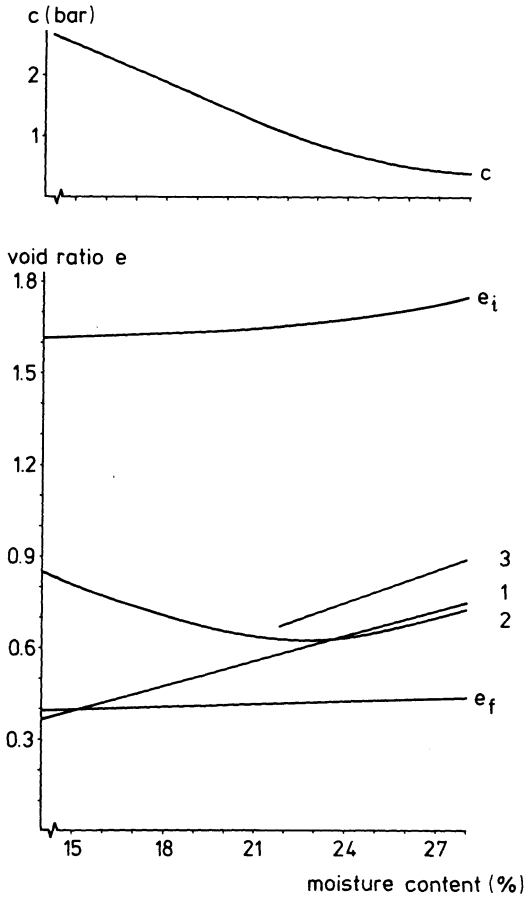

Fig. 2.24. Wageningen silt loam behavior in compaction

2.3 Elemental Treatment of Deformation (Distortion)

2.3.1 Occurrence of Distortional Strain

Loading of a soil volume element is generally accompanied by a certain degree of distortion of the element. The main variables with respect to distortion are load, soil density, and soil moisture content.

Tires, Wheels and Rollers induce relatively high stresses which, since the affected soil can move away rather easily, may induce large deformations. Consider first a vertical plane through a tire and its wheel axis. If tire sinkage is large there will be strong deformations in that plane. When the soil is wet or dense, deformations will take place at constant volume and the soil surface next to the tire has to bulge up. Under loose or drier circumstances the deformation will include compaction and there will be little or no bulging up beside the tire (Kuipers 1970). Now consider the vertical plane through the tire center in the direction of travel. There are

also deformations in this plane. If there is positive tire slip, soil in the rut is moved backwards. At normal pull a tire slips 15% – 20%. For current tractor tire sizes this means a backward movement of about 0.2 m. This movement decreases with depth and this gradient is manifested as deformation. A steep gradient indicates a large deformation that is restricted, however, to a thin layer. Such steep gradients occur, for instance, at high slip percentages on relatively firm soil with hardly any sinkage. A steep gradient will also occur if strength rapidly increases with depth due to a density increase or a moisture decrease.

Puddle Wheels. In wet rice fields puddle wheels may be used to obtain the desired puddled soil condition. Slip percentage and design of these wheels aim at strong deformations at a high stress level. Since soils are saturated at puddling, deformation will take place at near constant volume. The actions of smearing and mixing with superfluous water initiate swelling and therefore final pore space will be high.

Moldboard Plows have been developed mainly for dense, moist soil. They are designed in such a way that large deformations occur at low stresses. Deformation of dense soil at a low stress level increases soil volume. This phenomenon is known as *dilatation.* Dilatation is an unstable process because in spots where volume increases, the soil will become weaker which favors further deformation and volume increase. So, deformations tend to concentrate, ultimately leading to the development of fracture surfaces. Along such surfaces very thin dilatation bands are present having an increased pore space. Deformation in these bands is larger for shear failure than for tensile failure. For moldboard plows three levels of deformation should be distinguished,

- deformation on a micro-scale, within the dilatation bands along fracture surfaces,
- newly formed soil blocks rolling and sliding over each other. This gives a large volume increase, because the blocks are brought into a loose configuration,
- deformation within the soil blocks, which is possible because of the relatively high moisture content at plowing.

Plowing dry soils requires high cutting forces and results in low quality work because a coherent soil slice cannot be formed.

Tines are more suitable for dry, dense soil. Because the width of a tine is smaller, the cutting force is smaller. When the soil is firm, stresses will be transmitted far enough to make the actual working width acceptable. Soil deformation within blocks will be negligible under dry conditions. For a tine operating in wet soil actual working width would be small and deformation within that width would occur at a high stress level, inducing soil smearing.

2.3.2 Fundamentals

2.3.2.1 Introduction

Consider a soil volume that is being deformed from shape *A* into a widely different shape *B* under the condition that at any moment the state of deformation is the same in all points of the volume (homogeneous deformation). Such a deformation process can be understood better by assuming that this large deformation is the sum of a number of successive small deformations. Each of these small deformation steps (deformation increments) can be described by the incremental strain tensor applying to that step (see part 2.1.3). A new elemental cube should then be assumed within the soil at the start of each small step to allow for the matrix description. So, each step can be described by six numbers, being the six components of the matrix of the incremental strain tensor of that particular step.

There are many different possible ways of homogeneous deformation to get from shape *A* to shape *B*. Two possibilities are given in Fig. 2.25. It should be clear that the second deformation process influences the soil much less than the first; thus, deformation is "path-dependent".

Deformation and deformability are much more complex than compaction and compactibility. As a first simplification we shall distinguish between deformation at constant volume, distortion accompanying compaction, and deformation (expansion) at breaking. Under field conditions these different types of deformation generally do not occur in pure isolation, but normally one of the three types dominates.

2.3.2.2 Deformation at Constant Volume

Deformation at constant volume occurs especially in wet, deformable soils. The process will be described for deformations that can be realized in measuring apparatuses. We shall subsequently deal with the tri-axial test on cylindrical samples, the elemental torsion test, the tri-axial test on a soil cube, and tests with other rheological instruments. Each of these tests uses a specific deformation that is only a small part of the entire scala of possible deformations. It implies that care should be taken in generalizing measuring results.

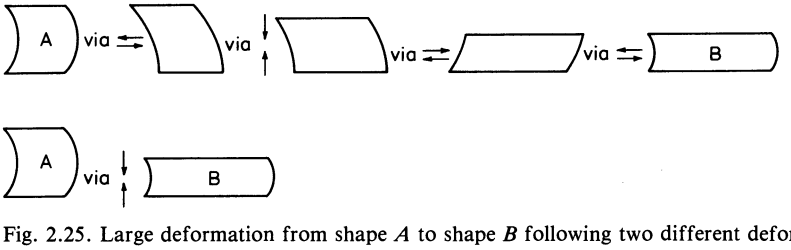

Fig. 2.25. Large deformation from shape *A* to shape *B* following two different deformation paths

Description of Deformability at Constant Volume Using a Tri-Axial Test on a Cylindrical Sample

A tri-axial apparatus is a very universal deformation measuring instrument. Its main restriction is that total deformation is limited. Suppose that a cylindrical sample of a wet deformable soil is subjected to a rapid tri-axial test, in which the sample is compressed axially over a relatively great distance, say to half the original sample height. During the test we keep the amount of water in the sample constant. The shortening of the sample at a certain moment t may be indicated by ε_1. However, it is better to think of the shortening occurring in small steps $d\varepsilon_1$. It can be calculated that

$$(\Sigma d\varepsilon_1)_t = \ln(1 - (\varepsilon_1)_t) .$$

If we want to keep the rate of deformation $(d\dot{\varepsilon}_1)$ constant during the experiment the loading ram speed should decrease during compression in such a way that ram speed times sample height is constant. Because there is no volume change (so that $d\varepsilon_1 + d\varepsilon_2 + d\varepsilon_3 = 0$) and because $\sigma_2 = \sigma_3$, it follows that $d\varepsilon_3 = -\frac{1}{2}d\varepsilon_1$ if the soil is isotropic. During the deformation principal stress directions do not change, so there is no kneading effect.

Figure 2.26a is the measuring result of such an experiment with a given σ_3 and a given rate of deformation $d\dot{\varepsilon}_1$. In the picture we see a threshold value A for σ_1; significant deformation only occurs if σ_1 is greater than A. In deforming from 0 to C, soil structure is changing which induces changes in measured σ_1. In this range σ_1 attains a maximum from which soil strength can be deduced (see Section 2.4). In C a certain equilibrium is reached, after which soil structure and σ_1 do not strongly change anymore. In the figure, B is shown higher than A, but that is not necessary. Relative positions of A and B depend on the initial and final structural state of the sample.

Resistance against deformation of wet deformable soil is very much rate dependent. At a higher $d\dot{\varepsilon}_1$, σ_1 will also be higher. This is shown in Fig. 2.26b (El-Domiaty and Chancellor 1970) for a saturated Grimes clay soil. To the right of C on the curve in Fig. 2.26a, an increase in σ_1 will result in a higher $d\dot{\varepsilon}_1$. This rate dependency is mainly caused by soil water viscosity.

If the tri-axial test of Fig. 2.26a were carried out at a higher value of σ_3, there would be two possibilities.

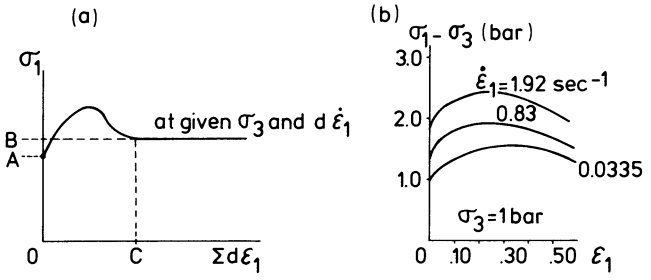

Fig. 2.26a, b. Resistance against deformation of a saturated soil in a tri-axial test (a). An example (El-Domiaty and Chancellor 1970) showing rate dependency of this resistance (b)

1. The sample is so well saturated that the increase in σ_3 is entirely supported by the soil water and forces between soil particles do not increase. That means that only normal stresses in the soil water are increased and not the normal stresses between soil particles. The higher normal stresses in the soil water do not lead to a higher shearing resistance of the sample. This resistance must be surmounted by shear stresses in the sample and these shear stresses are determined entirely by the difference $\sigma_1 - \sigma_3$. Therefore, in this case $\sigma_1 - \sigma_3$ does not change by an increase in σ_3.
2. Water content of the sample does not avoid that an increase in σ_3 results in some compaction with an increase in normal stresses between the soil particles. This increases the frictional forces between the soil particles and therefore $\sigma_1 - \sigma_3$ will have to grow when σ_3 is increased. This case is comparable to the phenomenon that resistance against break by shear is more sensitive for σ_3 as the angle of internal friction is larger (see part 2.4).

The drier the soil, the less probable it will be that deformation will occur at constant volume. Instead, deformation will include compaction if the soil is loose, and will involve unstable breaking if the soil is dense.

Torsion Tests

Figure 2.27 shows two methods for measuring deformation based on torsion. In both cases the soil sample is a thick-walled hollow cylinder. In Fig. 2.27a the sample wall is unconfined and torque is applied by rotating the upper ring relative to the lower ring. This measurement can only be applied on firm cohesive pastes. In Fig. 2.27b the inner cylinder is rotated relative to the outer cylinder. Now, the sample may even be a liquid. For both methods the rotational speed should be small because grip on the sample should not be lost due to inertia effects. In a short time interval, small volume elements $ABCD$ in Figs. 2.27a, b and c are deformed into elements $A'B'C'D'$. For this time interval it holds that

$d\varepsilon_1$ has direction AC and equals $\frac{1}{2}d\theta$
$d\varepsilon_3$ has direction BD and equals $-d\varepsilon_1$

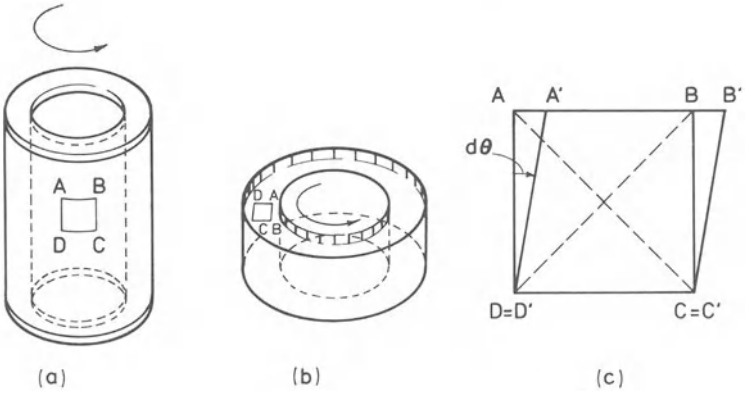

Fig. 2.27a – c. Measuring soil deformability using torsion tests (a and b) and soil elemental behavior in these tests (c)

$d\varepsilon_2 = 0$.
The element rotates as a rigid body over an angle of $\frac{1}{2}d\theta$.

In the next time interval the direction of $d\varepsilon_1$ is of course the same, but the soil material in the volume element is rotated slightly with respect to the position durng the first time interval. So, there is a kneading effect. The described deformation differs from that in the tri-axial test. There we found

$$d\varepsilon_2 = d\varepsilon_3 = -\tfrac{1}{2}d\varepsilon_1 \text{ and rotation } = 0.$$

During a torsion test the required torque is recorded as a function of $\Sigma d\theta$. From this torque, we can calculate or estimate the shear stress on a small plane through AB and perpendicular to $ABCD$. So, we actually measure for a certain $d\dot{\theta}$,

$$\tau_{AB} = f(\Sigma d\theta).$$

In general, other stress components cannot be measured and/or controlled.

Tri-Axial Tests on Cubic Samples

In principle, with tri-axial tests on cubic samples one should be able to measure

$$(\sigma_1(t), \sigma_2(t), \sigma_3(t)) = f(d\varepsilon_1(t), d\varepsilon_2(t), d\varepsilon_3(t)).$$

In fact, it is very difficult to do so and for agricultural soil there are no realistic measurements known. Moreover, function f is very complex for soil. To give some idea, f is given below for two very simple materials. For a relatively rigid, incompressible elastic material, f is given by

$$\begin{pmatrix} \sigma_1 - \sigma_m & 0 & 0 \\ 0 & \sigma_2 - \sigma_m & 0 \\ 0 & 0 & \sigma_3 - \sigma_m \end{pmatrix} = \tfrac{2}{3}E \begin{pmatrix} \varepsilon_1 & 0 & 0 \\ 0 & \varepsilon_2 & 0 \\ 0 & 0 & \varepsilon_3 \end{pmatrix}$$

where E is the modulus of elasticity. A firm soil sometimes behaves according to this function. For an incompressible Newtonian liquid, f is given by

$$\begin{pmatrix} \sigma_1 - \sigma_m & 0 & 0 \\ 0 & \sigma_2 - \sigma_m & 0 \\ 0 & 0 & \sigma_3 - \sigma_m \end{pmatrix} = 2\eta \begin{pmatrix} d\dot{\varepsilon}_1 & 0 & 0 \\ 0 & d\dot{\varepsilon}_2 & 0 \\ 0 & 0 & d\dot{\varepsilon}_3 \end{pmatrix}$$

where η is the viscosity. A slurry may behave in this way. It is interesting to observe that in both equations for positive σ_1, σ_2, and σ_3, deformation component $d\varepsilon_3$, and often also $d\varepsilon_2$, is negative.

Other Rheological Tests

In rheology many measuring apparatuses have been developed and sometimes these instruments are of use in soil mechanics. Two aspects are important.

1. The experiment should be technically feasible and results should be reproducible. Often the measurement can only be carried out for specific soil conditions.
2. The measuring results can often only be interpreted if certain material properties are assumed. Since most soils do not obey these assumed properties, the results are often only of comparative value.

Boekel (1978) determined soil deformability with a plasticity meter (an instrument that is mainly used in ceramic industries) by measuring the pressure needed to force the soil through a small dye. A wet plastic soil requires a small pressure and a dry crumbly soil a high pressure. Boekel tried to relate soil workability to this required pressure. Here, soil workability is defined as the soil ability to react as intended in a tillage operation, for instance the crumbling ability in seedbed preparation.

Minkin et al. (1972) used rotatory viscosimeters of the spherical and cylindrical type to investigate the relation between plasticity values and humus content, content of exchangeable sodium, and degree of dispersion.

Koenigs et al. (1976) measured shear stress with a rotary viscosimeter in air free suspensions and condensates. Yield stress appeared to be determined primarily by the distance between clay platelets, and not by the force needed to obtain this distance.

These examples demonstrate a major application of rheological measurements, namely the investigation of micro-structure through (macro-)mechanical properties.

2.3.2.3 Distortion Combined with Compaction

Distortion combined with compaction occurs in relatively dry soil at relatively high values of σ_3/σ_1. This kind of deformation is more complex than deformation at constant volume, because not only shape is changing but also volume. Compaction makes soil stronger and gives it a higher resistance against deformation. Deformation that includes compaction, therefore, works against itself, thus limiting total deformation. Discussion will be confined to cases where $d\varepsilon_2 = d\varepsilon_3$, $\sigma_2 = \sigma_3$, and $d\sigma_2 = d\sigma_3$.

Deformation has an elastic component (which recovers at unloading) and a plastic, permanent component. Because deformation and compaction are generally considerably greater than the elastic component, the elastic part can often be neglected. If not, the usual elasticity laws are adequate to account for it.

Consider a cylindrical sample loaded with σ_1 and σ_3. Load increments $d\sigma_1$ and $d\sigma_3$ are applied and the resulting strain increments $d\varepsilon_1$ and $d\varepsilon_3$ include volumetric strain and distortional strain. Volumetric strain $d\varepsilon_v$ equals $d\varepsilon_1 + 2d\varepsilon_3$. For distortional strain per unit of volumetric strain, different measures can be used. A very simple measure is

$$\frac{d\varepsilon_3}{d\varepsilon_1}$$

which will be intensively used in this text. In literature, other measures frequently occur. Roscoe and Poorooshasb (1963) used

$$\frac{d\varepsilon_v}{d\varepsilon_1} = \frac{d\varepsilon_1 + 2d\varepsilon_3}{d\varepsilon_1} = 1 + 2\frac{d\varepsilon_3}{d\varepsilon_1}.$$

Table 2.1. Limiting values of deformation measures for cylindrical samples

Type of strain	$d\varepsilon_3/d\varepsilon_1$	$d\varepsilon_v/d\varepsilon_1$	$d\gamma/d\varepsilon_1$	$d\gamma/d\varepsilon_v$
Compaction	$>-\frac{1}{2}$	>0	<1.5	$\geqslant 0$
No volume change	$-\frac{1}{2}$	0	1.5	$\pm\infty$
Dilatation	$<-\frac{1}{2}$	<0	>1.5	<0
Compaction under hydrostatic pressure	1	3	0	0
$d\varepsilon_1$ and $d\varepsilon_3$ both positive	>0	>1	<1	<1
Uni-axial compression	0	1	1	1
$d\varepsilon_1$ positive, $d\varepsilon_3$ negative	<0	<1	>1	>1 or <0

Chancellor and Korayem (1965) used

$$\frac{d\gamma}{d\varepsilon_1} = \frac{d\varepsilon_1 - d\varepsilon_3}{d\varepsilon_1} = 1 - \frac{d\varepsilon_3}{d\varepsilon_1}$$

where $d\gamma$ is the maximum shear strain in the time interval considered. Another possibility is

$$\frac{d\gamma}{d\varepsilon_v} = 1 - \frac{3}{2 + \dfrac{d\varepsilon_1}{d\varepsilon_3}}.$$

For cylindrical samples these different deformation measures have the limiting values listed in Table 2.1.

Suppose soil in a "point" is being compacted by an increasing load ($\sigma_1(t)$, $\sigma_3(t)$). In time interval dt, the load increase is ($d\sigma_1$, $d\sigma_3$). The central question is then: Which distortion per unit volume change will occur during dt due to ($d\sigma_1$, $d\sigma_3$)? For a perfectly elastic soil the answer is, simply and exactly:

- principal directions of the incremental strain tensor coincide with principal directions of the incremental stress tensor,
- volume change is determined completely by $d\sigma_m = \frac{1}{3}(d\sigma_1 + 2d\sigma_3)$,
- distortion is determined completely by $(d\sigma_1 - d\sigma_3)$.

For soils knowledge on this point is still incomplete, but as a first approximation, it may be assumed that

- volume change during dt is determined by a compaction criterium (see Section 2.2). In general, such a criterium states that volume change in dt is a function of ($d\sigma_1$, $d\sigma_3$), and that this function depends on the stress level ($\sigma_1(t)$, $\sigma_3(t)$),
- principal directions of the incremental strain tensor coincide with those of the stress tensor, but not necessarily with the principal directions of the incremental stress tensor,
- distortion per unit of volume change resulting from load increase ($d\sigma_1$, $d\sigma_3$) is determined completely by ($\sigma_1(t)$, $\sigma_3(t)$), and not by the increments ($d\sigma_1$, $d\sigma_3$).

The last two assumptions are known as "flow rule". Consider the relation between the ratio $\sigma_3(t)/\sigma_1(t)$ and the ratio $d\varepsilon_3/d\varepsilon_1$. The ratio $\sigma_3(t)/\sigma_1(t)$ ranges

from 1 to its value at the so-called "critical state" (about 0.1). If the flow rule applies then $d\varepsilon_1 \approx d\varepsilon_3$ when $\sigma_1(t) \approx \sigma_3(t)$. If $\sigma_3(t) < \sigma_1(t)$, then also $d\varepsilon_3 < d\varepsilon_1$. If $\sigma_3(t)/\sigma_1(t)$ equals the value prevailing in uni-axial compression then, per definition, $d\varepsilon_3 = 0$, and also $d\varepsilon_3/d\varepsilon_1 = 0$. If $\sigma_3(t)$ is yet smaller relative to $\sigma_1(t)$ than in uni-axial compression, the sample will expand radially and $d\varepsilon_3 < 0$, which means that also $d\varepsilon_3/d\varepsilon_1 < 0$. $\sigma_3(t)/\sigma_1(t)$ has a minimum value at the critical state. Then $d\varepsilon_3 = -\frac{1}{2}d\varepsilon_1$, so that $d\varepsilon_3/d\varepsilon_1 = -\frac{1}{2}$. Note that the relation between $\sigma_3(t)/\sigma_1(t)$ and $d\varepsilon_3/d\varepsilon_1$ is not influenced by the ratio $d\sigma_3/d\sigma_1$ if the flow rule applies. Also note that the total distortion (e.g. expressed by $\Sigma d\gamma$) is dependent on the path along which $[\sigma_1(t), \sigma_3(t)]$ is attained. If during the loading σ_3/σ_1 was small for a long part of the loading path, $\Sigma d\gamma$ will be large. It is said, therefore: "$(\text{porosity})_t$ is a point function, and $(\Sigma d\gamma)_t$ is a path function". Experiments have shown that the flow rule does not always apply and that sometimes distortion per unit of volume change from load increments $(d\sigma_1, d\sigma_3)$ are not only determined by $[\sigma_1(t), \sigma_3(t)]$ but also by the increments $(d\sigma_1, d\sigma_3)$. This is true, for instance, when $\sigma_1(t) \approx \sigma_3(t)$. Consider a sample under hydrostatic pressure. If the axial load is increased with $d\sigma_1$ at constant lateral stress $(d\sigma_3 = 0)$, the flow rule requires that the sample becomes thinner and shorter. We observe however that in such case $d\varepsilon_3$ is small and negative. The flow rule also does not apply for sand (Vermeer 1980).

2.3.2.4 Expansion at Breaking

When soil is relatively dense and σ_3/σ_1 is relatively small, loading may lead to breaking of the soil. Generally, this involves a zone along the failure plane where the soil expands slightly (dilates). We will discuss the phenomenon for shear-plane failure and for tensile failure.

Expansion at Shear-Plane Failure

Expansion at shear-plane failure of firm soil may be explained with the aid of Fig. 2.28. The very dense arrangement of soil particles in the left part of the figure is loaded by σ. Then, the soil is sheared by shear stress τ as shown at the right. The soil particles have to roll or to slide along each other. Because the arrangement was very dense, this rolling and sliding will result in a looser arrangement.

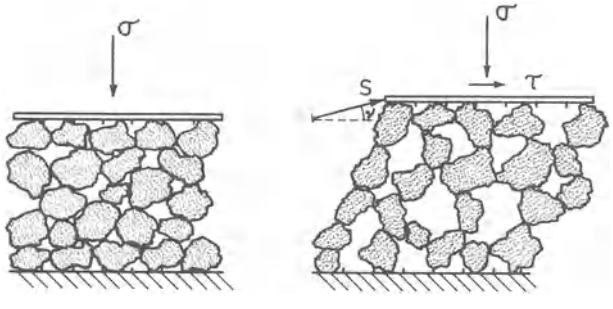

Fig. 2.28. Demonstrating expansion in shearing initially dense soil

This implies that the top plate not only moves horizontally to the right, but also upwards. The movement of the top plate is indicated by vector S and the direction of movement by ν, called the *angle of dilatation*. Let us assume that ν is constant during shearing, up to a certain moment when a state of equilibrium is attained. From that moment on, plate movement is purely horizontal. Equilibrium will be attained when τ reaches its maximum value. Note that ν is independent of sample height; a thicker sample will give a greater vertical movement of the load, but the horizontal movement required for equilibrium will increase proportionally. However, because of instability effects, the expansion is not likely to be as uniform over the entire soil height as indicated in the figure.

Now consider the more realistic situation of Fig. 2.29, showing a rectangular sample $ABCD$ of firm, dense soil. The sample is loaded to shear failure by (σ_1, σ_3). Shear normally occurs in a narrow band under a certain angle α with σ_1. The initial position of the band is shaded in the figure and the initial height of the sample is chosen such that the band coincides with a diagonal. Further assume that in the shaded zone the shear process occurs as sketched in Fig. 2.28. Then point A moves to A' along the displacement vector at a dilatation angle ν with the shaded zone. Suppose that the sample is compressed a distance Δh vertically and that this compression increased the sample width by Δb. From the position of the displacement vector AA', it can be deduced that

$$\frac{\Delta h}{\Delta b} = \tan\beta = \tan(90° - \alpha - \nu).$$

The initial sample height was chosen to satisfy

$$\frac{b_0}{h_0} = \tan\alpha.$$

Because $\varepsilon_1 = \Delta h/h_0$ and $\varepsilon_3 = -(\Delta b/b_0)$ we have

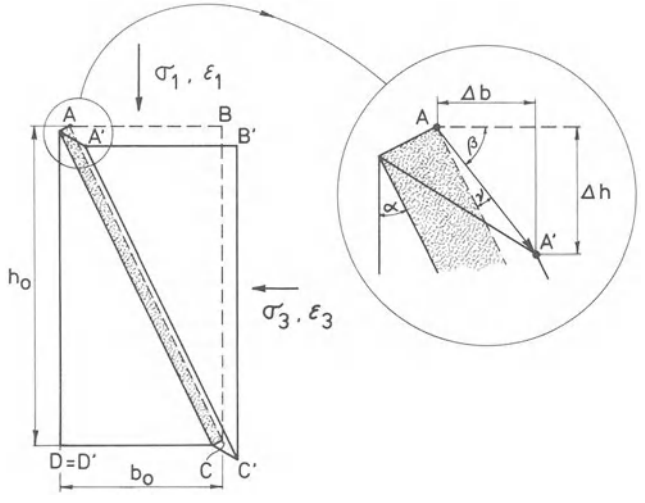

Fig. 2.29. Relationship between $\varepsilon_3/\varepsilon_1$ and the dilatation angle ν

$$\frac{\varepsilon_3}{\varepsilon_1} = -\frac{\Delta b}{b_0}\frac{h_0}{\Delta h} = -\frac{\Delta b}{\Delta h}\frac{h_0}{b_0}.$$

Using the first two formulas this can be written as

$$\frac{\varepsilon_3}{\varepsilon_1} = -\frac{1}{\tan\alpha\tan(90° - \alpha - \nu)}.$$

Note that this relation is independent of the band thickness. It would even apply when shear would occur throughout the entire sample. As soon as shear in the band reaches equilibrium, no further volume change will occur and, for this sample shape, $d\varepsilon_3 = -d\varepsilon_1$.

In reality deformation of rectangle $ABCD$ is more complicated. Suppose that the sample is loaded by (σ_1, $\sigma_3 = \sigma_1$) and that then σ_1 is increased while σ_3 is kept constant. During the increase, σ_1 will first slightly compact and distort the sample according to the elasticity law. If σ_1 increases further, compaction will turn into expansion. The rate of expansion, or rate of dilatancy, will increase and attain a maximum at shear failure, when σ_1 attains a maximum. It is better, therefore, to write the last formula in its incremental form,

$$\frac{d\varepsilon_3}{d\varepsilon_1} = -\frac{1}{\tan\alpha\tan(90° - \alpha - \nu)}$$

and to consider ν as the instantaneous angle of dilatancy, which depends on the loading stage. Roscoe (1970) reports that for leighton Buzzard sand $\nu = 24°$ at the condition of peak stress ratio. Rowe (1962) reports values of ν up to 30°.

Expansion at Tensile Failure

Consider a bar shaped sample with a slightly concave surface, so that the cross section is smallest halfway the bar. If such a sample is loaded under tension by moving the bar ends away from each other while remaining parallel, at a certain moment a fracture plane will be formed perpendicular to the axis of the bar at the

Table 2.2. Displacement at fracture (b) in simple tensile tests

	Moisture content (% by weight)	Porosity (%)	b (mm)
Wageningen silt clay loam	28.4	45.9	0.65
	27.3	55.3	0.39
	17.3	49.6	0.14
Lexkesveer loam	18.8	38.3	0.48
	18.2	51.0	0.30
	12.5	42.4	0.14
Schinnen silt loam	24.8	42.9	1.28
	24.3	50.6	0.47
	16.2	43.1	0.21
Ede sand	16.9	40.9	0.36
	17.1	49.3	0.37
	11.0	44.0	0.24

smallest cross section. If one end of the bar had moved a distance b relative to the other end at the moment of fracture, one might expect a movement of $2b$ in case the length of the bar were doubled. From observations we know that this value is much smaller than $2b$. The reason is that tensile loading results in only minor elastic deformation throughout the sample and that most of the observed bar length increase results from deformation in a very thin band at the place where the fracture surface will be formed. Therefore, it makes no sense to express this length increase as a percentage of the original length. Tensile tests in which bars with initial lengths of 15 cm were elongated at a rate of 5 mm/min, and in which bar ends were maintained parallel, resulted in the b-values listed in Table 2.2. The table shows that, in general, b decreases with moisture content and/or with looser conditions.

2.3.3 Applications

2.3.3.1 Stress-Deformation Models

Because real stress-strain relations for soils normally are complicated, often simplified models are used to describe these relations for a better understanding. There are mechanical, idealized, and curve fitting models.

Mechanical Models. Stress-deformation behavior can be represented visually by mechanical models. Figure 2.30a, b, and c show three elements of such models:

- a *perfectly elastic spring* to model a material for which deformation is proportional to stress and complete recovery occurs after unloading,
- a *perforated piston* moving in a cylinder containing a viscous liquid (called dash pot) to model a liquid for which stress is proportional to rate of deformation. As long as the load is acting, deformation will continue. As soon as the load is removed the material will come to rest.

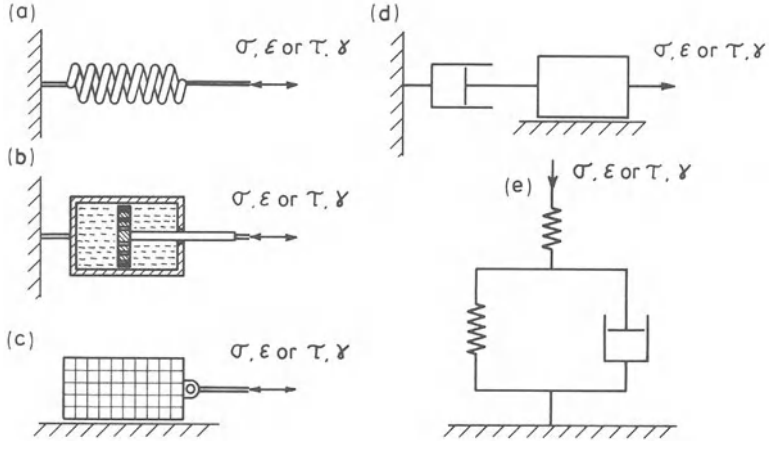

Fig. 2.30a – e. Mechanical stress-deformation models

- a *weight resting on a table top* with solid friction between both. In this case stress has to attain a certain value before deformation occurs. Attempts to increase the stress beyond that value by increasing the deformation rate, will fail.

Examples for these behaviors are steel in normal use, water and window putty, respectively. To represent more complex behavior, elements can be combined as in Fig. 2.30d, which is a model for a so-called *Bingham* body. In it stress has to reach a certain threshold value before deformation occurs, and above that value, rate of deformation is proportional to stress. Paint is an example of a Bingham body.

For soil also combinations of elements have been used (McMurdie 1963, Gupta and Pandya 1966, Sitkei 1972). Such combinations are often complicated and even then they are able to describe only a part of the soil stress-strain relations. Different combinations will be chosen for different purposes. Figure 2.30e shows Sitkei's model. It is a so-called visco-elastic model and was used to explain why tire rut depth depends on travel speed.

In general, a mathematical relation between stress and strain can easily be derived from the models discussed. A Bingham body, for instance, is described by

$$\tau = \xi + \eta \dot{\gamma}$$

where ξ and η are constants. When a mathematical relation for a model is obtained, it is possible to make further quantitative analyses.

Idealized Models. In rheology, which is the branch of physics that deals with the deformation and flow of materials, a number of idealized models have been described (Reiner 1960). An idealized model has the following characteristics:

- mathematical description of the stress-strain relations is relatively simple,
- deformation behavior is very characteristic,
- in nature there are materials that resemble these models closely.

Examples of idealized models are:

- the Euclid solid or rigid body. By considering soil blocks as rigid bodies, it is possible to predict soil forces on tillage tools with the aid of rigid body mechanics (see Section 2.4.3.3),
- the Hooke-solid or linear elastic body. Solutions for many loading problems based on this model have been published (Harr 1966). These solutions apply to firm soil at a stress level far below yield stress.
- the Newtonian liquid or linear viscous liquid. Soils with a moisture content higher than the upper plastic limit resemble this behavior.
- the St. Venant-body or perfectly plastic material. This corresponds to the weight-element of Fig. 2.30c; shear stress has to reach a certain value before deformation starts. Once this value has been reached, continuous deformation (flow) occurs. Shear stress cannot be increased beyond that value. A yielding, dense, saturated clay resembles this behavior.
- the Bingham body discussed above. It can model soil behavior during puddling of paddy fields (El-Domiaty and Chancellor 1970).

If soil behavior can be approximated by an idealized model, mathematical description of the stress-deformation relation is rather simple and for many loading problems solutions are available.

Simple Curve Fitting Models. In unconfined compression, direct shear, and tri-axial tests measured relations between stress and deformation are not at all linear. To describe such measured relations a best fitting formula may be calculated according to a curve-fitting technique. This first involves the selection of a suitable fitting formula.

For direct shear tests in sand Basak and Brahma (1974) give the fitting formula

$$\tau = \frac{\gamma}{a + b\gamma^n}$$

where a, b, and n are constants. For shear tests, Janosi's fitting formula (see Section 3.4.3.1) may also be used.

For a series of unconfined compression tests on Wageningen silty clay loam, a good fit was achieved by

$$\frac{\sigma_1}{(\sigma_1)_f} = (\tan\alpha)\left(\frac{\varepsilon_1}{(\varepsilon_1)_f}\right) + (3 - 2\tan\alpha)\left(\frac{\varepsilon_1}{(\varepsilon_1)_f}\right)^2 + (\tan\alpha - 2)\left(\frac{\varepsilon_1}{(\varepsilon_1)_f}\right)^3$$

where $(\sigma_1)_f$ and $(\varepsilon_1)_f$ refer to failure condition and $\tan\alpha$ is the initial tangent modulus of the $\varepsilon_1/(\varepsilon_1)_f$ to $\sigma_1/(\sigma_1)_f$ relation. The value of $\tan\alpha$ was about 2 and was hardly influenced by moisture content and pore space.

For tri-axial tests with constant σ_3, Kondner (1963) proposes

$$\sigma_1 - \sigma_3 = \frac{\varepsilon_1}{a + b\varepsilon_1}$$

with a and b as constants.

More Complicated Fitting Models. After introduction of the computer, numerical calculation methods, like finite element analysis, were developed for complicated loading problems. (Coleman and Perumpral 1974, Marchant 1980). These numerical calculations allow handling cases where the soil stress-strain relations are complicated, so that more realistic stress-strain relations can be developed. The procedure for a given loading problem is as follows:

1. decide what part of material behavior can be neglected for the given loading problem,
2. on this basis, formulate the general stress-strain relationship. This formula may include parameters which depend on previous loading and deformation,
3. determine these parameters by measuring mechanical properties.

An example of this procedure is Marchant's investigation on the behavior of grain in silos (1980);

1. Marchant assumed that $\sigma_2 = \sigma_3$, that principal directions did not change with time, and that there was no decrease of load at any time.

2. As general stress-strain relation he chose

$$\dot{\gamma}_0 = a_{11}\dot{\tau}_0 + a_{12}\dot{\sigma}_0$$

$$\dot{\varepsilon}_0 = a_{21}\dot{\tau}_0 + a_{22}\dot{\sigma}_0$$

where γ_0 is octahedral shear strain, ε_0 is octahedral normal strain, σ_0 is octahedral normal stress, and τ_0 is octahedral shear stress.

3. Parameters a_{ij} he determined from a series of tri-axial tests at constant σ_0 and a series of tri-axial tests at constant τ_0.

Much care should be exercised in generalizing such fitting formulas, because a certain part of material behavior has been neglected and another part may have been overlooked.

2.3.3.2 Determination of the Liquid Limit with a Rotary Viscosimeter

The liquid limit of a soil is a well-known Atterberg consistency limit, being the moisture content above which the soil exhibits a particular fluid-like behavior and below which a particular solid-like behavior. The classical determination is subjective to some extent (Freitag et al. 1970).

Hajela and Bhatnagar (1972) describe a straightforward method to determine the liquid limit with a rotary viscosimeter. A set of samples is prepared with different moisture contents around the expected value of the liquid limit. In each sample a number of measurements are carried out at different rotation rates. In each of these measurements one determines the torque required for a certain rate of rotation. This procedure yields a hysteresis curve as in Fig. 2.31a. The straight section of the falling part of the hysteresis-curve is extrapolated to the horizontal axis and the intersect is taken as the Bingham yield stress. Then, the different yield stresses are plotted versus moisture content, which generally results in a curve with a break point (Fig. 2.31b). The moisture content at this break point agrees very well with the liquid limit as found with the Cassagrande method.

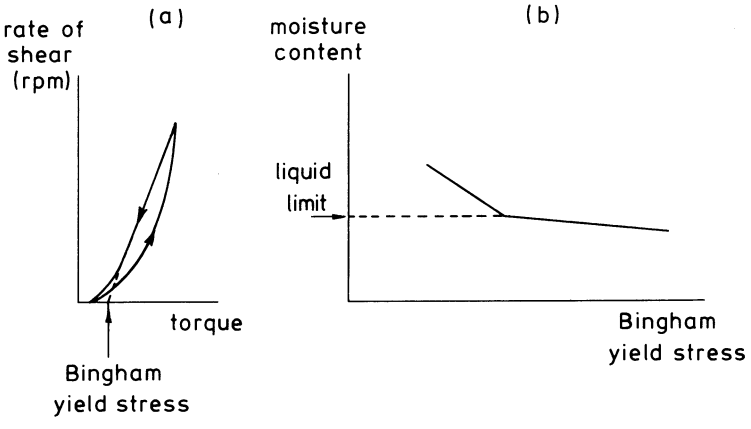

Fig. 2.31 a, b. Determining liquid limit using a rotary viscosimeter

2.3.3.3 Distortion Combined with Compaction, Estimated Using the Flow Rule

Consider a cylindrical sample being compacted under an increasing load $[\sigma_1(t), \sigma_3(t)]$. In time interval dt the load increases with $(d\sigma_1, d\sigma_3)$, and the resulting $(d\varepsilon_1, d\varepsilon_3)$ in dt can be estimated by one of two methods.

In the first method we assume that compaction depends uniquely on the largest principal stress, so that the compaction curve has the form (see Sect. 2.2)

$$\text{degree of compaction} = f(\sigma_1).$$

We further assume that the flow rule (Sect. 2.3.2.3) applies and has the form

$$(d\varepsilon_3/d\varepsilon_1) = F(\sigma_3/\sigma_1).$$

It is also assumed that, as a first approximation, F is the same for all soils. In Fig. 2.32, $d\varepsilon_3/d\varepsilon_1$ is plotted versus σ_3/σ_1. For hydrostatic compression, $\sigma_3/\sigma_1 = 1$ and $d\varepsilon_3/d\varepsilon_1 = 1$. The closed dots in the graph were measured in a tri-axial test on Wageningen silty clay loam at a moisture content of 20% by weight and at constant σ_3. The open dots were calculated from tri-axial tests published by Roscoe and Poorooshasb (1963) where σ_3 increased proportional to σ_1 in each test. The cross indicates a critical state measured by Bailey and VandenBerg (1968) on Lloyd clay.

For a cylindrical sample that is being compacted by load $[\sigma_1(t), \sigma_3(t)]$ that increases with $(d\sigma_1, d\sigma_3)$ during dt, the increments $(d\varepsilon_1, d\varepsilon_3)$ in dt can be predicted as follows:

1. From the function "degree of compaction $= f(\sigma_1)$" and from $d\sigma_1$, calculate $d\varepsilon_v = d\varepsilon_1 + 2d\varepsilon_3$. Suppose value a is found.
2. Determine ratio $\sigma_3(t)/\sigma_1(t)$ and read, in Fig. 2.32, $d\varepsilon_3/d\varepsilon_1$ belonging to that ratio. Suppose, value b is found.
3. The equations obtained are then

   $d\varepsilon_1 + 2d\varepsilon_3 = a$

   $(d\varepsilon_3/d\varepsilon_1) = b.$

   These two equations can be solved for $d\varepsilon_1$ and $d\varepsilon_3$.

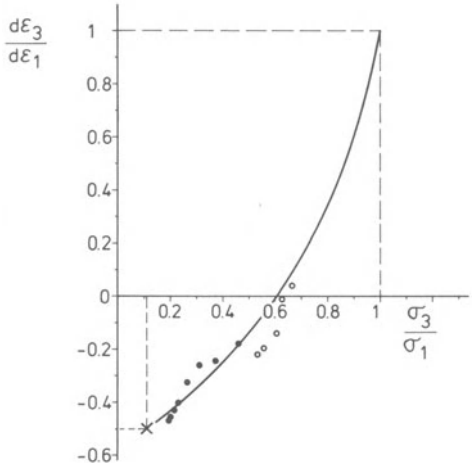

Fig. 2.32. Assumed form of the flow rule

The second method, which is somewhat more complicated, yields and estimate of $d\varepsilon_1$ and $d\varepsilon_3$ using critical state soil mechanics (Atkinson and Bransby 1977).

2.3.3.4 Estimation of Distortion Combined with Compaction for Sand

When a cylindrical sample of sand with a given initial bulk density is being loaded by (σ_1, σ_3), so that distortion and volume change occur, it is possible to estimate total compaction and total deformation using formulas given by Vermeer (1981).

Total compaction from (σ_1, σ_3) is $v = \varepsilon_1 + \varepsilon_2 + \varepsilon_3$.

Total deformation from (σ_1, σ_3) is $\gamma = \varepsilon_1 - \varepsilon_3$.

The author further defines $p = (\sigma_1 + \sigma_2 + \sigma_3)/3$ and $q = \sigma_1 - \sigma_3$.

Then γ is approximated by

$$\gamma = \gamma_0 \frac{p^\beta}{p_0^\beta} \frac{q/p}{a - (q/p)}.$$

The constant γ_0 is γ for $p = p_0$ and $(q/p) = a/2$. The reference stress p_0 can be chosen freely. Constant a is the maximum value of q/p and may be e.g. 6/5. The third constant β is normally between 1/3 and 1/2. v can be split into two parts, $v = v_c + v_d$, in which the compaction part v_c depends on the hydrostatic pressure p. Vermeer gives the following approximations:

$$v_c = v_0 \frac{p^\beta}{p_0^\beta} \qquad dv_d = \frac{k\sigma_3 - \sigma_1}{k\sigma_3 + \frac{1}{2}\sigma_1} d\gamma,$$

where $d\gamma$ is the increment of γ when the compaction part v_d increases by the amount dv_d. The approximations involve two new constants; v_0 and k. v_0 is v for isotropic compression up to p_0. Values of k are given by Rowe (1971). To find v_d the above differential equation has to be integrated. Therefore we need the function $\gamma = f(q/p)$ given above, and the path along which (σ_1, σ_3) has been reached. Integration should be carried out along this path. Note that in this case not γ but v is path dependent.

2.4 Elemental Treatment of Breaking

2.4.1 Occurrence of Breaking

Consider a cylindrical, relatively dense soil sample, about twice as high as its diameter, being under a relatively low hydrostatic pressure $(\sigma_1 = \sigma_2 = \sigma_3)$. If we increase σ_1 while keeping σ_3 constant, at a certain moment the sample will break; at a certain value of σ_1 a fracture plane is formed at an angle of $45° - 60°$ to σ_1. During and after fracture the two fracture surfaces rub (slide) along each other and traces of this rubbing will be visible when the two parts of the sample are separated. Such a fracture is called *shear failure.* Under field conditions fracture surfaces and their sliding directions can be recognized by such slide-traces.

If a cylindrical sample is loaded in tension by applying an increasing tensile force in axial direction, failure will also occur but now the fracture plane will be perpendicular to the cylinder axis. There will be no slide-traces on the fracture surfaces, soil micro-structure at the surfaces will be left intact. The two parts of the sample will still fit perfectly together. Such a fracture is called tensile of *brittle failure* and can also be recognized in the field.

During moldboard plowing the soil is taken up, led along the moldboard and deposited again. During *intake* the share of the moldboard may have a splitting action, especially on cohering soils. This will result in tensile failure planes. On less cohering soil the share will push the soil material away and this may lead to shear-failure planes. During *soil movement along the moldboard* the soil beam is mainly subjected to bending and torsion. The soil beam is twisted around the length axis and this may induce tensile-failure planes at angles of 45° to the length axis. This kind of failure can be demonstrated easily by twisting a piece of blackboard chalk. Bending of the soil beam may cause shear failure at the convex side. A piece of chalk will also demonstrate this if it is broken while at the same time axial pressure is applied. The bending may also cause tensile fractures at the concave side of the beam. When the soil is *deposited* from the moldboard the beam is stretched between the moldboard end and the soil already landed. Therefore, tensile failure may occur.

Tines working in soil will mainly have a pushing effect and, therefore, mainly shear failure is to be expected.

For clod crushing, rollers are a common tool. If a clod is pressed upon, at little lateral support, both compressive and tensile stresses will be generated in the clod. The highest tensile stress will be on small planes in the center of the clod that are parallel to the direction of the applied force. If the external force is increased, tensile stress on these planes will increase roughly proportionally until tensile strength is reached. So, the clod fails due to tensile fracture.

In wheel tracks and on cutting planes left by knives, shares, tine edges etc., we normally observe small tongues. They arise from tensile failure and point in a direction opposite to the direction of movement of the wheel or tool. The direction of movement can be deduced in the field afterwards from this.

In aggregates being wetted, entrapped air may be compressed by the advancing water fronts. This may cause micro-explosions and the resulting desintegration of the aggregates will be of the tensile failure type (Koenigs 1972).

Growing plants can also induce fractures in the soil. An emerging seedling breaking through a surface crust will cause tensile and shear failures like a plow bending the soil beam. An expanding root will cause outward radial movement of the surrounding soil particles. This must necessarily be accompanied by tangential extension of the surrounding soil, which may lead to tensile failure.

Loading rate in loading to failure varies strongly in agricultural practice. When rate of loading is relatively low, it is reasonable to assume that stresses on the faces of a small volume-element being on the verge of breaking, are at static equilibrium. In the case of high speed tools, such as rotary tillers, however, stress waves may occur. Principles of fracture under such conditions are not yet fully understood.

2.4.2 Fundamentals

We start with an elemental cube of relatively dense soil loaded by a rather low hydrostatic pressure $\sigma_m = \sigma_1 = \sigma_2 = \sigma_3$. Subsequently, we increase σ_1, keeping σ_2 and σ_3 constant, until fracture occurs. This combination of σ_1, σ_2, and σ_3 that gives rise to failure is indicated by $[(\sigma_1)_f, (\sigma_2)_f, (\sigma_3)_f]_1$. We proceed with a second but identical elemental cube. First, hydrostatic pressure is applied, then σ_3 is lowered slightly, and finally σ_1 is increased until fracture occurs. This gives a second combination that induces failure, $[(\sigma_1)_f, (\sigma_2)_f, (\sigma_3)_f]_2$. In this way an infinite number of failure conditions can be determined, if we keep σ_2 and σ_3 relatively low to avoid that compaction will take place instead of fracture.

When we have determined a number of such $[(\sigma_1)_f, (\sigma_2)_f, (\sigma_3)_f]$ combinations and plot each combination in a σ_1, σ_2, σ_3 space, then these points represent a surface in the coordinate space. Such a surface is called a yield surface. An example of a yield surface is Fig. 2.33, a cylinder around the space diagonal. Hydrostatic pressure is always on the space diagonal (for instance, point A) and will never give failure. As soon as one principal stress differs from the other two, one moves off the diagonal, for instance from A to B, but since B is still inside the cylinder no failure occurs. If the difference between principal stresses is increased the surface of the cylinder will be reached at a certain moment (for instance, in C) and failure occurs. Stress combinations outside the cylinder cannot exist. It should be mentioned that for soil the yield surface is more complex. Mathematically, a yield surface can be represented by

$$\text{if } f(\sigma_1, \sigma_2, \sigma_3) = \text{a certain constant} \rightarrow \text{fracture occurs}.$$

This formula represents a mechanical property and is the subject of this section. Use of this formula means implicitly

- failure is path-independent. In general, that is correct.
- loading rate has no influence. This assumption is made for simplicity, but in reality there are rate effects. These will be discussed in Section 2.4.2.4.

There is also a yield surface for tensile fractures. In Fig. 2.33 this lies around the origin. The yield surfaces for shear failure and for tensile failure have a

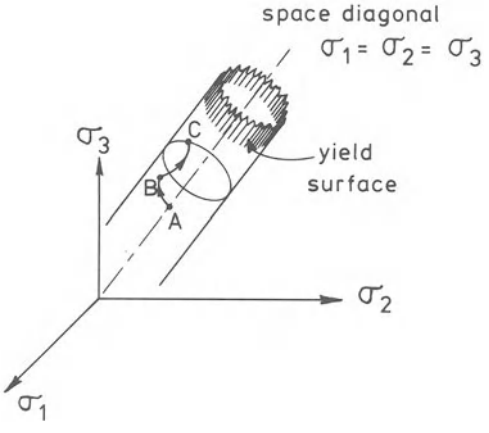

Fig. 2.33. Example of a yield surface of the form $f(\sigma_1, \sigma_2, \sigma_3) = \text{a constant}$

spatial curve in common in the σ_1, σ_2, σ_3 space. There, the transition occurs from tensile failure to shear failure.

2.4.2.1 Measures of Resistance Against Breaking

Direct Measures

Compressive Strength. When a cubical or cylindrical soil sample is loaded to failure by an increasing σ_1 under condition of $\sigma_2 = \sigma_3 = 0$, then σ_1 at the moment of failure is called compressive strength. This σ_1 should be calculated from the total compressive force exerted on the sample, and the area on which this force acts, both measured at the moment of failure. That area (A_f) can be estimated from ε_1 at the moment of failure [$(\varepsilon_1)_f$] with the formula

$$A_f = \frac{A_0}{1 - (\varepsilon_1)_f}$$

where A_0 is the initial area. This formula is derived assuming that sample volume is constant. The expression "unconfined compressive strength" is in use specifically for cylindrical samples with a height to diameter ratio of 2.

Tensile Strength. When a bar-shaped sample is loaded by an increasing tensile force in the direction of the bar axis until it breaks, and the bar surface is kept stress free, then the tensile force at the moment of breaking divided by the cross section of the bar perpendicular to the axis is called tensile strength.

Shear Strength in Tri-Axial Tests. When a cylindrical soil sample is under a hydrostatic pressure $\sigma_1 = \sigma_2 = \sigma_3$, and σ_1 is increased until the sample breaks at constant $\sigma_2 = \sigma_3$, then the difference between σ_1 and σ_3 at the moment of breaking is called shear strength. σ_1 at the moment of failure can be calculated from the axial load and from the sample cross section estimated in the same way as in the compressive strength determination. This concept of shear strength may be extended to indicate the difference between σ_1 and σ_3 for any tri-axial test.

In general, shear strength increases as σ_3 is increased.

Shear Strength in Shear Tests. Certain tests for determining resistance against breaking measure shear stress in the plane of breaking at the moment of failure. This shear stress is also called shear strength. It generally increases with increasing normal stress on the plane of breaking.

Indirect Measures

The direct measures indicate resistance to failure at only a certain stress level. There are also certain measures that pretend to describe resistance for a wide range of stress levels. They originate by describing the yield surface by a general mathematical formula. This formula will contain certain parameters (constants). The values of these parameters will depend on soil type, pore space, moisture content etc. They describe shear strength for a particular soil condition, but are only meaningful in relation to the selected mathematical formulation of the yield surface.

Constant K in Von Mises' Model. In this model the yield surface for shear failure is assumed to resemble the cylinder of Fig. 2.33. A mathematical expression for this cylinder was formulated by Von Mises in 1913 (Harr 1966):

$$(\sigma_1 - \sigma_2)^2 + (\sigma_2 - \sigma_3)^2 + (\sigma_1 - \sigma_3)^2 = 2K^2$$

where K is the number of stress units between the origin and each of the three points of intersection between the cylinder and the coordinate axes. Actually, K is the compressive strength. K describes failure behavior. A higher value of K means a higher resistance to failure.

Cohesion and Angle of Internal Friction in the Mohr-Coulomb Model. The best-fitting mathematical formula of the soil yield surface at shear is the Mohr-Coulomb model (Harr 1966)

$$\sigma_{max} = \sigma_{min} \tan^2(45° + \tfrac{1}{2}\phi) + 2c\tan(45° + \tfrac{1}{2}\phi)$$

where σ_{max} = major principal stress, σ_{min} = minor principal stress, ϕ is called angle of internal friction and c is called cohesion. c and ϕ are soil parameters indicating resistance against shear failure. The locus of this formula in a σ_1, σ_2, σ_3 space is pyramidal. The axis of the pyramid is the space diagonal and the top of the pyramid is in the neighborhood of the origin. Note that the intermediate principal stress does not play a role and that the formula generally predicts a higher shear strength at a higher stress level.

Constant L in Griffith's Model. For the soil yield surface at tensile failure, Griffith's model is available (Paul 1968):

When $\sigma_1 + 3\sigma_3 < 0$, $\sigma_3 = -L$

When $\sigma_1 + \sigma_3 > 0$, $(\sigma_1 - \sigma_3)^2 - 8L(\sigma_1 + \sigma_3) = 0$.

Constant L corresponds with the tensile strength discussed above. Note that the absolute value of σ_3 can be greater than σ_1 (compressive stresses being taken as positive and tensile stresses as negative). The correspondence between Griffiths's model and the true soil yield surface in tension is less satisfactory as the soil is less brittle.

2.4.2.2 Shear Failure

A General Model for Shear Failure. Coulomb's Law

The model presented by Coulomb as early as 1776, is very generally accepted as physical description of shear failure. Figure 2.34a shows a clod of precompacted soil loaded in such a way that a plane of breaking develops. Coulomb stated that this breaking requires a shear force which overcomes, firstly, the bonding force that existed between the soil particles across the failure plane and, secondly, the friction force between the two surfaces arising from the relative movement between these surfaces. Thus,

required shear force = bonding force + friction force.

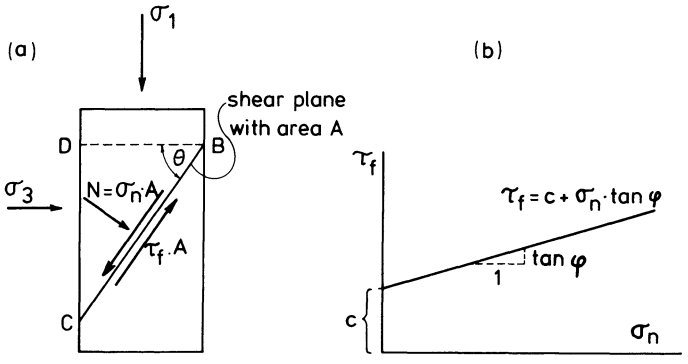

Fig. 2.34a, b. Coulomb's model of shear plane failure

According to the well-known law of friction,

$$\text{friction force} = N\tan\phi,$$

where N = force perpendicular to the plane of breaking, and ϕ = angle of friction between the two surfaces. Substitution gives

$$\text{required shear force} = \text{bonding force} + N\tan\phi.$$

Dividing by the size of the failure plane then yields

$$\tau_f = c + \sigma_n \tan\phi$$

where τ_f = required shear stress, c = bonding force per unit area, called cohesion, σ_n = normal stress on the failure plane, and ϕ = angle of internal friction. c and ϕ depend on soil type, moisture content, pore space etc., and can, therefore, be regarded as soil properties. The final formula is called Coulomb's law. It states that the shear stress required for breaking generally increases as the normal stress acting on the plane increases. If σ_n on a plane is infinitely large, there can be no failure along that plane. Coulomb's law can be represented graphically in a σ_n, τ_f co-ordinate system (Fig. 2.34b). The formula corresponds with a straight line that has a direction tangent $\tan\phi$ and intersects the τ_f axis in c.

In Fig. 2.34a, σ_2 is perpendicular to the plane of view which means that the failure plane is parallel to σ_2. This is in agreement with observations. So, if $\sigma_2 \neq \sigma_3$, σ_2 will influence the position of the failure plane. But, as a first approximation, c and ϕ may be considered as independent of σ_2.

Coulomb's Law in Terms of σ_1 and σ_3. The Mohr-Coulomb Law

For the failure plane in Fig. 2.34a at the moment of failure we obtained

$$\tau_f = c + \sigma_n \tan\phi. \tag{1}$$

According to the equilibrium conditions for block *BCD*, the following formulas also apply (Sect. 2.1.2.1).

$$\sigma_n = \sigma_1 \cos^2\theta + \sigma_3 \sin^2\theta \tag{2}$$

$$\tau_f = (\sigma_1 - \sigma_3) \sin\theta \cos\theta . \tag{3}$$

Elimination of τ_f and σ_n from equation 1 with the aid of Eqs. (2) and (3) gives

$$\sigma_1 = \frac{\sigma_3(\sin\theta\cos\theta + \tan\phi \sin^2\theta) + c}{\sin\theta\cos\theta - \tan\phi\cos^2\theta} . \tag{4}$$

This is a relation between σ_1 and σ_3 at the moment of breaking. This relation involves still one unknown quantity, the angle θ. This angle can be found from the reasoning that the failure plane will occur at that angle θ for which σ_1 (at constant σ_3, c, ϕ) according to Eq. (4) is minimal. At increasing load the failure condition is reached first in that plane. It can be shown, that Eq. (4) at constant values of σ_3, c, and ϕ attains a minimum at $\theta = 45° + \frac{1}{2}\phi$. Substitution of this angle in Eq. (4) yields

$$\sigma_1 = \sigma_3 \tan^2(45° + \tfrac{1}{2}\phi) + 2c \tan(45° + \tfrac{1}{2}\phi) . \tag{5}$$

Equation (5) represents Coulomb's law in terms of σ_1 and σ_3. This form is known as Mohr-Coulomb law (Note. It requires less mathematics to derive this formula from the graphical representation of Coulomb's law and Mohr's circle. See Harr (1966)). In section 2.4.2.1 it was already stated that Eq. (5) is an excellent mathematical model to describe the yield surface for shear failure in the (σ_1, σ_2, σ_3) space.

Coulomb's Law in Terms of τ_{max} and σ_m. Compaction Versus Shear Failure

If a soil sample is loaded by stresses σ_1, σ_2, and σ_3, then for this state of stress

$$\sigma_m = \tfrac{1}{3}(\sigma_1 + \sigma_2 + \sigma_3)$$

$$\tau_{max} = \tfrac{1}{2}(\sigma_1 - \sigma_3)$$

(see Sect. 2.1.2.1). One should distinguish clearly between τ_{max} and τ_f. τ_{max} characterizes a state of stress, while τ_f is the shear stress at failure in a failure plane. τ_{max} is always in a plane at 45° to the plane on which σ_1 acts. On most occasions the plane of τ_f is at an angle greater than 45° to the plane acted upon by σ_1. If we restrict ourselves to the condition of $\sigma_2 = \sigma_3$, the equations given above can be rearranged to

$$\sigma_1 = \sigma_m + \tfrac{4}{3}\tau_{max}$$

$$\sigma_3 = \sigma_m - \tfrac{2}{3}\tau_{max} .$$

Substitution of these expressions in Eq. (5) yields Coulomb's law in terms of τ_{max} and σ_m for the case $\sigma_2 = \sigma_3$:

$$(\tfrac{4}{3} + \tfrac{2}{3}\tan^2(45° + \tfrac{1}{2}\phi))\,\tau_{max} = (-1 + \tan^2(45° + \tfrac{1}{2}\phi))\,\sigma_m + 2c \tan(45° + \tfrac{1}{2}\phi) .$$

For soil at constant moisture content and varying *BWV*, this equation is well suited to distinguish between stress conditions that induce compaction and stress

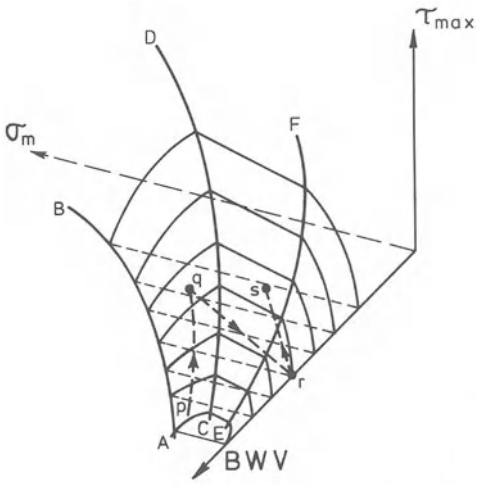

Fig. 2.35. Compaction surface, shear failure and tensile failure surface

conditions that induce shear failure. In such a soil, c and ϕ depend primarily on BWV and, therefore, the last equation can be written as

$$\tau_{max} = f_1(BWV)\,\sigma_m + f_2(BWV)$$

where f_1 and f_2 are functions of BWV. In a (σ_m, τ_{max}, BWV) space this formula represents a surface. An example is surface $CDEF$ in Fig. 2.35. All (σ_m, τ_{max}) combinations on this surface cause breaking. For a given BWV the relation between τ_{max} and σ_m at failure is linear. In a denser soil, stress must be higher to induce failure. We saw above that surface $ABCD$ in Fig. 2.11 was the compaction surface; on compaction, a stress path along this surface will be follwed. The yield surface can only be reached by loading a precompacted soil. This is demonstrated by the following example. Loose soil is compacted along path pq in Fig. 2.35. In q, stresses are removed and there will be a slight elastic rebound along path qr. In this way a precompacted sample is obtained. Subsequently, the soil is loaded again, but now at a relatively high σ_1/σ_3 ratio and, therefore, at a high τ_{max}/σ_m value. The loading path will now be steep and end at the shear surface, e.g. path rs. Along this path, deformation will mainly be elastic and when point s is attained, breaking occurs. Together with the breaking, the load falls off, and there is some elastic rebound. If the second loading path rs had been less steep it would not have come out at the yield surface but at the compaction surface and further compaction would have occurred. So, if for a precompacted soil the compaction surface and the yield surface are known, it is possible to predict for any stress path whether compaction or breaking will occur.

In an unconfined compression test (to determine unconfined compressive strength) the sample must always be precompacted to allow its existence without lateral support. In this test the loading path is always steep enough to reach the yield surface, because the condition of $\sigma_2 = \sigma_3 = 0$ involves $\tau_{max}/\sigma_m = 3/2$.

Measuring Soil Cohesion and Angle of Internal Friction

Tri-Axial Tests. The most accurate measurement of c and ϕ can be done with tri-axial tests (see Fig. 2.36). A precompacted cylindrical soil sample is placed between a bottom plate and a top plate. The cylindrical surface is covered with a rubber membrane that is fitted to the top and bottom plates with 0-rings. The top plate can be loaded by a loading ram. In this way σ_1 can be increased. A rigid cylinder is placed over the enclosed sample and filled partially with water, and partially with air under pressure. This air pressure, being transmitted to the sample, is σ_3 and contributes also to σ_1.

The experiment starts with adjusting σ_3 by adjusting the air pressure. Then the loading ram is moved downwards under continuous recording of the force required. This force is increasing as the ram is moving down, but, at a certain moment, the force will fall suddenly. At that moment the test is considered to be finished. From the recorded force, σ_1 is calculated as a function of ram displacement (Fig. 2.36). The maximum value of σ_1 is taken as σ_1 at breaking and the measuring result is a (σ_1, σ_3) combination leading to breaking, denoted by $[(\sigma_1)_{f1}, (\sigma_3)_{f1}]$. These values are substituted in the Mohr-Coulomb equation, giving

$$(\sigma_1)_{f1} = (\sigma_3)_{f1} \tan^2(45° + \tfrac{1}{2}\phi) + 2c \tan(45° + \tfrac{1}{2}\phi) . \quad (1)$$

This is an equation with two unknowns, which cannot be solved alone. We, therefore, prepare another sample of the same soil and subject it to a test at a different value of σ_3. This gives a second (σ_1, σ_3) combination leading to breaking, $[(\sigma_1)_{f2}, (\sigma_3)_{f2}]$. This combination is also substituted in the Mohr-Coulomb law,

$$(\sigma_1)_{f2} = (\sigma_3)_{f2} \tan^2(45° + \tfrac{1}{2}\phi) + 2c \tan(45° + \tfrac{1}{2}\phi) . \quad (2)$$

The set of Eqs. (1) and (2) can now be solved to give c and ϕ. In the practice of tri-axial testing, one does not use such sets of equations, but the graphical method discussed below.

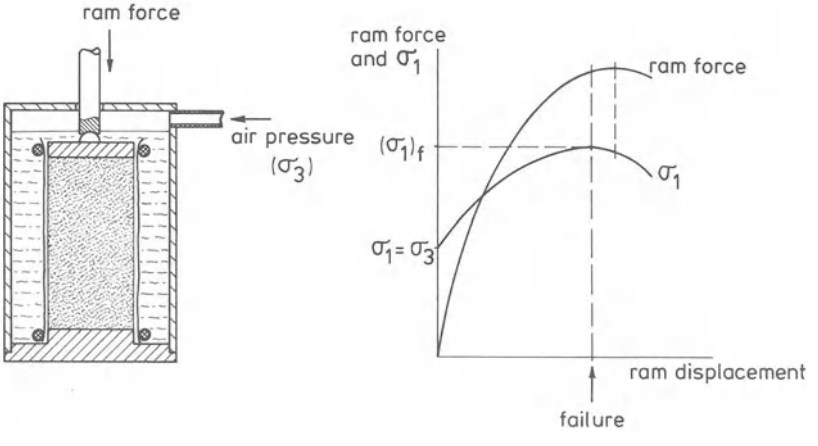

Fig. 2.36. Standard tri-axial shear test

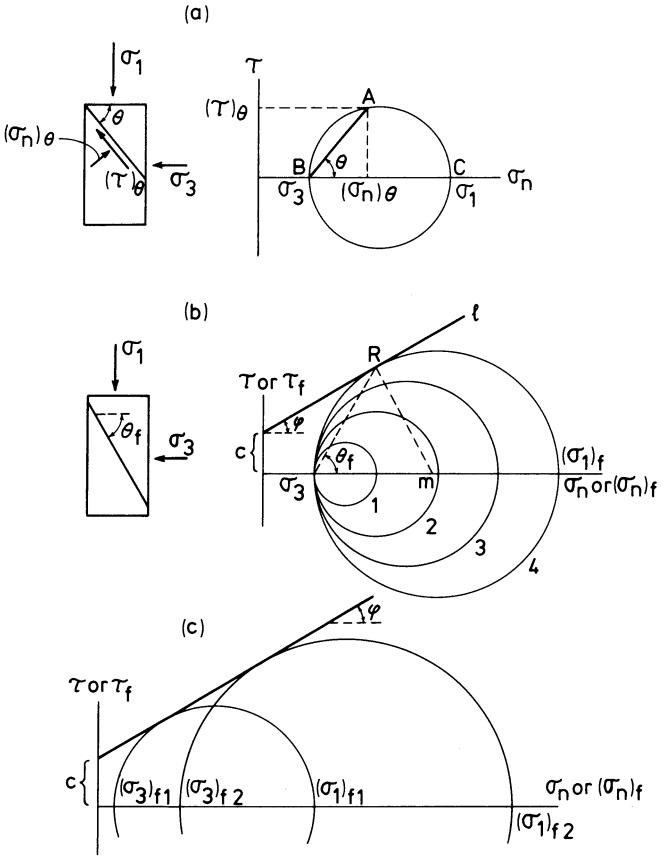

Fig. 2.37a – c. Graphical representation of tri-axial shear tests

Graphical Representation of Tri-Axial Shear Tests. Section 2.1.2.2 (Mohr's graphical representation of stress) presents the relation between (σ_1, σ_3) on a cylindrical sample and [$(\sigma_n)_\theta$, $(\tau)_\theta$] on an arbitrary plane through that sample (Fig. 2.37a). If for a certain θ, the prevailing $(\sigma_n)_\theta$ and $(\tau)_\theta$ values are known the corresponding σ_1 and σ_3 values can be found as follows. Plot [$(\sigma_n)_\theta$, $(\tau)_\theta$] in a $\sigma_n - \tau$ diagram. This gives point A. Draw line AB at angle θ. Then draw the circle through A and B with its center on the σ_n axis. Now B represents σ_3 and C represents σ_1. Figure 2.37b shows the change of Mohr's circle during a tri-axial test. When the hydrostatic pressure σ_3 is applied, σ_3 equals σ_1, and Mohr's circle is reduced to a point on the σ_n-axis (point σ_3). As σ_1 is increased, the circle grows from this point. A few stages have been drawn (circles 1, 2, 3). Suppose that a soil is tested that fails at stress conditions represented by line l (Coulomb's law). When with increasing σ_1 the circle grows so far that it touches line l (circle 4), then the breaking condition is reached for one plane through the sample and breaking will occur. According to Fig. 2.37a, θ for this plane (θ_f) must be the angle between line (R, σ_3) and the σ_n-axis. Between θ_f and ϕ a simple relation exists. Since

angle $RM\sigma_3 = 90° - \phi$ (M is center of circle 4)
and angle $M\sigma_3 R = \theta_f = \frac{1}{2}(180° - \text{angle } RM\sigma_3)$
it follows $\theta_f = \frac{1}{2}(180° - (90° - \phi)) = 45° + \frac{1}{2}\phi$.

Now, if two tri-axial tests for a certain soil resulted in the yielding conditions $[(\sigma_1)_{f1}, (\sigma_3)_{f1}]$ and $[(\sigma_1)_{f2}, (\sigma_3)_{f2}]$ and if c and ϕ are to be found, then Mohr's circles can be drawn for both conditions (Fig. 2.37c). If we then draw the mutual tangent to these two circles, this tangent must represent Coulomb's law. The direction of this line yields ϕ and the intersection with the τ-axis gives c.

A few special cases deserve our attention (Fig. 2.38).

Taking the Mean of Observations. If more than two observations are available a "mean" tangent line can be drawn to determine c and ϕ. For 4 observations this is demonstrated in Fig. 2.38a.

Shear Tests Involving Compaction. If σ_3 was chosen too high or if the soil was very loose at the start of the experiment, not a straight, but a curved tangent line will be found (Fig. 2.38b). In this case, the concept of failure as presented in this chapter, does not apply.

$c = 0$ *Soil.* Sand may have no cohesion at all, in which case the line of Coulomb's law passes through the origin. Then one tri-axial test is sufficient to determine ϕ (Fig. 2.38c).

$\phi = 0$ *Soil.* In general, saturated clay has no internal friction, so $\phi = 0$. The line of Coulomb will then be parallel to the σ_n-axis and only one tri-axial test is needed to determine c (Fig. 2.38d). It holds that $c = ((\sigma_1)_f - (\sigma_3)_f)/2$.

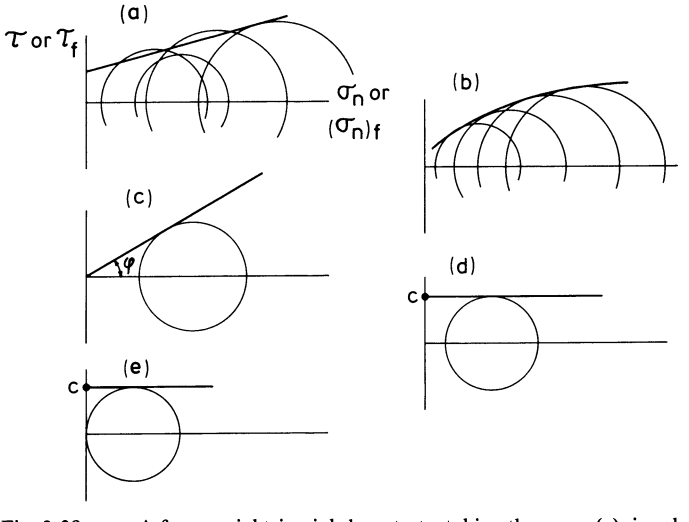

Fig. 2.38a – e. A few special tri-axial shear tests; taking the mean (a), involving compaction (b), $c = 0$ soil (c), $\phi = 0$ soil (d), and unconfined compression (e)

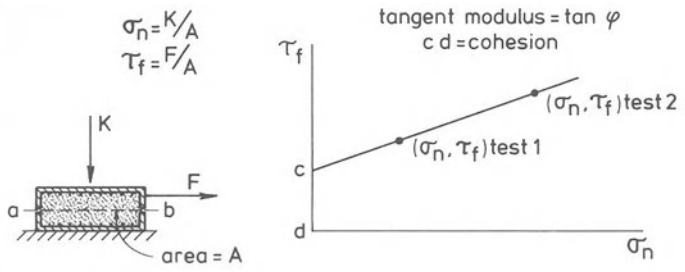

Fig. 2.39. Translational direct shear test

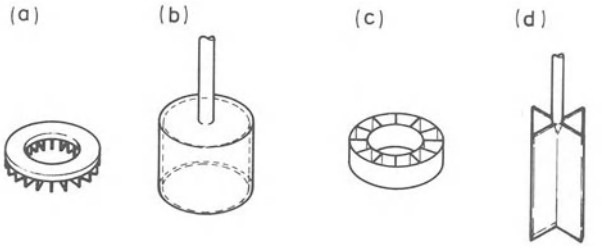

Fig. 2.40a – d. Torsional shear devices

Unconfined Compression Test on a $\phi = 0$ Soil. In general, a $\phi = 0$ soil will be firm enough to allow unconfined compression testing. See Fig. 2.38e. In that case c is half the unconfined compressive strength.

Direct Shear Tests. In contrast to tri-axial tests, the soil in direct shear tests is forced to break along a certain predetermined surface. We distinguish between translational and torsional shear tests:

Translational Shear Tests. A soil block is contained in an upper and lower box, see Fig. 2.39. The boxes are provided with lamellae to improve grip on the samples. A load K is applied to the upper box using dead weights. After loading the upper box is moved to the right and the soil must break along plane $a-b$ with known area A. The force F required for breaking is measured. Then σ_n on the failure plane is K/A and τ_f in the plane at failure is F/A. This (σ_n, τ_f) combination is a point of the line representing Coulomb's law in Fig. 2.39. To find a second point another test with a different vertical load should be carried out. This will give a second (σ_n, τ_f) combination. The line of Coulomb can now be drawn because two points are known, and from the line c and ϕ can be found. An important shortcoming of the translational shear test is that K and F are not evenly distributed over the failure plane because F is applied from one side.

Torsional Shear Tests. There are very differently shaped torsional shear devices. The most common type is shown in Fig. 2.40a, it is an annulus with grousers on the bottom (Bekker 1969, Bailey and Weber 1965). This annulus is pressed into the soil surface, loaded vertically and rotated. Torque needed to rotate attains a maximum when shear-plane failure starts and this maximum value is recorded.

Use and elaboration of the measuring results is comparable to the procedure in translational shear testing. Important differences are:

- the annulus can be applied directly in the field,
- in principle, it should be taken into account that failure occurs not only in a horizontal plane but also in the inner and outer vertical cylindrical surfaces of the annulus. Normal stresses on these vertical surfaces are considered to be zero,
- after rotation over a small angle, displacement in the potential failure surface will be greater near the outer side of the annulus than near the inner side. Therefore, breaking will not occur everywhere at the same time.

Figure 2.40b shows a cylindrical torsional shear box (Payne and Fountaine 1952). Figure 2.40c shows a shear annulus that consists of two concentric cylinders with connecting radial grousers (Söhne 1953b). Figure 2.40d finally shows a shear vane. The height of the blades is usually 1.5 – 2 times the diameter of the vane (Schaffer 1960).

2.4.2.3 Tensile Failure

Idealized Brittle Failure. Griffith's Model. Griffith (1920) developed a model for breaking of materials like glass. In such materials there are always small irregularities as microscopic cracks. As a result, on a micro scale stress distribution will be very irregular. Especially around tips of such small cracks high stresses may occur. When the material is loaded, and when its behavior is perfectly elastic, stresses will increase proportionally to the load, and elastic energy which is energy that will be released at unloading, will be stored. If the load has become so high that the energy required to let a microcrack grow a unit of length (fracture energy per unit of length, which is comparable to surface tension in liquids), is less than the elastic energy that will be released when this microcrack is elongated one unit of length, then cracking will start and the crack front will propagate through the material at a very high velocity. Such crack development is said to have a catastrophic character. Breaking that obeys Griffith's model is characterized by elastic behavior up to the moment of breaking and, subsequently, by fracture surfaces in which only separation of material occurs without any plastic flow.

Because tensile failure surfaces in soil exhibit more or less these characteristics, it is sometimes assumed that tensile failure in soil follows the Griffith model. For dry soils this is a reasonable approximation, but the wetter the soil and the higher its ability to deform, the more plastic flow phenomena occur, and the less applicable Griffith's model will be. As stress levels increase, micro-cracks are closed more and more, and friction according to Coulomb's model becomes more and more prevalent.

Griffith's Model in Terms of σ_1 and σ_3. In Section 2.4.2.1, Griffith's model is presented mathematically in terms σ_1 and σ_3 (Paul 1968).
According to the formulas

$$\text{tensile strength} = \text{compressive strength}/8 \; .$$

A comparison between tensile tests and unconfined compression tests shows that for rather dry soil this is indeed correct. For wet soil the ratio of tensile strength to compressive strength is greater (Farrell et al. 1967, Koolen 1977).

Griffith's Model in Terms of τ_{max} and σ_m. Griffith's model expressed in τ_{max} and σ_m is a function that can be represented by a surface in the (τ_{max}, σ_m, BWV) space. Hettiaratchi and O'Callaghan (1980) assume that the shape of this surface is as shown in Fig. 2.35 between line EF and the BWV axis.

Measuring Soil Tensile Strength. Tensile strength is measured by extending a vertical bar-shaped soil sample in axial direction until it breaks. It is advised to trim the bar in such a way that its surface is slightly concave. The fracture plane will then be in the middle part of the bar. During the test the ends of the bar should be kept parallel to ensure that failure will occur at the same time for each place in the potential failure plane. When soil strength is low, the weight of the soil between failure plane and force measuring equipment should be taken into account.

2.4.2.4 Loading Rate and Repeated Loading Effects

Tri-axial tests and unconfined compression tests are usually performed at such a low loading rate that stresses in a sample, considered at one moment, may be assumed equal in all points of the sample. If, however, loading rate is of the same order of magnitude as the velocity of stress propagation in the soil, this does not hold. The action of a suddenly applied stress is not transmitted at once to all parts of the soil sample. At the beginning the remote parts of the sample remain undisturbed, and deformations produced by the stress are propagated through the sample in the form of elastic/plastic waves. This should be realized when considering what follows. In unsaturated agricultural soils plastic wave velocity is about 10 – 12 m/sec (Hendrick and Gill 1973).

In general, soil is stronger as the loading rate is higher, but weaker at repeated loading.

Loading Rate Effect on Compressive Strength. Compressive strength increases linearly with the logarithm of the loading ram velocity up to a maximum and then decreases linearly with this logarithm of ram velocity. The velocity at which compressive strength is maximal, is called *critical speed.* Compressive strength at critical speed can be e. g. three times as high as at low speeds. Measured critical speeds were between 2 and 4 m/sec. Critical speed increases with increasing moisture content and increasing clay content of the soil (Lucius 1971, Kawamura and Umeda 1958).

Loading Rate Effect on Tensile Strength. Tensile tests of Rao and Hammerle (1973) on a sand-clay mixture showed that at a 5 times higher elongation speed, tensile strength was 1.3 times greater.

Loading Rate Effect on ϕ and c. Measurements indicated that ϕ is almost independent of loading rate (Wu 1971, Lucius 1971, Kawamura 1958). This means

that c has to depend on loading rate. This dependency of c has to account for the entire loading rate dependency of the unconfined compressive strength (u. c. s.). It means that the percentual change of u. c. s. with a change in loading rate will be accompanied by the same percentual change in c.

Repeated Loading Effects. Fatigue failures as known from steel and concrete may also occur in soils (Wu 1971). Consider a cylindrical soil sample loaded by $\sigma_1 = \sigma_3$. We increase σ_1 by $\Delta\sigma_1$ and then add a pulsating stress $(\Delta\sigma_1)_p$. If the sum $\Delta\sigma_1 + (\Delta\sigma_1)_p$ is high enough the sample will fail after a certain number of pulses, say N. N decreases with increasing $\Delta\sigma_1$, with increasing $(\Delta\sigma_1)_p$, and as σ_3 is decreased.

2.4.2.5 Soil Physical Aspects of Shear Strength

Soil Moisture. At the left side in Fig. 2.41, an elemental volume of saturated soil is shown. Line ab is a potential failure plane, σ_n is the normal stress on this plane. Soil water pressure is p_w. Suppose that the area of the potential failure plane is A and that a fraction f of this area passes through water. Normal forces between the soil particles across the potential failure plane are indicated by $\sum N$.

Equilibrium requires that

$$\sigma_n A = \sum N + A f p_w .$$

Points of contact between the particles will be small, so we may assume that $f \approx 1$, and obtain

$$\sum N/A = \sigma_n - p_w .$$

$\sum N/A$ is called the effective stress σ_n'. It is this effective stress σ_n' that makes shearing resistance increase according to the law of friction. Therefore, Coulomb's law for saturated soil is usually written as

$$\tau_f = c' + (\sigma_n - p_w) \tan\phi' .$$

The following terminology is used to distinguish between this formulation and Coulomb's law for drier conditions:

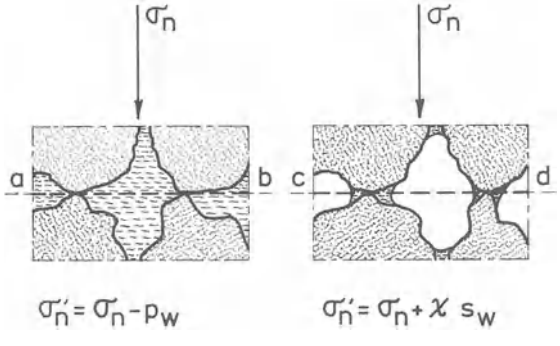

Fig. 2.41. Relation between effective stress (σ_n') and total normal stress (σ_n) for saturated (*left*) and unsaturated (*right*) soil

c = apparent cohesion

c' = true cohesion

ϕ = apparent angle of internal friction

ϕ' = true angle of internal friction .

For saturated soils it is common practice to use c' and ϕ' instead of c and ϕ, because drainage conditions in failure tests on saturated soil have a great influence on p_w.

The right half of Fig. 2.41 refers to unsaturated soil. Equilibrium implies

$$\sum N/A = \sigma_n' = \sigma_n + f s_w$$

where s_w is the suction prevailing in the soil water. Calculations show that f is equal to the degree of saturation χ of the soil. Coulomb's law can thus be written as

$$\tau_f = c' + (\sigma_n + \chi s_w) \tan \phi' .$$

This formula applies well for sands if $\chi > 0.5$, and for clays if $\chi > 0.9$. The formula is inaccurate for lower values of χ, because

- local differences in s_w will occur in the sample, due to the presence of isolated water pockets. In that case, s_w measured with an instrument differs from the strength determining, mean s_w.
- in aggregated soils the surface of breaking tends to run between aggregates. In that case f will be much smaller than χ.

In unsaturated soil it is common to use c and ϕ, and not c' and ϕ', because s_w can be considered constant during shear testing. Since

$$\tau_f = c + \sigma_n \tan \phi = c' + (\sigma_n + \chi s_w) \tan \phi' = c' + \chi s_w \tan \phi' + \sigma_n \tan \phi'$$

and s_w is constant, we have

$$\phi = \phi', \quad \text{and}$$

$$c = c' + \chi s_w \tan \phi' .$$

Thus, in unsaturated soil apparent cohesion is greater than true cohesion, the difference being caused by the clenching action of the suction in the soil water.

Figure 2.42 is an example of an apparent cohesion calculation based on the pF curve of a silty loam. In such soil c' is near zero and, therefore, apparent cohesion is $c = \chi s_w \tan \phi'$. Values of s_w can be found from the pF curve and ϕ' is supposed to be 35°. Then, c can be calculated as a function of χ and the result is shown in Fig. 2.42. Further information is provided by Lee and Donald (1968) and Towner and Childs (1972).

Mineral Parts. Mineral parts of the soil determine to a large extent the angle of internal friction. Two factors are especially decisive for ϕ.

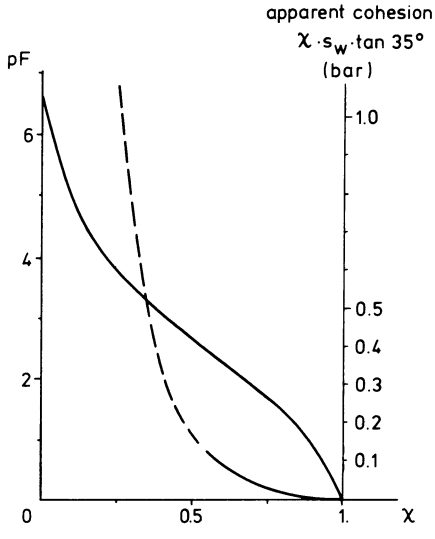

Fig. 2.42. Calculation of apparent cohesion from degree of saturation χ and soil moisture suction s_w

1. The friction angle between the surfaces of the minerals involved.
2. The angle of dilatancy. Dilatancy requires a certain amount of dilatancy-work, that must be supplied by the shear stress in the shear plane. [In Fig. 2.28 dilatancy work between the two given stages equals σ_n × rise of top plate × area of top plate (Rowe 1962).]

For unsaturated soil ϕ varies between 25° (moist, relatively loose, fine particles) and 45° (drier, relatively dense, coarse particles).

Packing density and arrangement of the mineral particles determine soil water suction at a certain moisture content (Sommer et al. 1972) and this is another influence of the mineral parts on soil strength.

Bonds. Besides the clenching action of the soil water suction, further bonds may occur between

- mineral particles (edge-to-plate forces and Madelung forces),
- mineral particles and organic matter,
- mineral particles and oxides/hydroxides,
- organic matter and oxides/hydroxides,

and, in a negative sense, between

- charged minerals (repulsive forces).

It is these bonds that cause true cohesion c'. In unsaturated soil they normally have no dominating part in c. In very aggregated soil, c' may have a high value within the aggregates. This will not show up in shear testing when the surface of breaking runs between aggregates leaving the single aggregates intact.

Finally it should be mentioned that in swelling soil these bonds may influence s_w (Koenigs 1961).

Measurements of c' in unsaturated soil are very scarce. Measurements of apparent cohesion have been carried out in a much greater number and appear to vary strongly. Söhne (1953b) mentions values of 0.09 – 0.43 bar. Fountaine and Payne (1954) give values up to 0.9 bar, but on most occasions they found $c < 0.2$ bar. Schaffer's results (1960) varied between 0.2 – 1.4 bar.

Explanation of Some Phenomena. Soil physics is able to explain a number of strength phenomena:

Changes in Strength on Aging. Immediately after precompaction of a loose soil, the *pF* distribution in the soil is more or less chaotic. Transport of water as liquid and vapor will re-establish gradually a moisture suction equilibrium. The accompanying local changes in soil water content and suction imply that soil strength changes with time. Observations show that strength increases on aging after precompaction until equilibrium has been attained. Failure resistance at one day after precompaction may be as much as 50% higher than immediately after precompaction.

Influence of Moisture Content at Precompaction. Consider a series of samples that are precompacted at different moisture contents and then dried or wetted to the same moisture content level so that samples have been obtained with equal moisture contents and equal pore spaces. If then shear strengths are determined, they are found to increase with increasing moisture content at precompaction. This increase may even imply a fivefold increase of soil cohesion. Further data are given in Koolen (1976). The phenomenon can be explained as follows. Precompaction of relatively wet soils will involve deformations at the contact surfaces between aggregates resulting in a large number of relatively small mutual pores at such a contact area. This allows the soil water suction to exert its clenching action between the aggregates as well.

Influence of Drying and Wetting Cycles. On drying, the relatively small particles of oxides, organic matter, etc. will move towards the points of contact between the relatively large mineral particles. This leads to a cementing effect (Gerlach 1953), which increases true cohesion.

Influence of Temperature on Shear Strength. Because the *pF* curve is temperature-dependent, it is to be expected that shear strength will also be temperature-dependent. Probably, the soil internal bonds also depend on temperature. Observation shows that shear strength decreases with temperature. A temperature increase of 20°C may decrease strength as much as 10% (NN 1969).

2.4.3 Applications

2.4.3.1 Methods to Determine the Measures of Strength Indirectly

When a value of a soil strength measure is required, it may save time and money to estimate this value from a related quantity that can be measured easily.

Estimation of Cohesion from Unconfined Compressive Strength in Unsaturated Agricultural Soils. In an unsaturated agricultural field soil, ϕ varies from 25° for moist, loose, fine textured soils to about 45° for dry, dense, coarse textured soils. In an "average" soil ϕ will be about 35°. Using Mohr's circle and the line of Coulomb's law it can be derived that for unconfined compression, and $\phi = 35°$,

$$\text{cohesion} = 0.26 \text{ unconfined compressive strength} .$$

For saturated soil, $\phi = 0$, and thus

$$\text{cohesion} = 0.5 \text{ unconfined compressive strength.}$$

Estimation of Tensile Strength from Unconfined Compressive Strength (Fig. 2.43 a). In section 2.4.2.3 we saw that for drier soils

$$\text{tensile strength} \approx \text{unconfined compressive strength}/8.$$

Estimation of Tensile Strength Using the Brasilian Test (Kirkham et al. 1959). If a cylindrical soil sample is crushed according to Fig. 2.43 b by a force F, then, at the moment of failure,

$$\sigma_t = \frac{2F}{\pi DL}$$

where F is vertical force at breaking, σ_t is tensile strength, D is sample diameter, and L is sample length. The formula is derived assuming perfect elasticity up to the moment of failure.

Estimation of Tensile Strength Using the Flexure Test. Tensile strength σ_t can also be estimated from a flexure test on a rectangular sample (Fig. 2.43 c) according to

$$\sigma_t = \frac{M}{Cbd^2}$$

where M is bending moment ($F \times L$) at failure, b is beam width, d is beam thickness, and C is a dimensionless parameter, depending on the shape of the stress-strain relationship in uni-axial loading of the soil. If that stress-strain relationship is linear, $C = (1/6) \approx 0.166$. If it is the relationship that applies to an ideal plastic material, $C = 0.25$. Farrell et al. (1967) measured C-values of 0.22 – 0.24 on ($2.5 \times 2.5 \times 7.6$) cm^3 loam soil samples, the value being independent of the soil moisture content. In the case of a non-linear stress-strain relationship, C probably also depends on beam dimensions. Maurer and Withey (1940) report tests with high loads on cast iron and wood, showing these dependences.

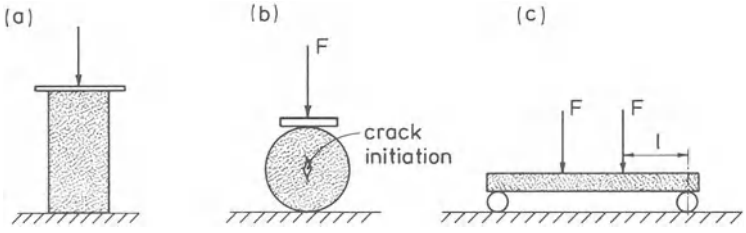

Fig. 2.43 a – c. Indirect determinations of soil tensile strength

2.4.3.2 A Few Applications of the Modulus of Rupture

Tensile strength calculated from bending tests under the assumption of elastic behavior is known as *modulus of rupture.* It implies that for C in Section 2.4.3.1 the value 1/6 is used. Because the true C in soil varies, its value being larger than 1/6 in most cases, this tensile strength value is generally larger than the true soil tensile strength value.

Modulus of rupture was used in testing soil conditioners (Allison 1956, Jamison 1954). Another application was in research to establish the resistance encountered by seedlings emerging from a crusted soil (Arndt 1965, Hanks and Thorp 1957). Finally, it is used as a measure of the influence of soil physical factors on soil strength (Gerard 1965).

2.4.3.3 Draft Calculations Using Hypothesized Mechanisms of Rigid Soil Bodies

Sometimes, the draft of a tine or a plowbody can be reasonably estimated by assuming hypothesized soil blocks piled up against the tool surface and considering the equilibrium of forces for each of these blocks. A very simple example is Söhne's model (1956), which applies to plane blades with small cutting angles. The model comprises one rigid soil block moving along the still undisturbed soil and along the tool. See Fig. 2.44. Line qr denotes a potential failure plane in which the force due to cohesion and the frictional force, are fully developed.

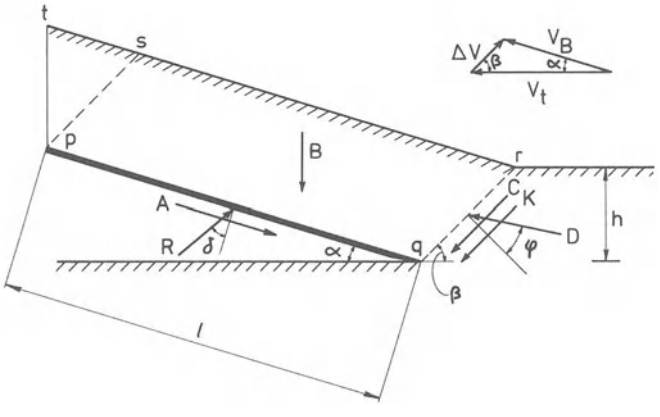

Fig. 2.44. Söhne's model

B = weight of soil body,
C = cohesive force,
K = force due to soil acceleration,
R = the normal force that the blade exerts on the soil plus the frictional force accompanying this normal force,
D = reaction force of the still undisturbed soil,
A = adhesive force,
l = blade length,
ϕ = angle of internal soil friction,
α = cutting angle,
β = shear angle, which has been assumed to be 45° in the model,
δ = angle of soil-metal friction.

It follows from the vector diagram

$$\Delta V = V_t \frac{\sin \alpha}{\sin(\alpha + \beta)} \qquad (V_t = \text{traveling speed}) .$$

The acceleration force can be calculated from ΔV. Soil particle acceleration takes place during a time interval Δt, so mean acceleration is $\Delta V/\Delta t$. The soil mass that is being accelerated at one moment equals $\rho\, b\, h\, V_t\, \Delta t$, where b is blade width, ρ is bulk mass per unit of volume and h is working depth. Using the previous formula we obtain

$$K = (\rho\, b\, h\, V_t\, \Delta t)\frac{\Delta V}{\Delta t} = \frac{\sin \alpha}{\sin(\alpha + \beta)}\, \rho\, b\, h\, V_t^2 .$$

It can further be derived that

$$C = \frac{h\, c}{\sin \beta} \qquad (c = \text{cohesion})$$

$$A = l\, a \qquad (a = \text{adhesion})$$

$$B = \rho g l h \frac{\sin(\alpha + \beta)}{\sin \beta} + \tfrac{1}{2} \rho g h^2 \frac{\sin(\alpha + \beta)\cos \beta}{\sin^2 \beta \cos \alpha} .$$

In this formula, the last term accounts for the soil in the triangle (s, t, p) and the next to last one for the soil in parallelogram (p, q, r, s). There are two forces in Fig. 2.44 still unknown, namely R and D. Using the equilibrium conditions in horizontal and vertical directions, two equations can be formed, which allow R and D to be calculated. Finally, A and R can be combined to find blade resistance. The horizontal component of this resistance is the blade draft.

2.4.3.4 The Influence of Moisture Content at Seedbed Preparation on Plowing Resistance After Harvest

The relation between moisture content at seedbed preparation and plowing resistance after harvest was investigated through simulation experiments in the laboratory using a series of cylindrical soil samples of Wageningen silty clay loam

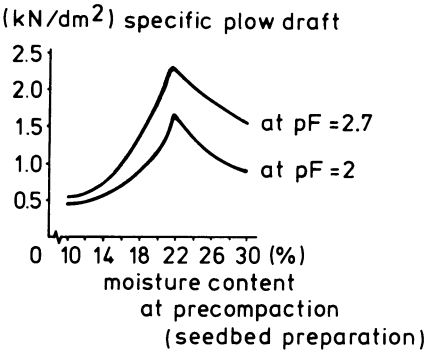

Fig. 2.45. Plow draft after harvest as affected by moisture content at seedbed preparation

(Koolen 1978). Compaction at seedbed preparation was simulated by uni-axial compression to 4 bar. Plowing resistance was calculated with the method of the previous Section 2.4.3.3, using c values calculated from unconfined compression tests assuming that $\phi = 25°$. Because of the necessary changes in moisture content between the different mechanical treatments, the experiments lasted 8 months. The result is shown in Fig. 2.45. The upper curve refers to the case of plowing at pF 2.7, the lower curve to plowing at pF 2. In the field, the workability limit of the soil used appears to be about a moisture content of 21%. If the soil is prepared before the growing season at this moisture content, and plowed at $pF = 2$ after harvesting, the graph predicts a specific plow draft of 1.4 kN/dm^2 for this plowing. If the preparation is delayed until the soil has dried to 20%, the predicted plow draft at pF 2 after harvest would be 1.2 kN/dm^2, involving a decrease of 0.2 kN/dm^2 = 14%.

2.5 Elemental Treatment of Soil-Material Friction and Adherence

2.5.1 Occurrence

In tillage and field traffic, boundary surfaces occur between soil bodies and other materials like steel and rubber, and also between adjacent soil bodies. A small element of such surfaces may be considered as a boundary between two rigid bodies. Sometimes there is relative movement in such a surface element, at other times not, but in general there is a stress acting across the surface element between the two bodies. The tangential component of that stress is the shear stress due to the friction at the surface element.

This shear stress is *fully developed* if sufficient relative movement occurs. Sometimes, the relative movement is not such large and the shear stress has a relatively low value. Conversely, if a small shear stress is applied, a small relative movement will occur and rest will be restored. Application of a greater shear stress initiates a relative movement that continues. Not fully developed shear stresses occur

- in parts of the contact surfaces of rollers, wheels and tires at low slip percentages,
- where a so-called soil wedge adheres to the material surface. Soil wedges may occur with tines, blades and shear elements,
- in the soil-material interface, if a thin soil layer adheres to the material. This may occur at rough tool surfaces and in sticky soils.

Fully developed shear stresses can be expected

- with rollers, wheels and tires at high slip percentages,
- with relatively sharp cones,
- with sleds,
- at soil-soil interfaces in shearing devices,
- in the contact surface of tools with small angles of approach under normal conditions.

For driven wheels shear stresses in the contact surface should be as high as possible to maximize pull. In other cases such as tines, plow bodies, and sleds, low values of the shear stresses in the contact surface are desirable. Also in research activities low values may be desired; for instance, for observations of soil-tool interactions through transparent soil bin walls, one tries to keep wall-interference as low as possible (Koolen 1977). The same holds true for the top and bottom plates in tri-axial tests and unconfined compressions tests, and for the cylinders in uni-axial compression tests.

2.5.2 Fundamentals

Figure 2.46 shows a shear stress τ that is exerted by a material on a soil body. Total stress S has a normal component σ_n. When there is significant relative movement in the interface, τ is fully developed. τ for this case will be denoted by τ_s (s from sliding). It is assumed that the surface element is fixed to the soil.

Measures. Frictional properties for a boundary surface are generally measured by measuring τ_s at different values of σ_n. Generally, τ_s at a certain moment can be approximated by

$$\tau_s = \mu \sigma_n \tag{1}$$

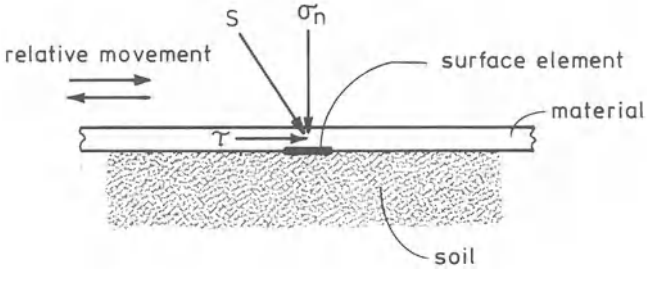

Fig. 2.46. Stresses on a soil surface element sliding along a material

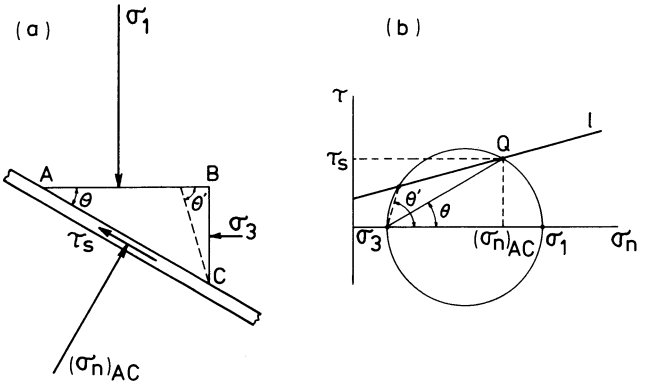

Fig. 2.47a, b. Graphically determined relationship between (σ_1, σ_3) and (τ, σ_n) on a sliding surface

or, more accurately, by

$$\tau_s = a + \mu' \sigma_n . \tag{2}$$

The parameters μ, a, and μ' are called apparent coefficient of soil-material friction, adhesion, and true coefficient of soil-material friction, respectively.

Sliding Conditions in Terms of σ_1 and σ_3. In Fig. 2.47a a soil element ABC slides along a material. The angle θ between the material surface and the plane on which σ_1 acts is given. In plane AC Eq. (2) must hold, so that

$$\tau_s = a + \mu' (\sigma_n)_{AC} .$$

According to Section 2.1.2.1,

$$\tau_s = (\sigma_1 - \sigma_3) \sin\theta \cos\theta , \qquad \text{and}$$

$$\sigma_n = \sigma_1 \cos^2\theta + \sigma_3 \sin^2\theta$$

and thus Eq. (2) for soil element ABC can be expressed as

$$(\sigma_1 - \sigma_3) \sin\theta \cos\theta = a + \mu' (\sigma_1 \cos^2\theta + \sigma_3 \sin^2\theta) .$$

The graphical representation using Mohr's circle (Section 2.1.2.2) is elucidating (Fig. 2.47b). Line l represents the sliding condition. Suppose that point Q on l represents the state of stress in the plane of sliding AC. Then the line through Q at angle θ to the σ_n-axis yields σ_3, and the circle through σ_3 and Q with its center on the σ_n-axis yields σ_1. Note that τ in the plane at angle θ' with the horizontal satisfies Eq. (2) as well. However, physically this equation is not valid for this plane, since it is not a soil-material interface. For planes at angles between θ and θ', the states of stress are represented by points above line l. Shear stresses in these planes may be much higher than the shear stress in the plane of sliding. Of course, high shear stresses can only exist if the soil is strong enough (Mohr's circle can never extend beyond the line of Coulomb's law). If, at fixed values of τ_s and σ_n in the plane of sliding, the angle θ between that plane and the plane perpendicular to σ_1 is different, other σ_1 and σ_3 values occur.

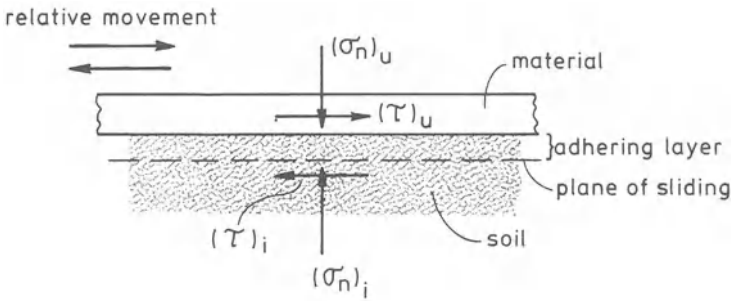

Fig. 2.48. Conditions favoring soil adherence

Adherence and Wedge Formation. Sometimes shear stresses in the soil-material interface are so great that sliding between the soil and the material not longer occurs; instead, shear planes are formed within the soil body. Whether or not these alternative shear planes develop depends on the ratio between the resistance against sliding along the material and the soil internal strength. Sliding resistance is characterized by a and μ', soil internal strength by c and $\tan\phi$ (c is cohesion, ϕ is angle of internal soil friction). Two cases may be distinguished.

1. Adherence of a thin soil layer of constant thickness as shown in Fig. 2.48. Equilibrium requires that

   $$(\sigma_n)_u = (\sigma_n)_i$$
   $$(\tau)_u = (\tau)_i .$$

   There is no sliding along the material and, therefore,

   $$(\tau)_u < a + \mu'(\sigma_n)_u .$$

   In the sliding (failure) plane, according to Coulomb

   $$(\tau)_i = c + (\sigma_n)_i \tan\phi .$$

   These four equations can be combined to show that adherence occurs if

   $$a + \mu'(\sigma_n)_u > c + (\sigma_n)_u \tan\phi$$

   or,

   $$\sigma_n < \frac{a - c}{\tan\phi - \mu'} .$$

   Adherence can be predicted if a, μ', c, $\tan\phi$, and σ_n are known. Scouring (sliding without adherence) is favored by increasing σ_n (think of slitted moldboards).

2. Soil wedges resting against material surfaces of tines etc. (Fountaine and Payne 1954). In contrast with case 1., this is a normal phenomenon, not conflicting with the intended action of a process (see Sects. 3.6 and 3.7).

Path Dependency of Instantaneous Values of μ, a, and μ'. Shear stresses just before movement between soil and material (static friction) are often different

from those immediately after the start of movement (dynamic friction). For steel on dry sand, Nichols (1931) found $\mu = \mu' = 0.26$ just before movement, and $\mu = \mu' = 0.23$ immediately after the start of movement.

Friction on the surface element in Fig. 2.46 may change with increasing length of sliding path and attain a constant value after a path length of one or more decimeters. With steel this change involves mostly an increase of μ, caused by changes in soil particle arrangement and in position and suction of soil water. In contrast, with rubber μ usually decreases, because the flexible rubber adjusts to surface irregularities and meets a smoother soil at a greater path length. In this way for steel μ may increase by e.g. 0.3 and for rubber it may decrease by e.g. 0.1 (Söhne 1953b).

The value of adhesion a seems to be especially sensitive to the highest value of σ_n that ever occurred on the surface element. A higher σ_n will give a closer contact. Söhne (1953b) reported up to fivefold increases of a upon tenfold increases in highest σ_n.

The Influence of Sliding Velocity. For wet soil and/or for speed variations over one or more orders of magnitude a speed dependency of μ should be taken into account. Increases of μ of $0.1 - 0.15$ have been measured due to higher sliding speed (Vornkahl 1967). It is likely that soil water viscosity plays a role in this.

Measuring Methods. A very elemental measuring method, the *plate method*, is shown in Fig. 2.49a. In this test, a soil surface of known size slides along another

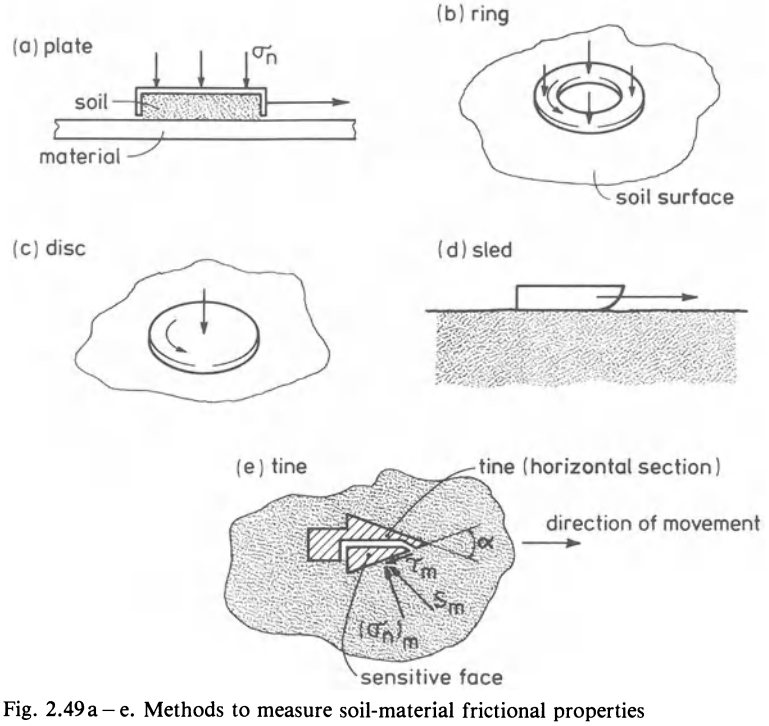

Fig. 2.49a – e. Methods to measure soil-material frictional properties

material. In fact, a small surface element sliding along a material is imitated. It is possible to measure the occurring shear stress in dependence of normal stress, sliding velocity and sliding path length. Before the test the contact may be improved by pressing the soil against the material. Initially, the shear stress will change with increasing path length, but after a certain length of time a steady state shear stress will be attained. During the test the soil element only meets fresh material surface. This differs from practical situations in which the material surface may be wet and soil particles may stick due to the sliding of preceding soil elements. In the *ring method*, (Fig. 2.49 b) an annulus resting on the soil surface is rotated and the required torque is measured. Ring and plate methods have the same characteristics, except that

- the annulus is better suited for long sliding paths,
- strictly, the sliding path along the outer circumference of the annulus is longer than that along the inner circumference. If outer and inner diameters are not too different, this is not a serious drawback and a mean sliding path length may be calculated according to

  $$\text{effective ring radius} = \tfrac{1}{2}(\text{outer radius} + \text{inner radius}) .$$

  If the inner radius is relatively small, the effect cannot be neglected, in particular not for the *disc method* (Fig. 2.49 c),
- during the test, the surface of the annulus may become wet and soil particles may adhere to the surface.

In the *sled method* (Fig. 2.49 d), a sled is pulled along the soil surface and the friction force is measured as soon as a steady state has been reached. Normal stress and sliding speed can be varied. In this method the sliding path length cannot be varied; at the front of the sled, it is zero and at the back it is equal to the sled length. If shear stress at small path lengths is smaller (higher) than at large path lengths, steady state shear stress measured with a plate will be higher (smaller) than with a sled. In the *tine method* (Fig. 2.49 e) a wedge shaped vertical tine is pulled through the soil. After a steady state has been reached the mean shear stress and also the mean normal stress are measured on one of the tine sides. Mean normal stress can be varied by changing the wedge tip angle α or by changing traveling speed. It is possible, therefore, to measure a mean shear stress in dependence of mean normal stress and sliding speed. The tine method has the same characteristics as the sled method, except that

- with a tine only mean stresses are measured,
- the tine method is very suitable for field soil.

Material Aspects. Surface *roughness* has a large influence on friction. For a rusted steel surface, the coefficient of friction may be as high as $\tan \phi$ (ϕ is angle of internal soil friction), and thus may exceed 0.8. If the rust is removed, friction will be considerably less but a high degree of surface polish will result in only a minor decrease. For a reasonably smooth, steel tool in an average, rather dry soil one may expect $\mu \approx \mu' \approx 0.25$ (Spoor 1969).

Also the *hardness* of the material surface plays a role. Nichols (1931) measured for steel at low soil moisture contents and short sliding paths

$$\mu = \mu' = 0.37 - 0.00015H$$

where H is Brinell hardness. H is about 650 for very hard tempered steel and about 125 for steel low in carbon. The influence of hardness was also discussed in the paragraph on sliding path length effects.

Regarding the type of material we should mention that, on soil that is not too wet and for short sliding path lengths, μ is about 0.2 higher for rubber than for steel. For soil-soil friction it is usually assumed that $\mu' = \tan\phi$.

Soil Physical Aspects. Soil moisture may strongly influence frictional behavior. Roughly one may interpret the law of friction

$$\tau_s = a + \mu' \sigma_n$$

[Eq. (2) mentioned in the beginning of this section] physically as follows (Fig. 2.50). An external load on a plate induces a normal stress σ_n on the soil. This σ_n contributes to the effective stress between the solid part of the soil and the plate (effective stress is the sum of the normal components of the contact forces between the plate and the solids, divided by plate area A). There may be water between the plate and the soil particles. If this water is under suction it will provide an additional effective stress. This additional effective stress is called σ_w. Real total effective stress is then

$$\sigma_k = \sigma_w + \sigma_n .$$

The friction between soil particles and the plate follows the well-known law of friction

$$\tau = \sigma_k \nu$$

where ν = coefficient of friction between the plate and single soil particles. Combination of these two equations yields

$$\tau = \sigma_w \nu + \sigma_n \nu .$$

A comparison of this equation with Eq. (2) ($\tau_s = a + \mu' \sigma_n$) shows that

$$\nu = \mu' \quad \text{and} \quad a = \sigma_w \nu .$$

Additional effective stress σ_w due to soil water can be expressed as

$$\sigma_w = sA_{\text{rel}}$$

where s is the soil water suction and A_{rel} is the wetted fraction of the plate area. The last two equations can be combined to

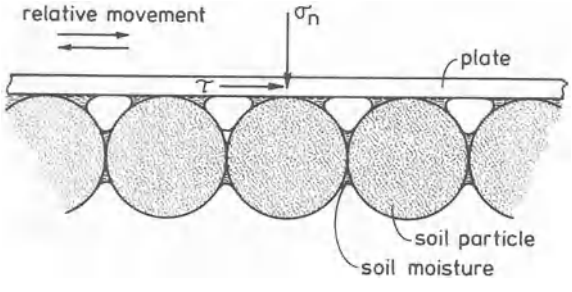

Fig. 2.50. The role of soil water in soil-material friction

$$a = vsA_{rel}.$$

Regarding this physical model the following remarks may be made.

- The occurrence of water between the plate and the soil particles requires good soil-plate contact. For this the duration of sliding, history of normal stress, and soil structure are important factors.
- Soil water suction depends on moisture content, soil structure and soil type.
- A_{rel} depends on the degree of contact, on soil moisture and on plate material.
- v is determined by surface roughness of the plate, and by the mineral type and shape of the soil particles.
- During the service life of a tool, the roughness of the soil-engaging surface is that of worn material. This roughness may be higher or lower than that of new material.
- At higher moisture contents, soil water may act as a lubricant and lower v drastically. The moisture range where this occurs is known as the *lubrication phase* of soil friction. In this range, v decreases with increasing moisture content.
- At lower moisture contents, water cannot be present between the soil particles and the plate. As a result, τ will not depend strongly on moisture content, and $a = 0$. This moisture range is called the *dry phase.*
- At moisture contents between the dry phase and the lubrication phase, A_{rel} increases strongly with increasing moisture content and, therefore, τ also increases (*adhesion phase*).
- Sliding velocity influences friction through soil water viscosity.

The mineral parts influence friction through type of mineral and packing density. For steel on dry sand friction was found to increase with packing density as a result of increased soil strength. Butterfield and Andrawes (1972b) found $\mu = \mu' = 0.17$ for a soil at a porosity of 43.7%, and $\mu = \mu' = 0.28$ at a porosity of 35.7%. Fine-textured soils have a higher coefficient of friction than coarse-textured soils. For small sliding distances of steel on soils with low moisture contents Nichols (1931) found

$$\mu = \mu' = 0.23 + 0.005\,(\% < 2\,\mu m) \quad \text{if this } \% < 32$$

$$\mu = \mu' = 0.37 \quad \text{if this } \% \geqslant 32\,.$$

2.5.3 Applications

2.5.3.1 The $\sigma_n - \sigma_1$ Ratio of a Soil Element at a Soil-Material Interface

If, in addition to a normal stress σ_n, a shear stress τ is present in a surface element of a soil-material interface, then for a soil volume element near that surface element, σ_1 is always larger than σ_n, and the direction of σ_1 is not the same as that of σ_n. Yet, in general, it is possible to estimate σ_1/σ_n. This will be shown for a soil element near the interface of a smooth tire, using

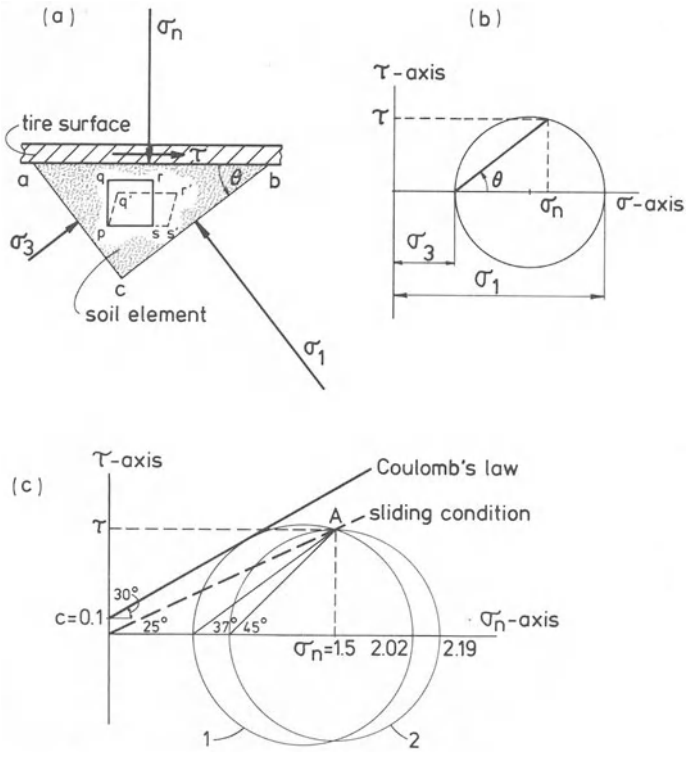

Fig. 2.51 a – c. Estimation of σ_1/σ_n at a soil-tire interface

$\sigma_n = 1.5$ bar
soil cohesion = 0.1 bar
angle of internal soil friction $\phi = 30°$
angle of soil-rubber friction $\delta = 25°$ ($\mu = \tan 25°$).

A soil element is selected with two faces being principal planes. It is shown as *abc* in Fig. 2.51 a, together with the stresses that act on it. According to Section 2.1.2.2, this state of stress can be represented by Mohr's circle of Fig. 2.51 b. σ_n is given and τ, σ_1, σ_3, and θ are unknown. Three considerations lead to the estimate.

1. Friction is fully developed, so Mohr's circle must pass through point A in Fig. 2.51 c.
2. Mohr's circle should not touch the line of Coulomb, so circle 1 is a boundary-circle. From this circle it follows that $\theta > 37°$ and thus $\sigma_1 > 2.02$ bar.
3. From observations we know that loading by a tire will deform element $pqrs$ into $pq'r's'$ in Fig. 2.51 a. This deformation may be assumed to be composed of a vertical compression with θ being 0° and a so-called pure shear ($\sigma_3 = -\sigma_1$) with σ_1 in the direction of qs and σ_3 in the direction of pr, so with θ

being 45°. Therefore, for the deformation from $pqrs$ to $pq'r's'$, θ must be between 0° and 45°. Hence, circle 2 is also a boundary-circle and $\sigma_1 < 2.19$ bar.

Combination of both boundary-circles imply that

$$2.02 \text{ bar} < \sigma_1 < 2.19 \text{ bar} .$$

Due to the shear stress in the interface, σ_1 in this example is about 40% larger than σ_n.

2.5.3.2 Attempts to Reduce Soil-Material Friction and Soil Adherence

For practical conditions, many attempts have been made to reduce friction on tool surfaces. Well known example are

- lubrication by adding water from an external source,
- lubrication by adding water extracted from the soil mass through electro-osmosis,
- reduction of adhesion by extraction of water through electro-osmosis,
- lubrication by air,
- replacement of sliding friction by rolling friction through rollers or conveyor belts,
- application of low wettability materials,
- slitted contact surfaces to increase normal stresses and to reduce the area where sticking can occur. Both aspects diminish the relative influence of adhesion,
- application of inert greases of high durability.

Up to now, such attempts have not been very successful for reasons of low durability, low profits, poor technical feasability, etc. If it is intended to reduce tool draft by such methods, the first step should be to examine how much reduction may be expected. This reduction is always limited because factors other than friction contribute to the draft as well. The highest reduction possible depends on tool shape, soil type, and friction properties of the conventional tool surface. Calculations of Söhne (1956) for a flat, inclined blade operating in a loam soil showed that if μ were reduced from 0.25 to 0.125, draft would decrease by 20%.

Part 3 Load Bearing and Soil Loosening Processes

3.1 General Aspects of Processes

3.1.1 Soil Tillage Processes Instead of Element Behavior

Soil influenced at a certain moment by a tool or wheel may be assumed to be composed of small volume-elements as demonstrated in Fig. 3.1 for a wheel. Such a volume element should be chosen so small, that there is an even stress distribution on each face, and at the same time the element should be so large that the soil in it may be treated as a continuum. Within such an element the state of stress does not vary from place to place but, in general, the stress state will change with time. Mechanical behavior of such elements was treated in Sections 2.1 – 2.5 as compaction, deformation, breaking, soil-material friction, and adherence, successively. Knowledge of such behavior should be obtained by *measurements.*

At a certain moment stresses will differ for different volume elements. Therefore, a situation as shown in Fig. 3.1 is called a soil tillage *process.* These spatial variations of stresses depend on the tool or wheel, the handling of the tool or wheel, and the soil. The spatial variation of the state of stress in a soil tillage process will, in general, be time-dependent. A formal definition is: "A soil tillage process of a given tool (wheel), tool (wheel) handling, and soil combination exists during the time the tool (wheel) interacts with the soil. At any moment, the process comprises the movements and forces in the soil caused by the tool (wheel)". For a maximum effect these processes must be optimized.

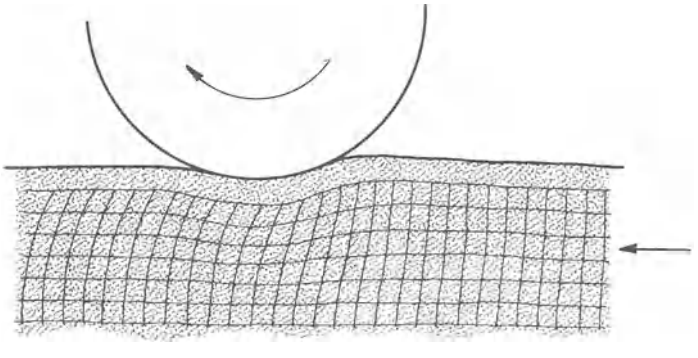

Fig. 3.1. Soil volume elements in a process

3.1.2 Description of the Variation of Forces and Movements in a Soil Tillage Process

3.1.2.1 Velocity Fields

The velocity of a soil particle in a soil tillage process can be indicated by a velocity vector, which is an arrow pointing from that particular soil particle in the direction of movement, with a length proportional to the absolute value of the velocity. Suppose that at a certain moment velocity vectors are assigned to all points of the process. If these vectors do not change with time we speak of a *steady process or flow* and if these vectors do change with time, we speak of an *unsteady process or flow*. Often a steady flow can be derived from an unsteady flow by selecting another coordinate system and redefining velocities. To illustrate this we consider the flow pattern under a roller with velocity V_0 relative to the x, y co-ordinate system in Fig. 3.2a. This is an unsteady flow field. The velocity in point (x_0, y_0) is at first zero, then increases due to the approaching roller, and becomes zero again after passage of the roller. A steady flow field is obtained by considering the u, v co-ordinate system fixed to the roller. The flow field relative to this moving co-ordinate system is shown in Fig. 3.2b. Velocity in point (u_0, v_0) that is fixed in the u, v system is independent of time because the point is fixed in a non-changing pattern. Note that the undisturbed soil has a velocity V_0 in the u, v system.

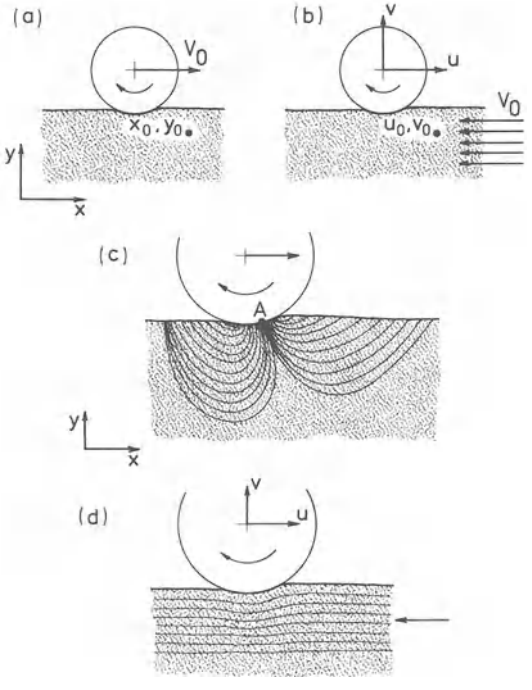

Fig. 3.2a – d. Unsteady (a) and steady (b) flow. Examples of streamline patterns for unsteady (c) and steady (d) flow

The flow system at a certain moment is sometimes presented by *streamlines.* These are curves tangent to the velocity vectors of that moment. With steady flow streamlines do not change with time. In that case, soil particles follow *streampaths* that coincide with streamlines (Fig. 3.2d). With unsteady flow a streamline pattern refers only to a single moment and there is no simple relation between streamlines and streampaths (Fig. 3.2c). Streamline patterns can be deduced easily from photographs that register the motion during a relatively large time of exposure. Another method is to provide the tool surface with a wearing finish like paint or a silicone compound. Soil particles scratch such a finish, showing the streampath pattern. Finally, it is possible to place markers on or in the soil and to determine their velocity field.

3.1.2.2 Strain Fields

Each volume-element of an instantaneous picture of a process, as in Fig. 3.1, can be subjected to a strain analysis. For each element, quantities like compaction, principal strains, and principal strain directions can be determined. By comparing such an instantaneous picture with a picture taken a time interval dt earlier, one can determine quantities like compaction rate and principal strain rates. Let us assume that the compaction of each volume-element in Fig. 3.1 is known. We can present this by numbers in the elements. In this field of numbers we can draw lines of equal density. If for each element in Fig. 3.1, direction of maximum principal strain rate is known, we can indicate this in each element by an arrow. If we now draw lines tangential to these arrows, we obtain a field of lines from which we can read the direction of maximum principal strain rates for the moment considered. To obtain an instantaneous picture as in Fig. 3.1, we will have to make a grid in the soil. This could be done, for instance, by inserting small lead balls, like hail shot, in the soil and taking instantaneous X-ray photographs while the roller passes over the soil. It is also possible to stop rolling suddenly and to dig out the balls and measure their positions. This method will always involve a certain disturbance by soil rebound and creep. Where process-boundaries coincide with soil block sides, the sides may be marked with paint. Photographs or movies may be taken from these marked sides through transparent soil bin walls.

3.1.2.3 Stress Fields

For an instantaneous picture as in Fig. 3.1, it is also possible to determine the state of stress of each element in an indirect way. The first step is to determine the strain state of the volume element. One then makes assumptions on the soil mechanical behavior (for instance, that the soil behaves as an elastic material). Using these assumptions one estimates the state of stress from the state of strain. In this way directions and magnitudes of principal stresses may be found. If for each element a quantity as the first principal stress is known, these values can be presented as well by numbers in the elements and lines (isobars) of equal first principal stress may be drawn.

3.1.2.4 Process Variations in Time

The Lagrangian Viewpoint. Variation in time can be studied by following a certain material volume element. For a volume element, changes can be considered as a function of time, and the path along which the element moves can be traced. One can draw such paths relative to the wheel or tool, or relative to the untouched soil. When the flow field is steady, the path of an element can be derived from the velocity field, and thus from an instantaneous picture.

The Eulerian Viewpoint. It is also possible to consider the process variation at a fixed point in a coordinate system, instead of following physical particles. Then, in general, soil at the considered point is continually exchanged by other soil. An example is the examination of stress fluctuating with time at the tip of a tine operating in brittle soil (implying a coordinate system fixed to the tine).

3.1.3 Basic Process Conditions

A process must satisfy three basic conditions: the mechanical property equations, the differential equations of equilibrium, and the boundary conditions.

The Mechanical Property Equations. Suppose that for the soil involved compactability, deformability, resistance against break, and soil-material friction and adherence properties are known. These mechanical properties for a volume element may be presented in the form of equations (stress-strain relations, yield conditions). Each volume element of the soil participating in the process has to satisfy these equations at any moment.

The Differential Equations of Equilibrium. A process was assumed to be composed of volume elements and the stress on a face of a volume element was assumed to be uniform, but in a process, variation is the important feature. In general, stress does vary slightly from point to point in an element. This is expressed in Fig. 3.3 for the stresses in the z-direction in the case of an incompressible material. Now it is true that, for elemental mechanical behavior, σ_{zz}, τ_{yz}, etc. are important, and not $(\delta\sigma_{zz}/\delta z)dz$, $(\delta\tau_{yz}/\delta y)dy$, etc. That is why in the mechanical property equations these increments do not appear. However, in mechanical equilibrium these variations do play a role and it turns out that σ_{zz}, τ_{yz}, etc. do not appear in the equilibrium equations of an element. Consider, therefore, the mechanical equilibrium in the z-direction of the volume element in Fig. 3.3. The sum of forces in the z-direction, df_z, is then

$$df_z = \frac{\delta\sigma_{zz}}{\delta z}\,dx\,dy\,dz + \frac{\delta\tau_{xz}}{\delta x}\,dx\,dy\,dz + \frac{\delta\tau_{yz}}{\delta y}\,dx\,dy\,dz\,.$$

The element is further subjected to the gravity force $g \times dm$ and the acceleration force $a_z \times dm$ (dm is mass of the element, g is acceleration of gravity, a_z is acceleration in z-direction). The differential equation in the z-direction is then,

$$df_z + g\,dm = a_z dm\,.$$

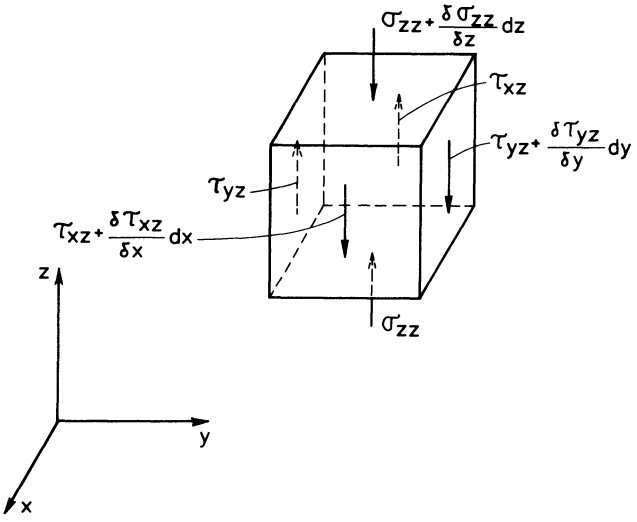

Fig. 3.3. Stresses in the z-direction on the faces of a volume element, taking into account stress variations

In this way one can also form differential equations of mechanical equilibrium for the x and y directions.

The Boundary Conditions. As a rule, external conditions are imposed on a process that must be satisfied at all times, for instance, the load on a wheel. It is also possible that rut depth is imposed. Note that both boundary conditions can not be satisfied at the same time; either one or the other applies. Plowing depth and plowing speed are other examples of boundary conditions.

If the mechanical property equations, the differential equations of equilibrium, and the boundary conditions for a process are known, it is, in principle, possible to calculate the forces and movements in the process. However, for tillage and wheel processes this is, in general, mathematically too complicated. Therefore, other methods were developed to predict forces and movements in such processes.

3.1.4 Prediction of Forces and Movements in Processes

It is useful to predict forces and movements in the process of a given tool (or wheel) that is handled in a certain way and operates in a certain soil. It is particularly useful to predict required pull, process types, and unwanted incidental effects. Such quantities to be predicted are called *dependent variables.* This section deals with prediction methods and is a summary of the work published in Koolen (1977). If we are to make predictions concerning a process, we need data on the characteristics of the tool (or wheel), the handling of the tool (or wheel), and the soil. Such characteristics are called *independent variables.*

In general, four different categories of independent soil variables can be distinguished.

Elemental Mechanical Properties, discussed in Sections 2.2 to 2.5. If these properties have been determined correctly, and if the volume elements in the process behave accordingly, then these soil data are ideal for prediction purposes.

Strength Determining Factors (soil physical factors), such as bulk density, moisture content, etc., discussed in Section 1.

Relationships Between Treatment and Behavior of the Soil. Soil behavior in a process depends on the treatment to which the soil has been subjected prior to the process in question. That treatment may consist of a series of tillage operations, wheel passes, wetting, drying, etc. A measure of soil behavior in tillage is, for example, the draft force needed in a process. Knowledge of the relationships between treatment and behavior may provide a basis for the prediction of process behavior in those cases where previous soil treatment is known.

Results of Characterization Processes, such as the cone penetrometer test, plate penetration test, determination of the Atterberg consistency limits, and drop shatter test. Such a test is relatively simple to carry out.

In order to predict one must select an existing prediction method, or develop one's own method. Two categories of prediction methods exist. The most important category is the so-called "black box" approach: the output of the box (the process) is observed for a given input, without paying much attention to what happens within the box. This category is discussed in the next section. The other category, to be discussed in Section 3.1.4.2, is mainly based on knowledge of the mechanism of the process, so on what happens within the box.

3.1.4.1 Prediction Methods Mainly Based on Observations of Relationships Between Independent and Dependent Variables

The main feature of these methods is that they involve the assumption that any dependent variable y is dependent on independent variables $x_1, \ldots x_n$ of soil, tool, and soil-tool system. This may be formulated as

$$y = f(x_1, \ldots x_n)$$

where f is the prediction function, defined for given ranges of x_i (the region delineated by these ranges will subsequently be referred to as the *domain* of f). Variables x_i should satisfy the following requirements:

- the function must be unique,
- the sensitivity of y to any x_i should be appropriate,
- no superfluous variables x_i should be involved.

The function is *unique* if, in reality, for each set $(x_1, \ldots x_n)$ only one value of y occurs. This is not the case, for instance, when the set $x_1, \ldots x_n$ does not cover all soil mechanical properties that are pertinent to the process and vary within the

domain. Then, additional variables should be introduced, which hopefully account for the overlooked mechanical properties. Scale model research has revealed many sets of $x_1, \ldots x_n$ for which the prediction functions are not unique.

The *sensitivity* of y to x_i may be represented by the differential quotient (dy/dx_i). When this quotient is large, the function can only be unique if x_i can be measured with a high accuracy. If a quotient dy/dx_i is small, x_i apparently is of little importance and can better be left out of consideration, because a prediction method generally becomes more simple as the number of x_i is reduced.

To develop a prediction method of the type under discussion, it must be decided which particular variables x_i are to be chosen. That decision may depend on many and various considerations:

Considering the Mechanical Processes to Be Mainly Determined by Soil Mechanical Properties. However true that may be in itself, this has often led to great disappointments for reasons as

- using a set $x_1, \ldots x_n$ that does not allow the function to be unique,
- underestimating the influence of speed in mechanical property measurements,
- the inability to measure soil mechanical properties correctly.

Assuming the Pertinent Soil Mechanical Properties, in Turn, to Be Completely Determined by Soil Physical Properties. Provided this is true, then the independent process variables are unique functions of soil physical properties. Use of soil physical properties may be, in prediction, advantageous since they are comparatively easy to determine. Texture, porosity, and moisture content are well-known soil physical variables. There are some cases in which soil mechanical properties are unique functions of texture, porosity, and moisture content, for instance, pure sand that has been allowed to equilibrate long enough to allow local soil moisture suction variations to disappear.

To Postulate That the Measuring Results of Characterization Processes are Preferred Because They Can Be Measured Quite Easily. This approach seems to be promising, as may be concluded from the success of predicting quantities of load-bearing processes based on cone penetrometer test results. Until now, the use of characterization processes has been limited to the prediction of a process quantity from the result of only one characterization process. Using a prediction method based on more characterization processes will be a logical development, leading to formulations as

> independent process variable $y = f$(result of characterization process 1, result of characterization process 2).

The characterization processes should be selected in such a way that each of them covers different soil mechanical properties.

In general, developing a prediction method will be easier as the number of independent variables x_i is smaller. Two methods for decreasing that number should be mentioned:

Decreasing the Number of Variables x_i by Reducing the Domain of the Problem. In that case, one or more x_i are in fact assumed to be constant. Of course, this implies that the prediction method can only be applied there where the x_i in question are equal to those constant values. Quantities that may be kept constant are:

- working depth. In agricultural practice a "most normal" working depth often exists for a tool type.
- traveling speed. A typical speed for agricultural practice may exist.
- shape of the tool.
- soil type. A prediction method which, for example, is only applicable to sandy soils, will be more simple than a universal prediction method.

Decreasing the Number of Variables by Using Buckingham's Pi-theorem. When for a process the relation between an independent variable y and dependent variables x_i can be written as

$$y = f(x_1, \ldots x_n)$$

and when the number of dimensions in which y and x_i can be measured equals b, then this theorem states that the above relation can be reduced to

$$Y = F(X_1, \ldots X_{n-b})$$

with the only restriction that Y and X_i are dimensionless and independent (Murphy 1950). Methods for calculating Y and X_i from y and x_i are given in (Murphy 1950). In tool and wheel processes force, length, and time are often the pertinent dimensions, and thus $b = 3$. Then, according to the theorem, the number of quantities that determine y can be reduced by three. This is illustrated with the following example. Sprinkle et al. (1970) state that the draft force of plane blades with a fixed length to width ratio satisfies

$$D = f(v, g, d, \alpha, \phi, \delta, c, \gamma)$$

where

D = draft force
v = traveling speed
g = acceleration of gravity
d = working depth
α = cutting angle
ϕ = angle of internal soil friction
δ = angle of soil-metal friction
c = soil cohesion
γ = bulk density of the soil.

These quantities involve the dimensions of force, length, and time. The sum of those dimensions is three and, therefore, according to the Pi-theorem, the eight independent variables can be reduced to five quantities, provided these quantities are dimensionless and independent. The following formula satisfies this.

$$\frac{D}{\gamma d^3} = F\left(\frac{v^2}{gd}, \alpha, \phi, \delta, \frac{c}{\gamma d}\right).$$

Quantities like the five in this formula are called Pi-terms. It should be realized that Pi-terms may have the disadvantage of being complex and difficult to imagine.

Prediction methods that are mainly based on observations of relationships between independent and dependent variables, may be divided into comparative methods and methods using empirical formulas or graphs.

Comparative Methods

The assumption that a process variable y depends on the independent variables $x_1, \ldots x_n$ of soil and tool, may be formulated as,

$$y = f(x_1, \ldots x_n)$$

where f is the function according to which y depends on $x_1, \ldots x_n$. When f is unknown, the above equation can still be used as a prediction method, for if it has been observed once that at certain values of $x_1, \ldots x_n$ a certain value of y occurs, then this particular value of y will be attained again when those particular values of $x_1, \ldots x_n$ re-occur. Prediction methods based on this principle are called comparative methods. Some of these will be discussed next.

Experience of the Farmer. An experienced farmer has had to make many decisions concerning tool and wheel processes in the field. He remembers relationships between dependent process variables and independent variables concerning soil and tool. These relationships usually are specific for a certain piece of land. The independent soil variables comprise those which can be sensory perceived, and those pertaining to previous treatments of the soil. However, it must be stated that this experience often does not suffice, for it happens frequently that a farmer readjusts or even stops a tillage process, based on his opinion on the desired effects.

Soil Tillage Record. The experience method may be improved by supporting memory by keeping notes, and by changing from (subjective) sensory perceptions to (objective) observations that can be quantified. Thus it is logical that on farms a soil tillage record is developed based on experience. Such a soil tillage record may be notes on quantifiable soil variables that were determined just prior to a tillage operation, on process quantities of tillage operations that were carried out, and on treatments to which the soil was subjected. When a farm consists of different pieces of land, such a record may be kept for each piece individually. The usefulness of such a record is demonstrated by the fact that soil workability limits often correspond with certain soil moisture suction values.

Mechanically Equal Soils Exhibit Equal Behavior. It appears reasonable to assume that mechanically equal soils exhibit equal behavior. This assumption leads to the following prediction method. For a series of standard soils and soil conditions a number of mechanical properties are measured and/or characterization processes performed. These properties and/or characterization processes should be selected such that each important feature of the soil mechanical be-

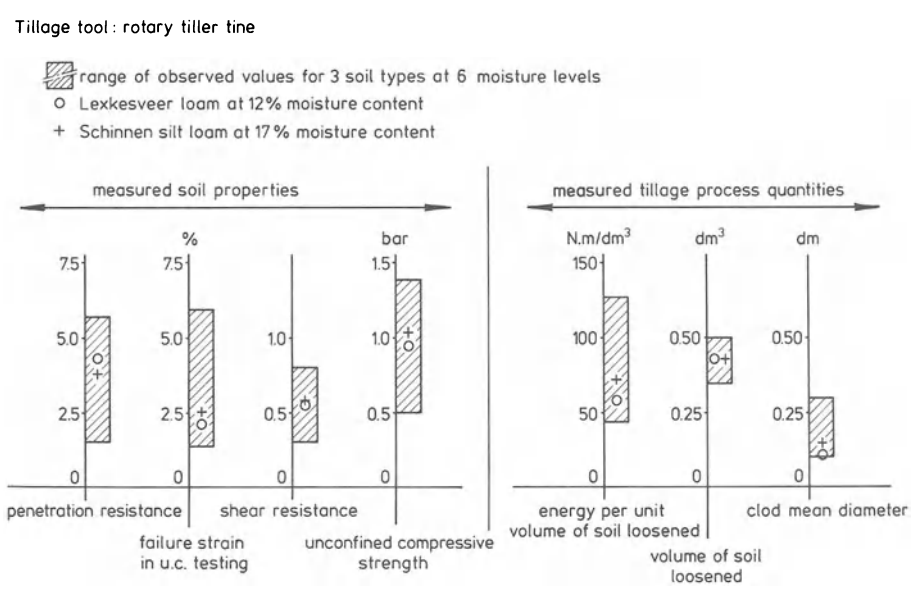

Fig. 3.4. Equal mechanical properties yield equal processes

havior is represented in at least one of these measured properties and/or characterization processes. For each standard, the pertinent tillage process variables to be predicted are also experimentally determined. Then, to predict the tillage process in question for another soil, the same mechanical properties and characterization processes must be measured to select the standard which most resembles the soil under consideration. The tillage process variables in this soil can then be assumed equal to the tillage process variables measured in the soil standard which resembles it the most.

That mechanically equal soils indeed exhibit equal behavior in tillage, was demonstrated in the following experiment. For each of three different soil types (Wageningen silty clay loam, Lexkesveer loam, Schinnen silt loam) two soil blocks were prepared at six moisture levels, giving 36 blocks in total. For each soil block the following quantities were measured:

- shear strength, using the torvane (NN 1971),
- penetration resistance, using the pocket penetrometer (NN 1971),
- unconfined compressive strength,
- the amount of strain needed to produce failure in the unconfined compression test.

The left part of Fig. 3.4 presents the ranges of these measuring results, together with the results for Lexkesveer loam at 12% moisture content and for Schinnen silt loam at 17% moisture content. This shows that these two soil conditions may be considered to yield the same mechanical behavior. Subsequently, each soil block was subjected to a tillage process in a pendulum-type impact machine, using a tine striking through the soil like a rotary tiller tool. For each tillage process were measured

- the energy consumption,
- the volume of the soil loosened,
- the mean aggregate size of the soil loosened.

The right part of Fig. 3.4 presents the ranges for these measuring results, along with the results for the two mechanically equal soil conditions mentioned above. It clearly demonstrates that mechanically equal soil conditions also yield equal tillage process quantities.

Scale-Model Testing. Scale-model testing is also a comparative method. It will be illustrated with a (very simple) example, which has the following domain:

- bulldozer blades having a given shape, a given height-width ratio, and a given cutting depth-height ratio,
- negligible velocity effects, thus excluding the dimension of time,
- mechanical behavior of soils which can be defined fully by cohesion, angle of internal soil friction, angle of soil-metal friction, and bulk density.

For this domain we may assume that

$$D = F(l, \gamma, c, \phi, \delta)$$

where D = horizontal pushing force at maximum blade load,
l = blade width,
γ = soil bulk density,
c = soil cohesion,
ϕ = angle of internal soil friction,
δ = angle of soil-metal friction.

Using the Pi-theorem this expression can be reduced to

$$\frac{D}{cl^2} = f\left(\frac{c}{\gamma l}, \phi, \delta\right).$$

Within the defined domain we consider two bulldozer blades, which will be labeled "prototype" (index p) and "scale-model" (index s), respectively. The prototype is intended to operate under practical conditions with known values of l, γ, c, ϕ, δ, for which the D-value is unknown. We want to know D but, due to the large blade size, it would be very expensive to measure D on the prototype. The scale-model, on the other hand, is very small but is well suited for the determination of its D. Using the last formula and designing the scale-model so as to satisfy

$$\left(\frac{c}{\gamma l}\right)_s = \left(\frac{c}{\gamma l}\right)_p$$

$$\phi_s = \phi_p$$

$$\delta_s = \delta_p$$

we obtain

$$\left(\frac{D}{cl^2}\right)_s = \left(\frac{D}{cl^2}\right)_p .$$

Using this equality, D for the prototype can be calculated from the value of D measured on the scale-model. The design condition

$$\left(\frac{c}{\gamma l}\right)_s = \left(\frac{c}{\gamma l}\right)_p$$

requires the scale-model soil to be different from the prototype soil, since, after re-arranging,

$$\frac{\left(\frac{c}{\gamma}\right)_s}{\left(\frac{c}{\gamma}\right)_p} = \frac{l_s}{l_p}, \text{ which is not equal to 1 .}$$

Scale-models are often run in artificial soil (oil-material mixtures), because artificial soils can exhibit the desired low c-values and have mechanical properties that do not vary much with time.

Further information on scale-model testing can be found in Wismer et al. (1976).

The Use of Empirical Formulas or Graphs

Methods using empirical formulas or graphs also start from the assumption that a dependent process variable y depends on independent variables $x_1, \ldots x_n$,

$$y = f(x_1, \ldots x_n) .$$

Again, f represents the funtion according to which y depends on $x_1, \ldots x_n$. In the methods under discussion f is known to such an extent that, within certain limits, y can be calculated for any arbitrary set $x_1, \ldots x_n$. f may be put in the form of a formula or a graph.

When f is a formula, the determination of f involves

1. assuming a general formula that incorporates $x_1, \ldots x_n$ as well as one or more (yet unknown) constants,
2. determining these constants empirically be measuring y for different sets $x_1, \ldots x_n$.

When f is a graph, the determination of f involves

1. assuming a graph shape,
2. drawing the graph from measurements of y at different sets $x_1, \ldots x_n$.

Examples of empirical formulas are presented by Perdok and van de Werken (1982) in their paper on power requirements in soil tillage. From the predictability point of view this article is interesting for two reasons. Firstly, plowing

Table 3.1. Characteristic data of drawn and multi-powered soil tillage implements

Soil tillage implement	Specific work kJ/m³	Tilth		Working depth m	Width per element m	Working speed m/s	Rps
		firm	loose				
Plow	A	×		0.25	0.40	1.5	–
Rigid tine cultivator	0.67A	×		0.25	0.25	1.5	–
Spring tine cultivator	0.67A		×	0.10	0.10	2.0	–
Oscillating harrow	1.47A		×	0.10	0.085	1.25	9
Powered rotary harrow	1.40A + 78		×	0.10	0.125	1.0	5
Rotary tiller with spikes	1.74A + 96		×	0.10	0.10	0.56	5
Rotary tiller with blades	5.64A + 22	×		0.15	0.15	0.56	3.3

is used as a characterization process to predict energy consumptions of other tillage implements as cultivators, harrows, and rotary tillers. Secondly, prediction was feasible by confining the domain of the problem to typical values of soil density, working depth, width per element, working speed, and *rps*. Table 3.1 presents their results.

Other examples of empirical formulas are Sections 3.6.3.1 and 3.6.3.2.

3.1.4.2 Prediction Methods Mainly Based on Knowledge of the Mechanism of the Process Under Consideration

These methods assume that the process under consideration is equivalent to a hypothetical process which proceeds according to a particular hypothetical mechanism. On the basis of this mechanism, values of dependent process variables can be derived from values of independent variables. Usually, such a hypothetical mechanism is composed of assumed failure patterns, compaction patterns, deformation patterns, and/or displacement (movement) patterns. For a hypothetical mechanism, dependent process quantities can be calculated using the condition of equilibrium of forces in the mechanism and conditions reflecting the elemental soil mechanical behavior.

Any method based on a hypothetical mechanism involves the following three features (which may easily be confused):

- the effectiveness of the method,
- the compatibility of the mechanism,
- the degree to which the hypothetical mechanism resembles the mechanism to be simulated.

A method is *effective* in the prediction of a dependent process quantity if for any arbitrary set of independent variables within the domain its mechanism predicts a value of this quantity which matches a measured value. Method effectiveness has to be determined experimentally. A mechanism is *compatible* if it can be realized physically and is able to function as it has been hypothesized. This is illustrated by the following example: if a hypothetical mechanism involves a frictional force in a contact surface between two lumps, and it has been hypothesized that this

frictional force is proportional to the normal force in the contact surface, then the mechanism is not compatible when this normal force is a tensile force. Many hypothesized mechanisms involve local incompatibility, which can be considered insignificant in most cases, for instance, at soil lump and tool edges. Incompatibility of the mechanism for some values of independent variables may reduce the prediction domain, but it has been shown that incompatibility does not have to affect effectiveness seriously (Witney et al. 1966). A hypothetical mechanism *resembles* the mechanism to be simulated if both mechanisms involve the same forces and movements. Almost always hypothetical mechanisms differ from real mechanisms to be simulated, because the latter mechanisms are very complex. Fortunately, large differences between hypothesized and real mechanisms need not be a serious drawback on the effectiveness of the hypothesized mechanism (Witney 1968).

Söhne's model to predict draft of a plane blade with a small cutting angle (see Sect. 2.4.3.3) is an example of a hypothesized mechanism that is composed of rigid soil bodies which may shear along each other. Mechanisms composed of rigid soil bodies have been used for

- tines (Payne 1956, O'Callaghan 1967, Hettiaratchi and Reece 1967),
- plane blades with large cutting angles and large working depth-blade height ratios (Osman 1964, Hettiaratchi et al. 1966), and
- bulldozer blades (Cook and Reece 1966).

In the mathematical theory of plasticity, mechanisms of non-rigid (plastic) soil bodies are discussed (Smits 1973, Butterfield and Andrawes 1972c, Yong 1973). In general, their predictive accuracy is low.

3.1.5 Types of Processes

In the following sections six types of processes are distinguished, namely those induced by

1. rollers, wheels and tires (Sect. 3.2),
2. penetrating bodies (wedges, cones, plates, wires, spheres) (Sect. 3.3),
3. sliding and shearing bodies (Sect. 3.4),
4. tracks, cage rollers, and cage wheels (Sect. 3.5),
5. tines (Sect. 3.6),
6. plow bodies (Sect. 3.7).

The first four types are load bearing processes and the last two loosening processes. Deformations are predominantly stable in load bearing processes and unstable in loosening processes. For each type of process the process fundamentals are discussed in the same order:

Kinematic Aspects

- kinematics of the tool or wheel itself (if its movement can be complex),
- movement at the tool (wheel)-soil interface,
- movement of the soil,

Dynamic Aspects

- forces on tool or wheel,
- forces in the interface,
- forces within the soil.

3.2 Rollers, Wheels, and Tires

3.2.1 Occurrence

Tires. Tires vary strongly in size, width-diameter ratio, tread pattern, and composition, because they are used for very different purposes requiring different tire properties. Requirements that mainly determine tire design, are

- bearing capacity. This relates mainly to tire inflation pressure and tire volume.
- strength and flexibility of the carcass (cord layers). Carcass strength is decisive for the highest allowable inflation pressure. Carcass flexibility determines the lowest allowable inflation pressure below which cord failure is likely to occur due to excessive tire deflection. These two aspects are actually conflicting.
- pull that a driven tire must be able to develop. Here, tread pattern, strength of tire side walls, and resistance against creep on the rim are important.
- sufficient heat discharge at the anticipated intensity of use and driving speed. Heat produced by deflection and recovery of a rotating tire must be discharged since rubber cannot withstand high temperatures.
- geometrical requirements. Examples are restricted width for use in row cultures or driving through open plow furrows, minimum axle height for sufficient clearance from the soil surface, sufficient height for cargo-space above a tire, sufficiently large steering angle, etc.
- prevention of excessive tire sinkage and rolling resistance in soft soils. This asks for low tire inflation pressures.
- some tire sinkage. To improve steerability in the case of unpowered tractor front wheels, for instance, rather small tires and rather high inflation pressures are used.
- sufficient stability to avoid excessive axle height variations due to in-service bumps. This is important for machines such as loaders, bulldozers, and graders.
- wear and impact endurance. This is especially important for vehicles intended to operate on rough, hard, rocky ground, such as earth movers.
- secondary tread requirements. These mainly concern prevention of problems such as clogging on sticky soil, damaging of turfs, aquaplaning of car tires on wet surfaces, etc.

Sometimes sub-optimal tires are used for economical reasons. For example, used truck and aircraft tires are often operated in agriculture at an inflation pressure that is too high regarding tire sinkage, and too low regarding deflection acceptable for the carcass.

Tire design is also strongly influenced by the ever-developing tire technology. Recent developments are

- stronger cord-materials. These result in fewer cord layers and more flexible tires which cause a more uniform stress distribution in the contact area and allow lower tire inflation pressures.
- radial ply tires. In general, these tires give a higher pull at lower slip, yield more uniform stress distributions in the contact area, and wear less, but cost more.
- so-called "low section height" tires. The height/width ratio of the cross-section of a normal tire is about one. For "low section height" tires, this ratio may be 0.7 or even 0.55. They allow for lower contact stresses and larger contact areas.

It is important to distinguish between the basic differences in design criteria for agricultural tires and automobile and truck tires. Automobile and truck pneumatic tires should provide a smooth ride and are not supposed to operate at noticable slip under normal conditions. Agricultural tires, being used on soft underfootings, should have a lower rolling resistance than comparable rigid wheels. For lower rolling resistance, inflation pressure should be decreased when the underfooting is soft, and increased when the underfooting is rigid and smooth (like a highway). Agricultural drive wheel tires, used in operations like plowing, etc., normally slip at a rate of approximately 15%. Here slip has a regulating function: when the drawbar load increases incidently due to field heterogeneity, slip increases, making the drawbar pull increase and forward speed decrease, so that the increase in engine power demand is relatively moderate.

Each field of application has its own tire assortment. This also holds for agriculture where very small as well as very large tires are used. In the smallest sizes there are hollow tires that are used un-inflated (semi-pneumatic tires) and solid tires. A classification of agricultural tires is given in Table 3.2, along with current tire inflation pressures. It should be noted that, to prevent wider tires from creeping on the rim at high pull, they should be inflated to a minimal pressure around 1.1 bar. Tires currently in use in the USA have been listed by the American Society of Agricultural Engineers (NN 1981). A few drive wheel tractor tires are given in Table 3.3, along with characteristic data. Table 3.4 shows some tires produced by a European company for trailers and farm implements. The lower part of this table shows tires exclusively intended for use on hard ground, involving a height to width ratio of the tire cross sections that is larger than in the upper part of the Table. Large trailer tire sizes are more current in Europe than in the USA. Sizes of semi-pneumatic tires can be found in the ASAE standards S 223 and S 224.1 (NN 1981).

Table 3.2. Current agricultural tire inflation pressures

Drive wheel tractor tires	0.8 – 1.7 bar
Tractor steering wheel tires	1.4 – 2.5 bar
Trailer and implement tires	1.5 – 3.5 bar
Semi-pneumatic tires	–

Table 3.3. Characteristic data of some current drive wheel tractor tires

Tire size	Tire width (cm)	Diameter (cm)	Maximum tire load at 1.1 bar inflation pressure (kg)	Maximum drawbar power (kW) (approximately)
14.9 – 28	37.8	135.0	1405	<30
16.9 – 30	42.9	147.5	1730	30 – 39
16.9 – 34	42.9	157.5	1830	40 – 49
18.4 – 34	46.7	164.5	2250	50 – 70
18.4 – 38	46.7	175.0	2380	>70

Table 3.4. Characteristic data for some agricultural trailer and implement tires

Tire size	Ply rating	Section height / section width	Tire width (cm)	Diameter (cm)	Static loaded radius (cm)	Tire load limits at extreme inflation pressures (kg-bar)	
10.0/75 – 15	6	0.75	26.4	76.0	34.4	880 – 1.50	1120 – 2.25
	8					1120 – 2.25	1330 – 3.00
	10					1330 – 3.00	1525 – 3.75
20.0/70 – 20	16	0.70	50.8	122.0	55.0	4000 – 2.00	5225 – 3.25
11.00 – 16	6	≈1	27.7	93.7	41.0	1155 – 1.25	1405 – 1.75
	8					1405 – 1.75	1760 – 2.50
	10					1760 – 2.50	1995 – 3.00

There is a large variation in agricultural tire tread patterns. Important tread patterns for *driven* tires are

- sports field tread (Fig. 3.5a). This tread has many low lugs and hardly damages a grass turf. It is easily clogged and cannot produce high pull. It is well suited for mowers on sports fields and in parks.
- road-field tread (Fig. 3.5b). This tread has a relatively large number of low lugs, which are often thicker near the center of the tire than at the sides. On the road this provides good traction and low wear. The tread does less damage to grassfields than the general purpose tread (below) and on loose sandy soil has a lower tendency to dig in. Clogging may be a problem on sticky soil. The tread is well suited for road transport and for use on grassland and loose, not sticky, sandy soil.
- general purpose tread (Fig. 3.5c). The lugs of this tread are spaced wide enough to prevent clogging on most circumstances. Except for very wet clay, grip on the soil is good. Grass turf damage as well as the tendency to dig in are within acceptable limits. A few companies offer comparable treads with slightly higher and wider spaced lugs, which produce higher pull on wet sticky soils.

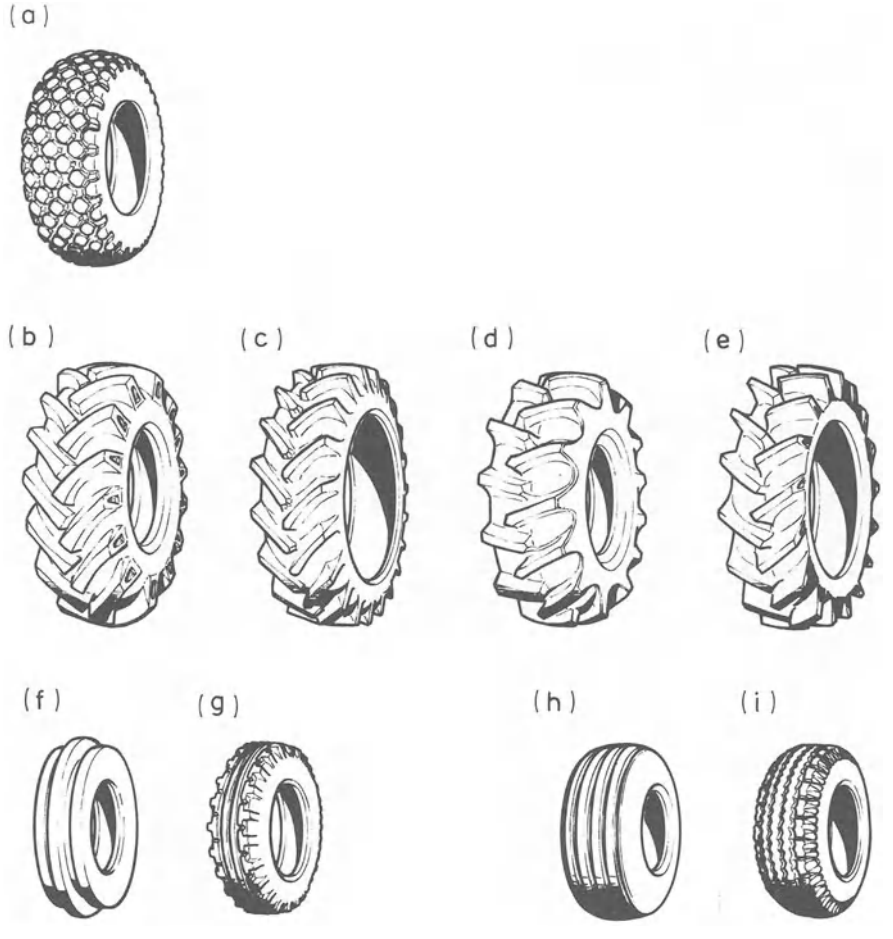

Fig. 3.5a – i. Current agricultural tire tread patterns

- low lug angle tread (Fig. 3.5d). This tread, being a variation of the general purpose field tread, has lugs at a smaller angle to the wheel axis (23° instead of 40° – 45°). This somewhat increases pull on non-sticky soils, but it also increases the tendency to dig in and to clog. Moreover, the risk of slide-slip on sloping is higher. This tread gives a less smooth ride on roads than the general purpose field tread. It is well suited for loamy sand and grassland.
- tread with high lugs (Fig. 3.5e). The high, widely spaced lugs of this tread penetrate deeply into loose or wet soil, and clogging hardly occurs. Therefore, grip is relatively good on wet, sticky soil. In field operations in the spring the tire "walks" on the lug tops, especially in the case of duals, and its action strongly resembles that of cage wheels. High lugs tend to bend at high pull on hard soil, which increases wheel slip. Bumping and high wear during road use can be prevented by lowering the inflation pressure until the lugs make contact with the road over the full width of the tire.

Towed front steering wheels (Fig. 3.5 f) require tires having one or more longitudinal ribs to allow accurate steering. Sometimes small climbing lugs have been added to make it easier to get out of a deep, hard rut, or to climb onto an elevated path (Fig. 3.5 g). Tires for trailers and farm implements do not usually need to produce pull; the main tasks of their treads are to prevent side slip and to maintain grip on braking. Besides their usual treads with rounded shoulders (Fig. 3.5 h), a zig-zag tread with sharp shoulders often occurs (Fig. 3.5 i). Semi-pneumatic tires normally have a smooth tread.

Finally, it should be mentioned that nearly all tire manufacturers publish tire tables containing much useful information.

Rigid Wheels. Depth control wheels, pressure wheels, and supporting wheels mostly are rigid steel wheels without tires. Important differences between tires and rigid wheels are:

- rigid wheels have a higher rolling resistance on soft soil than tires of comparable size.
- rigid wheels have maximum stability.
- rigid wheels cannot absorb shocks, which is a problem especially on hard ground.
- rigid wheels are not "self-cleaning", like tires. Therefore, they are often equipped with scrapers.
- rigid wheels are very reliable and require little care.

The rim of rigid wheels may be shaped in different ways. Often, the cross section is symmetrical, the shoulders rounded, and the middle of the rim exhibits a longitudinal welded joint. Asymmetrical cross sections occur for certain applications. A thin, high collar may be present along the circumference to penetrate the soil in order to resist side forces, or to improve steerability.

Rigid Rollers. Rigid rollers with closed surfaces are often used to control depth, to compact soil, or to ballast an implement and make it heavier. Sometimes stress in the contact area is increased using water-filled rollers. In general, stresses in the contact area of rigid rollers are much lower than those of tires or rigid wheels. Rollers may be powered to prevent soil from adhering to them and tearing up the surface. Sometimes, roller treads are provided with aids, e.g. cams.

Wheel–Roller Hybrids. Hybrids of wheels and rollers are used in seedbed operations. They consist of a series of wheels on a joint axle, making them roller-like implements. The wheels can rotate independently, which allows a certain self-cleaning and is easy in making turns. Sometimes scrapers are mounted. These hybrids are known as land rollers, roller packers, cultipackers, soil pulverizers, clod busters, plow packers, subsurface packers, etc. In addition to compaction, they are also used for crust breaking, clod breaking, leveling, mixing, and loosening and roughing the top layer. Two groups can be distinguished:

1. Hybrids without appreciable space between the wheels. The rim of each wheel can be *V* shaped or serrated. Sometimes, such wheels alternate with sprocket-tooth wheels mounted with very large clearance around the axle (Cambridge rollers).
2. Hybrids with much space between the wheels. Examples of these are treaders, of which the wheels have backwards-bent tines and an angled gang. Many packers also belong to this group, especially those that are intended to compact the lower layers of plowed soil.

For the moderate climate of West Europe an optimal subsurface packer was developed having the following characteristics:

wheel diameter:	70 cm
width of each wheel:	3 cm
spacing of wheels:	15 cm
weight:	400 – 600 kg/m.

Systems of Tires, Rollers, and/or Wheels. The hybrids mentioned above might also be classified as systems of tires, rollers and/or wheels. Several rolling elements may operate in one system. Examples are the tires of a tractor, tandem wheels of a trailer, and duals on a tractor. The towed front wheels of a tractor, followed by the drive wheels, followed on their turn by the tires of a trailer or implement, may also be considered as a system.

3.2.2 Fundamentals

3.2.2.1 Kinematic Aspects of Rolling Elements

State of Movement

Rollers, wheels, and tires can move in different ways. They may or may not rotate, the axis may move forward, or backward, or not translate at all. In the case of rotation and a translating axis, the most important aspect of the movement is the phenomenon of slip. This is usually expressed as the *slip percentage* defined as

$$S = \left(1 - \frac{V_{act}}{V_{th}}\right) \cdot 100\%$$

where S is slip percentage, V_{act} is actual forward speed of the axis, and V_{th} is theoretical forward speed of the axis, being the speed when slip is zero. For a rigid element on a hard surface, the definition of zero slip is very straightforward: no slip occurs at the line of contact between the element and the ground (Fig. 3.6a). For a rigid element on a soft soil, developing a significant rut, slip is defined to be zero if no slip occurs at the contact line between the element and a hypothetical plane AB (Fig. 3.6b). For situations involving tire deformations at the contact zone in vertical and horizontal directions (Fig. 3.6c), the definition is

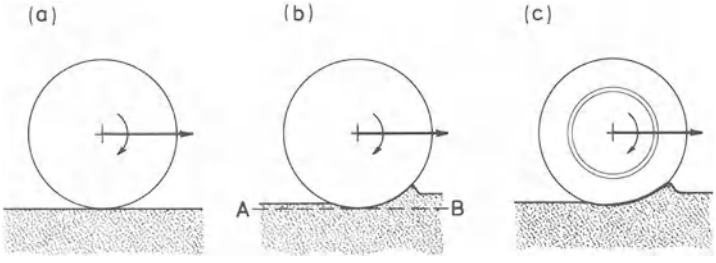

Fig. 3.6a – c. Illustrations of definitions of zero-slip

more complicated. Then zero-slip may be defined by one of the two following conditions (ASAE R 296.1 (NN 1981)):

1. The self-propelled point, which is the condition when a driven wheel develops no pull.
2. The towed point, which is the condition when the wheel axle exerts no torque to the element.

These two conditions are not the same and thus, when slip percentages of tires are presented, one should indicate to what condition they refer. Other zero-slip conditions are sometimes defined for practical reasons. In the case of tractor tires, for instance, the zero-slip condition is sometimes defined as that when the tractor rides on soft grassland without exerting a pull.

The slip percentage can be positive as well as negative. Negative values occur on braking, and with towed rigid wheels under a vertical load on soft soil.

Apart from using the slip percentage, slip can also be described using the effective radius or the instantaneous center of rotation. The *effective radius* r_r of a roller, wheel, or tire moving on soil is the radius of an imaginary, equivalent, rigid wheel having the same angular velocity and V_{act} as the element considered, but rolls without slip. So, $2\pi r_r n = V_{act}$ (n is number of revolutions per second of the rolling element), and effective radius r_r equals $V_{act}/2\pi n$. From $V_{th} = 2\pi r n$ and $S = (1 - V_{act}/V_{th})\,100\%$, it follows that

$$r_r = r\left(1 - \frac{S}{100}\right).$$

(Note. This relation does not apply to S as defined for deflected tires.) The equivalent, rigid wheel with imaginary radius r_r rolls without slip on a imaginary plane. The line of contact between this plane and the equivalent wheel (I in Fig. 3.7) is called the *instantaneous center of rotation*, since the instantaneous movement of each point of the rolling element is actually a rotation about this contact line. The above formula indicates that $r_r < r$ if the slip percentage is positive, and $r_r > r$ if the slip percentage is negative. If the slip percentage is positive the rolling element proceeds slower than would be expected from its size; the wheel seems to be smaller than in reality. For negative slip percentages the reverse is true. Note that the effective radius or instantaneous center of rotation

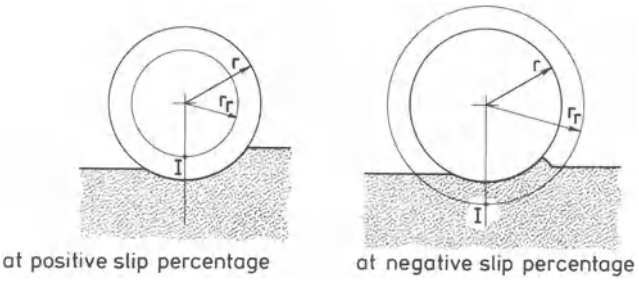

Fig. 3.7. Effective radius r_r and instantaneous center of rotation I of a roller with radius r

defines the slip phenomenon for tires more uniquely than the slip percentage does.

Tire deformation at the contact zone is rather complicated. It is discussed in the next section.

Contact Zone

To understand better the movements at the area of contact between element and ground, we will distinguish three cases: tires on hard surfaces, rigid rollers or wheels with sinkage, and tires with sinkage.

Tires on Hard Surfaces. A tire rolling on a hard surface deflects and becomes wider. Tire width reaches its maximum at some distance above the surface. The flattening involves a compression of the tire tread rubber. It deforms and rebounds as the wheel rolls further. This phenomenon is called *wriggling* and contributes to the slip. When a tire must develop more pull, the contact zone lags more behind the rest of the tire. If pull becomes extremely high, the sides of the tire may *buckle* leading to carcass failures.

Wriggling is accompanied by small relative movements between the tire and the supporting surface in the contact area. It is the major cause of tire wear. These relative movements increase with increasing torque on the tire, which also contributes to the slip. If the supporting surface is not completely rigid, the relative movement may make a thin soil layer move backwards. This backward soil movement can be large; in the case of a high slip percentage, it equals about the length of the contact area.

The shape of the contact surface depends on tire deflection. In general, the surface is slightly shorter and wider than would follow from an imaginary, intersecting plane between the tire in its unloaded shape and the supporting surface. The shape of the contact surface depends on the tire type but mostly resembles an ellipse (in the case of diagonal ply tires) or a rectangle (in the case of radial ply tires).

The shape and area of the contact surface that is obtained when a non-rolling tire is let down vertically onto a surface, is slightly different from that of a rolling tire.

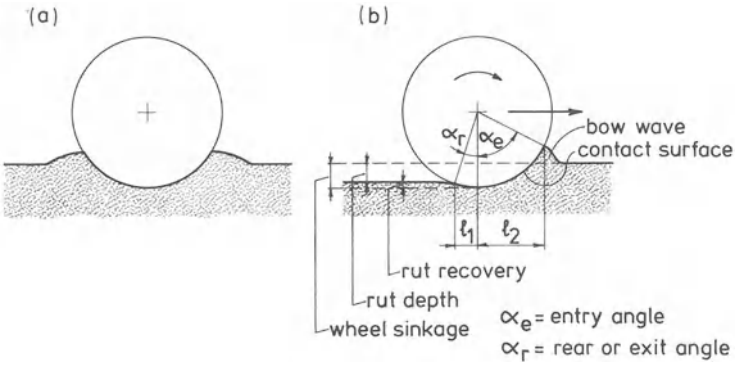

Fig. 3.8a, b. Sinkage of a roller. (a) let down vertically, (b) travelling

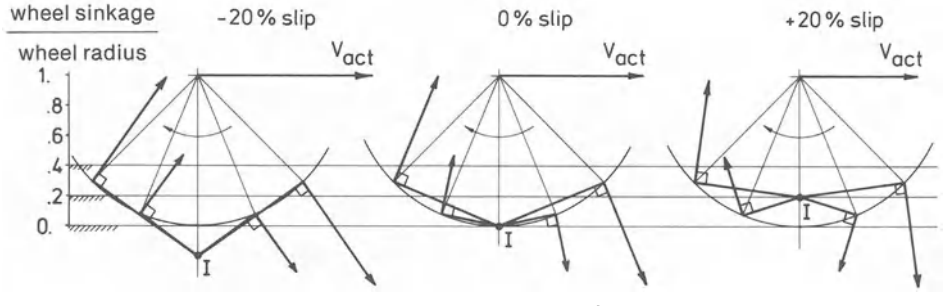

Fig. 3.9. Velocity vectors at equal angular speed

Rigid Rollers or Wheels with Sinkage. Figure 3.8a shows the cross section of the impression that is obtained when a non-rotating, rigid roller is let down vertically onto a soft soil. An entirely different cross section is found when the roller is moving over a soft soil (Fig. 3.8b). The figure also gives usual terms and symbols.

The direction of movement of a small roller surface element can be found from the instantaneous center of rotation, and thus from the slip percentage. To do this, a line is drawn between the center of the surface element and the instantaneous center of rotation. The instantaneous direction of movement is then the direction of a vector acting in the middle of the element and being perpendicular to this line. For slip percentages of -20%, 0% and $+20\%$, a few of these directions of movement are given in Fig. 3.9. Note the variation in the angle between the vector of movement and the normal of such an element.

The path that a roller surface element follows when the roller rolls over the soil surface is a cycloid, which can be found easily in a graphical way. In Fig. 3.10, a number of cycloids are given.

The movement of soil particles in the contact area depends on roller smoothness. It is often tried to avoid relative movement between roller and soil. For this the roller surface is made rough, for instance by providing it with cams. If there

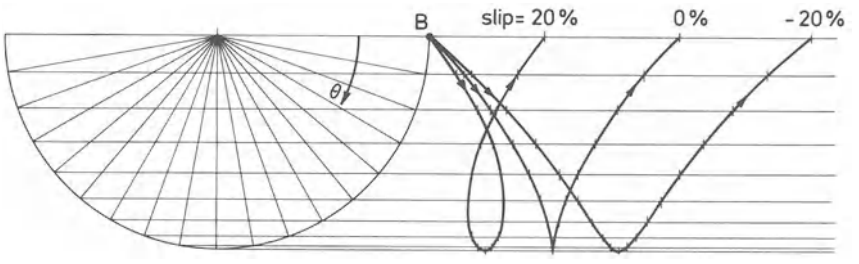

Fig. 3.10. Path of point B during a half wheel rotation, at different slip percentages. Horizontal path length projection = $(1 - s)r\theta + (\cos\theta - 1)r$ (s = slip percentage/100)

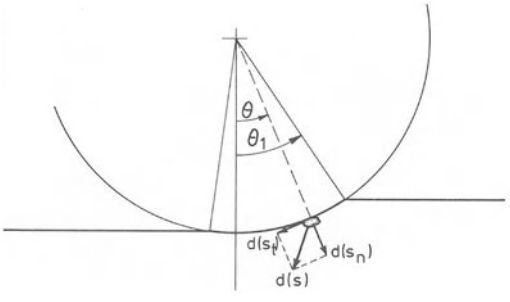

Fig. 3.11. Tangential displacement of soil particle

is no relative movement, the soil particles in the contact area will follow parts of cycloids as indicated in Fig. 3.10. Certain characteristics of such soil particle movement can be calculated, e.g. the *tangential displacement*. The tangential displacement of a soil particle against the wheel circumference (Fig. 3.11) will be referred to as J. A small displacement $d(s)$ of the particle can be resolved into a tangential component $d(s_t)$ and a normal component $d(s_n)$. Then tangential component $d(s_t)$ is equal to the increase of the tangential displacement dJ. J can be found as a function of θ by integrating over dJ. J increases with decreasing θ. Such integrations are given in Onafeko and Reece (1967), Wong and Reece (1967), and Janosi (1962). The simplest solution is that of Wong and Reece (1967):

$$J = r((\theta_1 - \theta) - (1 - i)(\sin\theta_1 - \sin\theta))$$

where θ_1 and θ are as indicated in Fig. 3.11, i is slip percentage/100 and r is rolling radius. For instance, for a very inflated, not deflected 11 – 38 tire on soft soil with a rut depth of 20 cm, r = 76 cm and θ_1 = 45°. If, in addition, θ = 0, then J = 19 cm for i = 25%, and J = 33 cm for i = 50%. Besides the tangential movement, the horizontal projection of the backward movement can be calculated as well. This can also be determined graphically with cycloids as those in Fig. 3.10. When there is no relative movement between a roller and a soil particle in the contact area, a tendency for such movement will still exist. At high positive slip percentages, such a particle tends to lag behind roller surface elements or, stated differently, it tends to move relative to the roller surface in the direction of travel. At high negative slip percentages soil particles tend to move relative to the roller

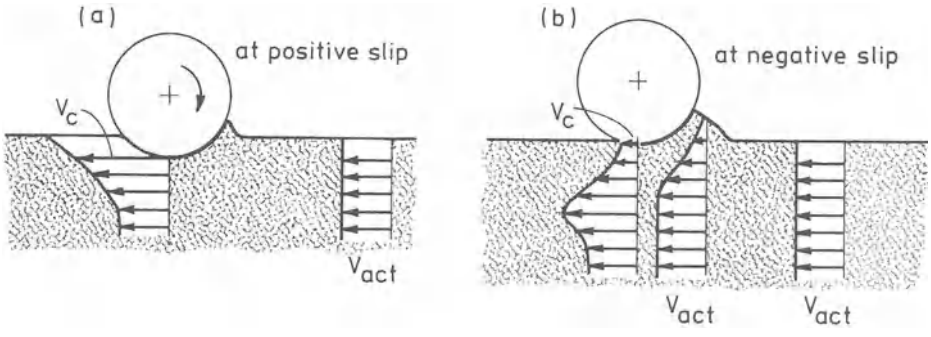

Fig. 3.12a, b. Velocity profiles deduced from continuity considerations

surface in a direction opposite to the direction of travel. Between these two cases there is a transitional range of slip percentages (including the towed condition) characterized by a contact area with two zones; a rear zone in which a tendency exists to move backwards, and a front zone in which this tendency is directed forward.

Relative movement, or sliding in the contact area, can arise with relatively smooth roller surfaces, relatively high slip percentages, and with clogging of roller treads (then the contact area is acutually a failure plane in the soil). The direction of relative movement follows from the movement tendencies as described above. It should be noted that though there is relative movement, the contact area may involve a zone where such movement does not occur. Such zone is then a central part of the contact area. Knowledge about relative movement in the contact surface is very limited yet.

Consideration of continuity requirements is very instructive when studying rut formation by rolling elements that are *infinitely wide.* If the soil is incompactible, application of the law of continuity (or of conservation of mass) leads to the following conclusions (see Fig. 3.12):

- after passage of an infinitely wide roller the soil surface is exactly at the same height as the untouched soil surface ahead of the element.
- if we consider an infinitely wide roller with a fixed axis and with the soil flowing toward the roller, the horizontal component of soil velocity varies with depth as is given for positive slip in Fig. 3.12a (because of positive slip, $V_c > V_{act}$). This velocity distribution must be accompanied by a sinkage of the surface under the roller. However, since the final soil level has to be unchanged, rut recovery must occur. This is achieved by the pumping action of the positively slipping roller.
- for a towed, infinitely wide roller, slip is negative, so $V_c < V_{act}$ and sinkage is not to be expected (Fig. 3.12b).

When the soil is compactible, permanent decrease in soil surface height or final rut depth, is a measure for the amount of compaction caused by the infinitely wide roller.

The quotient l_1/l_2 as defined in Fig. 3.8b is variable. Factors of influence are slip percentage, soil elasticity (the more recovery, the greater l_1), soil compactibility, and rut depth.

If we shift from infinitely wide rollers to wheels having *finite widths*, relative movements at the contact zone may have lateral components. Soil that has moved aside cannot contribute anymore to refilling of the rut; wheel sinkage is accompanied by less rut recovery and the *final rut depth is no longer a unique measure for compaction.* Recovery in the center of the rut is greater than near the sides. If after passage of the wheel a rut is left with the soil surface on both sides being bulged up, compaction is likely to be small but soil distortion is large. If a rut remains without bulges at the sides, much compaction occurred.

Tires on Soft Soil. Tires moving on soft soil deflect as well as sink to a certain extent. The process in the contact zone exhibits aspects of a tire on a rigid surface as well as aspects of a rigid wheel with sinkage. The higher the tire inflation pressure and/or the weaker the soil, the less the problem resembles the former and the closer the latter case. It is difficult to measure the shape of the contact surface of a moving tire (Gill and VandenBerg 1967). The few available data suggest a complicated arched surface. Figure 3.13 shows a few lines of an example of such a contact surface. The shape of curve AB, d, l_1, and l_2, as affected by inflation pressure, slip percentage, and soil hardness, were investigated by Freitag and Smith (1966). The depth d increases with increasing inflation pressure, increasing slip percentage, and decreasing soil hardness. The ratio l_1/l_2 decreases with increasing inflation pressure, increasing slip percentage, and decreasing soil hardness. A smaller l_1/l_2 ratio means that a smaller portion of the total contact length is behind the center line of the tire. The projected contact length $(l_1 + l_2)$ increases slightly with increasing inflation pressure, increasing slip percentage, and decreasing soil hardness. Note that the deepest point of the contact surface is not on the vertical through the axle.

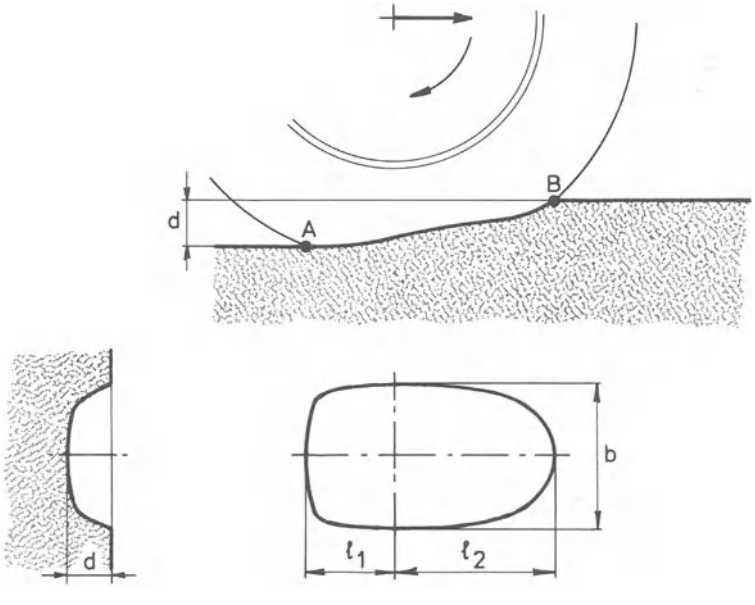

Fig. 3.13. Deflected tire-soft soil interface

Soil Movement

The movements of soil particles under and beside a rolling element are largely determined by

- the "foot print" of the rolling element (sinkage and shape of contact surface),
- the slip percentage,
- the geometry of the rut and the bulges left behind.

These all are geometric quantities. If one of these quantities changes significantly, the movements of the soil particles will also change. With infinitely wide rollers, soil movements only occur in vertical planes parallel to the direction of travel. With wheels and tires soil movements, in general, also have lateral components; only the movements of particles in the vertical plane of symmetry perpendicular to the wheel axis involve no lateral components. Therefore, the soil movements under infinitely wide rollers can fully be described by considering only one arbitrary plane, perpendicular to the axis of the roller. For wheels and tires, one mostly considers only the plane of symmetry perpendicular to the axis and the vertical plane including the wheel axis. In this way soil movements are only partly described. Describing soil movements is simplified considerably if movements of soil material points are distinguished from deformations (strains) of soil volume elements.

Movement of a Soil Material Point. Consider a point in the vertical plane of symmetry perpendicular to the axis of the rolling element, being in the sphere of influence of the element. Due to the passing of the rolling element, the point describes a path in the symmetry plane. The general shape of such a path is one of the curves of Fig. 3.14, being drawn relative to the untouched soil. When the roller has approached to where the point starts being influenced, the point starts to move forward and upward from position *i*. When the point is about under the front of the contact area, its movement changes into a forward and downward direction, followed by a backward and downward movement. Approximately under the axis, the direction of movement becomes backward and upward. The point leaves the sphere of influence of the rolling element at *f*. Thus, *i* is the initial position and *f* the final position of the considered point. The projected distance *j* between *i* and *f* is related to the slip percentage. *f* is ahead of *i* at negative slip and behind *i* at positive slip. When the slip percentage is close to zero,

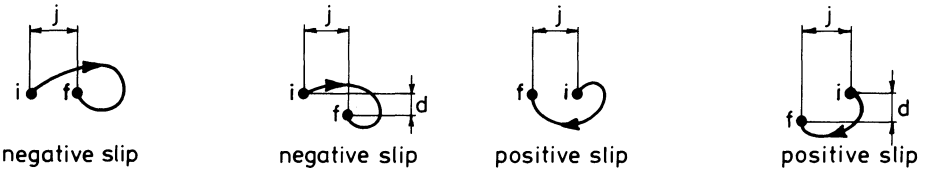

Fig. 3.14. Movement of a soil material point relative to the untouched soil, due to a roller passing from *left* to *right*

j will be very small. The deeper the element sinkage, the lower f will be than i. Several authors give such paths (McKibben and Green 1940, Gliemeroth 1953, Karafiath and Nowatzki 1978, Wong and Reece 1967).

A general picture of the streamlines under a rolling element, relative to the untouched soil, is given in Fig. 3.2c. This field of streamlines moves together with the rolling element and is therefore not a steady field. Two zones may be recognized, touching each other in A (point of separation). With increasing slip, A moves to the right. When the rolling element is being braked so that it translates without rotation, the rear zone will disappear and soil will pile up ahead of the braked element. The element together with the piled up soil then act as a vertical blade. There is no front zone when the slip percentage is 100%.

Figure 3.2d shows streampaths relative to the axis as if the soil moves instead of the axis. The flow is steady and, therefore, streampaths are also streamlines.

Deformation of Soil Elements. The movement of a single point tells nothing about the deformation of soil. For this we have to consider the movement of more points, not too far apart. The easiest way is to assume that the untouched soil is composed of small cubes, and to follow the deformation of such a cube (soil volume element) as the rolling element passes by. For this we only need to follow the positions of the corner points. Figure 3.15a shows subsequent stages of deformation of a soil element during the passage of a roller, when the undisturbed soil is considered not to move. Figure 3.15b shows the same deformation

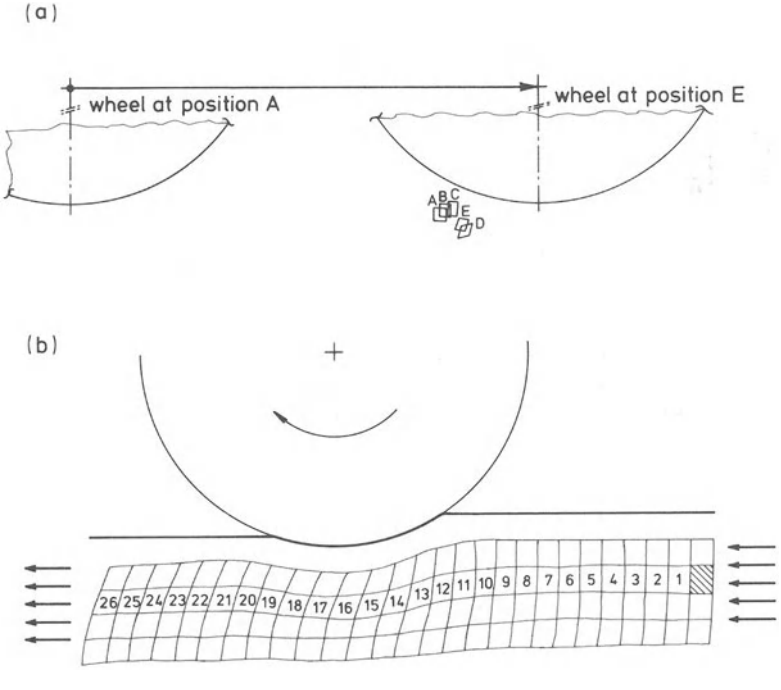

Fig. 3.15a, b. Displacement and deformation of a soil volume element relative to the untouched soil (a), and relative to the roller axis (b)

process, but now the axis is considered not to move. This figure should be interpreted as follows. The shaded soil element is yet undisturbed but as it flows toward the roller with a velocity equal to the roller traveling speed, the soil element is deformed by the roller. A series of positions and corresponding shapes have been drawn and numbered. The time interval between two successive numbers is equal to the traveling speed divided by the original soil element length. The influence of the roller ends at about position 21. Then again, the soil element flows with unchanging shape at a velocity equal to roller traveling speed.

Because the picture of Fig. 3.15b is steady, its determination is relatively easy. Although the picture as such is not an instantaneous picture, it can be obtained from an instantaneous picture of the soil interior, provided with an internal grid, when taken at the moment the roller is passing by. The reason for this is, of course, that all numbered elements, successively, behave identically. The accuracy of determining the deformation of an element can be relatively high, because observations for one element can be smoothed with observations from neighboring elements. A figure like 3.15a can be constructed graphically from a figure such as 3.15b.

Figure 3.15b is also well-suited for a strain analysis, that is the determination of strain quantities as volume change, changes in lengths of the sides, and angular change of an element. Such quantities can be represented in a similar picture, which shows the course of such quantities for an element during the time the roller is progressing. The same holds for derived quantities as ε_1, ε_3, γ_{max}, $\dot{\varepsilon}_1$, $\dot{\varepsilon}_3$, $\dot{\gamma}_{max}$, and rate of volume change. One then obtains a so-called field of a strain quantity. A few of such fields are presented by Chancellor and Schmidt (1962) and by Yong (1969).

Often strain analyses are less complete. For instance,

- only relatively large strains are determined, requiring a smaller accuracy in their determination,
- only the final volume change is measured from core samples under and to the side of a rut, after the rolling element has passed.

One should be aware that essential information may be missed in these cases. For instance, determination of the final γ_{max} tells nothing about the real distortions, since distortions occurring in front of the axis partly vanish due to distortions occurring behind the axis.

Important features of soil strains under wheels, rollers, and tires are

- ε_1 decreases with depth and γ_{max} reaches a maximum at a certain depth,
- compaction decreases with depth, or has a maximum at a certain depth. The latter case may be caused by a sensitivity of the soil to γ_{max} (Chancellor 1976).

3.2.2.2 Dynamic Aspects of Rolling Elements

Forces and Torques

Figure 3.16a shows a towed element carrying a vertical load W over a field. For this a pull P is required, because the element is subjected to a counteracting force

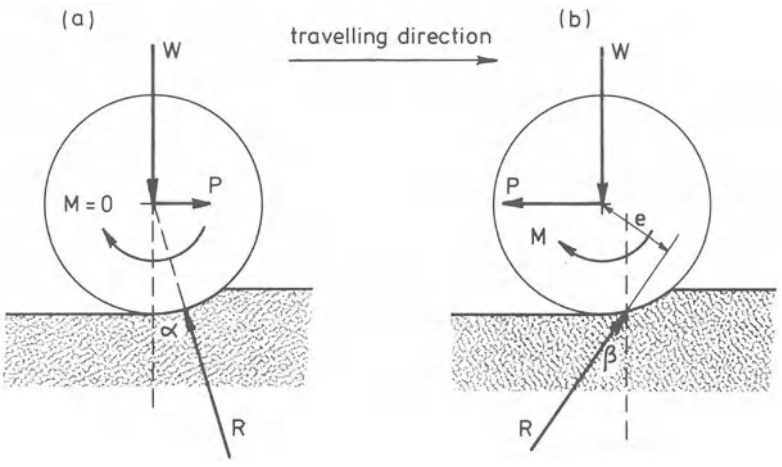

Fig. 3.16a, b. Forces acting on a transport device (a) and a traction device (b)

R in the contact surface. If friction at the axle is neglected, the torque on the wheel is zero. This means that R passes through the axis. The equilibrium of forces in horizontal direction implies that P must be equal to the horizontal component of R. This component is called *rolling resistance.* Force equilibrium in vertical direction means that the vertical component of R must equal W. As the field becomes more difficult to pass over, α and R increase, making also P increase. As W increases, R, and therefore P, will also increase. W divided by P, equal to the horizontal component of R, is called *coefficient of rolling resistance.*

Figure 3.16b shows a powered element intended to develop a *drawbar pull P.* For this a torque M must be applied to the axle to produce P, as well as to overcome the counteracting force R in the contact surface. The wheel must push itself off, so now the reaction force R is directed forward. When axle friction is neglected, torque $M = e \cdot R$. Equilibrium of force components requires that P is equal to the horizontal component of R, and that W is equal to the vertical component of R. As more pull is required, β and R increase. However, P cannot exceed a maximum, which depends on W. In general, the maximum value possible for P increases with increasing W, but W cannot be increased to an unlimited extent. As W increases sinkage interferes more and more with a proper action of the rolling element. P can also be limited by a limitation of the available torque M. Then, the engine of the vehicle stalls.

Considerations of conservation of energy for the powered pulling element leads to the following important quantities: apparent rolling resistance, thrust, and power efficiency. For a single revolution of an element with effective radius r_r:

$$\text{supplied energy} = 2\pi M$$

$$\text{drawbar energy} = 2\pi r_r P$$

$$\text{energy loss} = \text{rolling resistance energy} = 2\pi(M - Pr_r).$$

Apparent rolling resistance (force) S is defined as

$$S = \frac{\text{rolling resistance energy}}{\text{distance of travel}} = \frac{2\pi(M - Pr_r)}{2\pi r_r} = \frac{M - Pr_r}{r_r}.$$

The meaning of this quantity becomes clear when transforming the formula to

$$P = \frac{M}{r_r} - S.$$

M/r_r is called gross tractive effort or *thrust. Power efficiency* is

$$\frac{\text{drawbar pull energy}}{\text{supplied energy}} = \frac{2\pi r_r P}{2\pi M} = \frac{P}{M} r_r.$$

If required, r_r in the formulas can be replaced by a term that includes the slip percentage, s. For example by

$$r_r = \frac{V_{th}}{2\pi\omega}\left(1 - \frac{s}{100}\right)$$

where ω is angular speed. This term can be derived from

$$r_r = \frac{V_{\text{act}}}{2\pi\omega}, \quad \text{and} \quad V_{\text{act}} = V_{th}\left(1 - \frac{s}{100}\right).$$

One should be aware that, for $s = 0\%$, S does not need to be zero and power efficiency 1. The rolling resistance energy is dissipated in tire deformations, soil deformations and frictional movements in the contact surface.

The behavior of a towed tire is completely characterized by

unloaded tire diameter,
unloaded tire width,
inflation pressure,
traveling speed,
composition, construction, and tread.

Figure 3.17a shows the relation between P and W for a towed tire for different field conditions. Rolling resistance P is strongly dependent on the underfooting and W. The coefficient of rolling resistance also depends strongly on the underfooting, but less on W. The curves are bounded at the right, because the load W is at its maximum when the tire deflection is at its allowed maximum. With a larger tire size, the curves move to the right and upwards. Also, for a given W, P will be smaller. A higher inflation pressure raises the curves, while the curve bounds at the right also occur at higher W values. However, there is a maximum admissible pressure which depends on the tire carcass construction and increases with ply rating. The curves are slightly influenced by tire tread and traveling speed.

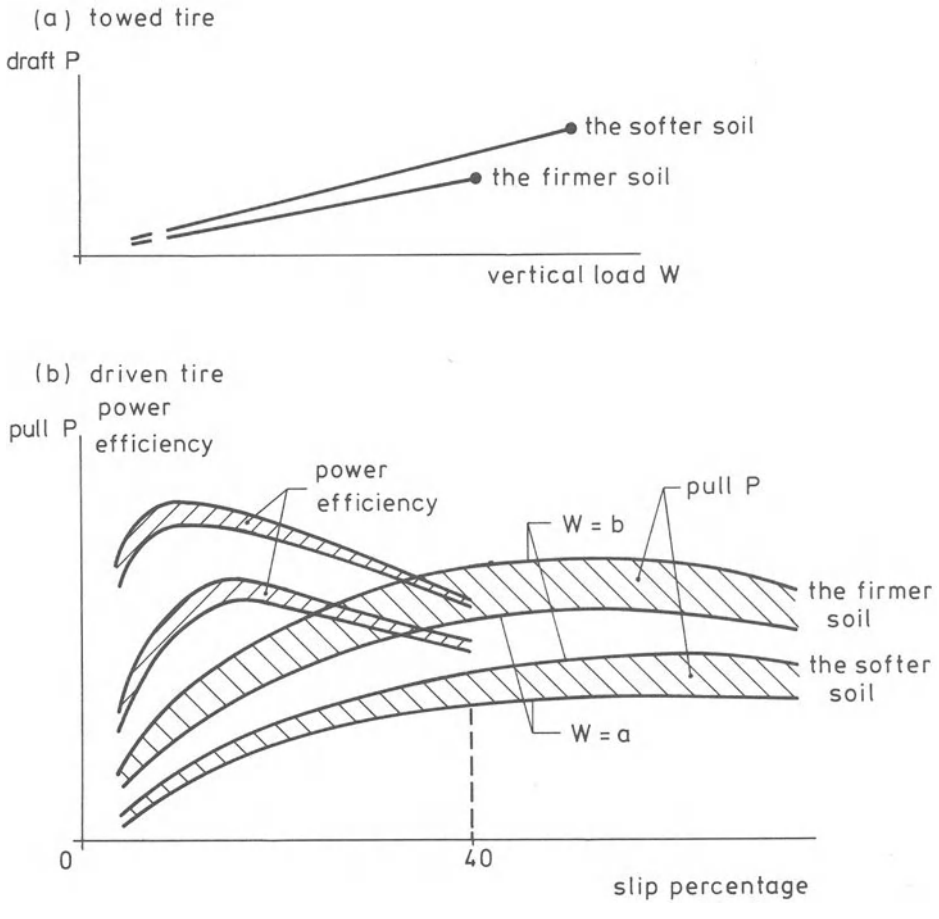

Fig. 3.17a, b. Behavior of a towed tire (a) and driven tire (b)

Figure 3.17b characterizes the behavior of a powered, pulling tire which is determined by

unloaded tire diameter,
unloaded tire width,
inflation pressure,
angular velocity,
composition, construction, and tread.

Drawbar pull P and power efficiency are related to slip percentage for different loads W and different field conditions. The figure shows that W, field conditions, and slip percentage all have great influence. W exhibits a maximum connected with the admissible tire deflection. The drawbar pull-slip curves show maxima at such high slip percentages that power efficiencies there are very low. Moreover, it is not practical to operate near a curve maximum; a small increase

in drawbar load would reduce the forward speed to zero. A larger tire size means that W can be greater before the maximum admissable tire deflection is attained and/or that energy losses due to rolling resistance are lower. Both aspects allow for a higher P. Lowering tire inflation pressure also makes P increase. However, inflation pressure is subjected to a lower bound as the admissible tire deflection may not be exceeded. A higher inflation pressure can increase P indirectly, as it allows a higher W. However, a maximum inflation pressure exists for each tire, depending on the carcass construction. The P-curves are influenced slightly by tire tread and by angular velocity.

Figure 3.17 concerns a towed element and a powered pulling element. Both loading types are of great practical importance. A summary of all possible loading types is given in Schüring (1968).

Stresses in Contact Surfaces

Introduction. Force R in Fig. 3.16 is the resultant of the normal and shear stresses in the contact surface between element and soil.

The stresses under a rigid element depend mainly on the size of the contact area. When the area of contact is small, stresses will be high. If the soil cannot bear these high stresses without being deformed, the element sinks into the soil, increasing the size of the contact area until the required soil bearing capacity is attained.

The essential difference between a rigid wheel and a wheel with a pneumatic tire is that a tire can deflect. As the tire is more deflected, the deflecting force increases, partly because the bearing area (at constant inflation pressure) increases, and partly because the tire carcass resistance against deflection increases. On soft soil a tire will exhibit a certain sinkage. With increasing sinkage, resistance against sinkage increases, partly because the bearing area increases, and partly because of soil compaction hardening. In general, a tire moving on soft soil will involve tire deflection and sinkage (rut formation) in such a way, that tire deflecting forces and soil sinkage reaction forces balance each other. Extreme cases are

- rigid soil surface, implying only tire deflection and no rut formation (apart from small elastic strains),
- high inflation pressure, implying only rut formation and no tire deflection.

In each point of the contact surface a normal stress and a shear stress occur. Moreover, a major principal stress and a major principal stress direction can be assigned to each point.

Normal Stresses. In general, the normal stress distribution in the contact surface is not uniform, so that the mean σ_n is smaller than the maximum σ_n. In general, normal stresses are compressive but, where the rolling element and the soil should separate, normal stresses may be tensile stresses due to soil sticking. Normal stresses concentrate more or less under lugs, ribs, etc. of the rolling element and often also near the boundary of the contact surface, since there the tire deflection resistance is the highest.

Shear Stresses. The soil particles in the contact surface move relative to the rolling element surface of contact, or tend to do so (Sect. 3.2.2.1). Because the coefficient of friction between soil and traveling element is usually not zero, this means that shear stresses must be present in the contact area. These shear stresses are opposite to the relative direction of movement. The value of the shear stress in a certain contact surface point is equal to the normal stress in that point multiplied by the appropriate coefficient of friction, plus the adhesion. The coefficient of friction and the adhesion depend on several factors, such as the amount of movement that occurred earlier (see Sect. 2.5.2). In the case of a rolling element with a tread pattern, a clear plane of sliding may be generated through the soil material, passing along the tops of the tread. In places where soil to soil friction occurs, the coefficient of soil to soil friction, of course, applies.

Principal Stresses. It is a common mistake to consider the normal stress σ_n on an element of the contact surface as a major principal stress. However, the simple fact that a shear stress τ also acts on the surface element means that, at the point considered, a normal stress must exist that is greater and has another direction than σ_n. Using Mohr's circle and making a few assumptions, it is often possible for such a point to estimate the largest normal stress (σ_1) and its direction from σ_n and τ (see Sect. 2.5.3.1).

Some Measurements. When stresses in the contact surface are to be known, they should be measured. Because such measurements are very difficult they have been carried out for only a few, mostly very simple cases. A few of them are summarized below. Seven cases have been distinguished:

1. Rigid Wheels. Measurements have been carried out by Hegedus (1965), Onafeko and Reece (1967) and by Krick (1969).
– Stress distribution in direction of travel – Maximum stress lies ahead of the wheel axis and stresses extend behind the axis. Wong (1967) relates the stress distribution to the observed zones (see Sect. 3.2.2.1 and Fig. 3.2c) under wheels:

- normal stresses are maximal near point of separation A in Fig. 3.2c,
- in the front zone (a), the soil exerts forward shear stresses on the wheel,
- in the rear zone (b), the wheel moves forward relative to the soil when the wheel is towed, implying that the soil exerts backward shear stresses,
- when the wheel is driven, both soil and wheel move backwards in zone (b), but since the wheel moves faster the soil exerts forward shear stresses on the wheel there.

So, in the case of towed wheels, shear stresses in the second zone (b) act in opposite direction, which is in agreement with the requirement that $M = 0$.
– Stress distribution in lateral direction – At the interface boundaries are stress concentrations, which diminish with increasing slip. Krick (1969) reports a $(\sigma_{\text{side}})_{\max}/(\sigma_{\text{center}})_{\max}$ value of 1.75 for the towed condition, and 1.4 at 40% slip for a powered wheel.

Table 3.5. Measurements on rigid wheels (Onafeko and Reece 1967)

Slip (%)		Drawbar pull (N)	Rolling resistance (N)	Sinkage (cm)	Maximum σ_n (bar)	Maximum forward τ_n(bar)	Maximum backward τ_n(bar)	Rolling resistance / vertical load	Drawbar pull / vertical load
Towed −44.5	a		4220	23	1.65	0.27	0.41	0.48	
Towed −51.6	b		4010	15	1.04	0.14	0.15	0.43	
Towed −24.5	c		2220	9	2.03	0.33	0.44	0.25	
3.1	a	0		20	1.58	0.49			0
	b	330		13	1.16	0.33			0.035
	c	110		9	2.09	0.61			0.012
22.1	a	890		23	1.48	0.66			0.10
	b	1560		17	0.98	0.44			0.17
	c	1120		13	1.86	0.96			0.13
41.4	a	930		–	1.65	0.72			0.11
	b	1560		19	1.23	0.48			0.17
	c	1420		14	1.75	1.04			0.16

– A few numerical values – Onafeko and Reece (1967) presented some experimental data for 125 cm diameter steel wheels with tri-angular cams (see Table 3.5). They distinguished three cases:

a) wheel width 15 cm, loose sand, vertical load 901 kg,
b) wheel width 30 cm, loose sand, vertical load 946 kg,
c) wheel width 15 cm, compacted sand, vertical load 905 kg.

σ and τ have been averaged over the wheel width; the exact σ_{max} and τ_{max} are thus, according to (Krick 1969), higher.

2. Tire Resting on a Rigid Surface (Söhne 1953a, VandenBerg and Gill 1962, Krick 1969). The mean stress in the contact surface equals the tire inflation pressure plus 0.25 – 1.25 bar. Stresses are not uniformly distributed; in the case of tractor tires, load is mainly on the lugs. The lugs cover 20% – 25% of the contact area and, therefore, stresses under the lugs are about five times as high as the mean stress. So, it is not surprising that the lugs almost always penetrate the field soil. Kraft measured about 25% higher stresses at the boundaries than at the centers of the contact areas of motorcar tires (Söhne 1953a).

3. Towed Smooth Tire on a Rigid Surface. VandenBerg and Reed (1962) give sizes of contact surfaces and stress distributions in contact surfaces for smooth, radial ply tractor tires and smooth, diagonal ply tractor tires driving on a hard underfooting, and exerting a drawbar pull of 0.1 times the vertical load. Tire size was 11 – 28, inflation pressure 1 bar, and vertical load 940 kg. They found

– contact surfaces of radial tires were narrower and longer,
– areas of contact were 700 – 900 cm^2,

- mean contact pressures were 1.05 – 1.35 bar,
- maximum contact pressure was about 2 bar.

VandenBerg and Gill (1962) made the following observations on a tractor having smooth 4 ply 11 – 38 tires, each with a vertical load of 975 kg, pulling a test vehicle:

- maximum stress at the boundary,
- contact area when a tire is at rest being smaller than contact area when the tire is moving,
- stress increasing rapidly at the front of the tire and decreasing at the same rate at the rear.

The results are summarized in Table 3.6. Figure 3.18 represents graphically measurements of stresses on a hard surface.

4. Towed Smooth Tire on Soft Soil. VandenBerg and Gill (1962) also investigated the case of a tractor pulling a test vehicle on a soft soil. Measuring results are also shown in Fig. 3.18. In general, maximum stress is ahead of the wheel axis and is, therefore, not covered by these graphs. It appears that on soft soil the stress builds up slowly and decreases rapidly.

Gill and Reaves (1956) made measurements with a smooth 11 – 38 tire and a smooth Rolligon tire (152 cm wide, 107 cm in diameter) on a Hiwassee sandy loam at a normal moisture content, that had been rotavated several times and finally leveled. Results are given in Table 3.7.

5. Driven Smooth Tire on Soft Soil. Krick (1969) tested a driven smooth 11.5 – 15 AM tire on a rotavated sandy loam at a moisture content of 19%

Table 3.6. Results for a towed smooth 11 – 38 tire on a rigid surface (VandenBerg and Gill 1962)

Inflation pressure (bar)	Contact area (cm^2)	Mean contact pressure (bar)	Maximum contact pressure (bar)
0.98	888	1.10	2.29
0.70	1092	0.89	2.25
0.42	1461	0.67	2.46

Table 3.7. Results for two towed smooth tires on soft soil (Gill and Reaves 1956)

Tire	Inflation pressure (bar)	Vertical load (N)	On hard surface		Tire moving on sandy loam		
			Contact area (cm^2)	Mean contact pressure (bar)	Contact area (cm^2)	Mean contact pressure (bar)	Rolling resistance (N)
11 – 38	0.82	10900	877	1.23	1374	0.79	1220
Rolligon	0.39	22200	5882	0.38	7740	0.28	2150

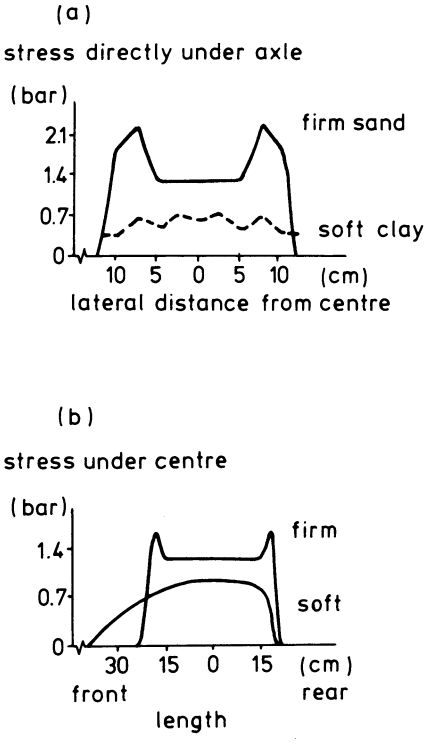

Fig. 3.18a, b. Lateral and longitudinal stress distribution under a towed smooth tire

and a relatively low vertical load of 545 kg. They found, for the lateral direction,

- stresses near the sides are higher with low, but not with high slip,

and for the travel direction,

- stresses are lowest at the front and the rear of the contact surface and maximum stress occurs slightly ahead of the wheel axle,
- only at high slip and in the middle of the track, stress maxima occur at the front and the rear.

Stress distribution was more uniform than under a rigid wheel. The measurements show that

- shear stresses are almost as great as normal stresses, when slip is high,
- the highest observed normal stress was 0.7 bar (being lower than the tire inflation pressure).

6. Towed Tire with Tread Pattern on Soft Soil. Baganz and Kunath (1963) made measurements on tires mounted on tractors driven backwards at zero pull on freshly plowed moist sand (*C*), and on freshly plowed moist loam (*D*). Results are given in Table 3.8. A comparison of tire inflation pressures with mean contact stresses suggest that the tires behaved as rigid wheels.

Table 3.8. Results for towed tires with lugs on soft soil (Baganz and Kunath 1963)

Tire	Inflation pressure (bar)	Vertical load (N)	Soil	Contact area (cm^2)	Mean contact pressure (bar)
9 – 36	1.6	9050	*C*	1620	0.56
11 – 38	0.8	7600	*D*	1615	0.47
11 – 38	2.0	7600	*D*	1440	0.53

7. Driven Tire with Tread Pattern on Soft Soil. Triabbic et al. (1959) did experiments using a 13.6 – 38.4 ply tire having a tread pattern, and exerting a vertical load of 1090 kg. The tire was operated in a 25.4 cm layer of spaded and leveled soil with a moisture content of 7.8% – 12.7%. In the tire surface, 4 × 10 load cells, being distributed over the entire width, were built in between lugs, on lugs and in the front and back faces of lugs. Independent variables were drawbar pull and inflation pressure.

- The effect of inflation pressure (at 809 kg drawbar pull) – As inflation pressure increases, the stresses in the center of the contact area increase, but stresses at the boundary decrease. This is because the tire is deflected less and slips more (see Table 3.9, top).
- Effect of drawbar pull (at 1 bar inflation pressure) – When drawbar pull increases, stresses on the leading lug faces and between the lugs increase. Stresses under the lugs decrease, because at increasing slip the lugs tend to slide off their supporting soil prisms. Stresses at the trailing lug faces also decrease (see Table 3.9, bottom).

Table 3.9. Contact pressures for a driven tire with lugs on soft soil (Trabbic et al. 1959)

		At the tread centre		At the tread sides	
Inflation pressure (bar)		0.7	1.3	0.7	1.3
Contact pressure (bar)	– between lugs	1.23	1.92	0.54	0.27
	– under lug	1.92	3.56	1.37	0.68
	– lug front face	1.43	3.42	0.20	0.14
	– lug back face	0.34	0.68	0.68	0.34
		At the tread centre		At the tread sides	
Pull force (N)		180	8000	180	8000
Contact pressure (bar)	– between lugs	1.23	1.51	0.14	0.27
	– under lug	2.68	2.33	1.03	0.75
	– lug front face	0.96	2.74	0	0.20
	– lug back face	1.03	0.41	1.03	0.41

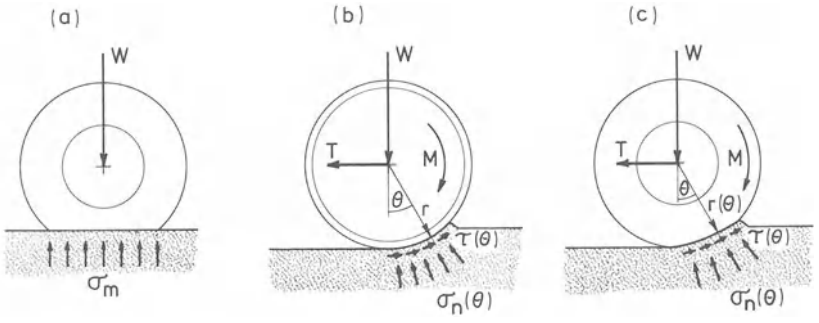

Fig. 3.19a – c. Refers to the equations of equilibrium

Slip at 1.3 bar inflation pressure and 809 kg drawbar pull was almost three times the slip at 0.7 bar inflation pressure and the same drawbar pull. Stresses under lugs were about 1.5 (at high drawbar pull) to 2 (at low drawbar pull) times higher than stresses between lugs. The horizontal force against the lugs can be of the same order of magnitude as under the lugs.

Considering the Equilibrium of Forces. In Fig. 3.19, W is the vertical load, T is the drawbar pull, M is the torque, r is the outer radius, θ is the angle of a radius with the vertical, τ is a shear stress in the surface of contact, σ_n is a normal stress in the contact surface, and σ_m is the mean normal stress in the surface of contact. Figure 3.19a shows a pneumatic tire on a hard surface. Equilibrium of forces in the vertical direction requires

$$W = \sigma_m A$$

where A is area of contact. Because of carcass stiffness, σ_m is always larger than tire inflation pressure.

Figure 3.19b refers to a rigid wheel forming a rut. σ_n and τ are functions of θ. The following conditions must be satisfied:

$$W = \sum \text{vertical components of } \sigma_n(\theta) + \sum \text{vertical components of } \tau(\theta)$$

$$T = \sum \text{horizontal components of } \sigma_n(\theta) + \sum \text{horizontal components of } \tau(\theta)$$

$$M = \sum r\,\tau(\theta) = r \sum \tau(\theta).$$

The summations should be performed over the entire area of contact. With respect to the last formula it is noted that $M = 0$ for towed wheels, implying that opposite shear stresses must occur. The first equation shows that W is partly borne by shear stresses.

Figure 3.19c shows a rut forming deflected tire. Now, r is a function of θ as well, and the formula for M becomes

$$M = \sum r(\theta) \cdot \sigma_n(\theta) \text{ component normal to } r + \sum r(\theta) \cdot \tau(\theta) \text{ component normal to } r.$$

Now, σ_n also contributes to the torque. The formulas for W and T are equal to those in the previous case.

Stresses Within the Soil

The stresses a rolling element exerts on the soil in the contact surface are accompanied by stresses within the soil under and aside from the contact surface. For certain special cases these stresses can be calculated. For example, when a smooth tire having very thin, flexible walls is supported by a rigid, perfectly smooth surface, normal stresses in the contact surface are evenly distributed and equal to the inflation pressure p_i. As the surface is perfectly smooth, there are no shear stresses in the interface. The area (A) of contact will be the vertical load divided by p_i. If it is assumed further that the contact surface is circular and that the soil behaves as an elastic medium, the stresses within the soil can be calculated using the solution of the problem of an evenly loaded circular area on a semi-infinite elastic medium. This solution can be found in numerous textbooks on elasticity.

However, in agriculture, the situation most times is different. Tires have tread patterns and soils are soft enough to allow ruts to be formed. At the contact surface shear stresses are induced due to the tread and due to soil-material friction. Tire flexibility is limited and this leads to a complicated stress distribution in the contact surface. The contact surface is hardly ever circular and when ruts are formed, soil behavior is clearly not elastic. All this means that isobars have very complicated shapes; there are no ready solutions for field situations. For these problems it is necessary to make assumptions and use approximations such as mentioned in Sect. 2.2.3.1. Stress measurements with load cells within the soil do not solve the problem, since their accuracy is poor. If the cell is stiffer than the soil, stresses concentrate on the cell, and if the soil is stiffer than the cell, it tends to arch around the cell, keeping the load away from the cell.

A few current ideas about σ_1-*isobars* under a rolling element are

- in the field, isobars will be asymmetrical because of rut formation and because the traveling process makes the soil properties change in the direction of travel.
- especially with pulling elements, shear stresses are present in the surface of contact. Then the directions of the longest axes of the isobars are no longer vertical, but are inclined backwards.
- when the soil profile is layered, especially when hard layers are present, the isobars will be of a very complicated shape. If hard layers occur at small depths and contact areas are large, isobars may run almost vertically from the element to the hard layer. This means that stresses hardly decrease with depth. Hard layers even may cause that maximum stress does not occur at the soil-element interface, but somewhere between the element and the hard layer. An important example of layered soil is arable soil tilled to a shallow depth, being a soft layer overlaying a rigid layer.
- the isobar shapes are also dependent on soil type. On a softer soil isobars tend to be more slender and more elongated in the vertical direction. This means that stresses reach deeper but less far in lateral direction.

- as a first approximation, it may be stated that the stress levels at the surface and in the soil are proportional. If interface stresses all double, the stress at an arbitrary point in the soil will double. Or, more generally, if stresses in the surface of contact are multiplied by a factor k, the isobar of stress p will become the isobar of stress kp.
- in a given situation, both the contact surface and the isobars have a certain geometrical shape. As a first approximation, one assumes this geometry to be independent of the length scale. Therefore, if length and width of the surface elements of the contact area are doubled, while the shape of the contact area and the stresses on the surface elements are kept constant, stresses in the soil will reach twice as deep. So, when the contact area is increased at a constant surface pressure, stress decrease with depth is less.
- at points not far below the contact surface, stresses are mainly determined by surface pressure and not by total load on the surface or by the size of the contact surface. For stresses at greater depth the surface load gets the character of a point load; total surface force is important and not interface pressure and size.
- for a soil where bulk density is mainly determined by σ_1 (see Sect. 2.2.2.2), a bulk density pattern can be calculated from a pattern of σ_1-isobars, using the relation between σ_1 and bulk density of this soil.
- the principal stress axes through an arbitrary point in the soil rotates during the passage of a rolling element. This rotation has a kneading effect, which may cause additional compaction.

As to the τ_{max}-isobars in agricultural practice, it is usually assumed that τ_{max} reaches a maximum value at a certain depth. For a soil with bulk density sensitive to shear stresses, this means that compaction under a rolling element has a maximum at a certain depth.

3.2.2.3 Systems of Rollers, Wheels, and/or Tires

For systems of rollers, wheels, and/or tires it is often assumed that the rolling elements do not interact (influence each other). But this is far from always true. Interacting systems that have been investigated to some extent are

- repeated wheel passes (the same tire moving one or more times over its own rut),
- two tires mounted side by side at close spacing, called usually duals.

Repeated Wheel Passes

If a rut has been made by a certain tire, and the same tire moves again along the same track, tire performance is generally better in the second than in the first pass. Dwyer et al. (1977) tested a 13.6–38 tractor tire at a vertical load of 1385 kg and an inflation pressure of 0.8 bar on 19 different plots. They found that "the performance during the second pass was generally better than during the first pass. On average, the coefficient of traction at 20% slip increased by 7%, rolling resistance reduced by 11% and maximum tractive efficiency in-

creased by 5%". Holm (1969) found that drawbar pull in the second pass was also influenced by the drawbar pull the tire had to exert in the first pass.

In the first pass the soil is relatively soft and sinkage is relatively large. Often, soil is bulldozed forward, in front of the tire. In the second pass no bulldozing occurs, and the tire meets a relatively firm soil by which the tire is more deflected (Holm 1969). Shape and size of the contact surface differ as well. Each pass repetition gives an additional sinkage. Causes for this, apart from vibration effects, time dependency of sinkage, and the so-called slip sinkage, are given by Wong (1978):

- when a tire is very inflated so that it behaves as a rigid wheel, it is obvious that the tire has to sink somewhat in the second pass before it is able to produce significant drawbar pull,
- the smallest dimension of the contact surface may be shorter at the second pass than at the first pass, which results in additional sinkage (compare with force-sinkage relationships in Sect. 3.3.2.2).

Soil compaction generally also increases as the number of passes increases (Holm 1969, Raghavan et al. 1976, 1977).

When the passes occur at relatively large sinkage, and thus mobility is relatively poor, tire performance decreases with increasing number of passes. This decrease in mobility is due to the ever-increasing friction between the rut walls and the tire, and to the fact that it is difficult to drive out of a deep rut. Mobility decreases with number of passes under such conditions until the no-go condition is reached. In practice, mobility of a vehicle or of a combination of vehicles and/or implements is not only dependent on tire sizes, treads, loads, inflation pressures, and on soil conditions, but it appears that available engine power and type of power transmission (mechanical or hydraulic) have small but significant influences.

Duals

In case two identically tired wheels, rigidly attached to each other and spaced far enough apart to avoid interaction, act side by side, the joint performance is twice the performance of a single tire. When the spacing is being reduced, at a certain moment they start to interact. Then the joint performance becomes more than twice the performance of a single, non-interacting, tire. Such tire combinations are called duals. The extra effect increases as spacing decreases and also as mobility conditions become worse. Melzer and Knight (1973) tested 9.00 – 14 tires on air dry dune sand. They found that

- the extra effect started to occur when the distance between the tires was less than 2 – 3.5 times the width of a single tire,
- in bad mobility conditions where drawbar pull to vertical load ratio for a non-interacting tire was 0.1, and at zero tire spacing, the extra effect was an increase of this ratio of 0.075.

Little is known yet about the effect of duals on stresses and compactions in the soil. As a first approximation it may be stated that

- at small depths, the situation under a tire which is part of a dual will not be different from the situation under a single tire,
- for points at greater depths, a dual acts as a point-load. When two non-interacting tires operating side by side, are brought together to form a dual, stresses at greater depths multiply by a factor 1.5 – 2.

Duals may also be obtained from singles by simply adding identical tires, keeping the axle load about the same. This is how farmers usually obtain duals. Then the load of a single tire is about halved. When adding the tires, farmers usually do not change tire inflation pressures. Therefore, soil stresses at small depth will not be diminished by changing to duals. The main effect is a reduction of the contact area per tire as the load per tire is reduced. In points at great depth, which experience a dual as a point load, stresses do not change either when duals are formed by adding tires. Such duals are mainly used in seedbed operations to leave a flat surface.

A third way to obtain a dual is replacing a single tire of a certain width by two tires with smaller widths. These usually are spaced wide enough to give room for a plant row or a ridge between the two tires. Such duals allow for sufficient bearing capacity, while causing less harm to the crop. They may be used, for example, in potato harvesting.

Trucks are often fitted with duals. When they are intended for off-road use, it may be advantageous to replace the duals by singles that are wider than the single tires in the duals, but less wide than the complete dual, and that have diameters larger than the duals. The advantage stems from a decrease in off-road rolling resistance.

3.2.3 Applications

3.2.3.1 Estimating the Pull a Tire is Able to Develop

It is important that the pull a tire is able to develop matches the required pull. Then the slip and the associated deterioration of the soil structure are within acceptable limits.

A very practical method to select a tractor for a given operation is using the ASAE tractor drawbar performance predictor for two wheel drive tractors (ASAE D 230.3 in (NN 1981)). Power, pull, slip, and actual speed on firm, tilled or soft/sandy soil can be determined for a tractor for which Nebraska test data (involving pull-slip measurements on concrete) are available. The method does not use particular tire data, so that, for example, the performance of alternative tires cannot be judged.

Size of the tires relative to the tractor size can be judged using a graph such as Fig. 3.20. This graph presents mean tractor weight as a function of drive wheel tire size for new 2-wheel drive tractors offered in Europe about 1981. Construction of such graphs is easy using tractor tables that are published in many countries.

Experimental data on the performance of single tires can be found in the Handbook of agricultural tire performance (Dwyer et al. 1974) which is based on

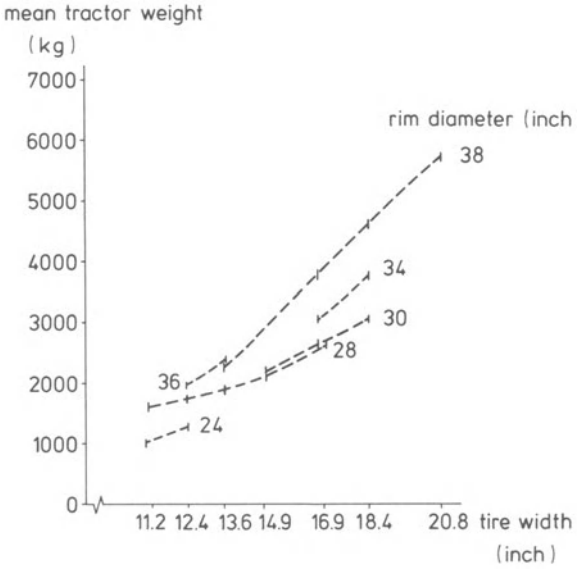

Fig. 3.20. Mean tractor weight as a function of drive wheel tire size for new 2-wheel drive tractors offered in Europe about 1981

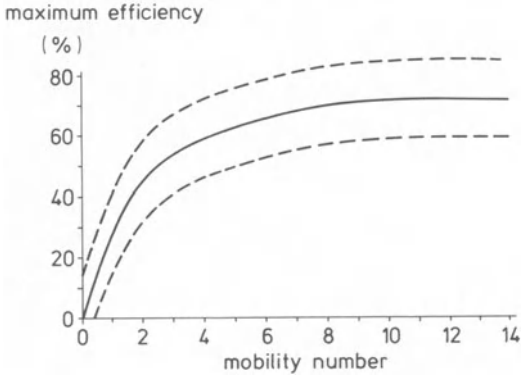

Fig. 3.21. Empirical relation between maximum efficiency and mobility number, with 95% probability limits

field work with a single wheel tester. Four soil conditions – good, average, poor, bad – are distinguished and described qualitatively. For these conditions and current tires the Handbook gives

- pull at 20% slip (this corresponds approximately to the highest pull at which a tractor can work continuously with reasonable efficiency when plowing or cultivating),
- maximum tractive efficiency,
- slip percentage at maximum efficiency (which percentage is about 10% in good, and about 20% in bad conditions).

Many empirical-analytical methods relate cone index (Sect. 3.3) and tire performance. A useful example is given in Fig. 3.21 (Dwyer 1973) where

maximum tractive efficiency of current tractor tires is plotted against the mobility number

$$\frac{Cdb}{W}\sqrt{\frac{\delta}{h}}\left(\frac{1}{1+\frac{b}{2d}}\right)$$

where C is cone index of the soil (defined in Sect. 3.3), d is tire diameter, b is tire width, W is vertical wheel load, δ is tire deflection, h is tire section height. Dwyer also indicates a way of using this graph: "from the graph it is possible to predict the improvements in performance likely to be achieved by changes in tire parameters. For example, if in a field condition with a particular cone index, the mobility number for a tire is 4, it can be seen from the graph that its maximum tractive efficiency is likely to be approximately 59%. If its mobility number could be increased to 8 in the same field condition by changes in tire parameters, its maximum tractive efficiency would be increased to approximately 70%. This could be achieved by doubling diameter or section width or increasing deflection by a factor of 4".

There may also be a relationship between tire performance on the one hand, and stress-sinkage relations of plates and shear-ring measurements on the other hand (Bekker 1960). Dwyer (1973) measured such relationships, but they were not very satisfactory.

A simple, analytical method to estimate maximum pull starts from the following assumptions:

- The soil-tire interface is a horizontal plane and the contacting lugs fully penetrate the soil.
- A plane of sliding exists in the soil which passes through the circumferential faces of the penetrating lugs.
- In this sliding plane, adhesion and soil-rubber friction under the lugs, and cohesion and internal soil friction between the lugs, are fully developed.
- Vertical stress in the plane of sliding equals tire inflation pressure p. Therefore, the area of contact equals vertical load W divided by p.

For these assumptions pull P can be calculated as

$$P = W\left(\left(\frac{c}{p}+\tan\phi\right)(1-m)+\left(\frac{a}{p}+\tan\delta_r\right)m\right)$$

where c is cohesion, ϕ is soil-soil friction angle, m is area of tire lugs as a fraction of tire peripheral area, a is soil-rubber adhesion, and δ_r is soil-rubber friction angle. Dwyer (1973) showed experimentally that approximately

$$\text{Pull at 20\% slip} = 0.8\,P.$$

Tire performance is primarily determined by tire size, inflation pressure, and soil conditions, but there are of course more factors of influence, such as lug angle (Taylor 1973) and tire cord direction (radial versus diagonal) (Taylor et al. 1976).

3.2.3.2 Estimation of the Mean Contact Stress of a Deflected Tire on a Rigid Surface

If a tire had a very thin flexible wall, like a balloon, the mean contact stress of a deflected tire would be equal to the air pressure in the tire. However, actual tires have carcasses with a certain stiffness and, therefore, tire deflection is accompanied by an additional reaction force making the mean contact stress higher than the tire inflation pressure. Several investigators examined the relationship between mean contact stress p_m and inflation pressure p_i for hard underfootings (Krick 1969, Söhne 1953 a, VandenBerg and Gill 1962). From this, certain rules of thumb have been developed. For example,

$$p_m = k p_i$$

where k can be found from the following table:

ply rating	4 and 6	8	10 and 12	16
k	1.1	1.15	1.2	1.25

Another rule of thumb is

$$p_m = p_i + p_k$$

where p_k accounts for the extra reaction force. Sometimes p_k is taken as a constant depending on tire type. For instance, Krick (1969) assumed that $p_k = 0.45$ bar for tractor drive wheel tires. Alternatively, p_k may be assumed a function of p_i, which decreases as p_i increases (Söhne 1953 a). In fact, p_k is a function of both tire type and inflation pressure.

3.2.3.3 Estimation of the Area of Contact Between a Tire and a Rigid Surface

A very simple method uses the equilibrium of vertical force components and an estimated mean normal stress p_m in the contact surface (see estimation of mean contact stress of a deflected tire on a rigid surface, Sect. 3.2.3.2). Equilibrium gives

$$\text{Vertical load} = \text{contact area} \cdot p_m .$$

If the vertical load and p_m are known, the area of contact follows from this formula.

A second method (Krick 1969) uses the amount of tire deflection f and the assumption that the shape of an undeflected tire is a torus (Fig. 3.22). On loading, the tire deflects, the chords AEC and DEF elongate as the tire bulges out, and the arcs ABC and DBF shorten to become chords AEC and DEF. The real lengths of the ellipse axes will be intermediate between the original lengths of the chords and the lengths of the respective arcs, but since the tire diameter is large, it may be assumed that chords AEC and DEF are not increased by the deformation. This implies that, when A is contact area, f is tire deflection, and a, b, r and R are as defined in Fig. 3.22,

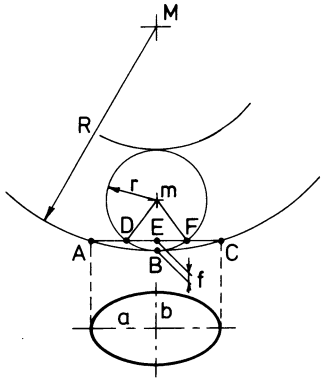

Fig. 3.22. Estimating area of contact between a tire and a rigid surface, when tire deflection is known

$$a = \sqrt{(2Rf - f^2)}, \quad b = \sqrt{(2rf - f^2)}$$

$$A = \pi ab = \pi \sqrt{(2Rf - f^2)} \cdot \sqrt{(2rf - f^2)} .$$

Since $f^2 \ll 2rf$ or $2Rf$, this reduces to

$$A \approx 2\pi \sqrt{Rrf^2} .$$

Note that this approximation implies the assumption that the contact surface on a rigid underfooting is an ellipse.

3.2.3.4 Relative Tire Deflection at Maximum Load

A good tire table gives tire deflection (f) at maximum load. Together with the cross section height of the unloaded tire (H), this yields the relative tire deflection at maximum load (f/H). From the data in such tables it appears that, for varying tire type and inflation pressure, this quantity obeys certain rules.

- using data on "Continental" – tractor drive wheel tires, Krick (1969) derived that on a rigid surface the highest admissible load is reached when $f/H = 0.13 - 0.17$,
- using data of diagonal ply – tractor drive wheel tires, Sitkei (1969) concluded that the highest admissible load is reached at $f/H = 0.15$.

These data on f/H can be used for estimating areas of contact on a rigid surface at maximum loads (see estimation of the area of contact between a tire and a rigid surface, see Sect. 3.2.3.3). They can also be used to judge whether inflation pressure may be lowered in a given operating condition to decrease soil compaction or increase tire performance.

3.2.3.5 Optimal Slip Percentage

At high slip percentages, soil structure is damaged and tire wear is high. At low slip percentages, drawbar pull/tractor weight ratio is low and sudden increases in pull demand may produce serious shocks in the engine and the drive train. Slip

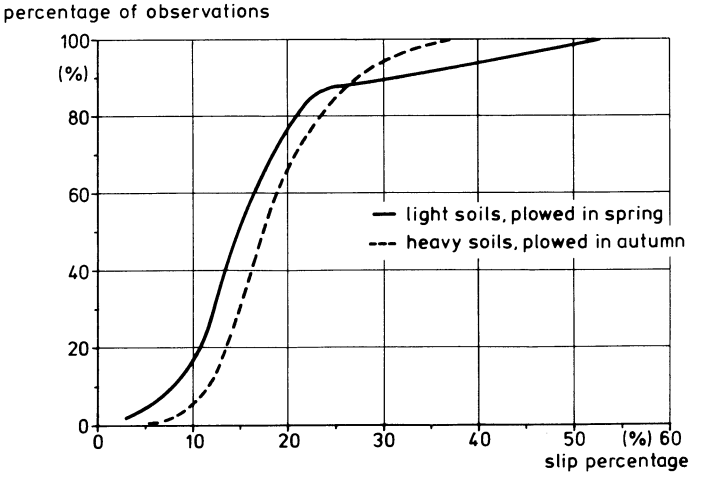

Fig. 3.23. Cumulative frequency curves of slip percentage in plowing light and heavy soils

percentage at maximum tractive efficiency varies from about 10% under good to about 20% under bad conditions (Dwyer et al. 1974). If slip percentage is very different from slip at maximum efficiency, fuel consumption is unnecessarily high. Sometimes it is stated that slip percentages lower than 10% and higher than 15% should be avoided.

In the field, slip percentages often deviate much from these values. With 12 arbitrary plowing tractors the slip percentage appeared to vary from 13 to 39% (NN 1978). Tijink and den Haan (1981) measured slip percentages on a great number of tractors at spring plowing of sandy soils, as well as autumn plowing of clayey soils (Fig. 3.23). It can be concluded that slip percentages very often are sub-optimal. Slip percentages can be influenced rather easily and it makes sense, therefore, to be able to estimate the slip percentage of a working tractor in a quick way. The following methods were described by Deere & Company (NN 1976):

– "Mark a spot on the ground and a chalk mark on one rear tractor tire. Then drive the tractor, under load with the implement in its normal operating mode, and count 10 complete rotations of the rear tire and place another mark on the ground. Repeat the trip without the implement and again count wheel rotations between the two marks. Estimate the fraction of the last rotation as nearly as possible. Check the number rotations counted on the second trip, using the chart below to determine the percentage of rear-wheel slippage.

Rotations	*Rear-wheel slippage percent*
10	0
$9\frac{1}{2}$	5
9	10
$8\frac{1}{2}$	15
8	20
$7\frac{1}{2}$	25
7	30

- slip can also be judged by observing tire-tread print in the rut. When tire slippage is too low, the tracks will be sharp and distinct in the soil. There is no evidence of slippage. The tires are figuratively "geared" to the ground. When tire-slippage is too high, the tread marks are entirely wiped out. In the case of proper slippage, the soil between the cleats in the tire pattern is shifted, but the tread pattern is visible. (NN 1976) presents rut photographs for each of these three slip levels.
- slippage under 15% is barely visible. So, as a rule of the thumb, if slippage can be seen, it is too much".

Slip percentage can be influenced by

- changing forward speed, if resistance of the pulled implement is speed dependent,
- adding or removing tractor ballast,
- changing tractor size and/or implement size.

3.3 Penetrating Bodies (Wedges, Cones, Plates, Wires, Spheres)

3.3.1 Occurrence

Wedges and plates are used frequently as aids to support machines that are standing in the field. These supports have complicated shapes. They may be circular or rectangular, flat plates or set to a shell form, with the hollow face upward or downward, horizontal *V*- or, *U*-shaped profile steel beams, etc. From a soil mechanics point of view, legs of cattle and horses may be considered as loaded plates. Wedges are also applied in a number of trench making machines. Wires are often used where plastic soil must be separated, like mud sticking to tires, shaping undried, unburnt brick in ceramic industry, etc.

Wedges, cones, and plates also play an important role in research. A penetrating wedge induces a two-dimensional process in the soil and is, therefore, well-suited for process-studies. Where a measure of resistance against penetration is wanted, the force required to press a cone or plate into the soil can be

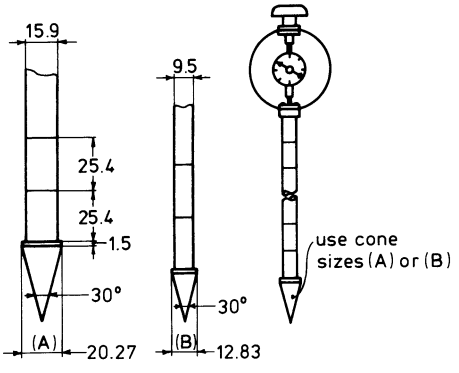

Fig. 3.24. ASAE standard cone penetrometer (NN 1981)

measured. When a cone with relatively small diameter and acute tip is used for this, the force needed may be supplied manually. Figure 3.24 shows a hand operated penetrometer of the ASAE standard type (NN 1981); the force is read from the scale of a spring balance and cone depth from the bar calibrated with incisions. Other manual penetrometers are instrumented to registrate the force-depth relationship continuously or in digital form. In plate sinkage tests plate diameters usually are relatively large, implying that the force demand cannot be supplied by hand but must be delivered by heavy powered equipment.

3.3.2 Fundamentals

3.3.2.1 Kinematic Aspects

Among the processes in the group of penetrating bodies, that of an acute wedge in a steady field, and at an early stage of penetrating, are basic.

Acute Wedge in a Steady Field. Suppose that an infinitely long, acute wedge is penetrating downwards into a soil at a constant speed, and consider a plane perpendicular to the longest axis. If penetration depth is large compared to the wedge width and height, the flow field in the considered plane may be assumed steady over a short length of time. Figure 3.25 a shows such a steady field for incompactible soil. Figure 3.25 b shows the same deformation but now relative to the untouched soil. The broken line in both figures surrounds the soil that is influenced by the wedge at a given moment, *the zone of influence.* In this zone the soil moves upwards relative to the wedge surface and the soil deformation is characterized by large compaction and/or shear strain. The deformation pattern depends on the soil compactability and deformability, the wedge dimensions, and the soil-wedge frictional properties.

Suppose now that the wedge is at rest and that the untouched soil moves upwards at constant speed as in Fig. 3.25 a. If much soil compaction occurs, the soil near the wedge will lag behind the upward movement of the soil as a whole.

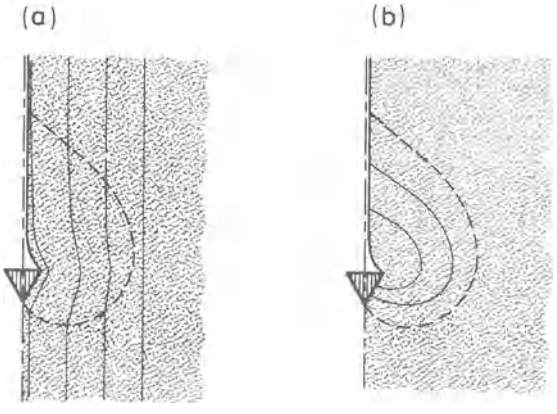

Fig. 3.25 a, b. Flow field in incompactible soil around a wedge relative to the wedge (a) and relative to the untouched soil (b)

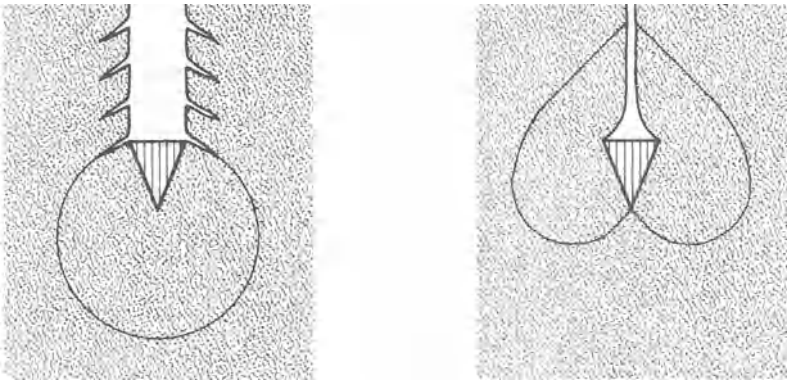

Fig. 3.26a, b. Steady state zones of wedge influence in compactible (a) and incompactible soil (b)

In the soil that has passed the wedge, tensile cracks will appear. If only little compaction occurs, the soil flow bends around the wedge to leave only very little empty space above it, because the area occupied by the soil in the considered plane cannot diminish much. In soil with low compactability, the zone immediately under the wedge tip is confined, which precludes significant soil movements in this zone. The above has consequences for the shape of the zone of influence. Figure 3.26a shows the general shape of this zone when much compaction occurs, and Fig. 3.26b refers to the condition of no compaction, only deformation.

As the tip angle and/or wedge surface roughness increase, the size of the zone of influence increases, and the soil near the wedge lags more behind in the upward soil movement (the soil near the wedge and the wedge act more as an entity). Compaction also increases. It is noted that

- in brittle soil, discontinuities (fractures) formed periodically by shear failure are to be expected,
- the deformation patterns to the left and to the right of the vertical center-line of the wedge may not be entirely symmetrical because of soil heterogeneity and instability,
- a higher penetration velocity is likely to result in a zone of influence that is smaller and shifted upward relative to the wedge.

Acute Wedge During Initial Penetration. Strictly speaking, a steady state can never exist because gravity induces a stress field in the soil that varies with depth; $(\sigma_z) = \rho g z$, with ρ is wet bulk density, g is acceleration of gravity, and z is depth. This depth-dependent stress field also affects the zone of influence. This gravity effect increases as

- the zone of influence is larger,
- the stresses due to internal soil friction and soil-wedge friction are more dominant than the stresses due to soil cohesion,
- the soil compactability decreases.

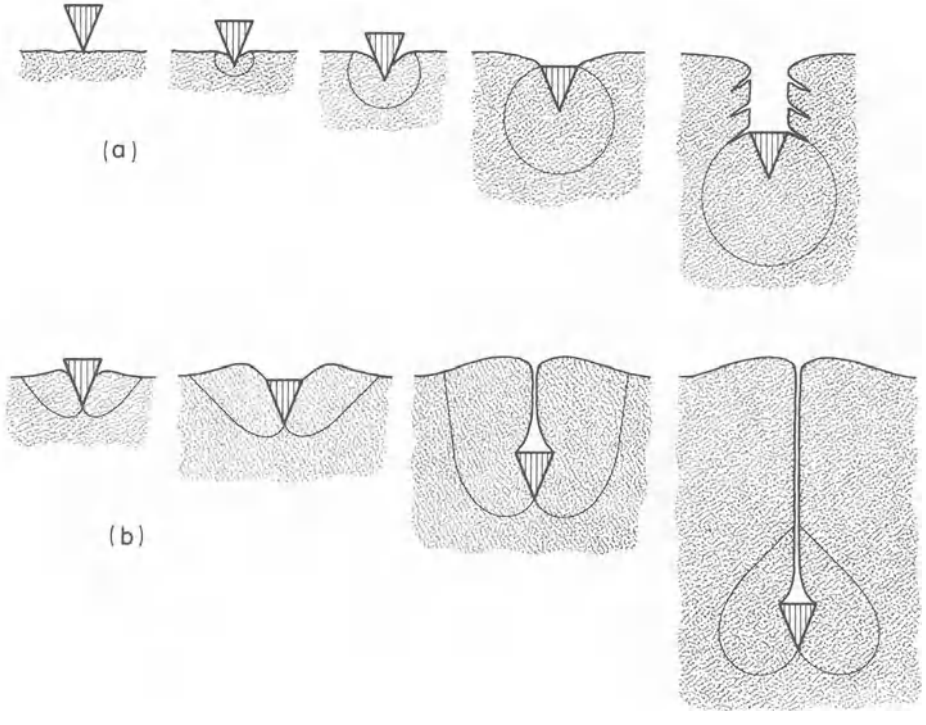

Fig. 3.27a, b. An acute wedge penetrating very compactible soil (a), and incompactible soil (b)

The initial phase of wedge penetration will be discussed further for the case of much compaction, and of little compaction.

With much compaction the zone of influence in the steady state will be as shown in Fig. 3.26a. When the tip starts penetrating (Fig. 3.27a), the zone of influence is still very small. As the wedge penetrates further, the active wedge width increases and the zone grows. From the moment the wedge is just entirely below the soil surface, the active wedge width does not increase anymore. But since the zone of influence at this moment is the result of a non-steady process, the shape of the zone is not yet that of the steady state. On further penetration the zone of influence still increases, while soil is entering at the lower boundary and leaving at the upper boundary. Initially, more soil is entering than leaving. After some time both quantities become equal and the steady state is reached. The steady state will be reached sooner as the exchange per unit length of wedge path increases. The exchange is larger with smoother wedge surface, smaller wedge tip angle, and less soil compactibility.

With little compaction the zone of influence in the steady state will be like that in Fig. 3.26b. When penetration starts (Fig. 3.27b) the zone is still very small. Because of the low compactibility, displacement of soil by the wedge has to be accompanied by a rise of the soil surface (free area) near the place of penetration. On further penetration, the active wedge width as well as the wedge depth increase, resulting in a larger rise of the soil surface and growth of the zone

of influence. As soon as the wedge is just entirely under the soil surface, the hole left by the wedge starts to contribute to the total free area, and soil will also flow towards this hole. Initially, the zone of influence keeps growing. As penetration depth increases, it gradually becomes easier for the displaced soil to flow to the hole than to the soil surface. In this transition stage the zone of influence reaches its maximum volume and becomes smaller thereafter. At a certain moment, the soil flow to the surface becomes zero, after which the steady state (as given in Fig. 3.26b) is soon attained.

Infinitely Long Strip in a Steady Field. When an infinitely long, flat, horizontal, rigid plate of constant width is forced into soil, a soil wedge is formed under the strip. Therefore, the steady state is essentially the same as in the case of an acute wedge, but now the wedge is built up of soil.

The angle of the soil wedge tip will be between 45° and 90° (the angle being larger as the angle of internal soil friction is smaller). If the soil is compactible, the soil wedge will be very compacted. No exchange of soil occurs between the wedge and its surroundings; the wedge and the plate move downward as a rigid entity, while the surrounding soil moves upward along the sides of the wedge. Frictional forces act on these wedge sides according to the soil-soil friction angle.

Infinitely Long Strip During Initial Penetration. If the soil cannot be compacted, the soil wedge is formed at the moment the downward moving plate starts to penetrate the soil. The wedge is already formed completely before any bulging up of the free surface occurs. For the rest, the process during the initial period resembles very much that for an acute wedge in a not very compactible soil.

If the soil is very compactible, the initial period will be longer because a relatively dense wedge can only be formed in the relatively loose soil after the strip has traveled a certain distance in the soil.

Related Bodies. The phenomena described above for an acute wedge and a strip also occur, in modified from, in the case of related bodies, such as

- an obtuse wedge,
- acute and obtuse cones,
- rectangular and circular plates,
- a wire,
- a sphere.

Under an obtuse wedge or cone, a soil wedge or soil cone is formed which moves together with the body and transforms the body into an acute wedge or cone. The division between acute and obtuse cones and wedges lies at a tip angle of about $90° - \phi$, where ϕ is the angle of internal soil friction. Ahead of a penetrating sphere, a small soil cone is built up that lies as a cap against a sphere sector (the heading part of a sphere may be considered to be obtuse and the side parts to be acute). Behavior with a round wire is similar.

3.3.2.2 Dynamic Aspects

Force-Sinkage Relationships

Acute Cone in Steady Field. The vertical force on an acute cone moving in a field that may be considered steady depends on base area, tip angle, soil-cone friction angle, soil properties, and penetration velocity. As a first approximation the vertical force is proportional to the base area. For this reason, cone resistance is usually expressed as the quotient of the vertical force and the base area, called *cone index (CI). CI* is insensitive to the size of the cone; except when the base area varies over a broad range, it decreases slightly with increasing base area. For example, Schothorst (1974) found that a ten-fold increase in base area gave a eight-fold increase in required force, and thus a 20% decrease of *CI*. This is because with larger cones, the importance of cohesive forces (so-called surface forces) decreases relative to gravity forces (so-called body forces).

The tip angle – cone index relationship is a curve with a minimum (Gill 1968) (Fig. 3.28). This minimum is a result of the large friction which the large surfaces of very acute cones encounter. This figure also shows the influence of the soil – cone friction angle δ; teflon cones have a much smaller δ than steel cones. For instance, for Decatur soil δ was 15° with teflon and 30° with steel (Gill 1969).

The penetration force also depends on the soil properties. This dependency is almost entirely determined by soil type, pore space, and moisture content; variations in soil structure of the same soil type, pore space, and moisture content have only minor influence on the penetration force for this load bearing process. The influence of moisture content and pore space is demonstrated in Fig. 3.29 for a cone with a diameter of 4 mm, a tip angle of 60°, and a velocity of 0.06 inch per second (Camp and Lund 1968). As for soil type, measurements in dry sands and gravels showed that *CI* increases with increasing particle sizes and increasing size uniformity (Melzer 1970).

The speed dependency of *CI* may be examplified by Fig. 3.30 (Freitag 1968). The soil strength ratio is defined as the ratio of the penetration resistance of a standard cone penetrating at 7.2 inches per minute and the penetration resistance of the same cone at a different rate of penetration. The speed effect decreases with soil clay content.

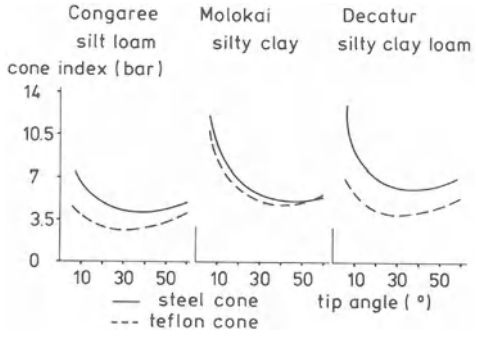

Fig. 3.28. Cone index as affected by cone tip angle and cone surface roughness (Gill 1968)

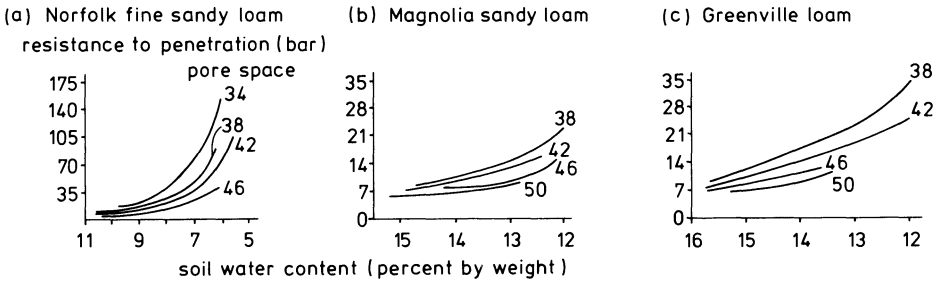

Fig. 3.29a–c. Resistance of a small cone as affected by soil type, pore space, and moisture content (Camp and Lund 1968)

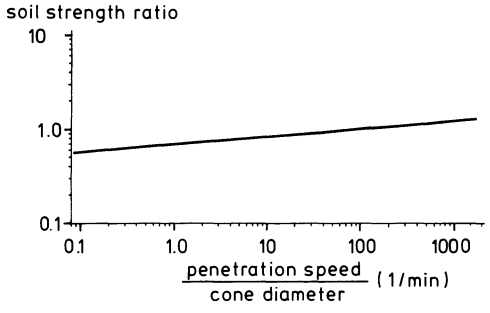

Fig. 3.30. Speed dependency of cone index (Freitag 1968)

If the soil is hard, and cracks develop in penetration, the penetration force fluctuates as the cone progresses, even in a homogeneous soil. In such unstable processes, the resultant force on the cone nearly always has a component in a horizontal direction (Butterfield and Andrawes 1972a).

Acute Cone During Initial Penetration and Acute Cone in Non-Steady Field. Initially, the penetration force increases with increasing depth. Thereafter, the force can usually be considered non-varying with depth. Cone index (*CI*) for a particular layer (also a top layer) is generally given as the average penetration resistance of this layer. If gravity plays an important role (as in dry sand), a constant resistance will never be found and a cone index gradient is used to describe penetration resistance to a certain depth z; namely the cone index at z divided by z (Melzer 1970). Experiments in cohesionless materials where acceleration of gravity g was varied (Costes et al. 1971) showed that gravity can play an important role.

In cone testing, the question arises whether penetration depth should be measured from the tip or from the base of the cone. When we want to determine *CI* as an average to a certain depth, then the best method is to measure depth from the base. In that case, zero cone depth corresponds with the cone base being flush with the soil surface, and the initial stage, where the active cone diameter is smaller than the real diameter, has no influence on the determined *CI* value. But when the vertical variation of a soil property is traced by measuring the cone

index – penetration depth curve, *CI* correlates best with the soil property if cone depth is measured from the tip of the cone (Williford and Larson 1968).

Plate. For a circular plate moving in a steady field, the penetration force is the same as for a cone having the same diameter, a tip angle of $90° - \phi$, and a soil-cone friction angle of δ.

However, plate diameters usually are not small relative to penetration depth and, therefore, plate penetrations usually correspond to the initial period. Because of this, force – depth relationships for plates during the initial period received much attention (Bekker 1969). Since at first contact with the soil a plate acts immediately over its full width, the penetration force at first increases relatively fast with depth. For this very first part of the initial period, solutions assuming elasticity are available (Harr 1966).

When a plate is used to trace a soil property varying with depth, it is advisable to take the presence of a soil wedge or cone in front of it into account.

When one changes from a circular to a non-circular plate, at constant plate width, the stress needed to reach a certain depth generally decreases slightly with plate aspect ratio (plate length/plate width) (Bekker 1969). This effect is small, however, and, therefore, it always holds that total penetration force increases with plate area.

Force – sinkage relationships for wires and spheres resemble in many aspects those for cones and plates.

Stress Distributions

Among the different bodies discussed, the circular plate and the infinitely long strip received most attention in research on stress distributions, because their shapes are best suited for this. In the beginning of the initial period, soil behavior was assumed elastic and stress distributions were calculated. They are published in numerous textbooks on elasticity. These calculations usually assume that the plate and strip are rigid and smooth. It appears that for this case normal stresses on the interface increase towards the edge, becoming, theoretically, infinitely large at the edge. As perfect smoothness has been assumed no shear stresses can occur on the interface. Within the soil, principal stresses decrease with increasing distance from the plate or strip, and shear stresses reach a maximum about under the sides of the plate or strip at a depth of about 1/4 of the plate or strip width. With further penetration, soil behavior deviates more from that of an elastic material. At first, maximum normal stresses in the contact area remain situated near the edge, and in some soils this does not change on further penetration. In other soils, normal stresses increase relatively more in the center of the interface, so that a stress distribution develops at the interface having peaks in the center and at the edge. As penetration continues, the central peak may grow so much that it overrules the outer peak, leading to a stress distribution with only a central peak.

In general, reproducibility of the stresses is low due to natural soil heterogeneity, to unstable deformation processes sometimes playing a role, and to the random build-up of the inner of the soil wedge as soil is exchanged.

With penetrating cones and wedges under normal soil conditions, highest stresses occur near the tips (Butterfield and Andrawes 1972a).

3.3.3 Applications

3.3.3.1 Fitting Formulas for Plate Tests

In a plate test, a force-depth curve is usually measured for the initial period. Several fitting formulas have been proposed for such curves. Parameters in such formulas may be considered soil mechanical properties characterizing soil resistance against penetration. Two formulas should be mentioned.

1. Bernstein's formula (1913)

$$p = kz^n$$

where k and n are soil mechanical properties which can easily be determined by plotting measured (p, z) combinations in a $(\log z, \log p)$ graph. Actually, k and n are not "true" soil properties; k in particular varies strongly with plate dimensions.

2. Bekker's formula (1960)

$$p = \left(\frac{k_c}{b} + k_\phi\right) z^n$$

where b is the plate width and k_c, k_ϕ, and n are soil mechanical properties. k_c, k_ϕ, and n can be determined from tests at two different b values ($b_2 > b_1$). By plotting the results of these two tests in a $(\log z, \log p)$ graph, we obtain for each plate width a straight line described by

$$\log p = n \log z + \log\left(\frac{k_c}{b_i} + k_\phi\right) \qquad i = 1, 2 .$$

The slopes of these two lines must be equal and from them n, being the tangent modulus of these lines, can be determined. The two lines intersect the $\log p$ axis in a_1 for plate width b_1 and a_2 for plate width b_2. It can be calculated that

$$k_\phi = (a_2 b_2 - a_1 b_1)/(b_2 - b_1)$$
$$k_c = ((a_1 - a_2) b_1 b_2)/(b_2 - b_1)$$

(Bekker 1960). It appears that k_c and k_ϕ and to a lesser extent also n, still depend slightly on b_1 and b_2. Other fitting formulas are presented in Sela and Ehrlich (1971), Reece (1965), and Wills (1966).

3.3.3.2 Bekker's Sinkage and Rolling-Resistance Theory for Rigid Wheels

To estimate rut depth of a rigid wheel on soft soil, Bekker (1960) developed the following approximation (Fig. 3.31). The vertical wheel load, W, is a *boundary condition.* Consider an arbitrary surface element on the wheel surface. The approximation involves two assumptions

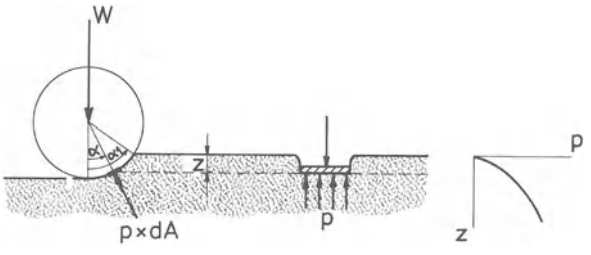

Fig. 3.31. Illustration of Bekker sinkage and rolling resistance theory

1. the soil reaction force on this surface element is perpendicular to the wheel surface and passes therefore through the wheel axis (the magnitude of this reaction force = stress $p \cdot$ elemental area dA);
2. the stress p is equal to the stress under a plate that has been pressed into the soil to the same depth as that of the surface element.

When the p-z relation is now determined with a plate, all stresses on the wheel surface are known. The plate test takes the place of the *soil behavior equations* (stress-strain relationships). Mathematically, the result of the plate test can be expressed as

$$p = \left(\frac{k_c}{b} + k_\phi\right) z^n$$

with k_c, k_ϕ, and n being soil properties (see previous section). Now an *equation of equilibrium* can be formulated by placing W into equilibrium with the sum of all vertical components of the stresses on the wheel surface. By solving this equation of equilibrium, the rut depth d can be calculated. The (simplified) result is

$$d = \left[\frac{3W}{(3-n)\, b\left(\frac{k_c}{b} + k_\phi\right)\sqrt{2r}}\right]^{\frac{2}{2n+1}}$$

with b is wheel width and r is wheel radius.

The approximation of the rolling resistance R is based on the assumption that the rolling resistance energy A, expended in making a rut of length l (so, $A = R \cdot l$), is equal to the energy expended in forcing a plate of length l and width b into the soil to a depth d. Hence,

$$A = Rl = \int_0^d blp\,dz = bl\int_0^d \left(\frac{k_c}{b} + k_\phi\right) z^n dz = bl\frac{k_c/b + k_\phi}{n+1} d^{n+1}$$

so that

$$R = b\frac{k_c/b + k_\phi}{n+1} d^{n+1}.$$

3.3.3.3 Correlations Between Cone Tests and Wheel Performance

Since cone tests and wheel processes both are load bearing processes, there must be some resemblance. Therefore, one has tried to predict certain aspects of wheel process from aspects of cone tests, which are easy to measure.

What aspects of cone processes can be used for this? Most often, the average *CI* of the top 15 cm of soil is used. When a great rut depth is expected it is better to select this 15 cm thick layer somewhat below the soil surface. A complication arises from the fact that soil properties change as a result of the rut formation, particularly with repeated passes in soils that compact easily. This is why sometimes the domain of a prediction method is confined by excluding very compactable soils, and why sometimes a rating cone index is used instead of the cone index *CI*. A rating cone index (*RCI*) is usually calculated by multiplying *CI* with the so-called remolding index *RI*. According to Turnage (1972), "the index *RI* is usually obtained by placing an undisturbed sample of the test soil, approximately 18 cm long and 4.8 cm in diameter, in a cylinder of approximately the same dimensions attached to a base plate, and subjecting the soil to 100 blows with an 11-*N* hammer falling 30 cm. For very weak soils (cone index values of about 70 and under), the sample is enclosed, and the entire test instrument is dropped 25 times onto a rigid surface from a height of 15 cm. Cone index measurements are made at the surface and at 2.5 cm-vertical increments to a depth of 10 cm before and after compaction. The ratio of the sum of cone index values obtained after compaction to the sum of those obtained before compaction, expressed as a decimal, is the remolding index. According to Knight and Freitag (1962), for fine-grained soils, correlations are of the highest quality when the rating cone index of the soil in the layer from 6 to 12 in. below the surface is considered. For very light vehicles the critical layer is 3 in. closer to the surface, and for very heavy vehicles the critical layer is 3 in. deeper". For cohesionless soils (Turnage 1972) one usually tries to find correlations with the quantity *G*, which is the slope of the curve of cone index versus depth, averaged over the depth within which changes in soil strength significantly affect tire performance (usually taken as 15 cm).

It has been tried experimentally to establish correlations of cone process aspects to various wheel process aspects. A very rough measure of wheel performance is the "go" or "no go" criterion for an entire vehicle, that is whether a vehicle is able to cross a piece of land or that its rolling resistance is too high for the vehicle to proceed in an acceptable way (Knight and Freitag 1962). A more detailed relation is the correlation between a cone test aspect and the rolling resistance or pull-slip relation (or part of it) of a given tire at a given vertical load and a given tire inflation pressure. Such correlations may be especially interesting in cases involving little variation at the vehicle side, but large variations at the soil side. This is usually the case in the agricultural practice on a farm. An even more detailed result is obtained if the mentioned wheel process aspects are considered for different tire sizes, vertical loads, and tire inflation pressures. The empirically determined correlations are then described by formulas, which apply to large domains. For the domain of terrain vehicles such formulas are found in Turnage (1972). Wismer and Luth (1973) presented such formulas for the domain covering agriculture, forestry, and earth moving.

For towed wheels Wismer and Luth propose

$$\frac{TF}{W} = \frac{1.2}{C_n} + 0.04$$

TF = towed force of wheel, parallel to soil surface,
W = dynamic wheel load, normal to soil surface,
C_n = wheel numeric $CI \cdot b \cdot d/W$ (dimensions must be selected such that the wheel numeric is dimensionless),
CI = cone index measured with a cone penetrometer as defined in ASAE R 313 (NN 1981),
b = unloaded tire section width,
d = unloaded overall tire diameter.

For driven wheels they propose

$$\frac{P}{W} = 0.75\,(1 - e^{-0.3 C_n S}) - \left(\frac{1.2}{C_n} + 0.04\right)$$

P = wheel pull, parallel to soil surface,
W = dynamic wheel load, normal to soil surface,
e = base of natural logarithms,
$C_n = CI\,b\,d/W$,
S = slip.

The formulas apply to the following conditions:

- the wheel should be provided with a pneumatic tire having a "conventional" tread design,
- the soil should not be a $c = 0$-soil,
- b/d should be about 0.3,
- tire deflection should be about 20%,
- the zero-slip condition is the self-propelled condition on a hard surface,
- CI should be measured before the soil is passed over and averaged over the top 15 cm of the soil. In case a greater rut depth is expected, this layer should be selected to be somewhat under the soil surface,
- the soil should not be highly compactible, such as freshly tilled soils.

These formulas were determined experimentally for the tires that were commonly used in the mentioned domain around 1972. The highest values for b, d, and W investigated were 840 mm, 1650 mm, and 3000 kg, respectively. CI varied from 20 to 500 psi. For the quality of these approximations, consult the original literature.

3.3.3.4 Quick Determination of a Soil Mechanical or Physical Property

With penetrometers quick measurements can be done. This is an advantage over many other methods to determine a soil property. In certain cases penetrometer readings have been used successfully to estimate cohesion, angle of internal friction, or pore space (equivalent to BWV or γ), moisture content, or soil water

suction. Measurements of the upper plastic limit *UPL* were very successful (Campbell 1975). Wedge-shaped bodies have been used to determine angle of soil-metal friction (see Sect. 2.5.2).

Cone resistance varies with cohesion and internal friction. This may be expressed for a given cone by

$$CI \quad \text{or} \quad G = f(c, \phi) . \tag{1}$$

The degree of uniqueness of this function depends on the domain that has been selected. The degree of uniqueness is very low if this domain has to cover all soils and all soil conditions, but if it is confined to one soil type, the degree of uniqueness can be great and the function can be determined through experiments. The measuring result is often presented as a calibration graph (Freitag 1968). Such a graph can be used to determine ϕ (or c) with a penetrometer if c (or ϕ) are known from another source. When the domain is confined to $\phi = 0$-soils, the function will have a high degree of uniqueness. Then it holds that $CI = 12.5\ c$, independent of soil type (Freitag 1968). There is also a unique relationship between G and ϕ when $c = 0$, but this relationship is specific for one soil type (Freitag 1968, Costes et al. 1971). The degree of uniqueness of Eq. (1) is not always large due to variations in soil-metal friction, and to compaction and deformation which change c and ϕ locally during cone penetration.

Cone resistance can also be seen as a function of soil physical properties that are related to the soil mechanical properties. This may be expressed for a given cone by, for example,

$$CI, G = f(\theta, P, \text{soil type, soil structure}) \tag{2}$$

with θ is moisture content and P is pore space. This function has a high degree of uniqueness, but it is difficult to express soil structure, especially binding and arrangement of soil particles, in a quantitative way. Fortunately, soil structure often plays a modest role in Eq. (2) because of the load bearing character of the process. Therefore, it is often acceptable to neglect soil structure as a factor, although under a few conditions structure differences can cause significant differences in *CI* (von Boguslawski and Lenz 1958). In experiments with artificially prepared soils, one often starts from a single mixture of soil and prepares the samples following a more or less uniform procedure. Then the effect of soil structure is "confounded" with that of soil moisture content and/or pore space, and the factor of soil structure can be omitted in Eq. (2). The question may arise whether it is not better to use soil moisture suction (pF) instead of moisture content in the formula. Since soil moisture suction may show considerable change locally on penetration, whereas moisture content will stay relatively constant, the formula is likely to have a higher degree of uniqueness when θ is used.

Confining ourselves to a single soil type, we may write,

$$CI, G = f(\theta, P) . \tag{3}$$

Such functions were determined experimentally by Taylor and Gardner (1963), von Boguslawski and Lenz (1958), and Camp and Lund (1968). Figure 3.29 was taken from the last article. General properties of Eq. (3) are that cone resistance

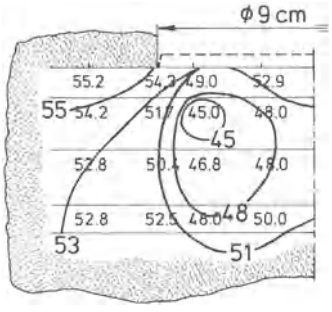

Fig. 3.32. Lines of equal pore space under a plate impression, determined through micro-penetrometer measurements (numbers are pore spaces expressed as percentages)

does not depend much on moisture content in loose soil, and that cone resistance is not much influenced by pore space at high moisture content. For instance, the relation between CI and θ in wet soil is not much influenced by small variations in pore space.

When, furthermore, moisture content is kept constant, Eq. (3) changes into

$$CI, G = f(P) . \tag{4}$$

An application of this formula is given in Fig. 3.32. Resistances of a micro-penetrometer were measured for a Lexkesveer loam soil at a moisture content of 16% by weight, and an initial pore space of 55%, which was impressed with a max. mean pressure of 1.5 bar by a rigid circular plate with a diameter of 9 cm, at different places and depths under the impression. After making for the same soil and the same moisture content a "calibration curve" $P = f(CI)$ with the same micro-penetrometer, the penetrometer readings could be transformed into pore space data, which are given in the figure. These data made it possible to draw lines of equal pore space, as shown. G-P relations for air dry cohesionless material are given by Freitag (1968), Melzer (1970), and Costes et al. (1971).

When P is kept constant instead of moisture content Eq. (3) becomes

$$CI = f(\theta) . \tag{5}$$

Using an empirically determined calibration curve of this form, the penetrometer can act as a moisture content meter under conditions of constant soil type and constant pore space at varying moisture content.

3.3.3.5 Determination of the Maximum Normal Stress That Has Ever Acted on a Soil Surface

Consider the surface of an initially loose soil, immediately after it has been loaded by a body (for example, by a plate, a wheel, a tire, or a plow body). Imagine this surface divided into small surface elements which are the upper faces of cube-shaped volume-elements located in a layer immediately under the surface. During the loading the normal stress on each surface element varied. The maximum value of the normal stress on such an element will be designated by σ_n. Subsequently, we measure the penetration resistance R in the center of

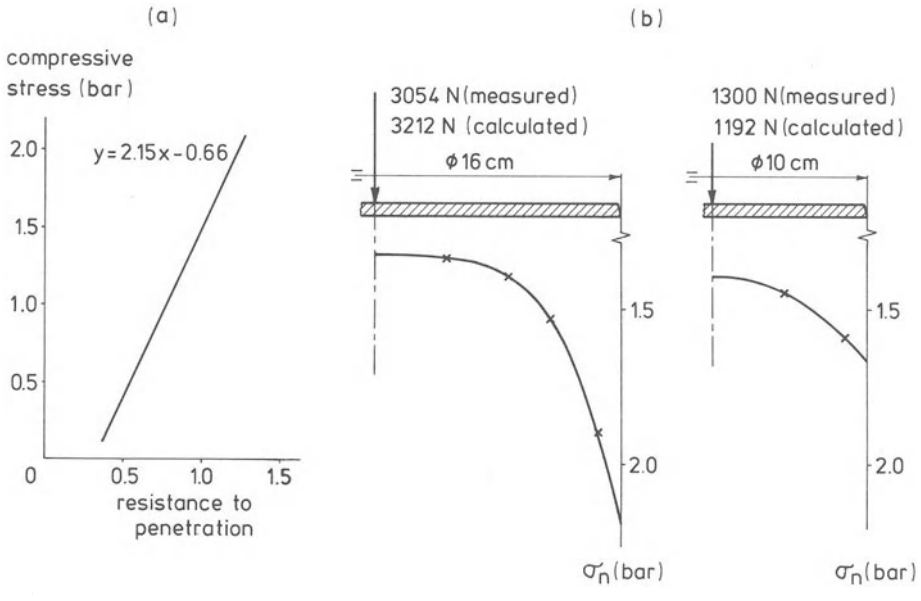

Fig. 3.33a, b. Stress distributions underneath plates (b), determined with pocket-penetrometer after removal of the plates, using the calibration curve (a)

each surface element with a micro-penetrometer. The penetrometer should be small enough and the surface element large enough to prevent neighboring measurements from influencing each other. The penetration depth may not be so large that the variation with depth of the maximum principal stress was significant above this depth.

For each surface element, a close relation exists between σ_n and R, because

1. on a surface element σ_n is often nearly equal to the maximum principal stress σ_1 in the adjacent volume element during loading (relationships between σ_n and σ_1 have been discussed in Sect. 2.5.3.1),
2. the pore space of the volume element is generally mainly determined by σ_1 (see Sect. 2.2.2.2),
3. R is determined by pore space.

To determine σ_n-values from R-values a calibration curve is needed. To obtain this, fill a number of cylinders having a sufficiently great diameter-to-height ratio from the same batch of loose soil. Then, compact the soil in each cylinder under a piston to a given maximum stress (σ_n), in such a way that a broad range of σ_n-values is obtained. Now, determine R in each cylinder with the micro-penetrometer and, using the measured σ_n-R combinations, compose the calibration curve.

An example of this method is the following experiment. Lexkesveer loam soil that passed a 5-mm-screen, was moistened to a moisture content of 20% by weight and precompacted to a pore space of 50%. Two circular plates with diameters of 10 and 16 cm, respectively, were pressed into this soil to a depth of

10 cm and maximum pressing forces were measured. After removal of the plates, shallow micro-penetrometer tests were carried out with a "Soil-test" pocket-penetrometer (NN 1971). The calibration curve shown in Fig. 3.33 a was obtained by plotting measurements in 11 cylinders with a diameter of 15.3 cm and a height of 12 cm. The observed patterns of penetrometer readings from the soil beneath the two plate impressions were then transformed into σ_n-distributions, using the calibration curve. The obtained distributions of σ_n-values under the plate impressions are shown in Fig. 3.33 b. From each stress distribution, a maximum pressing force could be calculated using a summation procedure. Measured and calculated maximum pressing forces are also presented in Fig. 3.33 b. Agreement is very satisfactory.

3.3.3.6 Other Applications of Penetrometers

Rootability. There is a relationship between *CI* and rootability. Investigations show that if $CI \approx 30$ bar or higher, root growth is almost impossible (Taylor and Burnett 1964, Taylor and Gardner 1963, Camp and Lund 1968, Van Dam and Hulshof 1967, Houben 1970). In Dutch sandy soils plant roots often approach the groundwater table close enough to assure their water demand even in dry periods. If a soil is so dense that plant roots cannot reach deep enough, subsoiling may give considerable improvement. The benefit that may be derived from subsoiling depends on

1. *CI* as a function of depth,
2. depth of groundwater table,
3. rooting depth in loose soils under normal conditions.

Resistance Against Trampling of Grassland. Penetrometer measurements were carried out on many Dutch grasslands and the measured average bearing capacities were related to observed trampling damage from cattle. This showed that grassland with an average *CI* of 5 bar will be severely trampled in grazing, whereas a *CI* of 7 bar or higher indicates that trampling resistance is sufficient (Schothorst 1963).

Kop (1960) also measured resistance against trampling of Dutch grassland. For a cone with 5 cm^2 base area, he found $CI = 6$ and $CI = 9$ as the boundary values between grasslands having low, medium, or high resistance against trampling.

Sportsfield Damage. Van Wijk and Beuving (1975) state that *CI* must be at least 14 bar on intensively used parts and 10 bar on extensively used parts of a soccer field when severe turf damage as a result of soccer playing is to be avoided. The *CI* values were measured at 2 – 3 cm depth with a steel cone having a tip angle of 60° and a base area of 1 cm^2. These *CI*-values apply to Dutch circumstances.

Uniformity Tests. Suppose that a series of tires or tools must be tested under equal soil conditions. Penetrometer tests are then very feasable to check the uniformity with place and time of the selected test area. The same holds for soil bins or containers that are prepared for laboratory tests.

3.4 Sliding and Shearing Bodies

3.4.1 Occurrence

Sliding and shearing bodies occur very frequently. On many occasions their role is of minor importance, on others their function is essential. Examples are the slade and heel of plows. Implements like rotavators, spading machines, and cultivators are often carried by sleds. Sleds are also used as a means of transport. Drainage machines may use large plates to retain the sides of the trenches as the drain is brought in. In this group, we also find track shoes, cams on cage wheel treads, etc.

In research one uses sliding and shearing bodies to measure frictional properties and to estimate soil strength and deformability.

3.4.2 Fundamentals

Sliding and shearing bodies may be separated into

- bodies having only a slight tendency to induce horizontal soil movements, like smooth plates and sleds,
- bodies that do feature this tendency, but induce deformation patterns that do not vary strongly in horizontal directions, such as shear plates and shear annuli,
- bodies having the same tendency, but now with strong horizontal variations in the deformation patterns, e. g. shear elements.

3.4.2.1 Kinematic Aspects

Smooth Plates and Sleds

When a smooth sled is moved over a soil surface, shear stresses in the contact plane will be so small that hardly any soil displacement occurs. But vertical movements may occur, depending on (Bernacki and Haman 1973)

- the sled angle of inclination,
- whether the sled is forced to follow a particular path (displacement-controlled) or is subjected to a particular vertical load (force-controlled),
- soil compactibility and deformability.

Force-Controlled, Pendulating Sled. In general, the point about which the sled can pendulate is at 1/3 of the sled length from the trailing end (Bekker 1956). The sled is provided with an upward bended nose to avoid penetration, which is especially important on uneven surfaces. Figure 3.34a shows such a sled on a relatively hard soil and Fig. 3.34b on a soft soil. As the soil is softer and/or the load is larger, the inclination is greater. For intermediate soil conditions (relatively soft, but precompacted soil), a situation as given in Fig. 3.34c can be expected; the sled does not fully contact the soil.

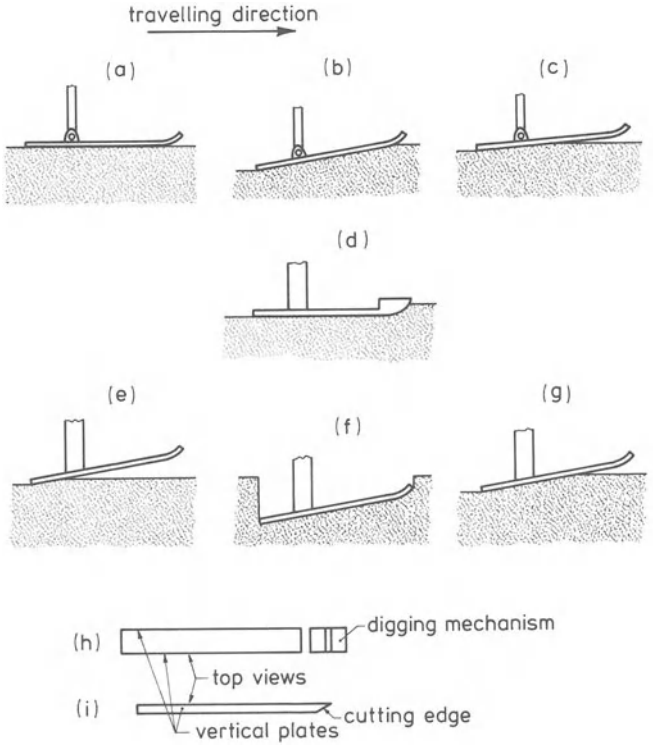

Fig. 3.34a – i. Sleds and smooth plates

Force-Controlled, Not Pendulating, Horizontal Sled. On a hard soil such a sled will not penetrate. On a relatively soft soil, a situation as in Fig. 3.34d will occur; the nose compacts the soil to a higher bearing capacity, and the sled is supported by soil having this higher bearing capacity. A heavier load and/or a shorter sled and/or a softer soil will give greater sinkage.

Force-Controlled, Not Pendulating, Trimmed Sled. This sled is not horizontal but has a fixed inclination. Figure 3.34e applies to hard soil. Contact stresses at the rear of the sled can be so high that some sinkage occurs even on hard soil. The situation of Fig. 3.34f may occur on very soft soils unless the mean stress is very small. The deep sinkage prevents the sled from moving forward. An intermediate case is shown in Fig. 3.34g. Sinkage and contact area increase with increasing load and/or softer soil. For a given soil and load, a greater inclination will cause a greater sinkage and a smaller area of contact.

Displacement-Controlled Plate with Zero Trim Angle. When a plate moves through soil in the direction of its length, an aid is needed to clear the path. This aid can be a digging mechanism (Fig. 3.34h), but also a cutting edge on the plate (Fig. 3.34i). In the latter case the soil is pushed aside and the plate moves along soil that has been freshly precompacted, or along precompacted soil that has been compacted further. A disc coulter is an example of such a plate with cutting

edge. To a first approximation, a disc coulter moves through the soil at a slip percentage of zero (Bernacki and Haman 1973).

Ruts left behind by a sled or plate often feature small inclined cracks in a forward and downward direction. Sleds can be very rigid, but sometimes they are flexible, so that the ends of the sliding surface are bent upward.

Shear Plates and Annuli

Shear plates and shear annuli are so designed that they cannot slide along soil easily. This is often achieved by lamellae that are pressed into the soil, or by sand grains glued to the surface. When such a plate is pulled tangential to the soil surface, soil particles tend to move together with the plate, so that the horizontal displacement of soil is usually not negligible. Furthermore, vertical soil movement may occur. In practice, only force-controlled, horizontal, not pendulating plates are important.

Infinitely Large Plate. When an infinite, horizontal plate is loaded, the degree of sinkage depends on the soil compactibility. If, in addition, a horizontal stress is applied, while the normal stress is not too small, the soil will deform according to a pattern as in Fig. 3.35a, until it breaks along a plane as in Fig. 3.35b. In the

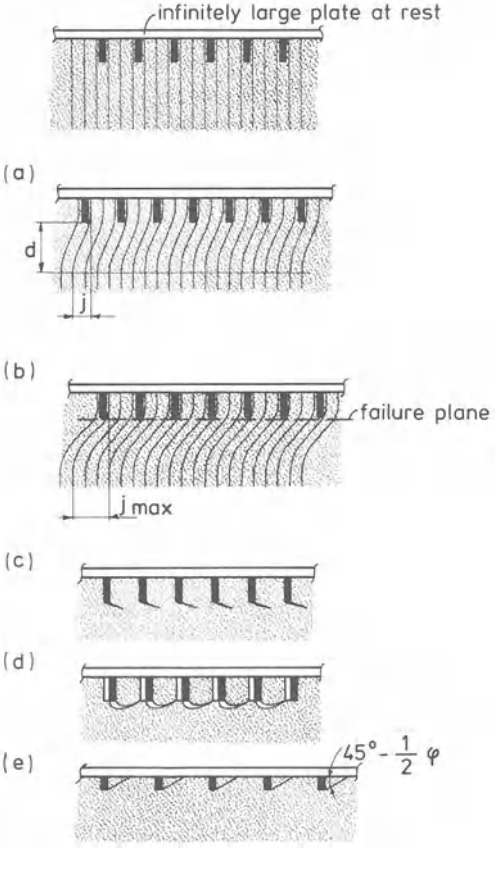

Fig. 3.35a – e. Soil behavior under an infinitely large shear plate

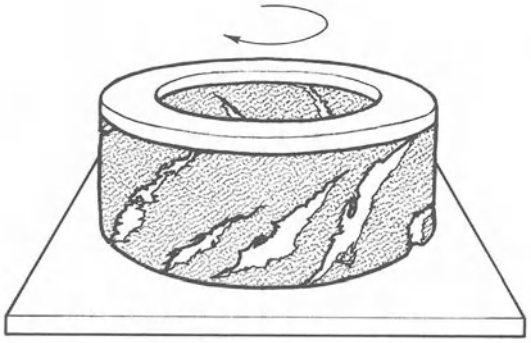

Fig. 3.36. Tensile cracks due to pure shear

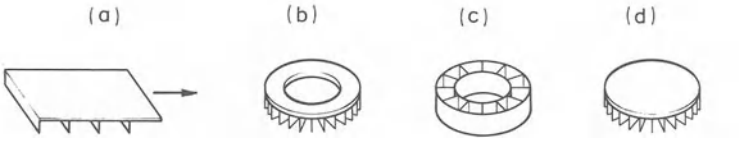

Fig. 3.37 a – d. Finite shear plate and shear annuli

case of lamellae, the plane of breaking will pass through the lamella tips. Usually, the breaking plane does not develop instantaneously over its full size; "progressive failure" occurs with crack fronts propagating from the lamella tips in a horizontal and forward direction. The breaking plane is complete as soon as each crack has reached an adjacent crack. Depending on the magnitude of the vertical stress and the soil properties, dilatancy may occur, involving plate movement upward and inclined to the horizontal. Usually, the tangential plate movement is accompanied by additional sinkage, called *slip sinkage.*

The process described above can only exist with an infinitely large plate, if soil strength increases with depth. If this is not the case, sinkage as a result of applying a vertical stress will be infinitely large and the zone of influence of a horizontal plate displacement will extend infinitely deep. Thus, soil profile variation with depth determines the maximum value of j and the value of d (Fig. 3.35 a and b).

When the vertical stress on the plate is small, the soil is cohesive, and lamellae are present, a tangential movement of the plate will induce tensile cracks running in an inclined forward and downward direction (compare with Fig. 3.36, showing torsion cracks in a twisted thick-walled hollow soil cylinder). These cracks start from the tips of the lamellae (Fig. 3.35 c). With proceeding movement, the cracks develop further. They bend around and end at the tip of the preceding lamella (Fig. 3.35 d). In this case the displacement of the plate is forward and upward.

With small vertical stress on the plate, relatively short lamellae and low cohesion, tangential plate movement will cause the development of inclined shear planes in a forward and upward direction in front of each lamella (Fig. 3.35 e). This phenomenon is accompanied by inclined, forward and upward, plate movement.

Finite Plate. With finite plates, the zone of influence is finite as well. The size of this zone depends on plate size and vertical load. The edges of finite plates vary widely in shape. A few examples are given in Fig. 3.37. The edges may induce local side effects in the soil at the front, back, and laterally. The character of these side effects may be deduced from the effects described in the following section on shear elements. Ring-shaped plates, of course, show no front- and back-side effects.

Shear Elements

Shear elements have very different shapes of which Fig. 3.38 shows examples. The usual initial positions relative to the soil surface are indicated by the dotted lines representing the soil surface. Shearing takes place in the plane of view. The dimension of a shear element perpendicular to the plane of view is generally large compared to the other dimensions. In Fig. 3.38 the three basic shapes can be distinguished: a shear element with vertical grouser, an inclined shear element, and a horizontal flat shear element. However, the shape has no great influence on the size of the zone of influence (Jaworski et al. 1978).

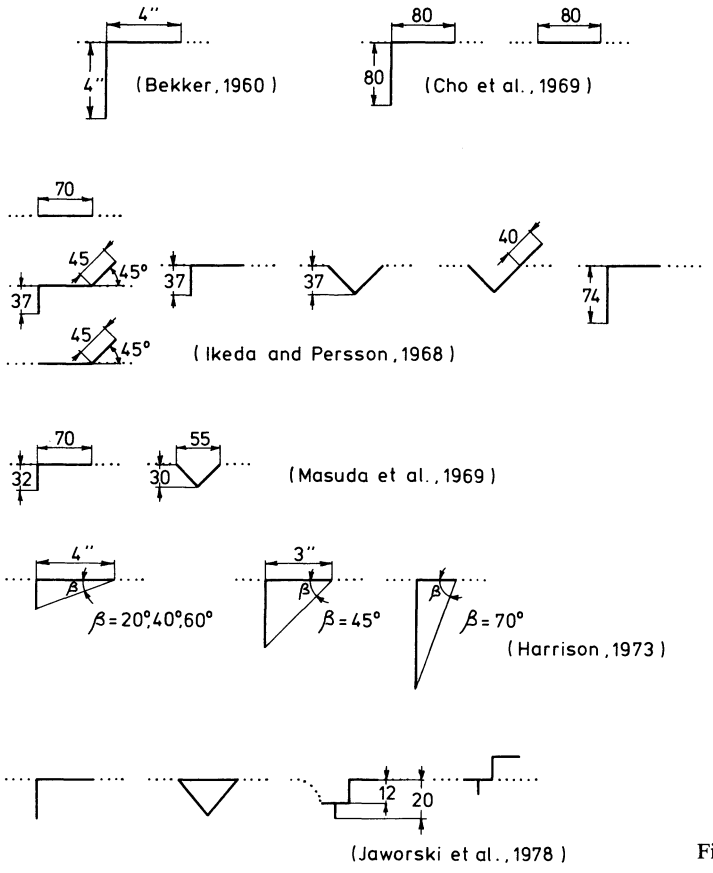

Fig. 3.38. Shear elements

Movement in the plane of view can be very complex. In the literature two types prevail: (1) sinkage due to applying a vertical load, followed by a translational movement due to applying a horizontal load, (2) translational movement due to applying an inclined load. In both types rotation of the element is prevented, for example, by using parallel guides.

Further distinction should be made between a relatively small vertical load being accompanied by a relatively small zone of influence, and a relatively high vertical load influencing a relatively large zone of soil.

Shear Element with a Vertical Grouser and a Small Vertical Load. When soil cohesion is low a shear failure plane, like *a b* in Fig. 3.39a, will develop (Bekker 1960). In soils with higher cohesion, tensile failure occurs and the crack front may run up to the surface (Fig. 3.39b). In both cases the element moves in an inclined, upward and forward direction. Both types of failure are sometimes called *grip failure.*

Shear Element with a Vertical Grouser and a High Vertical Load. When element movement is of type (1), the vertical loading will cause one of the two patterns

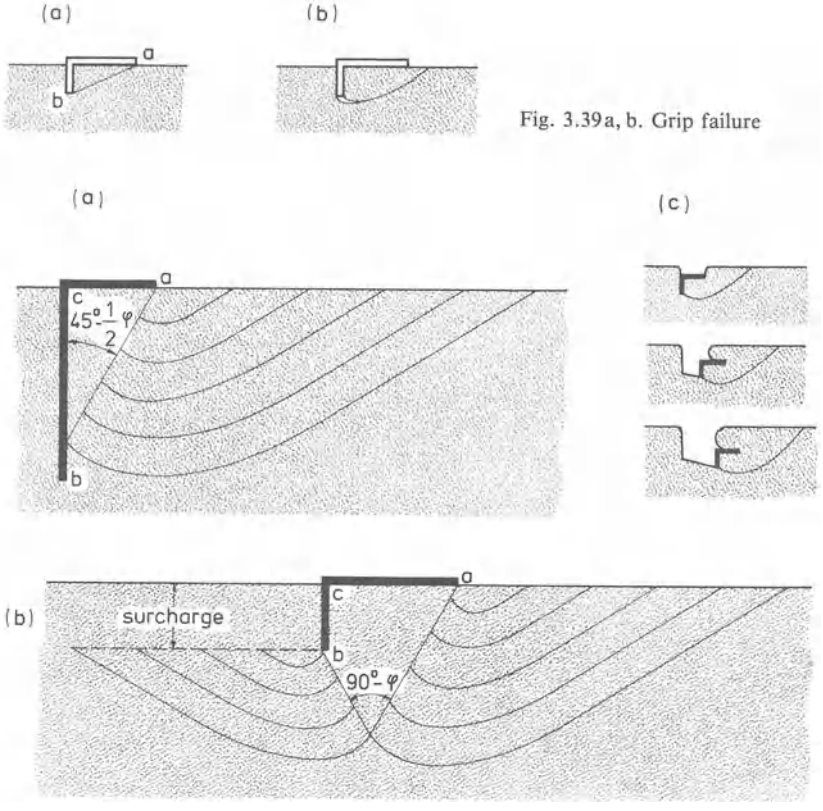

Fig. 3.39a, b. Grip failure

Fig. 3.40a – c. Soil deformation when a shear element is loaded in a direction that is vertical initially (a) or (b) , and then horizontal (c)

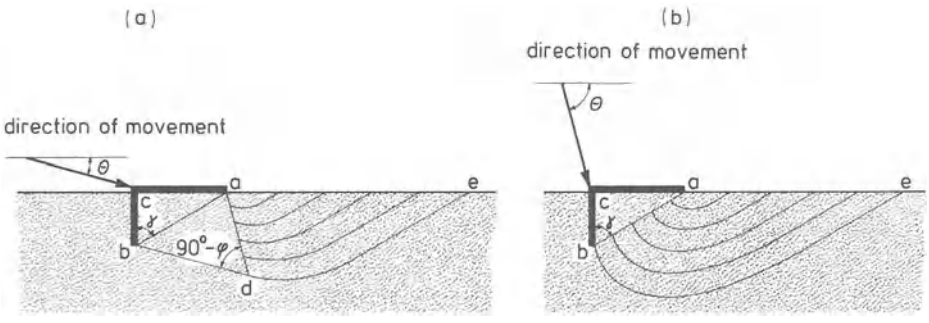

Fig. 3.41 a, b. Soil deformation when a shear element penetrates along an inclined direction

shown in Fig. 3.40a and b (a wedge and one or two flow zones). Which of the two will prevail, depends on the *ac/bc* ratio. Strictly, this stage belongs to Sect. 3.3. When, subsequently, a horizontal load is applied, the pattern starts to follow the rules that apply to the type (2) movement of elements. Here, slip sinkage may occur (see Fig. 3.40c).

Figure 3.41 refers to type (2) movement (Harrison 1972, 1973). In this figure θ indicates the direction of movement of the element. The deformation pattern shown at the left occurs when $\theta < \gamma + \phi$ (ϕ is angle of internal soil friction, γ as defined in the figure). This pattern is characterized by

- a "dead" soil volume *abc*,
- a soil wedge *abd*, with angle $adb = 90° - \phi$, and *db* parallel to the direction of movement of the element,
- a zone *ade* in which soil flow occurs.

The pattern shown at the right in Fig. 3.41 occurs when $\gamma + \phi \leqslant \theta < 90°$. Now the wedge is absent. When an element sinks deep, a pattern as in Fig. 3.40c is obtained.

Inclined Shear Element. This can be treated by replacing the inclined element by an imaginary comparable element with a vertical grouser plus a dead soil volume. For example, in the case of an inclined shear element with position *ab* in Fig. 3.41, *acb* is the replacing element.

Horizontal Flat Shear Element. At a relatively small vertical load, this element may be treated as a sled on a hard soil.

At a high load and element movement of type (1), vertical penetration may be treated as with the plate in chapter 3.3. With subsequent horizontal loading, the behavior conforms again to sled behavior.

With a high vertical load and element movement of type (2), soil deformation will be as in Fig. 3.41a for many directions of element movement. Under the plate a soil wedge is then present with its base parallel to the plate displacement vector (Harrison 1973).

3.4.2.2 Dynamic Aspects

Smooth Plates and Sleds

Section 2.5 (soil-material friction and adherence) is very relevant to the behavior of plates and sleds.

A sled is subjected to a vertical load and a horizontal force must be exerted to move the sled along. This horizontal force depends on the length of the sliding path with the understanding that for path lengths greater than the sled length the force – path diagram shows a constant force value. This constant value of the horizontal force and the sinkage depend on

- magnitude of the vertical load,
- frictional properties of the sled-soil friction,
- soil compactibility and deformability,
- the nose properties when the sled nose is in contact with the soil,
- sled shape and dimensions,
- trim angle, in case of rigidly mounted sleds,
- the pivot position in case of pendulating sleds (the trim angle is then a dependent variable strongly connected with depth of sinkage).

Compared with a wheel, a sled demands less pull on soft wet soils, and more pull on normal soils and hard soils (Gill and VandenBerg 1967).

Sled loading is correct if the point of action of the vertical load is at one third of the contact length from the sled rear end. This explains the pivot position of pendulating sleds. This pivot should further be positioned as low as possible to minimize the moment about this point of the shear stresses in the contact surface; to balance this moment, extra normal stresses are needed in the contact surface.

Kinematic behavior of a sled and the point of action of the vertical load can well be explained assuming that the normal stress σ_n in a point of the contact surface may be expressed as

$$\sigma_n = A z + B$$

where z is depth and A and B are constants (Bernacki and Haman 1973). Constant B is zero for loose soil, and greater than zero for precompacted soil. This formula leads to a stress distribution in the contact surface characterized by a linear increase of σ_n from front to back. This linear stress distribution does not occur if the sled bends significantly (Bekker 1956), or if sinkage is great.

The correct length-to-width ratio of the sled depends on its purpose. Width should be great when, for instance in swamps, a high flotation is required rather than a low motion resistance. Where a small motion resistance is wanted, a large length to width ratio may decrease drawbar pull demand if water is squeezed out of the soil under the front part of the sled, reducing the friction under the back part.

Sleds in which the displacement is controlled often do not follow a straight path, but wringing movements may be superposed. This may locally induce high normal stresses on the plate which, in turn, strongly increase pull demand.

Shear Plates and Annuli

Many direct shear devices (Sect. 2.4.2.2) are identical with shear plates and shear annuli; therefore, the text on these devices is very relevant.

With sleds the main interest is in the force after a starting period. With shear plates and annuli, most interest is in the force-displacement diagram before the steady state is reached. Such a force-displacement diagram depends on

- soil properties. Often, a curve is found without a clear maximum, but for brittle soils the curve usually exhibits a clear maximum, as in Fig. 3.42a and c, where τ = shear force/shear area is plotted against tangential displacement j. Soil plasticity is one of the factors that determine the steepness of the curves,
- the change of the soil properties with depth. The more soil strength increases with depth, the steeper ("compressed" horizontally) the curve may be,
- the normal stress. Normal stress determines in the first instance curve level. This is best illustrated by plotting curve maxima against corresponding normal stresses. See Fig. 3.42b and d (Bernacki and Haman 1973). Normal stress may also influence curve shape; curves at lower normal stresses tend to have clearer maxima (Bekker 1969),
- edge effects. A good treatise on this subject can be found in chapter 3 of Bekker (1969),
- grousers. The influence of grousers is only small. The weight of the soil between the grousers contributes to the normal stresses on the potential surface of breaking, and this soil weight increases with increasing grouser height. With greater grouser spacing, the process is more characterized by "progressive failure" and an exactly horizontal shear plane is less likely to occur.

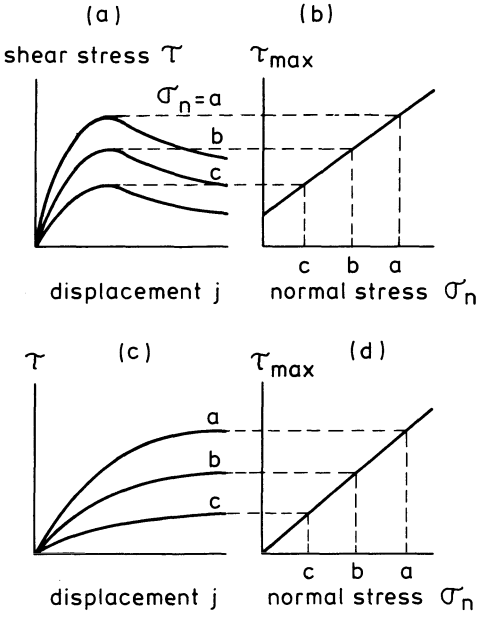

Fig. 3.42a – d. Shear stress on shear plate or annulus as affected by shear displacement and normal stress. Clear peak values occur in (a), but not in (c)

Measured curves can be found in Bekker (1969), Masuda et al. (1969), Oida (1975), Reece (1965), Wong (1970), Janosi (1962), Sela (1964), and Dwyer (1973). A measured curve is often treated incorrectly as a soil property. Objections are that the shape and size of the plate or annulus play a role, and that the variations with depth of the soil properties have a large influence on the measuring result.

Shear Elements

For a shear element the relationship between horizontal force and horizontal displacement depends on

- magnitude of the vertical load with movement of type (1),
- penetration angle with movement of type (2),
- size of the element, especially height. The shape of the element is less important (Ikeda and Persson 1968, Jaworski et al. 1978),
- element width. As a first approximation, horizontal force per unit width may be considered independent of the element width (Harrison 1973),
- soil properties.

Type (1) Movement. Force-displacement diagrams are given in Ikeda and Persson (1968), Masuda et al. (1969), and Cho et al. (1969). The shapes of these force-displacement diagrams are similar to those of the curves of shear plates and annuli (Fig. 3.42). Soil piling up in front of the element may prevent a steady state being reached.

Type (2) Movement. Force measurements are given in Bekker (1960), and Harrison (1973). The last article also presents relationships between the element direction of movement θ and the direction of the resulting force on the element ξ (Fig. 3.43). By and large for this type of movement, the horizontal and vertical forces both increase with increasing penetration, the direction of the resulting force remaining more or less constant.

Grip Failure. For this we refer to Sect. 3.4.3.2.

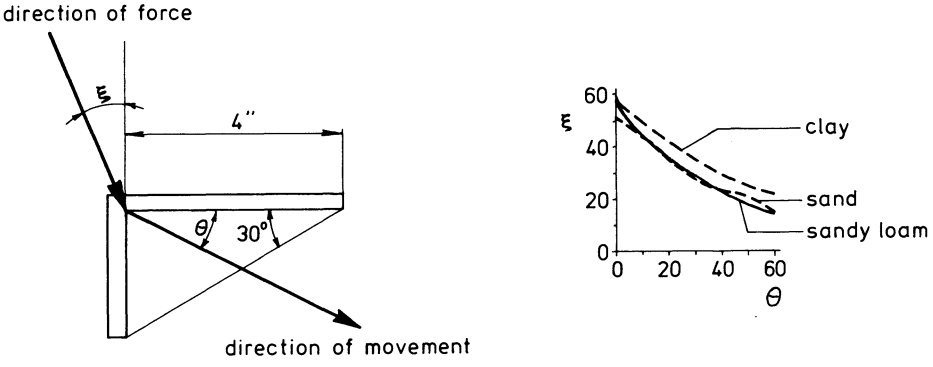

Fig. 3.43. Direction of resulting force on shear element when the element penetrates the soil along an inclined direction

3.4.3 Applications

3.4.3.1 Fitting Formulas for Shear Force-Horizontal Displacement Relationships

Measuring with a shear plate or annulus often results in a set of curves as shown in Fig. 3.44a. The curves feature no clear peak value but rather approach an asymptotic value. Each curve in such a series refers to a particular normal force. A very common fitting equation is (Janosi 1962)

$$s = (c + p \tan \phi)(1 - e^{-j/K})$$

where s is shear stress, c is soil cohesion, p is pressure normal to the shear plane, ϕ is angle of internal friction, j is shear deformation, and K is so-called modulus of a soil shear stress-strain curve. K must be in the same units as j. In older Anglo-Saxon literature these are often inches. To find a value for K (Fig. 3.44b) start from a representative curve somewhere in the middle of the family of curves. In the point $j = 0$ draw a line tangent to the curve. The point of intersection of this tangent line with the horizontal asymptot of the curve determines K. This graphical solution is possible, since

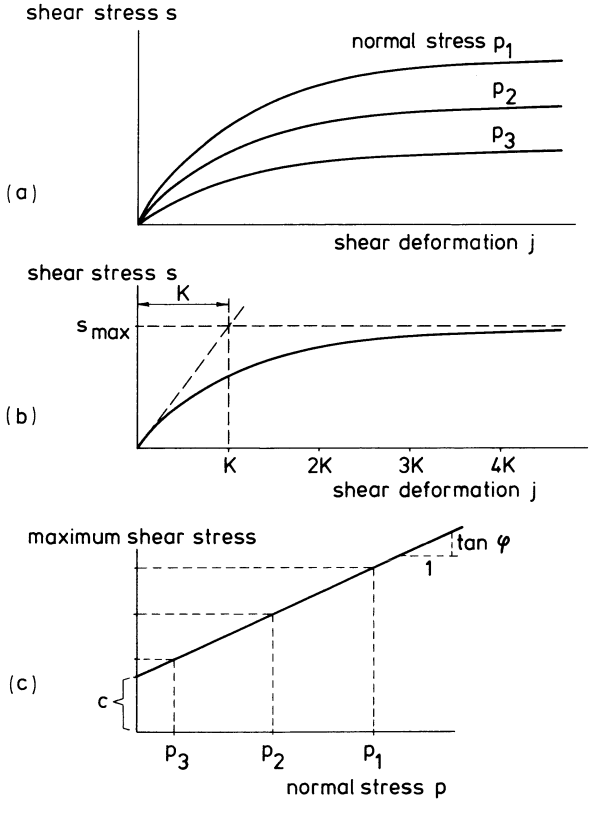

Fig. 3.44a – c. Deriving c, ϕ, and K values from shear stress – shear deformation relationships

$$\frac{ds}{dj} = \frac{c + p\tan\phi}{K}.$$

Of course, K could also be determined from a measured curve using a least-squares curve-fitting technique. K can also be found by comparing visually the measured curve with a family of theoretical curves (Wills 1960). Reece and Adams (1966) present the following method. "When an experimental set of curves such as those in Fig. 3.44a has been obtained, the appropriate K value can be found for each curve in the following way. The first equation can be re-written as

$$1 - \frac{s}{s_{max}} = e^{-j/K}$$

and taking logarithms of both sides yields

$$\ln\left(1 - \frac{s}{s_{max}}\right) = -j/K.$$

K can then be simply determined from the shape of the straight lines that are obtained by plotting the last equation on log-linear graph paper". The value of K is a good visualization of the soil deformability (Fig. 3.44b). Values of c and ϕ can be found by plotting the curve maxima against p, as in Fig. 3.44c. This will yield a straight line that intersects the vertical coordinate axis at c, and has a tangent modulus equal to $\tan\phi$.

Sometimes the force-displacement diagram is a curve with a clear peak, as in Fig. 3.42a. A fitting formula for this case is given in Bekker (1960)

$$s = (c + p\tan\phi)\frac{\{e^{(-K_2 + \sqrt{K_2^2 - 1})K_1 d} - e^{(-K_2 - \sqrt{K_2^2 - 1})K_1 d}\}}{y_{max}}$$

where d denotes the shear deformation, K_1 and K_2 are slip parameters, and y_{max} is the maximum value of the function enclosed between brackets $\{\}$. c and ϕ can be found as indicated above. To find K_1 and K_2 Bekker (1960) gives a graphical method. A second method is described by Soltynsky (1968).

Another fitting formula for diagrams with clear peaks is given by Sela (1964). Sela's formula can describe a curve whose shape depends on the normal stress:

$$s = c\frac{d}{d_c}e^{(1 - d/d_c)} + p\tan\phi(1 - e^{-(d/d_\phi)})$$

where c, d_c, ϕ, and d_ϕ are constants depending on the soil. The second term in the formula represents a cohesive component, the third a frictional component. Note the resemblance of this third term to Janosi's formula at the beginning of this section.

3.4.3.2 Resistance Approximations for Sliding and Shearing Bodies

The resistance of smooth plates and sleds can be calculated from soil-metal frictional properties. The effect of a non-zero trim angle or sinkage should be taken

into account. Trim angle or sinkage can be estimated with the aid of Section 3.4.3.4.

The resistance of shear annuli and shear plates can be estimated using c and ϕ values of the soil considered.

Theories on the resistance of shear elements may be found in Karafiath and Nowatski (1978), Cho et al. (1969), Harrison (1972), and Bekker (1960). Bekker also presents a calculation for grip failure. It must be noted that these theories are complicated and often not very satisfactory.

3.4.3.3 Pull-Slip Relationships for Spaced-Link Tracks

Suppose that for a particular soil and a particular shear element (length l and width w), shear force-displacement curves at different normal stresses have been measured, and represented in Fig. 3.45 a. Then consider a spaced-link track composed of the same shear elements as used for the figure. The number of elements in contact with soil is n, and the normal stress on each element is the same and

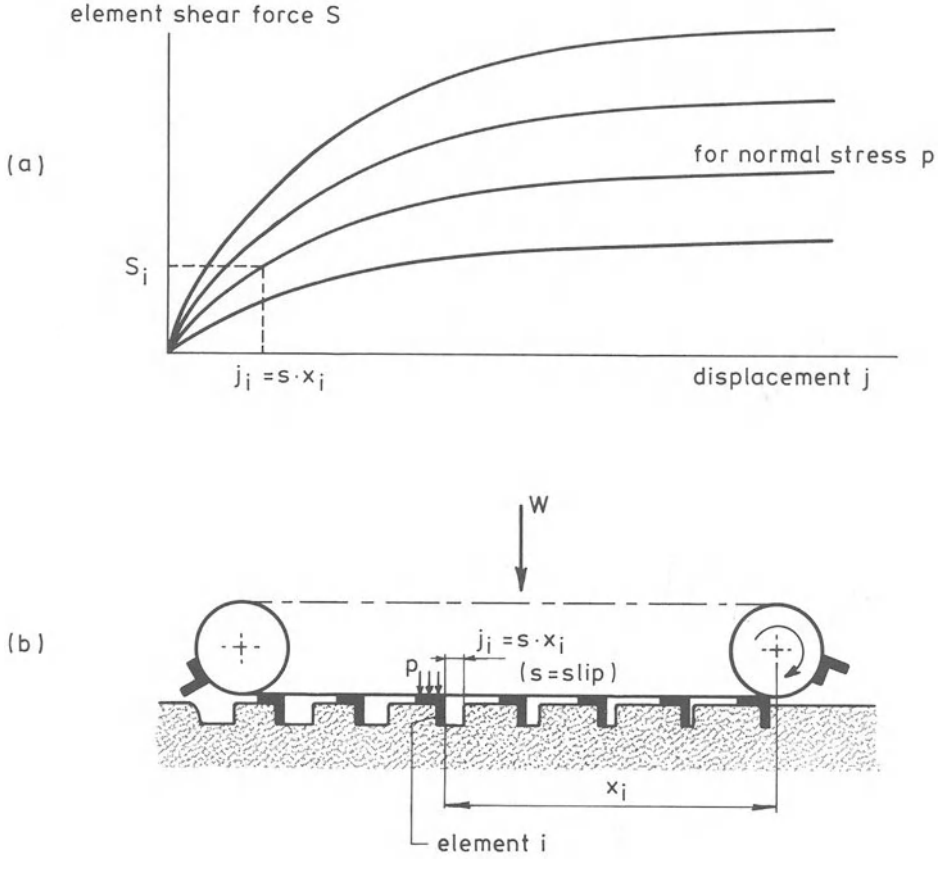

Fig. 3.45 a, b. Shear force of track element i (b) derived from shear force – element displacement curves (a)

equal to p (p equals vertical load W divided by lwn). The fractional reduction in forward speed due to slip is s (s = slip percentage/100). We want to estimate total pull force P at slip s of the spaced-link track in the same soil for which Fig. 3.45a was measured, assuming that the elements neither interact, nor that p varies. For this, we consider element i. By definition, $j_i = s \cdot x_i$ (Fig. 3.45b). Now read in Fig. 3.45a the S_i-value for the given values of p and j_i. Summation for all elements yields

$$P = \sum_{i=1}^{n} S_i .$$

This sum is the total pull force for slip s and normal stress p. Selecting another slip value results in another P value. In this way a complete pull-slip curve can be found, belonging to a particular p. It was assumed that no interaction occurred between neighboring elements. However, narrower spacings will lead to more interaction. This can be taken into account by determining Fig. 3.45a in the presence of a leading and following element, spaced as in the track considered. For an example, see Cho et al. (1969). Basically, using zero spacing, a closed track may be approximated. Complications arise from p not being evenly distributed and from track rollers acting as repeated loads. A summation procedure for uneven p-distributions is given in Kogure and Sugiyama (1975). Further complications are that

- a part of the gross pull force is lost in the track due to bearing friction, etc.,
- a non-zero trim angle will occur, depending on the slip-sinkage, depth to which the stresses extend, etc.,
- energy is dissipated in the immediate rut formation by the first track shoe.

Summation procedures are also given in Reece and Adams (1966). Komandi (1966), Bekker (1960), and Oida (1975).

3.4.3.4 Estimation of Rut Depth and/or Trim Angle of a Sled

For this estimation Bernacki and Haman (1973) introduce the volumetric specific compaction force q_0, expressed in kg/cm^3, which is the force needed to push a volume (rut) of 1 cm^3 aside in loose soil. For small sinkages, q_0 is independent of the particular shape of this 1 cm^3 volume, and thus independent of pushing area A and penetration depth x. Accordingly, for the plate sinkage in Fig. 3.46,

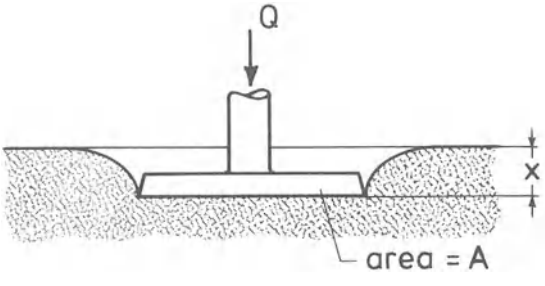

Fig. 3.46. Illustration of specific compaction force $q_0 = Q/Ax$

Table 3.10. Typical values of the specific compaction force q_0, in kg/cm^3 (Bernacki and Haman 1973)

Loose soil	Settled medium soil	Settled heavy soil	Settled heavy dry soil
0.5 – 1.5	3 – 8	6 – 10	12 – 20

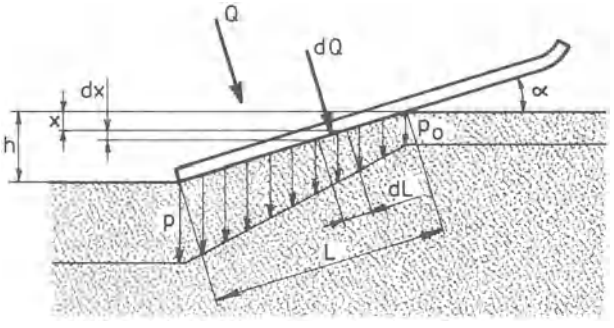

Fig. 3.47. Sled with sinkage h and trim angle α, operating in precompacted soil

$$Q = A q_0 x$$

where Q = plate penetration force. Table 3.10 gives a few values of q_0. For precompacted soil, the formula should be written as

$$Q = A q_0(x + x_i) = A x q_0 + A p_0$$

where x_i is sinkage at precompaction and p_0 $(= x_i q_0)$ is precompaction stress. Application of this result to a sled yields the following differential equation (Fig. 3.47).

$$dQ = B dL\,(q_0 x + p_0)$$

with B as sled width. Because $dL = dx/\sin\alpha$ this becomes

$$Q = \frac{B}{\sin\alpha}\int_0^h (q_0 x + p_0)\,dx = \frac{Bh}{2\sin\alpha}(q_0 h + 2p_0)\,.$$

3.4.3.5 Estimating c and ϕ Using Shear Plates or Annuli

In principle, it is possible to estimate c and ϕ from measured $\tau - \sigma_n$ relations (Dwyer 1973, Bailey and Weber 1965, Dunlap et al. 1966, Freitag et al. 1970, Bekker 1969; also Sects. 3.4.3.1 and 2.4). The value of σ_n can be found by dividing the normal force by the area of the plate or annulus. The method to determine τ requires some explanation.

For a rectangular plate, τ is equal to the measured shear force divided by the plate area. In the case of a circular plate or an annulus, for which the torque is measured, the calculation is more complicated. We have to start from the differential equation

$$dM = 2\pi r^2 \cdot \tau \cdot dr$$

where M is the resisting moment, r is the radius of the elemental ring dr and τ is the shear stress on the elemental ring. To proceed, a uniform stress distribution across the plate or annulus (τ = constant) is assumed. For an annulus with outer and inner radii of R_0 and R_i, respectively, the result after integrating and solving for τ is

$$\tau = \frac{3M}{2\pi(R_0^3 - R_i^3)}.$$

For a circular plate and a uniform stress distribution

$$\tau = \frac{3M}{2\pi R_0^3}.$$

Both formulas are of the same form,

$$\tau = \frac{M}{R_e A}$$

where R_e is the effective radius and A is the area of the given plate or annulus.

For a small surface element, initially $\tau = 0$ and τ grows with increasing soil deformation up to a maximum where c and ϕ are fully developed. It is usually assumed that in a test this maximum is reached in all elements at the same time. In reality, this is not true, because the soil deformation under the plate or annulus is not uniform. Under a rectangular translating plate, for example, soil deformation is always zero at the front, increases with increasing distance from the front up to a certain value, and remains constant at that value with further increase of distance. Under a rotating plate or annulus, soil deformation increases with increasing distance from the center. Therefore, Cohron assumed for a rotating shear plate that a linear stress distribution existed under the plate when the peak moment was reached. In that case

$$\tau = r\frac{\tau_0}{R_0}.$$

Substituting this value for τ in the differential equation, integrating, and solving for τ_0 yields

$$\tau_0 = \frac{2M}{\pi R_0^3}.$$

This τ_0 is the shear stress at the outer radius and is four-thirds of τ calculated assuming a uniform stress distribution. The validity of the assumption of a linear distribution depends on the shape of the stress-displacement curve. For the assumption to be accurate, there must be a large and instantaneous drop in shear stress immediately after the peak stress is reached. Cohron's concept is similar to the concept of progressive failure.

Edge effects may influence the measuring results. This is especially clear in the case of a rectangular plate piling up soil with its leading edge. Often, soil that

piles up is removed before the measurements. The sides are often guarded by vertical walls with a cutting edge to facilitate penetration into the soil. For an annulus this leads to the shape shown in Fig. 3.37c. Dwyer (1973) did not use guarding steel cylinder walls in his annulus, but the accounted for the edge effect by assuming a shear surface that included the two short cylinder walls along the inner and outer edges of the grousers. No normal stress acts on these vertical parts of the shear surface. For an annular shear ring with 300 mm outside and 200 mm inside diameter and 25 radial grousers 25 mm high, Dwyer found

$$M_{max} = 0.025\,\pi c + V \tan \phi$$

where V is the vertical load on the annulus (M_{max} in Nm, c in kN/M^2, V in kN).

At low normal stresses a flat horizontal surface of shear failure passing through the grouser tips does not develop, but upward or downward inclined cracks run from each grouser tip. In that case the estimation of c and ϕ is not correct. In the "ideal" case a horizontal plane of shear failure develops instantaneously along the bottoms of the grousers. The measured c and ϕ-values then apply to this depth.

In a relatively loose soil and with relatively high normal stress, the application of the normal stress may have induced compaction at the depth where the failure plane is formed. This may result in a curved rather than a linear σ_n-τ graph having a slope decreasing with higher normal stress.

3.4.3.6 Wall Friction of Cone Penetrometer Rods

If the rod diameter of a penetrometer were equal to the cone diameter, friction and adhesion at the rod surface would make the measured resistance much greater than the "true" cone penetration resistance. It is necessary, therefore, to keep the rod diameter smaller than the cone diameter.

In dry, loose sand, however, the produced cavity is filled by sand flowing around the cone, and friction is only partly eliminated. According to Meyerhof, this residual friction is negligible to a depth of about 10 m (Sanglerat 1972).

Wet, soft clay soil will also flow around the cone and fill the cavity. Due to the adhesion, the shear force on the rod may then be significant even at small depths. The error introduced will be smaller as the rod diameter – cone diameter ratio is smaller. A measured example is given in Freitag (1968), being the result of penetration tests made with an ASAE standard cone in soft clay. For a 5/8 in. shaft the increase in penetration resistance at a depth of about 6 in. was believed to be due to the adhesion of the soil to the shaft. Use of a 3/8 in. shaft avoided the shaft drag problem for penetration depths of at least one foot.

Modern penetrometers eliminate the drag problem by using electric force transducers immediately above the cone.

3.5 Tracks, Cage Rollers, and Cage Wheels

Tracks, cage rollers, and cage wheels are load bearing, rolling bodies having in common that they are composed of elements that in a way act separately, but

also interact to a lesser or higher degree. They feature many of the aspects mentioned in the sections on

- rollers, wheels and tires,
- penetrating bodies,
- sliding and shearing bodies.

3.5.1 Occurrence

3.5.1.1 Tracks

Basically, tracks have the same function as wheels and tires. The difference between a rigid wheel, pneumatic tire, and track is that, in this order, the area of contact that can reasonably be realized in a vehicle or implement increases. Large contact areas are useful as they allow for

- high pull forces,
- high bearing capacities,
- low sinkages (rolling resistances).

Tracks vary strongly with respect to size and shape of the track shoes, pitch, number of track rollers, diameter of the rollers, number of track shoes, spring action of the track rollers, track tension, and track shoe material. These variations arise out of performance requirements. The requirements that mainly determine track design are:

The Required Bearing Capacity, which relates mainly to the size and shape of the area of contact, to the number and diameter of the track rollers, and to the pitch.

The Required Pull. This depends strongly on the same factors, and furthermore on the vertical load and the track tread and strength.

The Required Speed Range. With higher speeds, spring suspensions and small pitch are required.

An Acceptable Durability. This often limits the maximum speed, and led to the design rule that track shoes should not be wider than strictly necessary. Sufficiently high grousers reduce the risk of track shoe cracking and breaking. Durability is directly related to proper track tension. For a particular undercarriage, there is a particular, correct track tension.

Geometrical Requirements, like maximum width on public roads and steerability. The ratio of track gauge to track length should be 0.7 or greater to provide good steering characteristics and optimum maneuverability. Also, required clearance for mounting implements in or under a machine can be a decisive factor.

Secondary Requirements for the Shoe Shape, for instance, to prevent packing with soil or damaging the underfooting.

Several track applications occur in agriculture, such as with combine-harvesters (in rice production) and trailers (in sugar cane production), but the most important application in agriculture is the crawler tractor as an alternative for the wheel tractor. Crawlers differ from wheel tractors in

- a higher pulling capability per unit of vehicle weight,
- usually, a lower coefficient of rolling resistance in off-road conditions,
- lower forward speeds,
- less engine power per unit of vehicle weight (approximately, fly wheel power/unit vehicle weight is 9 kW/ton for crawlers and 17 kW/ton for wheel tractors),
- a higher pulling capability at comparable size (length and width),
- usability on soil having less bearing capacity and/or with less soil structure deterioration and smaller sinkage,
- being more bound to off-road use,
- less maneuverability, if soil structure damage is to be avoided,
- often longer service life.

Wheel tractors are common on farms, because of their maneuverability, usability in road transport, and large range of forward speeds. Performance in soil tillage is obviously not decisive. Crawlers are common where the development of high pulls on land is the main requirement, because they have a higher pulling capacity at comparable size and weight, and perform better under bad conditions. Soil amelioration, land clearing, and earth moving activities are well-known fields of application for crawlers.

Figure 3.48 shows the right side of the undercarriage of a track layer. The sprocket is normally at the back. Note the position of the grouser on a track shoe relative to the direction of travel. The roller frame is provided with a recoil spring to put the track under tension. Depending upon type of machine and expected operating conditions, compressed load on each recoil spring should be 65% to 100% of the total machine weight. The track rollers, being unsprung, are rigidly mounted on the roller frame. Maximum traveling speed is generally lower than 10 km/h. Note that the track shoe dimension in the plane of view is greater than

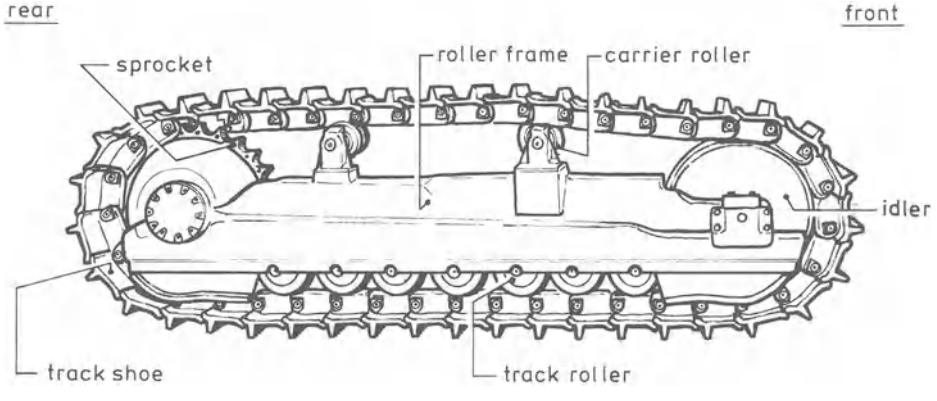

Fig. 3.48. Right half of a track layer undercarriage

Table 3.11. Characteristic data of three current agricultural track-type tractors *A*, *B*, *C*

	A	*B*	*C*
Weight (kg)	7620	10704	13064
Width of standard track shoe (mm)	405	455	510
Optional shoe widths (mm)	455/510/560	510/560/610	560/610/660
Length of track on ground (mm)	1840	2180	2360
Ground contact area with standard shoe (m^2)	1.50	1.99	2.41
Mean ground pressure (bar)	0.50	0.53	0.53
Number of track rollers	5	6	6
Track pitch (mm)	172	172	203
Flywheel power at 2000 RPM (kW)	67	89	123
Maximum drawbar pull at lug in lowest gear (kg)	5960	8070	11120
Drawbar pull at rated RPM, at a speed of 7.5 km/h (kg)	2420	2950	4080
Maximum forward speed (km/h)	7.5	9	8.8
Grouser height (mm)	48	60	60

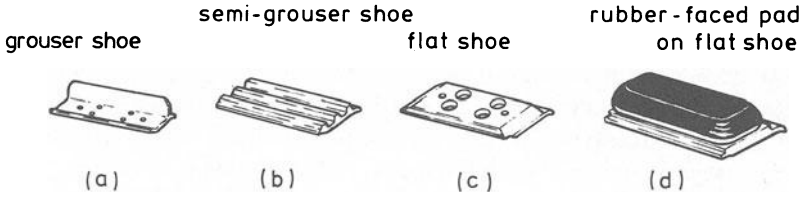

Fig. 3.49a – d. Track shoes

the track pitch. The center of gravity of a crawler is low and is sometimes brought forward using extra weight in the radiator area. Table 3.11 gives a few technical data of current agricultural crawlers, indicated as *A*, *B* and *C*. The track shoe shape shown in Fig. 3.49a (a flat plate with a single high cleat or grouser across it) is considered standard. It gives good traction and protects from side slipping, but tears up the soil surface. Digging-in may occur with slip. Semi-grousers (Fig. 3.49b) are flat shoes that carry two or three low cleats. They tear up less and allow better maneuverability, but provide less pull and stability than full grousers. Also available are flat shoes (Fig. 3.49c) and rubber-faced pads (Fig. 3.49d). Track shoes may have a center hole, allowing the sprocket to extrude packed material as mud from between the sprocket teeth and the track.

3.5.1.2 Cage Rollers

Figure 3.50 shows a few cage rollers that are common in agriculture. They are often mounted behind a field cultivator or harrow and serve for levelling the soil,

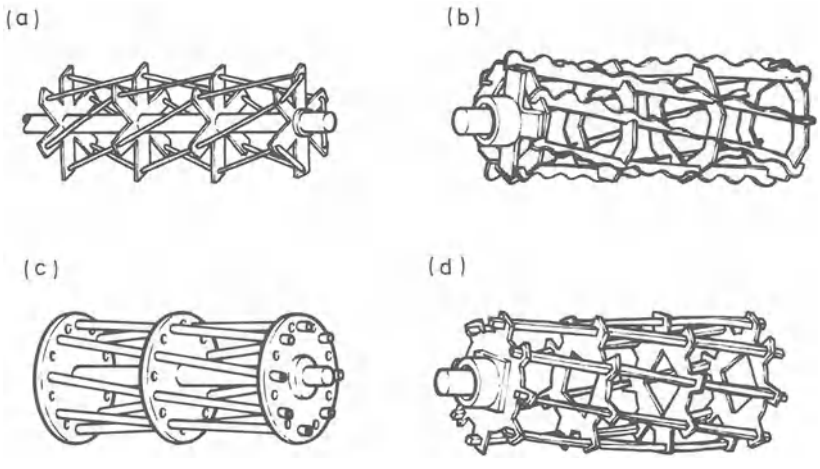

Fig. 3.50a – d. Some current agricultural cage rollers

for further crumbling and compacting of the top layer, as well as for supporting and controlling the field cultivator or harrow. They are known as crumbler or "Krümelwalze". Diameters range from 25 to 35 cm and working width per element is 95 to 145 cm. The rollers are not driven and working speed is 8 to 12 km/h. The bars may be straight and parallel to the axis of rotation, bent according to a screw curve or straight but not parallel to the axis of rotation. The bars may be solid and round, rectangular profile steel, round tubes, or with teeth. Bar thickness varies from less than one cm to several cm's. The rollers do not always have an axle over the full width. Bars can be connected to the axle in such a way that the connections hardly touch the soil, but in other rollers those connections (plates or discs) clearly contribute to the tillage effect. Vertical load is about 100 to 300 kg per meter width. Operating depth may reach up to 5 cm.

3.5.1.3 Cage Wheels

Cage wheels are used, firstly to diminish compaction and soil damage when driving on the field. Here, a cage wheel replaces a pneumatic tire or is attached to a tire. When the latter is the case, the cage wheel diameter should be slightly less than the tire diameter to allow driving on roads. The bars are simple, mostly round bars or rectangular profile steel. Secondly, cage wheels are used for puddling wet rice fields to contribute to the puddling effect and to develop the pull force for the puddling tool attached to the tractor. The bar shapes may have a complicated form, but also simple forms are known, as in the so-called "Koga" type wheel (see Fig. 3.51 a).

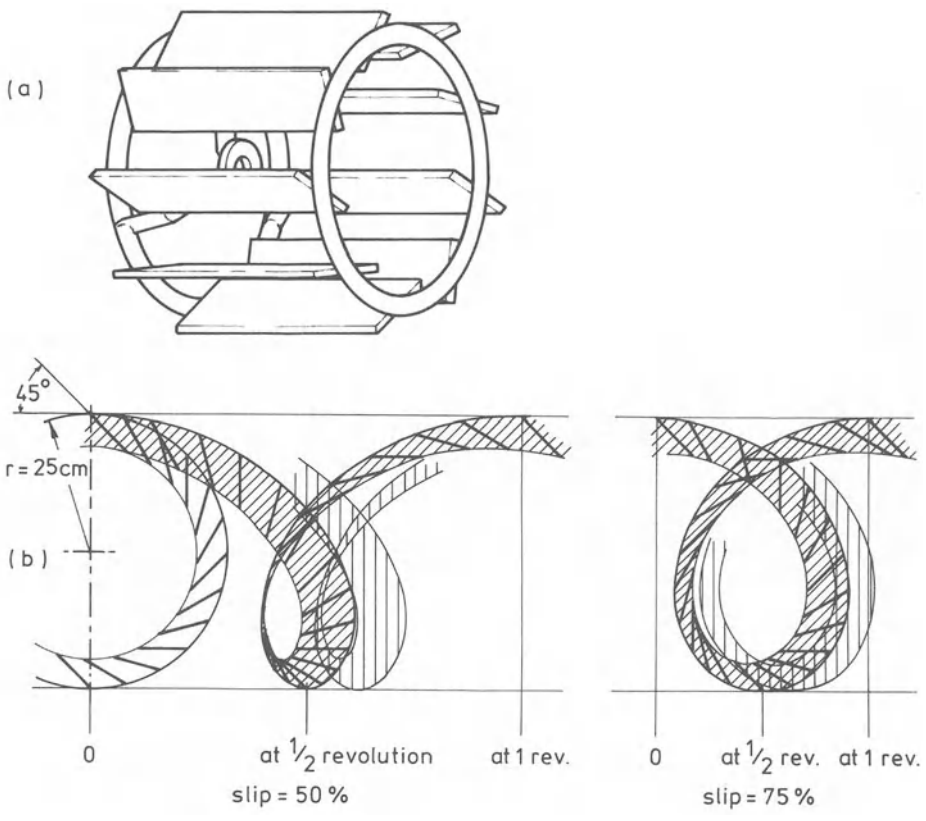

Fig. 3.51 a, b. Koga-type puddle wheel (a). Grouser paths at slip percentages of 50% and 75% (b)

3.5.2 Fundamentals

3.5.2.1 Kinematic Aspects

Tracks. Consider the undercarriage of Fig. 3.48 and suppose that the track is moving ahead under a vertical load and a drawbar pull, on a soil that is soft enough to let the grousers penetrate completely. In this case the line of contact is not straight but waves somewhat, with the track rollers in the wave-hollows. Waving is stronger with increasing distance between the rollers, with decreasing roller diameter and with decreasing pitch. Among the entire arsenal of tracks, those used in agriculture feature a relatively small degree of waving. The track chain sags slightly between the front carrier roller and the idler. In the case of a hard underfooting, track sag would be about 40 mm. In the given situation the track will slip slightly (for the definition of zero slip, see Sect. 3.2.2.1). The track will sink somewhat and due to slip sinkage a trim angle will be formed. The trim angle also depends on the position of the center of gravity and the drawbar height. The track chain is not completely tight, so that the contact line may

rumple when moving backwards under load. Because of the relatively rigid assembly of a crawler, vibrations of the engine and the transmission may be transferred to the soil through the contacting track shoes. These vibrations can be measured with acceleration transducers on shoes.

The backward displacement of a soil particle carried along in the contact area can be estimated with the formula

$$Q = \frac{s}{100} x$$

where Q is the backward displacement at a particular moment, s is the slip percentage, and x is the distance at the considered moment of the considered soil particle measured from the front of the contact area. Since traction development is related to backward displacement of soil, the maximum Q for a track is comparable with the maximum Q of a tire. However, the contact surface length is much greater with a track. So, in view of the formula above, it is easily understood that the range of normal slip percentages for crawlers is from 1/4 to 1/3 of the range for wheel tractors. The width of the rut is, of course, equal to the track width and, therefore, comparable with single tires but far smaller than those of duals. Rut depth is primarily determined by the contact pressure. For a tracklayer this contact pressure is about half the pressure under a single tire of a wheel tractor. So, tracks have a smaller sinkage. Contact pressure of duals may be comparable to the pressure under tracks. In that case, rut depth will also be comparable. The degree of soil break up in the rut increases with increasing slip percentage.

To form an idea of the movement of a soil particle that is influenced by a track, it is useful to imagine, for a moment, that the chain is not present and the rollers and the idler are being driven. The soil particle is then influenced by the subsequent wheels, and the influence of each wheel can be derived analogously to the path descriptions in Sect. 3.2.2.1 on rollers, wheels and tires. So, repeated loading occurs, and the soil particle will follow a path with many loops. The less the contact line is wavy, the less the influences of the individual wheels are manifested. The compaction in a particular point under the track will depend primarily on the pressure in the contact area, and the width of contact area. And thus, in general, total compaction with a crawler track is less than with a wheel tractor track. Further research is required with respect to the compacting effects of vibrations.

Cage Rollers and Cage Wheels. The state of movement of cage rollers and cage wheels can be very complicated:

- when the bars are parallel to the axis of rotation, a bumpy gait may occur. Shocks can be eliminated with bars curved according to a screw-line,
- when the bars are straight and not parallel to the axis of rotation, the effective roller or wheel radius (defined in Sect. 3.2.2.1) decreases with increasing distance from the bar supports,
- when the cage wheel or roller is mounted to another body, for instance a tire, the state of movement is more or less determined by this other body,

- at a particular traveling speed, a "free" bar and a "free" bar support each would have their own circumferential speed. But since they are connected, each of them features a slip. The ratio between bar slip and bar support slip depends on the diameter ratio and on the degree in which the bar supports participate in influencing the soil,
- even without this interaction slippage occurs because the wheel or roller penetrate the soil (compare Sect. 3.2).

In general, the bars describe a path through the soil. Figure 3.51 b illustrates this for a puddle-wheel at slip percentages of 50% and 75%. The grousers of the puddle-wheel are at 45° to the wheel circumference. From the figure it can be seen easily, that radial grousers produce an extreme digging action, and tangential grousers an extreme pressing action.

3.5.2.2 Dynamic Aspects

Tracks

Forces and Torques. Motion resistance of tracked vehicles consists of two principal components; internal friction and external soil resistance. *Internal friction* includes scrubbing of pins and bushings, friction between links, and roller and idler turning friction. It varies with age of track components and tension on track chain. *Soil resistance* includes scrubbing of grousers during penetration, the force needed to compress the soil, and the friction resulting from soil packed around idlers, rollers and other components. On a rigid underfooting, *the motion resistance* of a track is comparable with that of a pneumatic tire (coefficient of rolling resistance ≈ 0.02). When the grousers penetrate and the soil is hard, additional power is required to push the grousers into the ground and even more to spade out soil on the back side of the grouser as the track is lifted to travel around the radius of the sprocket. The force required to move a crawler on a hard field soil may be as much as 10% to 15% greater than in loose soil (NN). When the whole shoe track penetrates, rolling resistance is mainly determined by the rut depth and width. Since at comparable rut widths, tires generally make deeper ruts than tracks, the coefficient of rolling resistance on soft soil is generally greater with tires than with tracks. The rolling resistance

- increases with increasing weight,
- decreases with increasing track length,
- does not react very clearly to an increase in track width,
- increases with increasing contact line waving,
- depends on track shoe shape,
- increases if the resultant force in the soil-track interface acts at a greater distance from the contact area center.

Figure 3.52 represents the system of forces on a pulling crawler. Equilibrium of forces implies that,

- the vertical component of R equals W,
- the horizontal component of R equals P,
- R, P, and W all pass through one point (in this case point b).

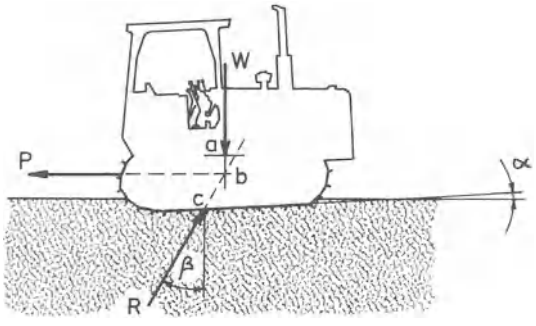

Fig. 3.52. System of forces on a pulling crawler

Point *a* is the center of gravity. The position of the point of action *c* varies with the position of *a*, with the magnitude of *P* and with the height at which *P* acts. Also, the trim angle α has a small influence. Unlike the situation with tires, there is now no simple relation between *R* and the torque supplied to the sprockets (see: stresses in the contact area).

At the University of Manitoba (NN), crawler *B* in Table 3.11 was compared to a heavy four-wheel drive, articulated tractor with duals. Figure 3.53a shows pull-to-weight ratio versus slip curves, and Fig. 3.53b power efficiency versus speed curves. General pull-to-weight ratios for wheels and tracks on different surfaces are given in (Nichols 1976). The pull capacity

- increases with increasing *W*, as long as the sinkage is not extreme,
- increases with increasing track length,
- does not react clearly to an increase in track width,
- usually increases if point *C* in Fig. 3.52 is displaced backwards (as long as the trim angle remains small),
- increases with decreasing waving of the contact line (this is unlike the situation with tires where the pull force increases with increasing tire flexibility),
- does not depend much on track shoe shape (Kuether and Reed 1964).

Stresses in the Contact Area. Force *R* in Fig. 3.52 is the result of normal – and shear – stresses in the contact area between track and soil. We will simplify the discussion by assuming

- the grouser penetration to be complete,
- the track to be closed,
- the surface passing through the grouser tips (the so-called shear surface) to be the contact surface,
- the thickness of the grousers to be negligible.

1. Normal Stresses. Generally, normal stresses are not evenly distributed, mainly for two reasons. Firstly, stress peaks occur under the sprocket, idler and rollers, so in the hollows of the wave line. Under practical conditions the maximum stress in the contact area is 1.4 – 3.0 times the mean normal stress. The multiplication factor is small if the waving of the contact line is small. For agricultural crawlers this factor is about 1.4. Secondly, point *c* in Fig. 3.52 may not be in the center of

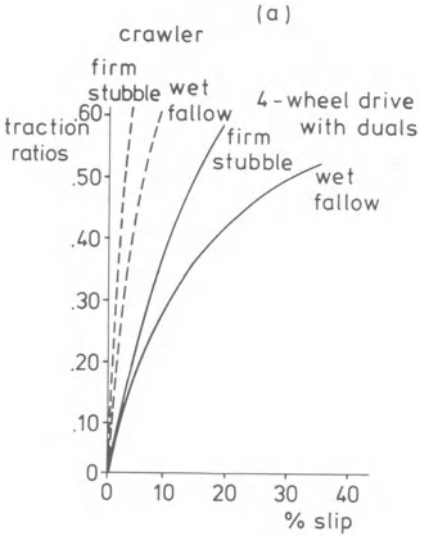

tractive efficiency under full load at varying speeds

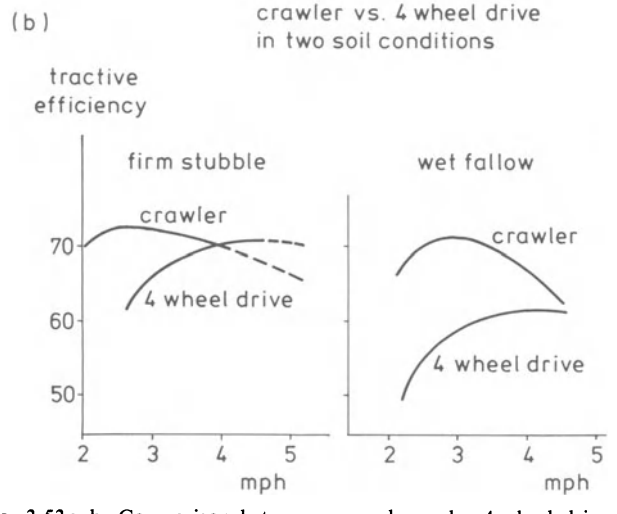

Fig. 3.53a, b. Comparison between a crawler and a 4-wheel drive articulated tractor with duals. (a) traction ratio-slip curves; (b) tractive efficiency

the contact area. If c is behind the center, the normal stresses increase in backward direction. For measured normal stresses under tracks we refer to Rowland (1972), Kogure and Sugiyama (1975), Oida (1975), Bekker (1969), and Karafiath and Nowatzki (1978). So, the maximum normal stress is greater than the mean (nominal) normal stress. Essentially, rut depth (and therefore rolling resistance) depends on maximum, and not mean stress. Relatively high stresses at the back side will induce a large trim angle.

2. Shear Stresses. As soon as some slip occurs, normal stresses will be accompanied by shear stresses. From the theory of shear elements (Sect. 3.4) we know that for a surface element of the contact area the shear stress is greater as

- the normal stress on this surface element is larger,
- generally, backward displacement of the element is larger. This backward displacement increases with increasing slip percentage and/or as the considered surface element is at a greater distance from the front of the contact area.

The summation procedure for successive shear elements (Sect. 3.4.3.3) can be applied to the distribution of normal stresses and deformations to get an idea of the sum of the shear stresses, and thus of the thrust. From this we shall only be able to draw qualitative conclusions due to the interactions of the shear elements. Since, approximately,

$$\text{shear stress} = (k_1 \cdot \text{normal stress} \cdot \text{deformation}) + (k_2 \cdot \text{deformation})$$

where k_1 and k_2 are constants, the highest shear stress can be obtained by applying the normal stress there, where the deformation is the largest. A backward shift of the center of gravity may increase thrust, as well as an elongation of the contact surface, at unchanged vertical load. The latter effect is strengthened by a decrease in sinkage, and thus in rolling resistance. Increasing the width of the contact surface has no clear influence since, as the rut depth decreases, the rut width increases also. Increasing the width is advantageous if k_2 in the formula is relatively important (cohesive soil!). Elaborative summation procedures for different normal stress distributions are given by Wills (1960), who reports theoretical effects of normal stress distributions, at constant contact area and vertical load, on the pull force of up to 20% pull.

Equilibrium Considerations. In Fig. 3.54, M is the torque exerted by the axle on the sprocket, r_e is the active radius of the torque, τ is a shear stress in the contact surface, and σ_n is a normal stress in the contact surface. τ and σ_n are functions of x, being the distance from the contact surface front. Equilibrium of forces implies that

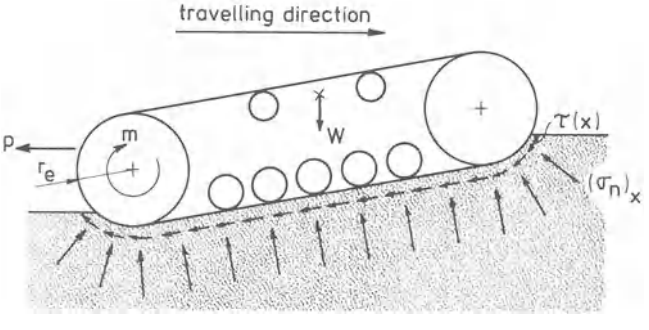

Fig. 3.54. Refers to the equations of equilibrium

$$W = \sum \text{vertical components of } \sigma_n(x) + \sum \text{vertical components of } \tau(x)$$

$$P = \sum \text{horizontal components of } \sigma_n(x) + \sum \text{horizontal components of } \tau(x)$$

where the summations should be made over the entire contact area. If we assume that the contact surface is a plane having unit width, then

$$\frac{M - M_0}{r_e} = \sum \tau(x)$$

where M_0 is the torque needed to overcome the internal rolling resistance of the undercarriage and the resistance due to soil packed in the undercarriage. Thus, M_0 does not correspond precisely with the internal rolling resistance. Under field conditions the contact line is wavy. Then, $\sigma_n(x)$ also contributes to the torque and this complicates the relation between M and $\tau(x)$ appreciably.

Stresses in the Soil. For the special case of a perfectly flat, rectangular, rigid, smooth contact surface, without sinkage and pull development, stresses within the soil can be calculated using the so-called solution of a rigid, smooth, rectangular plate on a semi-infinite elastic medium.

In agricultural practice, the situation is mostly different: the track shoes have grousers, the contact line is wavy, there is sinkage and a non-zero trim angle, and the main objective is developing pull. Handy solutions for this are not available, but the insight obtained through approximations and experiments with tires (Sect. 3.2), applies here as well. In addition,

- if the length of the contact surface is much larger than the width (which is the case with tracks as well as with tires), the stress at a particular depth in a particular soil is mainly determined by (1) the mean stress in the contact area, and (2) the width of the contact area. This was affirmed by measurements of Reaves and Cooper (1960). If the mean contact pressure under a track is half of that under a tire of the same width, then the stress level within the soil is also half as high under the track than under the tire.
- compared to a tire, a track transmits more vibrations to the soil, and gives, because of the stress peaks under the rollers, etc., a more pronounced kneading effect. Since a track is longer than a tire, and a crawler travels mostly at lower traveling speed, the load duration in a particular point is longer under a track than under a tire. When a soil is sensitive to vibrations, kneading, and/or load duration this can cause extra compaction. Before statements on vibration effects can be made, more research is needed.

Cage Rollers

Tillage effects of cage rollers are:

Crumbling. Cage rollers are not used on homogeneous, firm soil, but on soils that have been loosened and broken up into smaller and larger clods or aggre-

gates. If a clod or aggregate is hit by the roller, it is pressed between the roller and the soil underneath with hardly any lateral confinement. This is a process intermediate between load bearing and soil loosening. Crumbling will be favored by the beating action of a bumpy gait. A higher speed will give more intense strokes. Also inside the rollers aggregates may be crumbled by hitting the roller bars. This shuttling effect also increases at higher speeds.

Compacting. Compaction will occur only spotwise under the areas of contact between the soil and the roller.

Mixing. The roller slip and the strikes of the roller bars, both at a small degree of soil confinement, have an intensive mixing effect. An initially undulating soil surface, for instance, as a result of tines, may be left behind as a flat surface without large holes.

Piling Up. The soil in front of the roller may pile up. This unwanted secondary effect increases as a soil is pushed more easily (light soil), and the roller has a larger tendency to drag. Drag tendency can be diminished by not using a central axle over the full width and by selecting a greater roller diameter.

Cage Wheels

Cage wheels used in agriculture are driven wheels. The influence of wheel dimensions, etc., on rolling resistance, pull force, and rut depth follow rules that are comparable with the rules given in the sections on rollers, wheels and tires, and tracks. In general, cage wheels have a lower power efficiency than tires because of a higher rolling resistance. Pandey and Ojha (1978) determined which cage wheel design gave the highest pull in saturated soil (wet rice fields) for a wheel diameter of 685 mm and a vertical load of 490 – 980 N.

Cage wheels compact soil less than a comparable tire, especially the top layer. Soil compaction by cage wheels decreases as the bars are more radial and rectangular, because then compaction is more concentrated and radial, thin bars have a digging, loosening effect. When a cage wheel is mounted to a tire, compaction is usually reduced only a little because the load is still mainly supported by the tire.

3.5.3 Applications

3.5.3.1 Estimation of the Maximum Stress in the Contact Area of a Track on Soil

The maximum stress in the contact surface of a track is not equal to the mean (nominal) pressure, but higher, and the more so as the waving of the contact line is more pronounced. Rowland (1972) presented an empirical formula to estimate this maximum stress;

$$MMP = \frac{0.63\,W}{mb\sqrt{pd}}$$

MMP = mean maximum pressure, "mean"because stress peaks under the different rollers are not exactly the same (N/m^2),
W = vehicle weight (N),
m = number of rollers in one track,
b = track width (m),
p = track pitch (m)
d = outer diameter of track road wheel (m).

3.6 Tines

3.6.1 Occurrence

When a soil has to be loosened, a body (operating tool) can be moved through the soil. Such a body will be labeled a tine if the loosening effect reaches considerably further than the width of the body, and plow body if the loosening effect is mainly confined to the soil within the width of the operating tool.

Tines occur in chisel plows, spike-tooth-harrows, cultivators, p.t.o.-driven implements for seedbed preparation, weeders, and subsoilers (Krause and Lorenz 1979, Davis et al. 1972, Bernacki and Haman 1973).

Chisel Plows. The main objective of chisel plows is a coarse loosening of dense soil. Other objectives are control of perennial weeds and mixing of crop residues and fertilizers. Operating depth can be roughly equal to the depth of the arable layer. There are rigid tines, spring-mounted rigid tines and spring tines (see Fig. 3.55 a). Tines having some flexibility are able to move around obstacles and have a better self-cleaning action and sometimes a better crumbling action, than non-flexible tines. A share is mounted at the bottom end of a tine. Shares have many shapes and are usually wider than their shanks. The latter increases the loosening effect with a smaller soil displacement. Wear is concentrated mainly to the share area. Shares are exchanged when they are worn, or for purposes of tillage effects. Tines usually have a curved shape, the share cutting angle being between $30° - 60°$. The larger this angle, the less upward is the soil movement, but the higher the draft, the more the crumbling, and the more difficult it is for the tine to penetrate. Larger tines often have a smaller cutting angle than smaller tines. The set working depth is generally stabilized by supporting wheels. Normal range of traveling speeds is $6 - 8$ km/h. Crumbling increases with increasing traveling speed.

Spike-Tooth Harrows. Spike-tooth harrows are mainly used for shallow crumbling of soils that have been broken up earlier into coarse soil parts, thus in seedbed preparation. They also have mixing and leveling effects. Sorting occurs with mixing; larger aggregates are transported upwards. Working depth is up to about 8 cm. The tines are mounted in relatively small frames so they can follow uneven surfaces. The tines (Fig. 3.55 b) are usually rigid and vertical, with a

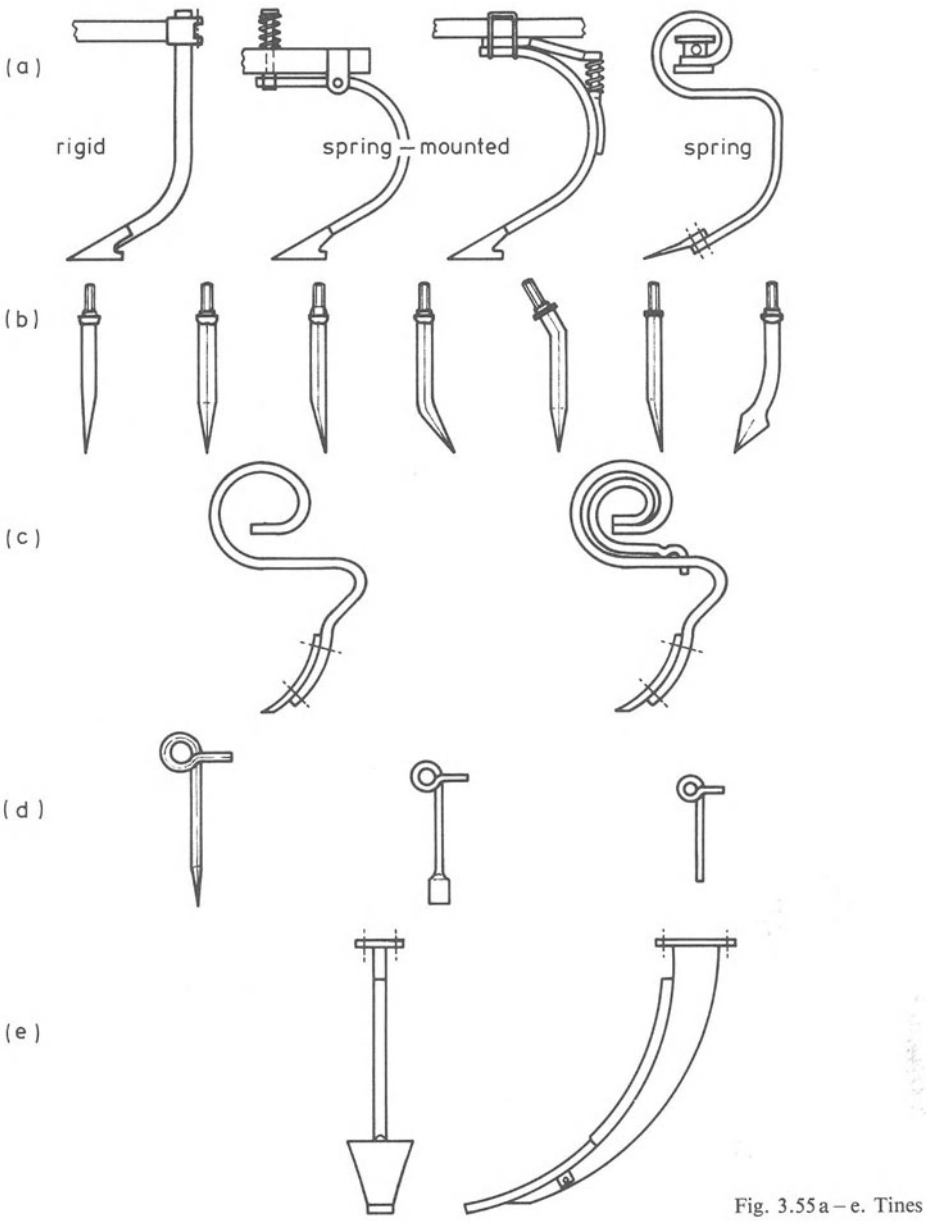

Fig. 3.55a – e. Tines

square cross section. Sometimes, the lower part is bent. Forward bending causes deeper penetration, backward bending results in a smaller working depth. The square cross section contributes to the crumbling effect. Working depth increases with increasing weight per tine, with decreasing tip cutting angle, with smaller inclination of the pull force direction, and which decreasing speed. Spike-tooth

harrows have no wheels or other supports. Operating speed should be at least 8 km/h to obtain the desired effect; a higher speed causes more crumbling.

Cultivators. Cultivators are intermediate between spike-tooth harrows and chisel plows. They are used mainly in seedbed preparation, postharvest operations, and weed control. Working depth reaches to about half the depth of the arable layer. The tines (Fig. 3.55c) are of the spring-type and may or may not have shares. Tine thickness varies, for instance, from 35 mm for light soils to 10 mm for heavy soils. Cutting angle is rather large to suppress bringing wet soil up to the surface. Depth control receives much attention, for which either supporting wheels or cage rollers may be used. Sometimes, when the tine itself acts like a spring, a second spring is used to make the working depth insensitive to tine spring action (Fig. 3.55c, right). Working speed may be up to 10 km/h, or higher.

P.T.O.-Driven Implements for Seedbed Preparation, such as rotating and reciprocating harrows. These tools feature a high capability of crumbling soils to large depths. The intensive crumbling is reached by a high tine speed and a great tine path length per unit area of land. At the same time, the degree of crumbling can be regulated over a broad range. The tines are simple, and often vertical. Depth control is by supporting wheels or cage rollers. Tine speeds may go up to 8 m/sec. Traveling speed of the tool should be less than about 6 km/h to keep the effect of the p.t.o. tine powering.

Weeders. Weeders are used for mechanical weed control. They will uproot weed seedlings and/or cover them with soil. Sometimes, they are used to break soil crusts. Working depth is very shallow, but tines may be up to 30 cm in length. In order that the tines will follow the soil surface irregularities, they are either spring-loaded or assembled to form a flexible frame. Sometimes the tine tips are pointed or chisel-shaped. The tine cross section is mostly circular. The tines are either straight (fig. 3.55d), or the lower part is raked forward. Tilling intensity increases with traveling speed, which may be up to 12 km/h.

Subsoilers. Subsoilers are used to loosen soil locally under the arable layer. Working depth may even be well over one meter, but most types are suited for depths less than one meter. The tine shank is equipped with a share, which is wider than the shank and has a very small cutting angle. The shank is rigid and much steeper than the share. Fig. 3.55e shows a subsoiler tine in front and side view. The subsoiler is ususally rigidly connected with the tractor, so that the tractor wheels also serve for depth control, but sometimes depth is controlled by wheels, rollers, or sleds. To reduce the power demand, traveling speed is low especially when used with crawlers which have a relatively low power-to-pull ratio.

Oscillating Tines. Sometimes, the above mentioned tines are vibrated. Particularly, oscillating subsoilers have gained some practical significance. The imposed oscillations are intended to reduce the draft force, but there are also secondary effects such as more crumbling, less compaction, less clogging, less adhesion, and better wear characteristics. The amplitude of the imposed vibra-

tions ranges from 1 to 25 mm and the frequency from 5 to 50 Hertz. Drawbar pull reductions as large as 70% have been reported, as a result of vibration, but the reduction in drawbar work generally is less than or equal to the extra energy consumed in the vibrations. Probably, the extra energy is lost mainly in the transmission system, so that further improvements of such transmissions may improve the energy balance and make oscillating tools more attractive for practical use. Literature on oscillating soil tools was reviewed by Verma (1971) and Blight (1970 – 1971).

3.6.2 Fundamentals

3.6.2.1 Kinematic Aspects

Motions of Tines

A rectilinear movement is very common for tines. Tines operating at very shallow depths usually follow soil surface irregularities, so that their paths are clearly curvilinear. A third type of movement occurs with powered tines, namely combinations of a rotating or reciprocating movement with a uniform forward movement. Well-known powered-tine paths are

- a sinusoidal curve in the horizontal plane, as obtained with a reciprocating harrow,
- a cycloid in the horizontal plane, as obtained with a rotating harrow,
- a cycloid in the vertical plane, as obtained with a normal rotary tiller with horizontal axis and radial tines.

These powered tines feature relatively large amplitudes and relatively low frequencies of the movement superposed on the uniform forward movement. The direction of movement of these powered tines is always about opposite to the direction of the soil flow. This is not true for vibrating tines. They feature high frequencies and small amplitudes, and during part of each vibration period the soil flow and tine movement are in about the same direction, at a tine velocity greater than the soil flow velocity. This is as if the soil flow were stretched. Eggenmüller (1958) introduced the quantity z^1 as a measure of this effect:

$$z^1 = \frac{\text{forward speed of implement}}{\text{amplitude} \cdot \text{frequency}}.$$

If $z^1 > 2\pi$, the tine movement is always forwards, and there is no soil flow stretching.

Flexible tines also have a complicated form of movement.

Contact Surface

In general, tines are not streamlined; they are intended primarily to break up and/or crumble soil. So, the process is periodical. This implies that the pattern of soil movement in the contact surface is not steady. Velocities and directions of

movement of soil particles vary from place to place and with time. Sometimes, there may be locally no relative movement between the tine surface and soil, for instance, where pronounced wedge formation occurs in front of the tine. Vertical soil movement is generally accompanied with lateral movement. This is especially the case near the soil surface. When the tine tip is blunt, the soil there is pushed downward, causing downward movements of soil particles in the contact surface.

The movements in the contact surface are more complicated as the tine movement itself is more complicated.

Soil Movements

Three movement patterns typical of soil influenced by a tine can be distinguished: the shear type, the flow type, and the type with open crack formation. *The shear type* is by far the most important and has been investigated most throughly. We will describe this type extensively for a straight vertical tine without profile (see Fig. 3.56, Koolen (1977)). Figure 3.56a is an instantaneous picture of the tine moving through a soil block, and the accompanying process. In front of the tine there is a compact soil mass, which can clearly be distinguished from the surrounding soil. This soil mass, usually called soil-wedge, is indicated by *ABCDEF*. Surface *GHIJKCBAG* is the boundary between the loosened and uneffected soil. The loose soil in front of and beside the wedge has just been loosened, and will be called crescent soil. The tine has made a furrow, which has been only partly refilled with loose soil. There always remains a small trench behind the tine. Another part of the loose soil has moved outside the lines *HL*

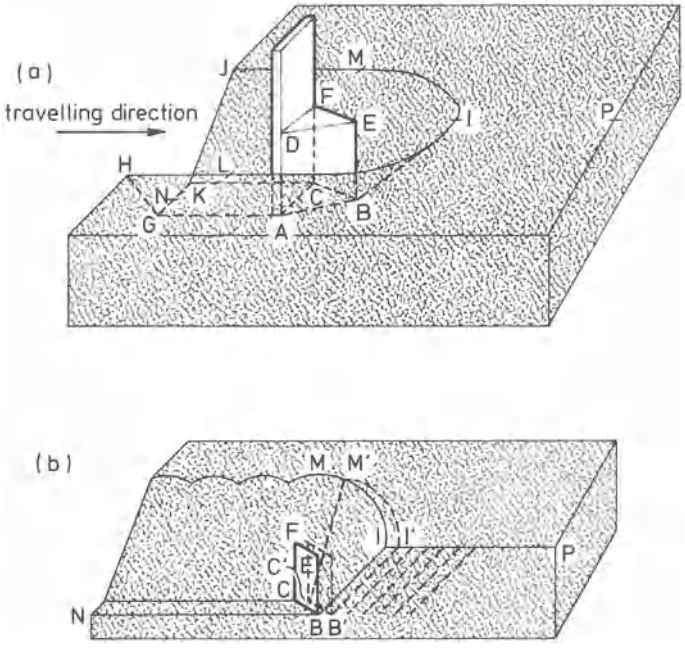

Fig. 3.56a, b. Tine inducing the shear-type process

and *JM* and rests on top of the firm soil surface. Where Fig. 3.56a is an instantaneous picture, Fig. 3.56b presents the progress in time of the soil breaking process. The plane through *NBIP* is a vertical plane of symmetry through the tine in the direction of travel. At a given moment plane *CBEF* is one side of the soil wedge and surface *CBIM* is half the boundary between firm and loose soil in front of the tine. As the tine moves further to the right, surface *CBIM* will be loaded by the underside of the wedge and by the loose soil present in front of the tine (this loose soil actually transmits the loading exerted by the vertical sides of the wedge). At a given moment, the load on *CBIM* has become so large as to cause failure along a new failure surface $C'B'I'M'$ and the soil from $CBIMC'B'I'M'$ will partly join the compact wedge, and partly the loose soil (distance $BB' = II'$ is sometimes called natural period of soil shear). When the tine moves further, the process is repeated. During the forward movement of the tine the wedge moves slowly upwards, the upper part being broken off and left aside at regular intervals. There is loose soil in front of and to the sides of the tine being transported in forward, upward, and sideways directions, as well as loose soil falling back into the furrow behind the tine.

The Soil Wedge. The soil wedge that moves upwards will be refilled from beneath with soil from the lower part of the tilled layer (Payne 1956, Willatt and Willis 1965b). It consists of compacted soil, the density being higher at the tine side than at the tip (Willatt and Willis 1965b). The wedge shape almost follows the outline of Fig. 3.56a, with the edges rounded (Payne 1956). The upward wedge speed fluctuates. Sometimes the wedge, or part of it, tends to adhere to the tine. In the literature the soil adhering to the tine is sometimes called "cone". Distinct cone formation may occur at low speeds and/or when the soil-metal friction angle is large (Tanner 1960, Willatt and Willis 1965b, Payne 1956).

The Crescent Soil. The degree of crescent soil pulverization can vary strongly. An extreme case happens when, after shearing, there is little or no further pulverization of the soil in $CBIMC'B'I'M'$. Then the freshly formed soil lump will keep its crescent-like shape (Payne 1956). However, in most cases some further pulverization occurs, which is more pronounced at higher speeds and at greater natural soil heterogeneity (Payne 1956).

The Furrow. Furrow width values (*HJ* in Fig. 3.56a) are given by Payne (1956), O'Callaghan and Farrelly (1964), and Willatt and Willis (1965a). A unique relationship appears to exist between the ratio's furrow width/tine width and tine depth/tine width (O'Callaghan and Farrelly 1964). The relationship between the ratio's distance from tine to tip of crescent/width of tine and tine depth/tine width is also unique (Payne 1956). These relationships apply to different tine widths and working depths, but are slightly dependent on soil type (Payne 1956) and on traveling speed (Willatt and Willis 1965a). The furrow walls and bottom can exhibit fissures. The longer axes of these fissures are perpendicular to the traveling direction of the tine (O'Callaghan and Farrelly 1964).

The Loose Soil Left Behind. The loose soil pushed away by the tine partly falls back into the furrow, and partly comes to rest outside the furrow on top of the

still firm soil surface. Usually, a small trench is left in the middle of the furrow, with a small ridge on either side. If there is not much crescent soil pulverization, the soil clods that have come to rest can have equal shapes and positions and exhibit a very regular pattern (Payne 1956). In the loose soil left behind mixing and sorting occur often. For these processes we refer to Kouwenhoven (1979).

The shear type, described for the straight vertical tine without profile, may also occur with

- the straight, slightly forward-raked tine without profile,
- the straight, slightly backward-raked tine without profile,
- the straight, very backward-raked tine without profile,
- the straight, vertical, wedge-shaped tine.

We observe the following pertinent extensions:
With increasing forward rake of the slightly forward-raked tine

- the soil wedge become less compacted (Willatt and Willis 1965 b),
- the wedge shape is more irregular (Payne and Tanner 1959),
- there is more upward movement of the wedge and less adhering to the tine (Tanner 1960),
- the furrow width increases and the length of the horizontal projection of the distance between the tine tip and the furrow tip decreases (Payne and Tanner 1959).

With increasing backward rake of the slightly backward-raked tine

- there is less upward movement of the wedge and more adhering to the tine (Tanner 1960),
- the furrow width decreases and the length of the horizontal projection of the distance between tine tip and furrow tip increases (Payne and Tanner 1959).

With the very backward-raked tine there is no relative movement between the tine and the soil wedge, so the wedge becomes part of the tine. The wedge neither crumbles off nor is refilled (Payne and Tanner 1959, Tanner 1960). For the wedge-shaped tine, provided the tip angle of the wedge shape of the tine is small enough, there is no soil wedge, its function being taken over by the wedge-shaped tine (O'Callaghan and McCullen 1965).

The described configuration of the shear type of soil reaction cannot exist at a small working depth/tine width ratio. The soil wedge in Fig. 3.56 a has the form of a standing prism. When the tine width is increased or the working depth decreased, at a given moment a standing prism cannot be found anymore, and we may state that the tine has *changed into a plow body* (soil wedges also occur with plow bodies, but those are lying prisms). The change occurs at a working depth/tine width ratio of 0.5 – 2.5 (Payne 1956, Payne and Tanner 1959, O'Callaghan and Farrelly 1964, O'Callaghan and McCullen 1965).

The described shear type can also not exist at a large working depth/tine width ratio. In that case the described process will not reach to the bottom of the tine, but to a smaller depth, which is called the *critical depth.* The tine part below the critical depth acts as a penetrating wedge (Sect. 3.3), displacing soil only in forward, sideward, and backward directions without vertical soil movements.

Here, soil compacting should be expected (whereas tines are intended to loosen the soil). The critical depth is smaller as the soil is looser. It increases with increasing soil angle of internal friction, increasing tine width, and increasing forward rake of the tine (Godwin and Spoor 1977, Spoor and Godwin 1978). For example, for a 25.4 mm wide, vertical, tine without profile, the critical depth in a dense soil appeard to be 120 mm.

With tines having a small cutting angle, *the type with open crack formation* instead of the shear type should be expected, like, for instance, with very forward-raked tines and curved tines. The cutting edge splits the soil at tine depth, inducing a crack that propagates in a more or less horizontal direction. An indication for this can be deduced from Willatt and Willis (1965a), who stated that "a deeper rut is created by a curved tine than by a plane vertical tine".

In *the flow type*, the soil is mainly deformed and no or only a few failure surfaces develop. Soil bulges up on both sides and in front of the tine. The furrow is a narrow trench bounded by a permanent bulge on either side. This type of process occurs with narrow tines, wet soil, and high speeds (Payne 1956, Payne and Tanner 1959, Stafford 1979).

3.6.2.2 Dynamic Aspects

We discuss only straight tines, without profile, inducing shear type processes.

Force measurements on tines can be found in Payne and Tanner (1959), Dransfield et al. (1964), Verma (1971), Spoor and Godwin (1978), and Stafford (1979). The draft force fluctuates with time as soil blocks are torn out, and increases with depth of operation. In non-cohesive soil this increase is about linear with depth, and in highly cohesive soil approximately quadratic. A tine with "zero" width still exerts a finite draft, whereafter draft increases linearly with width. At constant working depth the horizontal force depends on the cutting angle α (see Fig. 3.57). This force is infinitely large for $\alpha = 0$ as well as for $\alpha = 180°$ (an infinitely large backward rake). The horizontal force attains a minimum at $\alpha = \alpha_{min} \approx 20°$, and increases as α differs more from α_{min}. In general, a tine also exerts a vertical force on the soil. Magnitude and direction of this force can be deduced from the magnitude of the horizontal force and angle β in Fig. 3.57. At a cutting angle α of about 45°, β is about zero and, therefore, the vertical force is about zero. For cutting angles smaller than about 45° the tine exerts an upward vertical force on the soil, and β increases with decreasing α.

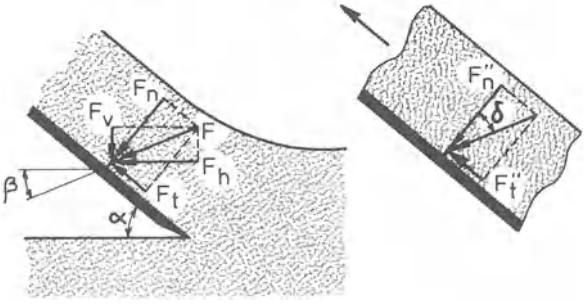

Fig. 3.57. Vertical force F_v/horizontal force $F_h = \text{cotan}(\alpha + \delta)$, provided some conditions are satisfied (see text)

For cutting angles larger than about 45° the tine exerts a downward vertical force on the soil and β becomes more and more negative with increasing α. The draft is speed-dependent. For the shear type process the draft increases quadratically with speed. For an oscillating tine the draft decreases with increasing frequency and amplitude. This decrease is less at higher traveling speeds. With increasing frequency and amplitude, the energy consumed in the vibration increases rapidly. For a tine, there must be equilibrium among the following forces: the force that the soil exerts on the tine, the tool weight, the draft, and if supporting wheels or similar aids are present, the appropriate reaction forces. As a rule of thumb, the tool should be designed and adjusted so that, on the average, the reaction force on the supports is zero, in order to avoid unnecessary rolling or drag energy losses. Supports should only stabilize working depth.

At the soil-tine interface in Fig. 3.57, the force that the soil exerts tangentially on the tine is labeled F_t, and the force that the soil exerts perpendicularly to the tine F_n. Both forces consist of two components:

$$F_t = F_t' + F_t''$$
$$F_n = F_n' + F_n''$$

- F_n' and F_t' are the components of the force at the cutting edge that tries to push the tool upward. This force is significant when the cutting edge is blunt, or in soils exhibiting significant elastic recovery (Payne and Tanner 1959).
- F_n'' is the normal force that the soil exerts on the tool surface.
- F_t'' is the friction force between the soil and the tool surface.

Provided a soil flow exists along the blade, not involving any sideways movements,

$$F_t'' = F_n'' \tan\delta$$

where δ denotes the soil-metal friction angle. Sometimes there is no soil flow, but a soil wedge that is more or less stationary. Then

$$F_t'' < F_n'' \tan\delta .$$

At cutting angles larger than 90° the soil wedge may tend to move downwards. In that case F_t'' changes direction, but, because the subsoil prevents the wedge from traveling downwards, it is still true that $F_t'' < F_n'' \tan\delta$ (Payne and Tanner 1959). When the soil flow involves sideways movement, it is still true that the *algebraic sum* of the friction forces equals $F_n'' \tan\delta$, but the magnitude of the *vector sum* of the friction forces is smaller than $F_n'' \tan\delta$. Hence, provided

- the cutting edge is sharp,
- there is not much elastic recovery,
- a soil flow is maintained, not involving a significant sideways component,

$$F_t/F_n = F_t''/F_n'' = \tan\delta$$

and $\beta = 90° - (\alpha + \delta)$. Under field conditions, the cutting angle is not ideally sharp, there is elastic recovery, there are lateral soil movements, and sometimes stagnating soil wedges occur, so that $\beta \neq 90° - (\alpha + \delta)$.

Between the tine and the still unbroken soil, there are soil blocks which are completely separated or in the process of being torn up. Those soil blocks can be considered as rigid bodies, on which the following forces may act:

- the gravitational force (weight),
- an inertia force, if the block is accelerating of decelerating,
- a soil-metal frictional force and an adhesion force, if the soil element is adjacent to the tine surface,
- soil-soil frictional forces with adjacent soil or soil blocks,
- cohesive forces if a part of its surface is a developing failure surface.

All these forces have to be in equilibrium and this allows the draft of a tine to be estimated. For a very simple two-dimensional example of such an estimation, see Söhne's model in Sect. 2.4.3.3. Such models are often able to explain the character of the draft force. The formulas for Söhne's model demonstrate that

- weight force B partly increases quadratic with depth h. In non-cohesive soil, soil weight is responsible for draft and, therefore, the draft increases on such soils more than proportionally with depth.
- cohesive force C is linear in h and, therefore, a linear relation between draft and depth should be expected on highly cohesive soils,
- all forces are linear in width b,
- acceleration force K is proportional to the square of the velocity. It is understandable, therefore, that the draft increases more than proportionally with speed.

An oscillating tine has a lower pull demand because

- the vibration influences the equilibrium of forces in the soil volume as described above. Frictional forces may change direction, and normal forces may decrease. It appears that a strong draft reduction can occur when the vibration frequency approaches the natural frequency of shear.
- the vibration reduces the soil-metal friction angle δ.
- the vibration reduces soil strength (see Sect. 2.4).

3.6.3 Applications

3.6.3.1 The Profile of a Furrow Made by a Tine

Willatt and Willis (1965a) present prediction formulae for the (upper) width b and the area A of a section through a furrow (boundary between still firm soil and loosened soil) made by a tine. These prediction formulae have been tested for

- plane, vertical tines and curved tines,
- soils ranging from sandy loams to clays, located in wheat growing areas of New South Wales,
- working depths between 2 and 7 in,
- tine width of 2 in,
- a traveling speed of 4 – 5 ft/s,
- the shear type process.

The following independent variables were involved:

- tine width w,
- working depth d.

During the measurements no influence was seen of soil type or moisture content. Assuming

- a trapezoidal cross-section of the furrow, with upper width b, height d, and bottom width equal to the tine width w,
- a constant inclination of the non-horizontal trapezium sides,

a general prediction formula has been established as,

$$b = k_1 d + w$$

where k_1 is a constant. For measured values of b and d linear regression yielded $k_1 = 2.42$. According to the assumptions the section area A is

$$A = k_2 d^2 + wd$$

where k_2 is a constant. From measured values of A and d, it followed $k_2 = 1.03$.

3.6.3.2 Draft of Plane Blades and Tines Operating in a Saturated Clay

Wismer and Luth (1972) presented a method for predicting draft force of plane tines and blades within the following domain:

- a specific saturated clay, irrespective of its packing state,
- plane steel tines and blades having a specific surface finish.

The following characteristics were selected:

- tool width b,
- tool length l,
- tool operating depth z,
- cutting angle α (radians),
- operating velocity v,
- soil cohesion c,
- internal friction angle ϕ,
- unit weight γ,
- shear rate factor β,
- acceleration of gravity g,
- coefficient of soil to metal friction μ.

Application of Buckingham's Pi-theorem resulted in

$$\frac{F}{\gamma l^3} = f\left(\frac{L_1}{L_2}, \frac{L_1}{L_3}, \alpha, \frac{v^2}{gL}, \mu, \phi, \frac{c}{\gamma L}, \beta\right)$$

where F is the draft force and L represents unspecified length variables of the tool. (According to the Pi-theorem, the L's can be interchanged and mixed, the only requirement being that the terms remain dimensionless and that L_1/L_2 and

L_1/L_3 are not identical.) Measurements on the clay in question showed that the packing state did not affect ϕ and μ, so these characteristics could be left out of consideration. Preliminary research justified the quantities $c/(\gamma L)$ and β to be replaced by one quantity,

$$\frac{CI}{\gamma z}\beta$$

where CI is the cone index of the clay, determined according to a standard method. This yielded

$$\frac{F}{\gamma L^3} = f\left(\frac{L_1}{L_2}, \frac{L_1}{L_3}, \alpha, \frac{v^2}{gL}, \frac{CI}{\gamma z}, \beta\right).$$

Further tests, in which the relationship for each independent quantity with the dependent quantity was determined at constant values of the other independent quantities, indicated that the following general formula might satisfy:

$$\frac{F}{\gamma b z^{0.5} l^{1.5}} = \alpha^{k_1}\left(\frac{z}{l\sin\alpha}\right)^{k_2}\left[\left(\frac{CI}{\gamma z}\beta\right)^{k_3}\left(k_4\left(\frac{z}{b}\right)^{k_5} + k_6\right) + k_7\frac{v^2}{gl}\right].$$

Consequently, k_1 through k_7 were calculated from measuring data by multiple regression. This resulted in the following prediction formula:

$$\frac{F}{\gamma b z^{0.5} l^{1.5}} = \alpha^{1.15}\left(\frac{z}{l\sin\alpha}\right)^{1.21}\left[\left(\frac{CI}{\gamma z}\beta\right)^{1.21}\left(0.055\left(\frac{z}{b}\right)^{0.78} + 0.065\right) + 0.64\frac{v^2}{gl}\right].$$

The standard error of estimate of F was 43 lb. F varied from 17 to 550 lb and the standard error of estimate, expressed as a percentage of the mean, was 20%. This is a good result, since the prediction formula is intended for:

- plane tines with small cutting angles,
- plane tines with large cutting angles,
- plane blades with small cutting angles and small working depth-blade height ratios,
- plane blades with large cutting angles and small working depth-blade height ratios,
- plane blades with small cutting angles and large working depth-blade height ratios,
- plane blades with large cutting angles and large working depth-blade height ratios.

3.7 Plow Bodies

3.7.1 Occurrence

A body that is being pulled through soil to loosen it, and does so over a width about equal to the width of the body, will be called a plow body. A plow body always resembles more or less a so-called two-dimensional blade, that is an infinitely wide blade with a horizontal cutting edge perpendicular to the direction of travel, and with a shape that does not vary across the width. The action of a two-dimensional blade depends especially on the cutting angle, the blade shape, the inclination at the rear end, the blade size, and the operating depth. Very much like a two-dimensional blade are, for instance, dozer blades and sweeps.

Krause and Lorenz (1979) gave a survey of *tillage tools.* The operating parts of many of these tools can be considered as plow bodies.

This holds true, for instance, for moldboard-plows. These are used to loosen and invert the soil, and to bury plants or manure. At the front of the plow body a slice of soil (furrow slice) is cut free. Vertical cutting is performed by a coulter, acting as a wedge (see Sect. 3.3) and as a sliding body (see Sect. 3.4), independent of the plow-body action. Horizontal cutting is performed by the share which has a small cutting angle. The share has a strong influence on the action of the plow body. The furrow slice that has been cut free, moves along the plow body and is deposed after undergoing a turning of $120° - 150°$. This involves twisting and bending of the furrow slice, which causes cracking. The loosening and the crumbling depend on the shape of the plow body, traveling speed, and soil conditions. Mixing hardly occurs in the furrow slice. As the conditions for plowing vary in practice, the shape of share and moldboard also vary. Important characteristics of this shape are the steepness (cutting angle), the angle between the cutting edge and the direction of travel (if this angle is large, the moldboard is said to be short or abrupt) and to what degree the moldboard is cylindrical and/or twisted. The shape of share and moldboard are designed to handle the furrow slice correctly, and not to minimize reaction forces. Consequently, supports of a plow body have to withstand considerable forces. Usually, support is provided by the so-called landside with heel. The reaction forces cause friction on landside and heel and this friction contributes significantly to the draft. Sometimes support is provided by an inclined wheel that runs in the corner of the open furrow.

A second example of plow bodies are the blades of rotavators. Here the shank acts more or less as a wedge and/or sliding body (Sects. 3.3 and 3.4). The path of a rotavator blade through the soil during one revolution is curved, and the thickness of the soil slice that is cut off varies along this path. For blades that rotate in the same direction as the tractor wheels this thickness is large at the start and zero at the end of a bite. The soil slice is relatively short, so that intake and output effects are relatively important. When the velocity of rotation is high, the force system on the small soil beam and the blade involves significant centrifugal forces.

Hillers, duckfoot sweeps, and blades of rotary diggers also resemble, more or less, a two-dimensional blade. In dry-land farming it is customary to loosen the top layer of the soil without inversion. A special tool for this purpose which resembles a two-dimensional blade is the sweep. For irrigated crop production a level soil surface is required, for which the leveler/smoother is available. Ridges for directing surface water can be made using a ridger/furrower. These implements also belong to the group discussed here.

Other agricultural machines with plow bodies are root crop harvesters, soil fumigators, manure injectors, vertical augers for making bore holes, and non-vertical augers for clearing ditches.

Plow bodies occur also in *earth moving* equipment (Nichols 1976), such as blades of bulldozers and graders, shares of scrapers and buckets, and augers.

3.7.2 Fundamentals

Plow body fundamentals have been discussed in detail by Koolen (1977). Figure 3.58 represents some plow bodies. The plow bodies *a* through *h* can be called two-dimensional blades. They are characterized by an infinite width, a horizontal cutting edge that is always perpendicular to the direction of travel, and a shape that does not vary across the width. In this way the process does not vary in the horizontal direction perpendicular to the travel direction, not considering soil heterogeneity effects. For two-dimensional blades important characteristics are the shape of the surface, the cutting angle, and the working depth in relation to the size, i. e. the height of the tool. If, for each of these three characteristics, two categories are chosen, a set of eight standard blades arises, according to Table 3.12. The other plow bodies in Fig. 3.58 are more widely known in agricultural practice: a moldboard plow (*i*), a rotatiller blade (*j*), a sweep (*k*), and a potato harvester lifting blade (*l*). For these blades and tools it is useful to define the following process parts: intake, main flow, and output process. The intake process separates a soil-strip from the untouched soil. The main flow is the process during which the soil-strip flows along the plow body. The output process includes the changes after the soil strip has left the plow body. For each plow body process in Fig. 3.58 the intake is indicated by *A*, the main flow by *B*, and the output by *C*. As can be seen from the figure, the process parts may not be all clearly present for each plow body. Blade *a* – a curved blade with a small cutting angle and a small working depth/blade height ratio – occupies a special place.

Table 3.12. Two-dimensional blades

Cutting angle	Small				Large			
Shape	Curved		Plane		Curved		Plane	
Working depth/blade height ratio	Small	Large	Small	Large	Small	Large	Small	Large
Type in Fig. 3.58	a	b	c	d	e	f	g	h

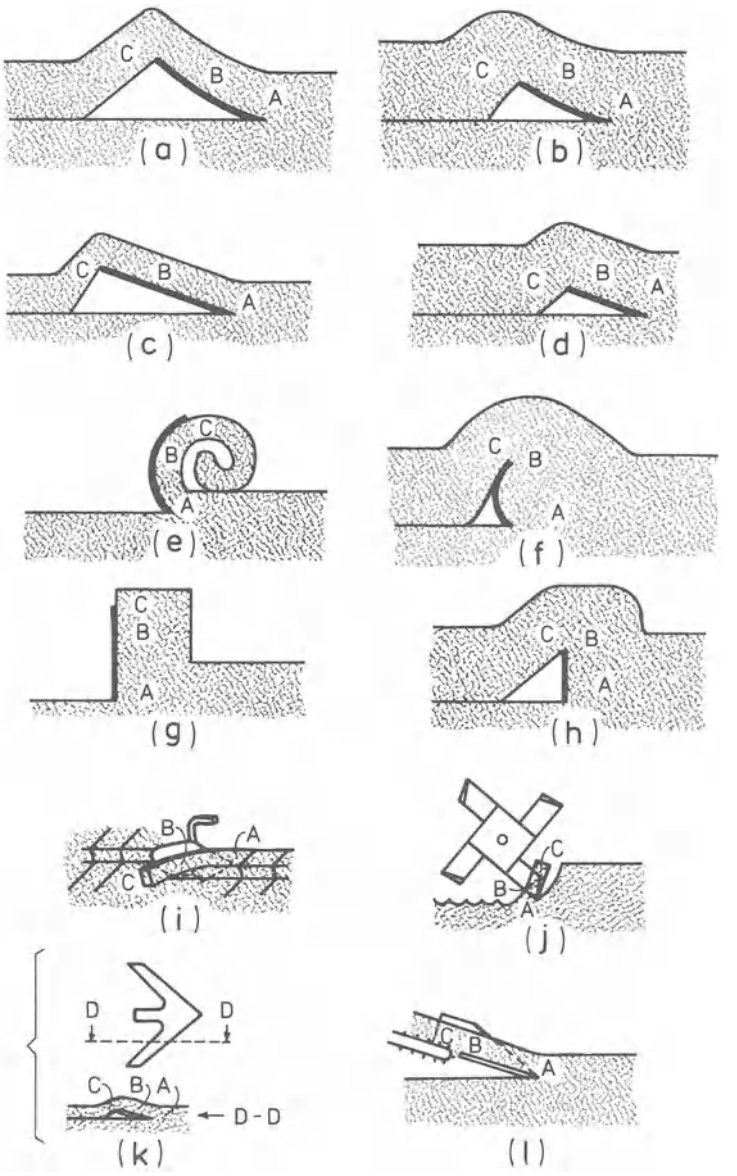

Fig. 3.58a – l. Plow bodies

On the one hand it is very suitable for experiments, on the other hand it exhibits a large number of phenomena that also occur with more complicated plow bodies. Therefore, kinematic aspects of this blade will be discussed first in detail, demonstrating many aspects of the behavior of other plow bodies which are less feasible in experiments (Sect. 3.7.2.1). After this, the kinematic aspects of other types of plow bodies will be discussed only briefly (Sect. 3.7.2.2).

3.7.2.1 Kinematic Aspects of Two-Dimensional, Curved Blade with a Small Cutting Angle and a Small Working Depth/Blade Height Ratio

Intake

The different shapes of intake processes can be categorized as follows (Fig. 3.59):

- intake with open cracks. Cracks develop from the edge of the blade (share) and the share penetrates the cracks like a wedge,
- intake by shear-plane failure. Failure surfaces occur, and normal stresses act on (almost) all parts of these surfaces,
- intake by steady cutting. Failure surfaces do not (or seldom) occur.

Intake by Open Crack Formation. Figure 3.60 shows successive instantaneous pictures of the formation of an open crack. In picture 1, the leading edge of the share has penetrated the still firm soil so far that a crack is being initiated in which the share tip can penetrate as a wedge. In pictures 1, 2, and 3, the crack propagates at a larger velocity than the traveling speed of the share, so that the crack front is heading the share tip more and more. In pictures 4, 5, 6, and 7 the rate of propagation of the crack reduces to zero so that the share tip gains somewhat on the crack front. In picture 7 the share tip starts again to penetrate into

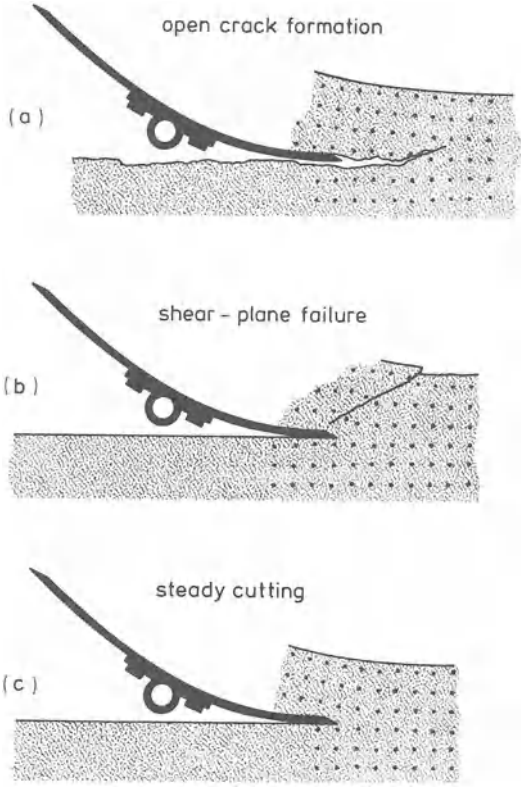

Fig. 3.59a – c. Types of intake

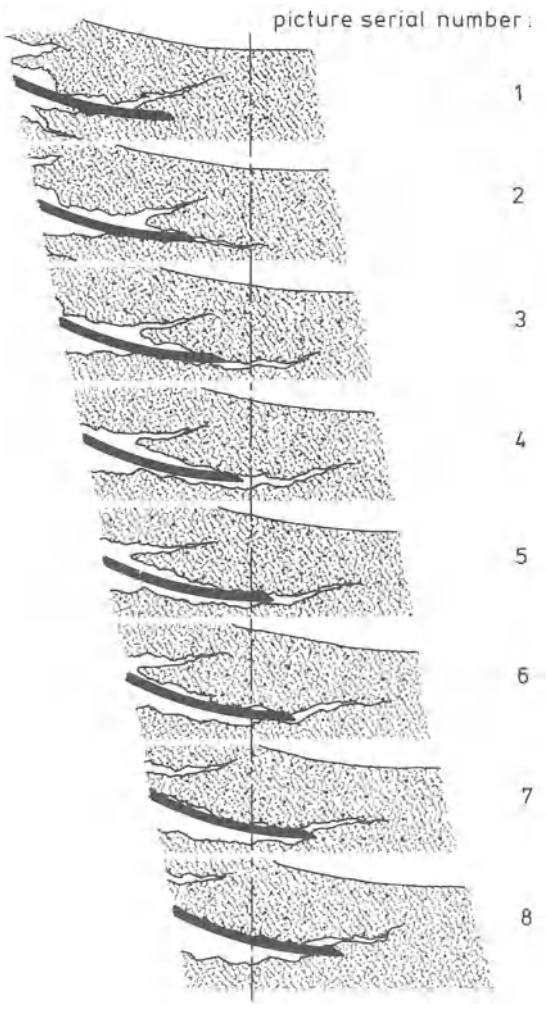

Fig. 3.60. Series of instantaneous pictures of open crack formation by a penetrating blade

firm soil and the process is repeated. The crack propagation between pictures 7 and 8 should be attributed to the fresh soil beam being lifted (bent upward) by the blade and is, therefore, a feature of the main flow. The crack in Fig. 3.60 starts in a somewhat downward direction, but the share tip is able to penetrate the crack. Subsequently, crack direction bends upwards, making the share tip meet again still firm soil at a given moment, as shown in picture 7. This path of cracking causes the formation of a hole in the furrow bottom and of a tear in the bottom side of the soil beam. The cracking path can vary strongly and feature phenomena other than hole formation (Fig. 3.61). When crack-fronts come to rest below the share tip, this leads to tongue formation in the furrow. When a crack front moves below the share tip path, the blade tip penetrates the soil beam bottom, and the crack front eventually moves above the share tip path, then a free soil slice is formed in the bottom of the furrow. In a similar way free slices

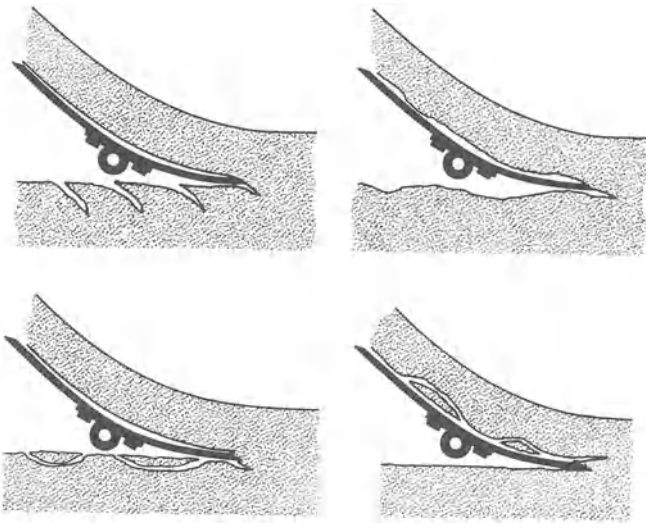

Fig. 3.61. Formation of tongues, holes, and slices during intake with open crack formation

can be formed in the bottom part of the soil beam. When the level of the crack front is only slightly higher than the share tip path, only soil crumbs will be separated, which is called planing. A survey of observed crack paths is given in Table 3.13.

The thickness of the soil beam is hardly ever the same as the nominal working depth, as can be seen in Fig. 3.60, where a hole develops in the bottom of the furrow. Also in case of tongue formation the thickness of the soil beam exceeds the working depth; the soil in front of and above the tongue is pushed in an upward and forward direction before being cut off. The additional thickness of the soil beam corresponds with the open space under the tongues left behind. This effect is pronounced, especially in plastic soils. The degree of stability of the cracking varies. A crack may propagate at a high velocity, bend upwards and run to the soil surface, separating a soil piece. The opposite is a crack propagating horizontally with a constant crack front speed equal to the traveling speed of the share. Here, the distance between the share tip and the crack front may be large.

Sometimes a running crack splits into two cracks, being known as fork formation.

Intake by Shear-Plane Failure (Fig. 3.59b). The cutting edge of the tool tries to push the soil upwards, thus inducing a field of increasing stress. As soon as the shear stress has become equal to the soil shear strength (sum of soil cohesion and internal friction), a failure plane is initiated, which will extend very quickly up to the soil surface. The failure plane separates a soil lump moving upwards along the tool and the still firm soil. After the soil lump separates, the cutting resistance falls until the pushing action of the cutting edge makes it rise again. Then the process is repeated and the following lump will be formed (Söhne 1956).

Table 3.13. Open crack phenomena

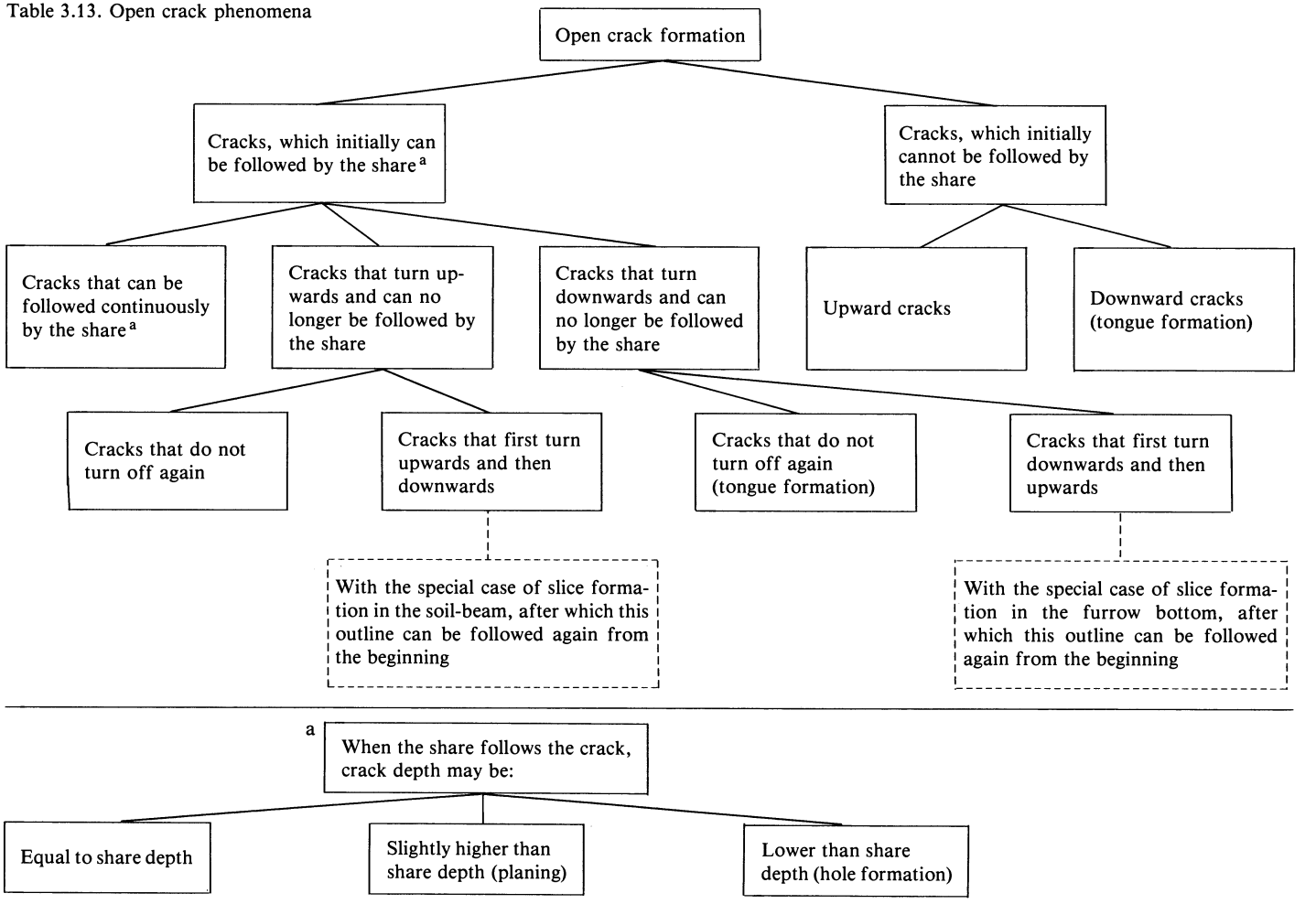

Intake by Steady Cutting (Fig. 3.59c). Each volume element of soil being taken in deforms so as to enable the soil beam to follow the change in direction at the cutting edge without breaking or tearing.

Starting and Running-Out Processes. In soil tillage we are primarily interested in processes occurring at constant tool speed which are not affected by starting or running-out phenomena. This is comparable to fluid mechanics where pipe flow studies have been concentrated on the equilibrium situation some time after initiating flow. The simplest equilibrium situation involves pressures, flow rates, etc. that do not change with time. Fluid mechanics uses the term "steady state" for this. Flow in a given coordinate system is said to be steady if at any point belonging to the flow system and fixed in the co-ordinate system, the velocity vector does not vary with time. The steady state concept has been adapted to turbulent flow by using mean velocity vectors instead of actual vectors. For this the time interval over which velocities are averaged must be taken so large that the mean vectors are indeed constant with time (Shames 1962). This concept seems applicable also to soil tillage processes. However, because soil break-up is more structured than the turbulent flow of water, the following definition is chosen: a tillage process is called a steadily fluctuating process if, at any point fixed relative to the tool, the flow properties are repeated periodically, apart from incidental effects. Returning to the blade, the question arises over what distance the blade has to travel before the process is steadily fluctuating. Consider the soil that successively is in the intake zone. At the start of the tool run, the soil being taken in is influenced only by the tool share, which causes a specific process. As the tool progresses the blade is filled with soil, and this soil influences the intake process. This influence is dependent on the way in which this soil was taken in (unsteadily fluctuating). If that dependence is negligible, then the intake process will attain its steadily fluctuating character as soon as the blade is completely filled with soil, that is, when the amount of soil approaching the blade equals the amount leaving the blade. As soon as the output of soil is also fluctuating steadily, the entire tillage process can be considered steady. Hence, it can be stated that, generally, the starting period will be shorter as:

- the intake zone is smaller,
- the external influences on the intake process are smaller (external influences are the main flow, the subsoil, and the load to which the soil was subjected prior to the time under consideration),
- the tool is shorter and, therefore, is filled faster,
- the thickness of the soil mass on the tool does not exceed by much the depth of cut (which means that less soil is needed to achieve complete filling),
- the filling efficiency is higher (filling efficiency is low if there is a significant output before complete filling occurs).

The starting process exists over a distance that is never shorter than about one tool length and may comprise many tool lengths.

When the blade is approaching the end of a soil mass, the intake process in its steadily fluctuating state will at a certain moment no longer fit in that part of the mass which is in front of the tool. The intake process then starts to differ.

Products of the Intake. The intake process delivers a soil beam and a furrow bottom. The tool caused a plane of separation between them. This plane of separation usually does not pass along the soil particles that were originally at the nominal working depth. This is true, for instance, when the soil is pushed upwards at intake and cracks extend below the share depth, whereas all the soil above the crack is taken in by the blade. Also, the depth of the furrow bottom is not always equal to the share depth, for instance, when the soil is pushed upwards and forwards in the intake zone, and part of the furrow bottom behind the share is taken along. This is always accompanied by widening of cracks in the furrow bottom. Also, tongues can stick to the bottom of the tool and are consequently moved forwards, and therefore, also upwards.

The bottom of the furrow may be composed of cutting planes, failure planes, and cracks under tongues. At the bottom of the furrow slices and holes may be present. The cutting planes usually are not completely smooth, but often have very small cracks that are similar to the larger ones under the tongues. These small cracks are inclined forwards and downwards with respect to the cutting direction; they may help to determine the cutting direction from an existing cutting plane. The upper part of the soil under the furrow bottom has usually been moved forwards to some extent.

The bottom of a soil beam that has just been taken in may exhibit phenomena very much resembling those described for the furrow bottom (cutting planes, failure planes, cracks above tongues, and slices). The soil beam may be torn, broken, or deformed, and may have a thickness equal to or larger than the nominal working depth.

Main Flow

The basic types of main flow depend on the variation of the blade curvature. The following blade shapes may be distinguished:

- curvature increasing towards the end,
- curvature decreasing towards the end,
- constant curvature (arc of a circle).

Blades with Increasing Curvature. The soil from the intake process is transported to the output process by the main flow process. During this main flow process the soil can be changed to a certain extent. The shape of the soil-strip that is delivered to the main flow is determined by the intake process. If the intake process is pure steady cutting, the strip will be continuous. If open cracks are formed during the intake process, the main flow normally will receive a soil-strip that is more or less cracked at the lower part. Parts of the soil-strip above these cracks act as hinges. An intake process with shear-plane failure gives a strip of moving pieces separated by parallel failure planes. Thus, three main types of soil-strips can be delivered to the main flow (Fig. 3.62):

Type I. unbroken strip,
Type II. strip of pieces connected by hinges,
Type III. strip of pieces moving along each other.

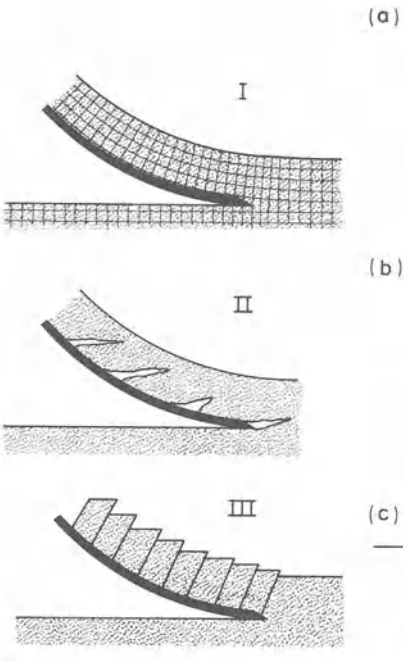

Fig. 3.62. Main flow: Types of soil strips

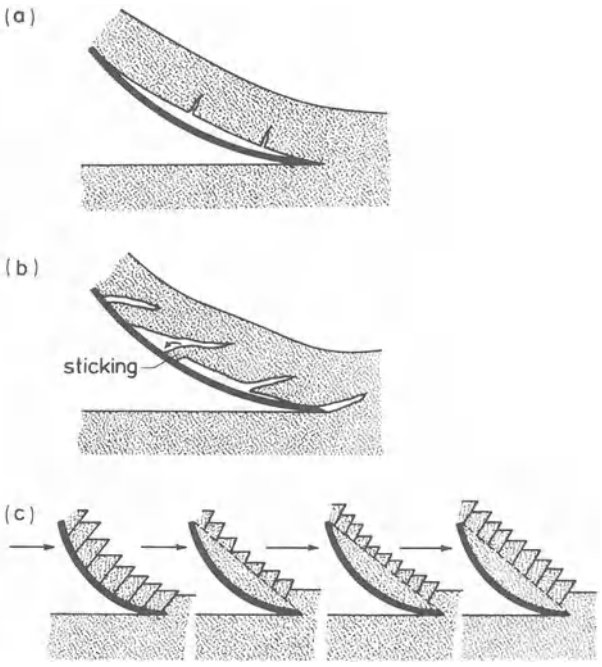

Fig. 3.63a – c. Some main flow phenomena. (a) Tensile cracking due to partial loss of soil-tool contact; (b) rotation of an adhering tongue; (c) filling up of the hollow of the blade

Type I an unbroken soil-strip. If there is continuous contact between the blade and the soil-strip, the whole strip must be deformed during its movement along the blade, because blade curvature is not constant. Sometimes contact between blade and soil is lost. Then tension cracks may develop in the lower part of the strip (Fig. 3.63a).

Type II a strip of soil pieces connected by hinges. If the hinges are not much weaker than the pieces themselves, its behavior will very much resemble that of an unbroken strip. If the hinges are much weaker than the pieces, every change in curvature will be absorbed entirely by the hinges and the pieces will move as rigid bodies along the blade. Because the curvature is increasing, the cracks under the hinges will be widened. Old crack fronts may become active again. Usually, cracks that produce hinges run from the bottom of the strip in a forward and upward direction, causing the pieces to be pointed. These points crumble during the main flow process, especially in drier soils. Occasionally, these points stay somewhat behind causing a certain rotation (Fig. 3.63b) and pushing the soil beam slightly upwards like a prop. A hinge can be disturbed to the extent that contact between hinge halves is lost, and the piece behind slips over the piece in front. By this mechanism a main flow of pieces moving parallel to each other can develop.

Type III strip of soil pieces moving parallel to each other. This parallel movement keeps pieces parallel to each other while following the blade curve. If binding forces within the pieces on the curved blade are small, the bottom parts of

these pieces will crumble and fill up the blade curvature. Then the blade is changed more or less into a plane plate and the pieces will not have to move parallel to each other any more (Fig. 3.63 c).

Blades with Decreasing Curvature. The above descriptions of types I, II, and III apply, with the understanding that, in the case of type II,

- cracks below hinges close as the strip travels over the blade,
- there is much less falling behind of pointed ends of soil pieces.

Blades with Constant Curvature. Here, too, all three above-mentioned types of soil-strips may occur. Although blade curvature is constant, relative movements between parallel moving soil pieces will be maintained, allowing the pieces to follow the blade curvature without any rotation. If the main flow receives an unbroken soil-strip or a strip composed of pieces connected with hinges, a process type will occur that does not involve any soil deformation when the soil beam follows the blade curve.

Output

The output process concerns the changes after the soil-strip leaves the blade. When the soil-strip is extended beyond the end of the blade, the cross section above the end is stressed more and more. At a certain length this extending part starts to break or shear off. When the failure surface is complete, a piece of soil is formed and falls down freely. Normally these pieces have other dimensions than those formed by the intake process and the main flow. The free fall ends in a collision in the furrow with previously formed pieces. At the same time the main flow produces the next piece and the process is repeated.

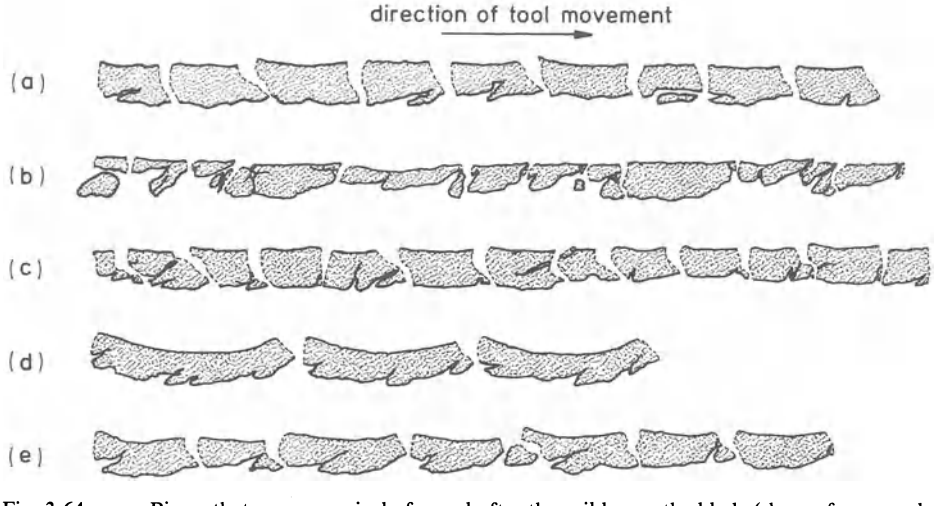

Fig. 3.64 a – e. Pieces that are successively formed after the soil leaves the blade (shown for several processes)

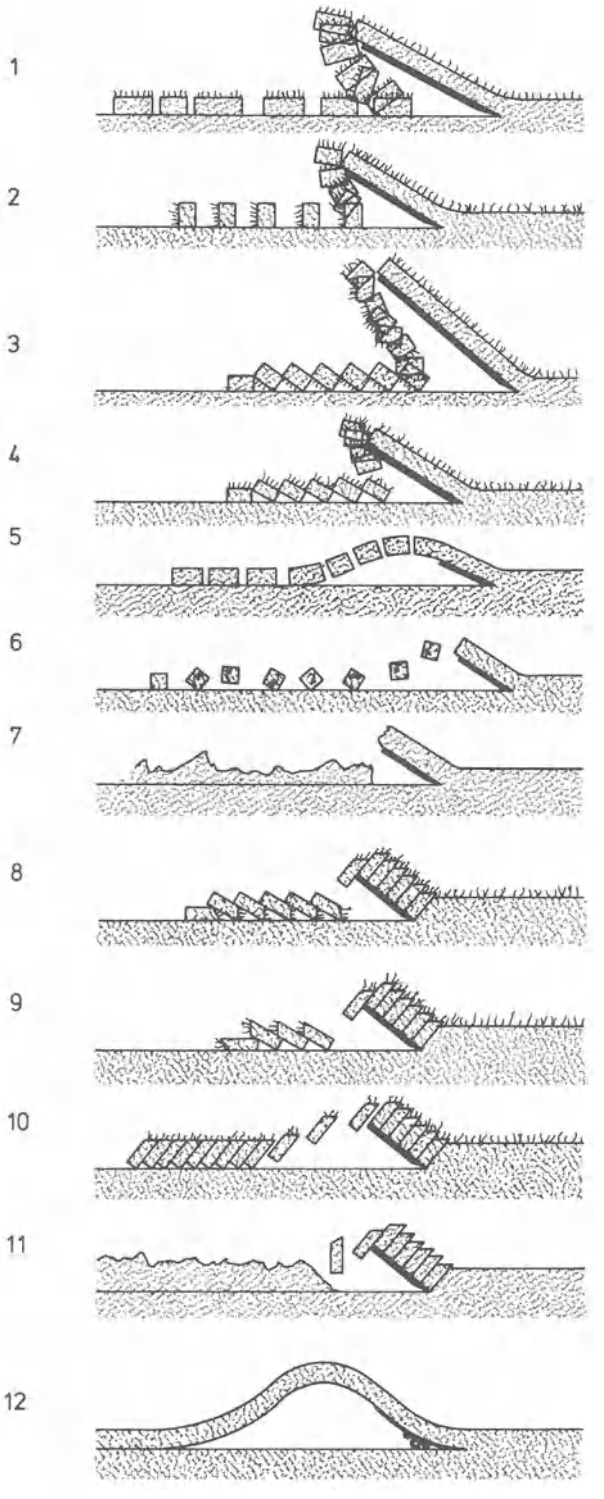

Fig. 3.65. Output processes

The length of the pieces formed in this breaking process depends on soil strenght and the degree of weakening by the intake process and the main flow. This is illustrated in Fig. 3.64 which shows the pieces that are successively formed by several processes after the soil leaves the blade. In this figure the cracks that are formed during input and main flow are indicated by solid lines, and the cracks that are formed after the soil leaves the blade are indicated by broken lines. In Fig. 3.64a the intake process produced a few cracks but they did not weaken the soil-strip to the extent of influencing the position of the output cracks. In contrast, in Fig. 3.64b intake and output are so closely related that output cracks nearly always coincide with input cracks. This is also the case in Fig. 3.64c. The relatively long output pieces in Fig. 3.64d are caused by high cohesion of this soil-strip. Nevertheless, output cracks have a certain preference for places where input cracks are present. In Fig. 3.64e there is a relationship between intake and output cracks at some places and not at others. Obviously, there is only a relationship if the intake crack is in a position favorable for breaking during the output.

A piece breaks off the strip by starting a rotation and, therefore, the piece has a certain angular speed when it starts falling. The value of the angular speed depends on the length of the piece, soil plasticity, and the position of the output-crack relative to the input-crack. The fall of the piece ends in a collision with the bottom of the furrow or with foregoing pieces. If cohesion is low, the soil may crumble at this collision. The series of fallen pieces shows a geometry that is determined by the shape of the falling pieces and by the angular speed obtained in the breaking process. Some types of this geometry are shown in Fig. 3.65. Cases 1, 2, 3, 4, 8, and 9 represent processes in which the velocities are very low. In cases 1 and 5 the soil-strip is compacted and deformed. At higher speeds cases as 5, 6, 10, and 12 (which is well-known in practice) can be observed. Low-strength soil may lead to 7 or 11. Note that the inversion in cases 3 and 8 is similar to that with moldboard plows.

3.7.2.2 Kinematic Aspects of Other Plow Bodies

Curved Two-Dimensional Blade with Small Cutting Angle and Large Working Depth/Blade Height Ratio

If the working depth of the blade discussed in Sect. 3.7.2.1 is increased to obtain a large working depth/blade height ratio (Fig. 3.66), some important changes result:

- the main flow becomes smaller in relation to the other process parts,
- the soil has to curve more during the intake,
- the ratio between height of fall in the output and working depth becomes smaller.

Such a blade (like all following plow bodies) is able to cause many of the phenomena discussed for the previous blade, but only observations by Nichols et al. (1958) are available, showing intake by shear-plane failure. The same authors investigated the importance of the shape of the cutting edge for the process, as

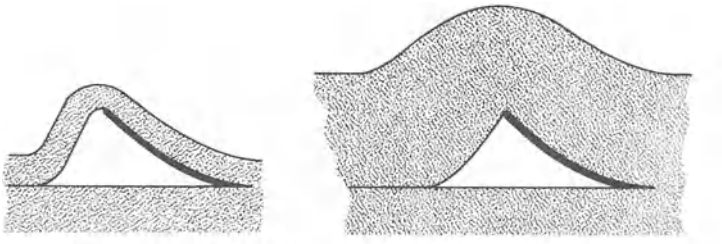

Fig. 3.66. Increase of working depth/blade height ratio

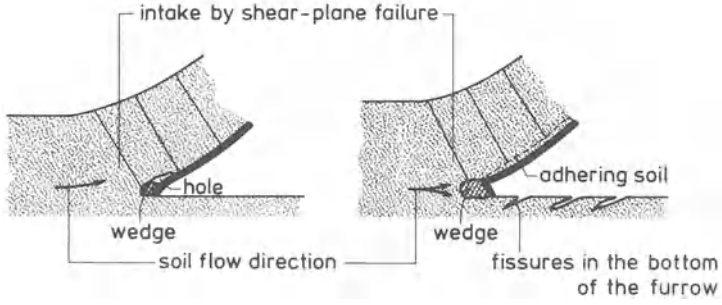

Fig. 3.67. Some cutting edge phenomena. (Nichols et al. 1958)

illustrated in Fig. 3.67. Of course, such cutting edge effects will not be restricted to this type of blade.

Plane Two-Dimensional Blade with Small Cutting Angle and Small Working Depth/Blade Height Ratio

Intake. The intake processes of this blade can be classified into the types defined previously:

- intake with open crack formation (Selig and Nelson 1964, Kawamura 1952, Drees 1956, Elijah and Weber 1968),
- intake by shear-plane failure (Söhne 1956, Drees 1956, Selig and Nelson 1964, Elijah and Weber 1968),
- intake by steady cutting (Söhne 1956, Drees 1956, Elijah and Weber 1968).

Main Flow. In soil moving over a plane blade, changes are minor. Nevertheless, some changes occur due to friction at the blade surface. Elijah and Weber (1968) measured stresses at the soil-blade interface, and found the locations of stress to move along the tool. Stresses sometimes disappeared suddenly, probably due to rotation or pulverization of the soil. Quite often the highest stresses were not measured at the bottom of the tool. A stress transducer gave a zero signal for 20% – 80% of the time, the percentage being strongly dependent on soil type, and tending to increase with soil strength.

Output. For the output the reader is referred to Sect. 3.7.2.1.

Plane Two-Dimensional Blade with Small Cutting Angle and Large Working Depth/Blade Height Ratio

If a plane blade with small cutting angle is changed from a small to a large working depth/blade height ratio, then

- the main flow becomes smaller in relation in the other process parts, and
- the height of fall/working depth ratio is decreased.

Diminishing the importance of the main flow influences the intake. Selig and Nelson (1964) presented the development of the process pattern in time from the very start for a plane blade with small working depth/blade height ratio. It appeared that at the start, where a main flow had not yet developed, the process shape differed from that occurring after some decimeters of tool travel, where a main flow and an output were present.

All intake processes described in the literature for plane two-dimensional blades with small cutting angles and large working depth/blade height ratios can be divided into:

- intake with open crack formation (Kawamura 1952),
- intake by shear-plane failure (Söhne 1956, Siemens et al. 1965, Olson and Weber 1966),
- intake by steady cutting (Söhne 1956, Olson and Weber 1966).

Blade with Finite Width

For a plane blade with a small cutting angle and a large working depth/blade height ratio, that has a side running through an open furrow, the intake will follow the pattern indicated in Fig. 3.68 (Söhne 1956), when the intake is assumed to be of the shear-plane failure type. There are additional cracks, being more or less parallel to the furrow.

Blades with Small Cutting Angles Versus Blades with Large Cutting Angles

The characteristics of the plow processes of blades with large cutting angles are rather similar to those of blades with small cutting angles, but there are also many differences, such as:

- intake by open crack formation is not likely to occur when the cutting angle is large,
- during the intake of a blade with a large cutting angle, a soil wedge tends to form which can be considered as part of the blade,
- the outputs of blades with large cutting angles are not always directed backwards, but can occur in a forward direction.

Curved Two-Dimensional Blade with Large Cutting Angle and Small Working Depth/Blade Height Ratio

Intake. Drees (1956) reports two types of intake, namely intake by shear-plane failure and intake by steady cutting. Sometimes the intake is accompanied by

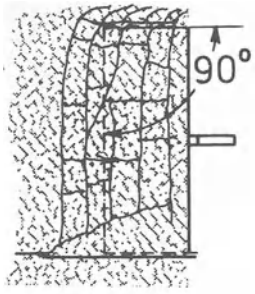

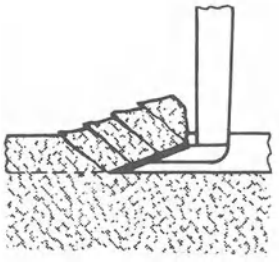

Fig. 3.68. Additional cracks due to one side of the blade traveling through a furrow. (Söhne 1956)

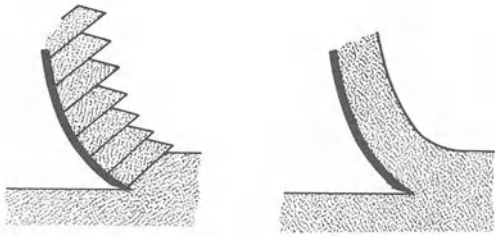

Fig. 3.69. Types of main flow at large cutting angles and backward directed output

cracks that start from the cutting edge and travel at an acute angle downward from the forward horizontal. These cracks can later be found in the bottom of the furrow.

Main Flow. Depending on the type of intake, one of the two types of "main flow" presented in Fig. 3.69, will occur. Especially in the case of this blade it is useful to realize that the length of the main flow cannot exceed a certain limit. Several reasons for this can be indicated. An obvious one is if the soil reaches the blade end. Then there is output as defined for the blades already discussed. Another cause involves a main flow that curls up, giving rise to a curled up soil beam in front of the main flow. Blade curvature can favor this action (Drees 1956). See Fig. 3.70a. A third cause is represented in Fig. 3.70b. The soil is bent forward so far that it fails or rolls, and falls forward and downward (Drees 1956). Figure 3.70c demonstrates a last cause. Here, the length of the main flow is limited as shear stress in the first part of the main flow reaches the soil shear strength. The shaded part of the soil is loaded by a stress p that originates from the blade-soil friction force W and the weight G of the soil which is on top of the shaded part. With the increase in main flow length the forces W and G increase, and so does p. If p becomes large enough to make the soil in the shaded part fail, a failure plane develops that nearly follows the broken line in the shaded area. The column above the broken line slides forward and downwards, which can be

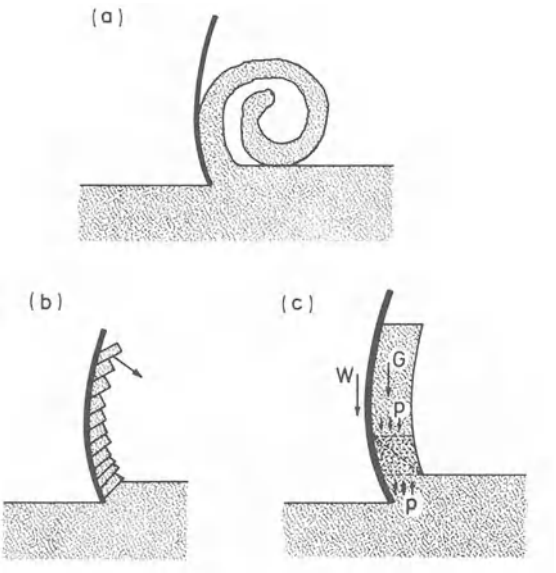

Fig. 3.70a – c. Cases where the main flow length is limited

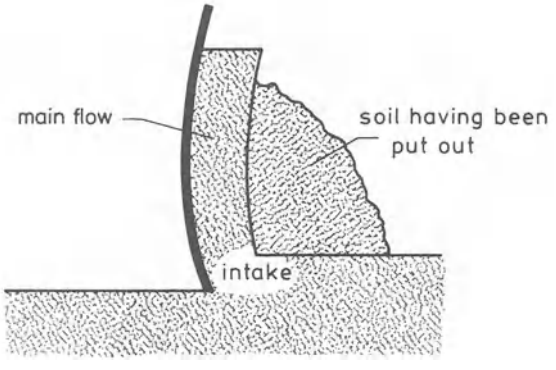

Fig. 3.71. Permanent influence of soil having been put out

considered to be the output process. The process is repeated periodically, piling up an increasing amount of soil in front of the main flow. It should be noted that soil strength involved in such cases is often very low because of soil heterogeneity and the soil weakening that has occurred during the intake.

Output. If there is an output directed backwards, then it will very much resemble that which is defined for the previous blades. In the case of forward output, soil will fall in front of the blade on top of the still firm soil (see Fig. 3.71), which has two significant consequences. Firstly, the weight of the soil having been put out rests on the intake zone, and this additional load influences the shape of the intake process. Secondly, the main flow has to push forward the fallen soil like a dozer blade, which gives rise to a mutual influence between the main flow and the soil that has been put out.

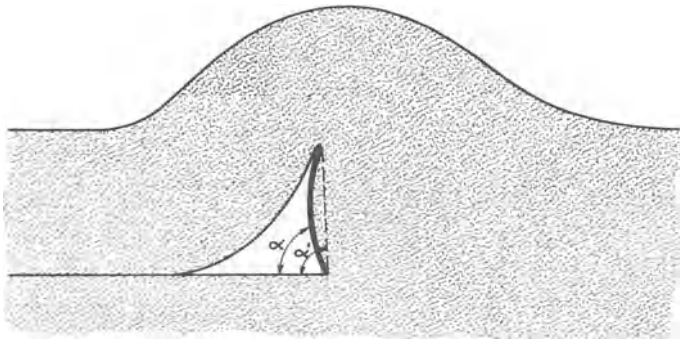

Fig. 3.72. A curved blade being filled up

Curved Two-Dimensional Blade with Large Cutting Angle and Large Working Depth/Blade Height Ratio

If for the blade discussed in the preceding section the working depth/blade height ratio is altered to a large value, then the following changes will occur:

- the main flow becomes much smaller,
- the soil must curve more at intake,
- although some soil may fall forward, output is always directed backwards, because in this case the main flow can hardly exert any pushing action.

According to observations by Osman (1964) there are two types of intake:

- intake by shear-plane failure,
- intake by steady cutting.

At large blade curvatures the blade may be filled up with immobile soil that should be considered part of the blade (Fig. 3.72). In that case the blade acts like a plane blade with a cutting angle equal to α' and a soil-tool friction angle equal to the angle of internal soil friction.

Plane Two-Dimensional Blade with Large Cutting Angle and Small Working Depth/Blade Height Ratio

Sometimes a wedge tends to be formed, as shown by Selig and Nelson (1964). Two types of intake can be distinguished:

- intake by shear-plane failure (Payne 1956, Selig and Nelson 1964, O'Callaghan and Farrelly 1964),
- intake by steady cutting (the next section provides evidence for this possibility).

Large cracks that travel forwards and downwards at an acute angle with the horizontal may develop from the cutting edge (Selig and Nelson 1964).

Plane Two-Dimensional Blade with Large Cutting Angle and Large Working Depth/Blade Height Ratio

Siemens et al. (1965) reported a tendency for wedges to be formed. Two types of intake appear to be possible:

- intake by shear-plane failure (Osman 1964, Siemens et al. 1965, Olson and Weber 1966),
- intake by steady cutting (Osman 1964, Olson and Weber 1966).

More Complicated Plow Bodies

Plow bodies used in practice often have a more complicated shape than the two-dimensional blades already discussed. Only a few investigations have been conducted into the process patterns of these more complicated plow bodies. It can be seen easily that many of the phenomena defined for blades will also occur with the more complicated plow bodies such as the moldboard plow, blade of rotary tiller, sweep, lifting blade of potato harvester, etc. Indeed, a good observer of tillage processes will often see phenomena such as tongues in the bottom or wall of a furrow, holes in a furrow bottom, and a strong regularity in the soil beam left by a moldboard plow.

Chase (1942) made observations from sweeps that show the possibility of the main flow length being smaller than the tool length. He reports: "If the blade is flat, it will slip through the soil disturbing it or the vegetation very little, but if the angle of the blade to the horizontal is too great, so much resistance to the movement of the earth over the blade is set up that the soil and trash jam together and cause not only a mixing of the mass but an uneven distribution on the fixed soil, and entirely too often a complete clogging of the gang of tillers". The same paper reports the following on the significance of the cutting edge, which normally has a bevel side at the bottom: "Sweeps were also tried with the bevel side up and the same pitch for the body of the blade. We found this gave better penetration in hard ground, but also introduced a scouring problem in many fields and especially when the ground had to be tilled the second time after the first. Just at the rear of the break between the bend and the body of the blade is an area of reduced pressure, and unless the soil is in a very dry condition, it will adhere at this point and eventually cause choking".

The main flow has a limited length, as indicated by the choking of the lifting blades of potato harvesters (Hawkins 1957).

For subsoilers, Nichols and Reaves (1958) reported wedge formation and indications for the possibility of shear-plane failure and steady cutting.

Nichols and Reed (1934) define the process of moldboard plowing under "normal conditions" as follows. Near the plow share shear planes develop, which separate soil blocks. These planes are called primary shear planes. As these blocks are traveling over the moldboard, failure planes (called secondary shear planes) develop perpendicular to the primary planes. The formation of primary shear planes described in this paper should be considered as intake by shear-plane failure and the formation of secondary shear planes as a phenomenon belonging to the main flow.

Finally, it is noted that moldboard shape classifications can be found in Söhne and Möller (1962), Hénin et al. (1969), and Dalleinne and Billot (1975).

3.7.2.3 Dynamic Aspects

The presented kinematics of plow bodies indicate that many dynamic aspects can be expected. Many will correspond to aspects mentioned in previous sections, for instance, the tine section. Here only a few comments will be made.

Intake. To understand the different types of intake, it is convenient to consider open crack formation as normal. Open crack formation is a splitting process involving cracks that extend due to tensile failure at the running crack tip. How large a distance the crack front can be ahead of the blade tip, and the direction of cracking, depend on the forces and moments exerted by the main flow on the intake, the working depth, the traveling speed, and the soil mechanical properties. Intake by steady cutting can be considered a special case of open crack formation in which the distance between crack front and blade tip is always near zero. Intake by shear-plane failure occurs at relatively low cohesion values; before significant splitting occurs, the soil fails through the formation of an upward shear-plane.

Main Flow. In comparison with the intake and output, the main flow is usually simple. Changes in the soil are mostly minor. Energy is consumed to increase the soil potential energy (to lift the soil to a higher level), and to overcome soil-tool, and often also soil-soil, friction.

Output. Important aspects of the output are:

- the forces and moments that it exerts on the main flow,
- its influence on the soil configuration left by the process,
- consumption of energy obtained from the main flow in the form of potential energy, kinetic energy, and flow work (Shames 1962).

The amount of flow work that is supplied per second equals the vector product $K\,V$, where K is the (vectorial) force exerted by the main flow on the output, and V is the (vectorial) soil velocity at the main flow end. When the output is hindered the flow work may be significant and may increase tool draft.

The form of the output can differ widely, and this is most striking at low forward velocities and small linear dimensions. At higher speeds and larger linear dimensions the inertia forces prevail in the process, and the output varies less with varying circumstances. The soil received by the output may be classified into six classes, characterized by:

- the main flow delivers a rigid, coherent flow without any cracks,
- the main flow delivers a rigid soil beam, with cracks only in a thin lower part,
- the delivered soil beam exhibits cracks extending far into the beam from the bottom,
- the main flow delivers short pieces, separated by parallel failure planes,

- the main flow only delivers chunks and crumbs,
- the delivered soil beam is able to deform strongly before a crack develops.

Each of these classes give rise to a specific *type of output.* The output process of a soil piece may be separated into a number of *stages*:

- the start of breaking as a soil beam extends far enough behind the blade,
- the breaking period,
- the free fall of the piece,
- joining the earlier pieces (landing).

On the basis of these output types and stages, Koolen (1977) was able to explain how and when the configurations in Fig. 3.65 occur. Many of the statements made in that explanation have not been verified by experiments. This is also not very urgent, in view of the current character of soil tillage in practice. Verification and quantification will be necessary to develop tools which are intended to work in specific soil conditions, based on full control of the soil movements during the tillage process. The possibility of designing such tools has been shown already clearly.

3.7.3 Applications

3.7.3.1 Plowing Draft as Affected by Soil Moisture Content

The total draft K of a drawn plow may be predicted using a method that has the following domain:

- all current types of drawn moldboard plows,
- "normal" plowing speed,
- one piece of land.

The independent variables are:

- soil moisture content in percentage of weight (m),
- plowing width (b),
- plowing depth (d).

A general formula for K is assumed to be:

$$\frac{K}{b\,d} = k_1 - k_2 m + k_3 m^2$$

where k_1, k_2, and k_3 are positive constants. This is the formula of a parabola with its vertex being a minimum value. The soil moisture content at this minimum is called optimum moisture content. Constants k_1, k_2, and k_3 must be determined empirically by measuring plow drafts on the piece of land in question at different moisture contents (Bakhtin et al. 1968, Ometto 1970, Florescu and Canarache 1973).

The assumption of a parabolic relationship having a minimum value quite often appears not to be valid. In some cases the relationship between K and m involves a parabola with a maximum value (Bakhtin et al. 1968). Also the rela-

tionship may be a decreasing function in the range of moisture contents that are relevant in practice (Ometto 1970). This was confirmed by Canarache (personal communication) who found that on many occasions the soil had to be moistened artificially to obtain measurements in the rising part of the parabola. The function is not unique, because plowing resistance is also affected by moldboard shape, plowing speed, soil bulk density, and soil structure, which are all allowed to vary within the domain (Poesse and Van Ouwerkerk 1967).

3.7.3.2 Plowing Draft as Affected by Speed

The draft K of a moldboard plow may be predicted by the method known as Gorjatchkin's formula, which was published in 1898 in Gorjatchkin's book "Uber Streichbleche" (Vornkahl 1967). The domain is very limited, namely:

- one moldboard type,
- one piece of land in a particular condition.

The characteristics are:

- working width (b) of the plow body,
- working depth (d) of the plow body,
- plowing speed (v).

Probably on the basis of his knowledge of fluid mechanics, Gorjatchkin stated the following general formula:

$$\frac{K}{b\,d} = z + \varepsilon v^2$$

where z and ε are constants which must be determined from K-measurements for different values of b, d, and v. The method has been adopted by many investigators (Söhne 1960, Söhne and Möller 1962, Poesse and Van Ouwerkerk 1967, Bernacki 1963, Zoz 1974).

Sometimes the accuracy of the formula leaves much to be desired. This would be true especially for heavier soils (Poesse and Van Ouwerkerk 1967). An additional constant x may be used to increase the accuracy:

$$\frac{K}{b\,d} = z + \varepsilon v^x$$

where the constants z, ε, and x must be determined experimentally (Telischi et al. 1956). Some investigators tried to enlarge the domain by using

$$\frac{K}{b\,d} = z + c(1 - \cos\phi)\,v^2$$

where z and c are constants. It would apply to any series of moldboard plows that differ only in side angle ϕ at the trailing edge of the moldboards. According to Söhne (1960) and Bernacki (1963) this seems to be true, but Poesse and Van Ouwerkerk (1967) did not observe any relationship between K and ϕ. Vornkahl (1967) also applied Gorjatchkin's formula to tines.

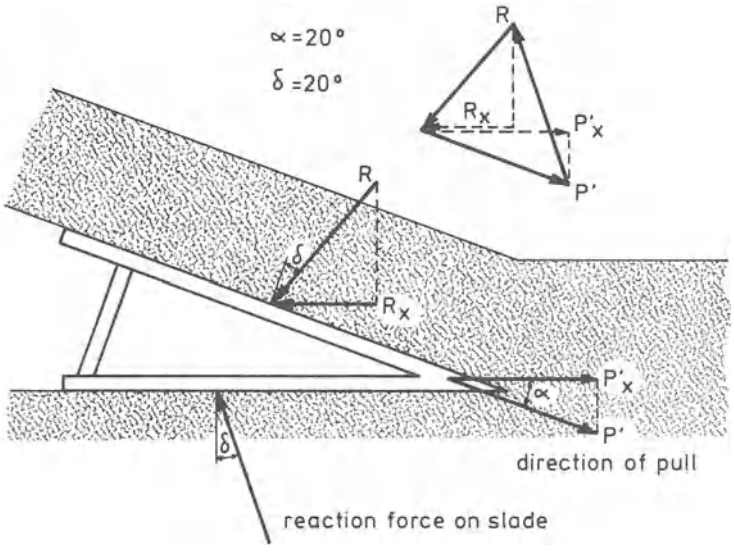

Fig. 3.73. R_x is horizontal component of soil resistance. P'_x is horizontal component of pull. $P'_x > R_x$ due to the influence of slade and direction of pull on tool draft

3.7.3.3 Draft Force as Affected by Slades, Supporting Wheels, and Inclined Directions of Pull

The vertical component of the reaction force that the soil exerts on a plow body is often balanced by a slade or supporting wheel. In addition, the direction of pull is often not the same as the traveling direction. These circumstances occur with the plane two-dimensional blade in Fig. 3.73, where the direction of pull is parallel to the blade surface. Soil above and in front of the blade exerts a force R on the blade. R is inclined to the blade normal by the soil-metal frictional angle δ. The pull force is P', its horizontal component is P'_x. From the system of forces it follows that, if $\alpha = 20°$ and $\delta = 20°$,

$$P'_x = 1.65\, R_x.$$

This implies that the slade and the inclination of the direction of pull increase z and ε in Gorjatchkin's formula (Sect. 3.7.3.2) by as much as 65%, when P'_x is considered instead of R_x.

3.7.3.4 Predicting Type of Intake from Unconfined Compression Tests

For a particular two-dimensional curved blade (shaped as in Fig. 3.59, 7.5 cm high, and 18 cm long), operating at a depth of 3 cm and traveling at a speed of 32 cm/sec, the types of intake in different soils could be predicted from the results of unconfined compression tests (Koolen 1977). Intake by steady cutting occurred in soils failing in unconfined compression at strains larger than 0.185. Intake by shear-plane failure occurred when the two conditions, unconfined

compressive strength <0.075 bar and failure strain in unconfined compression <0.03, both were satisfied. For the remaining soil conditions intake by open crack formation occurred.

Generalizing these findings, it may be stated that for any particular body, operating at a particular depth and a particular speed, the type of intake can be predicted from unconfined compression tests, whenever the appropriate correlations have been established through experiments.

Appendix Mathematical Treatment of Finite Homogeneous Strains in Two Dimensions

Finite Strain and Rotation. Although the description of large deformations of a body is rather complicated the principles may be demonstrated by considering a plane rather than a volume. This is equivalent to assuming that the body is not deformed along one direction and we speak of a two-dimensional or plane strain. To describe deformations and displacements of a body, a grid of squares is fitted to the undeformed body, perpendicular to the direction that will be kept free from strain. After deformation all these squares will be deformed. If these squares become parallelograms (which usually occurs when these rectangles are small in comparison to the deforming body), it is said that there was a *homogeneous strain* in the neighborhood of each square. This is normally intended in experiments in which a grid of squares is fixed to a soil surface. While the squares should be kept relatively small, it must be realized that the smaller the squares, the less accurate the measurements on such squares will be. Any homogeneous strain of a square can be treated as a combination of three reactions: a volume change by equal elongation or shortening in all directions, a deformation without volume change by a combination of elongation and shortening in perpendicular directions, and a rotation of the deformed square. This can be proved with the aid of the strain ellipsoid (Nadai 1950). If desired, the first and second reactions can be considered as one. We will use the following definitions.

Treatment is the final result of deformation and displacement.
Volume change = change in length equal in all directions.
Distortion = deformation without volume change.
Deformation = volume change + distortion.
Rotation = angular displacement of the element.

With the aid of a numerical example we will show how a square in a given position can be changed into a parallelogram in a certain position through volume change, distortion and rotation (Fig. A.1a). The treatment can be seen as three steps:

- a relative shortening of 0.2 in all directions, which is a volume change (Fig. A.1b),
- a relative elongation of 0.667 along an axis at an angle of 27°10′ to the horizontal and a relative shortening of 0.4 along an axis perpendicular to the former. See Fig. A.1c (for instance, $a'b' = ab\ (1 - 0.4)$ and $ob' = ob\ (1 + 0.667)$). This is distortion because a square with unit area will become a parallelogram with an area of $(1 + 0.667) \cdot (1 - 0.4) = 1$,
- a rotation of −16°25′ (Fig. A.1d).

If we consider volume change and distortion as one step, called deformation, Fig. A.1e applies. This represents a relative elongation of 0.34 along an axis at

27°10′ to the horizontal and a relative shortening of 0.515 along an axis perpendicular to the former. In this case a square of unit area will become a parallelogram with an area of $(1 + 0.34) \cdot (1 - 0.515) = 0.6499$.

Mathematically, the treatment in Fig. A.1a is a linear transformation, and the different steps in Figs. A.1b to e are also linear transformations. A vector $\boldsymbol{x}$ on the original body is transformed by the treatment into vector $\boldsymbol{x}'$ through an operation B, or $\boldsymbol{x}' = B\boldsymbol{x}$. Written in full,

$$x_1' = ax_1 + bx_2$$
$$x_2' = cx_1 + dx_2 .$$

Or in matrix notation,

$$\begin{pmatrix} x_1' \\ x_2' \end{pmatrix} = \begin{pmatrix} a & b \\ c & d \end{pmatrix} \begin{pmatrix} x_1 \\ x_2 \end{pmatrix} .$$

Or $X' = BX$ with

$$B = \begin{pmatrix} a & b \\ c & d \end{pmatrix} \qquad X' = \begin{pmatrix} x_1' \\ x_2' \end{pmatrix} \qquad X = \begin{pmatrix} x_1 \\ x_2 \end{pmatrix} .$$

For Fig. A.1a matrix B is found as follows. Point (15, 0) is transformed into (18, 0) and point (0, 15) into (8, 8).

$$(15, 0) \rightarrow (18, 0) \text{ means: } (1, 0) \rightarrow \left(\frac{18}{15}, 0\right) = (1.2, 0)$$

$$(0, 15) \rightarrow (8, 8) \text{ means: } (0, 1) \rightarrow \left(\frac{8}{15}, \frac{8}{15}\right) = (0.533, 0.533) .$$

Substitution of $(1, 0) \rightarrow (1.2, 0)$ in

$$x_1' = ax_1 + bx_2$$
$$x_2' = cx_1 + dx_2$$

gives,

$$1.2 = a \cdot 1 + b \cdot 0 \qquad \text{Hence } a = 1.2$$
$$0 = c \cdot 1 + d \cdot 0 \qquad \text{Hence } c = 0 .$$

Substitution of $(0.1) \rightarrow (0.533, 0.533)$ yields

$$0.533 = a \cdot 0 + b \cdot 1 \qquad \text{Hence } b = 0.533$$
$$0.533 = c \cdot 0 + d \cdot 1 \qquad \text{Hence } d = 0.533$$

therefore,

$$B = \begin{pmatrix} a & b \\ c & d \end{pmatrix} = \begin{pmatrix} 1.2 & 0.533 \\ 0 & 0.533 \end{pmatrix} .$$

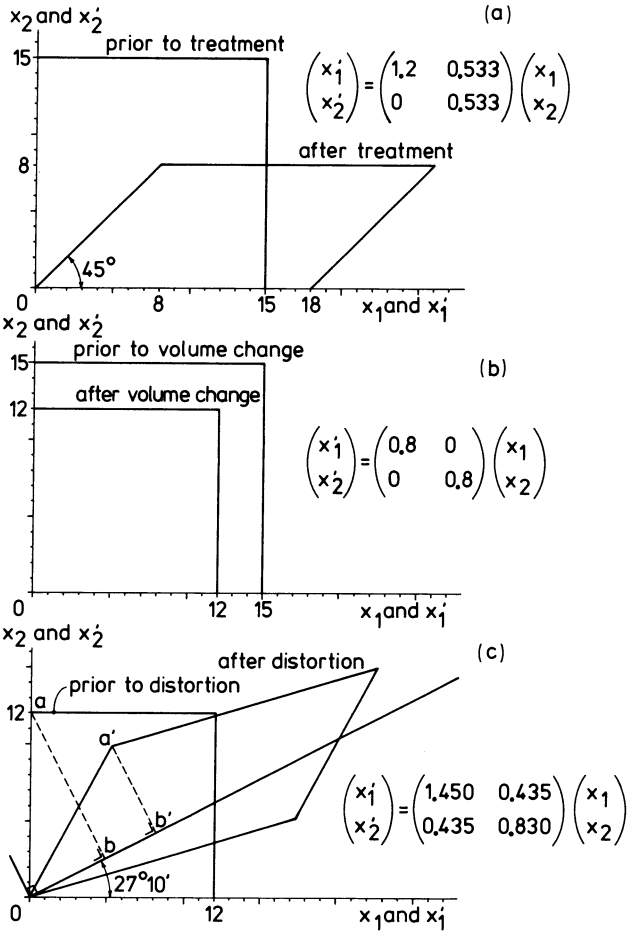

Similarly, the transformation matrices can be found for the other steps. The final result is

$$\text{Matrix of the overall treatment } B = \begin{pmatrix} 1.2 & 0.533 \\ 0 & 0.533 \end{pmatrix}.$$

$$\text{Matrix of volume change} \qquad C = \begin{pmatrix} 0.8 & 0 \\ 0 & 0.8 \end{pmatrix}.$$

$$\text{Matrix of distortion} \qquad Z = \begin{pmatrix} 1.450 & 0.435 \\ 0.435 & 0.830 \end{pmatrix}.$$

$$\text{Matrix of rotation} \qquad R = \begin{pmatrix} 0.9592 & 0.2826 \\ 0.2826 & 0.9592 \end{pmatrix}.$$

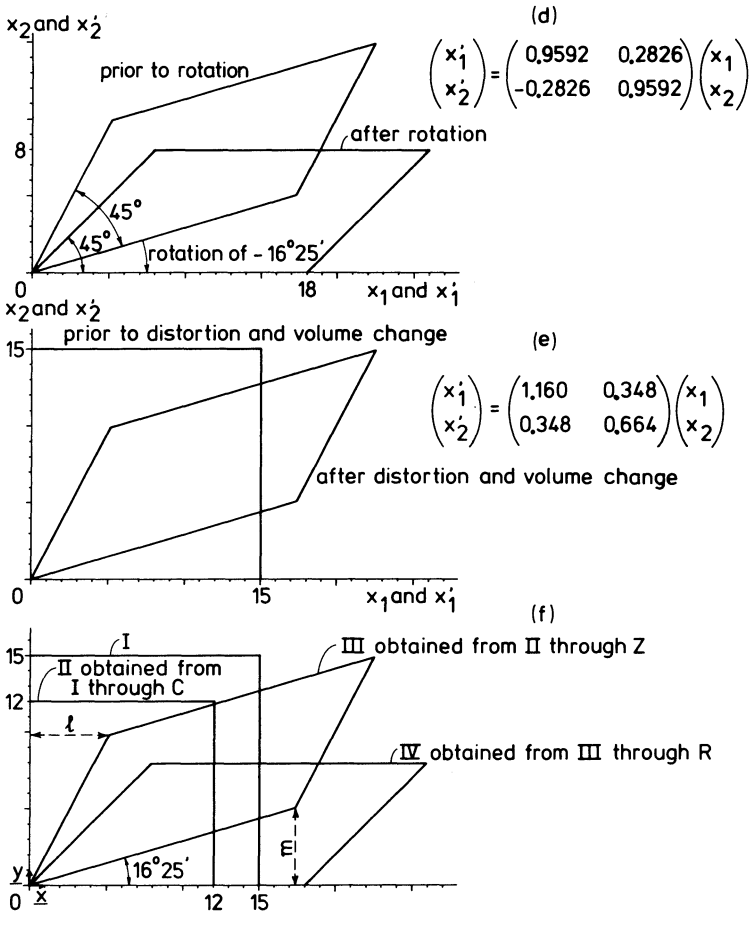

Fig. A.1 a – f. Treatment (a) may be separated into volume change (b), distortion (c) and rotation (d), or into deformation (e), and rotation (d). (f) Refers to the construction of quadrangles II and III when I and IV are known

$$\text{Matrix of deformation} \quad V = \begin{pmatrix} 1.160 & 0.348 \\ 0.348 & 0.664 \end{pmatrix}.$$

Matrix C is isotropic. Matrix R is orthogonal. Also, $B = RZC$ (but $B \neq ZCR$) and $V = ZC = CZ$ and therefore, $B = RV$ (but $B \neq VR$). An important fact is that matrices V and Z are symmetrical. This can easily be understood if we let the coordinate directions coincide with the directions of elongation and/or shortening, as in Fig. A.2, and note that a symmetrical matrix will not loose its symmetry on transformation.

Application of Theory. In experiments the initial state of a grid mesh (square) is frequently compared with its final state (a rotated parallelogram) in order to

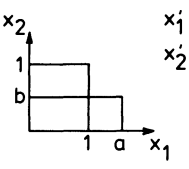

Fig. A.2. Demonstration of the symmetry of the deformation matrix

derive the matrices of volume change, distortion and rotation for that mesh. In the case of the numerical example (Fig. A.1f), this means that states II and III with the appropriate transformation matrices, and the matrix of rotation, must be derived from states I and IV. This can be done in the following way. We measure the area of IV, which appears to be 0.64 times the area of I. Since area IV = area II, it follows that area II = $0.64 \cdot$ area I. This means that the side length of square II must be 0.8 times the side length of square I. So we can draw square II and calculate maxtrix C. We can determine the rotation, starting from IV and using the fact that for 2 vectors y and x and the symmetrical matrix Z, $(Zy, x) = (Zx, y)$. If we choose $y = (0, 1)$ and $x = (1, 0)$, this means in Fig. A.1f that $l = m$. Therefore, to find III we have to rotate parallelogram IV until $l = m$, and measure the rotation. We find an angle of $-16°25'$, and from this we can find matrix R (clockwise rotation is negative by convention). Now it is possible to calculate matrix Z from II and III. Unknown are still the principal strain directions (principal strain is defined in Sect. 2.1). These directions can be calculated from Z, using the fact that a vector pointing in a principal direction at the start of distortion keeps coinciding with that principal direction during the distortion. Mathematically, this means that vectors in principal directions are eigenvectors, corresponding to the eigenvalues of Z. Those eigenvalues can be calculated. We find 1.67 and 0.61. The eigenvalue 1.67 corresponds with the eigenvector $\beta(1, 0.5076)$, where β is any constant, not zero. This vector (and therefore this principal strain direction) has an inclination of arctan (0.5076) = 26°55′ with the horizontal, which is in good agreement with the value given before (27°10′). The other principal strain direction is perpendicular to the one calculated here. The eigenvalues are equal to (1 + relative elongation) = (1 + 0.667) and (1 − relative shortening) = (1 − 0.4). The eigenvalues indicate by what factor lengths in principal directions are multiplied due to the distortion. Hence, eigenvalues give principal strains and eigenvectors principal directions. V of the numerical example and the corresponding elongation, shortening and principal directions can be determined using the same procedure as for Z.

Infinitely Small Strain and Rotation. The preceding discussion concerned finite strain and rotation. This means that the period between initial and final state may be so long, or that the grid geometry may be changed so much, that deformation and rotation may not be uniquely related to a current stress field. It is, therefore, also useful to consider deformation in an infinitely small time increment dt, rather than the overall deformation. The deformation in dt will then also be infinitely small.

The result of a treatment for a two-dimensional body can be described by the functions

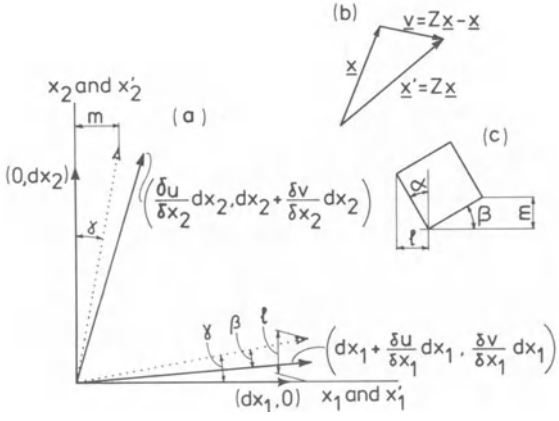

Fig. A.3. Diagram for infinitely small homogeneous strain

$$u(x_1, x_2)$$
$$v(x_1, x_2)$$

where $u(x_1, x_2)$ is the movement of a point (x_1, x_2) in the x_1-direction and $v(x_1, x_2)$ is the movement of this point in the x_2-direction. If deformations and displacements are infinitely small, then

$$\frac{\delta u}{\delta x_1}, \frac{\delta u}{\delta x_2}, \frac{\delta v}{\delta x_1}, \frac{\delta v}{\delta x_2}$$

are all much smaller than 1. The result of a treatment of a square with sides $(dx_1, 0)$ and $(0, dx_2)$ is shown in Fig. A.3a. The transformation of $(dx_1, 0)$ is

$$\left(dx_1 + \frac{\delta u}{\delta x_1} dx_1, \frac{\delta v}{\delta x_1} dx_1\right)$$

and the transformation of $(0, dx_2)$ is

$$\left(\frac{\delta u}{\delta x_2} dx_2, dx_2 + \frac{\delta v}{\delta x_2} dx_2\right).$$

To eliminate rotation we rotate in such a way that $m = l$ and we obtain the dotted vectors. Because

$$dx_1 = dx_2 \approx dx_1 + \frac{\delta u}{\delta x_1} dx_1 \approx dx_2 + \frac{\delta v}{\delta x_2} dx_2$$

the dotted vectors will be at equal angles to the coordinate axes. This angle will be denoted by Γ. Because this angle is infinitely small,

$$2\Gamma = \frac{\delta v}{\delta x_1} dx_1/dx_1 + \frac{\delta u}{\delta x_2} dx_2/dx_2$$

$$\text{or} \quad \Gamma = \frac{1}{2}\left(\frac{\delta v}{\delta x_1} + \frac{\delta u}{\delta x_2}\right).$$

The rotation is denoted by β and, obeying the sign convention,

$$\beta = -\left(\Gamma - \frac{\delta v}{\delta x_1}\right) = \frac{\delta v}{\delta x_1} - \frac{1}{2}\frac{\delta v}{\delta x_1} - \frac{1}{2}\frac{\delta u}{\delta x_2} = \frac{1}{2}\left(\frac{\delta v}{\delta x_1} - \frac{\delta u}{\delta x_2}\right).$$

The coordinates of the dotted vectors are, respectively:

$$\left(dx_1 + \frac{\delta u}{\delta x_1}\, dx_1,\ \Gamma dx_1\right) \quad \text{and}$$

$$\left(\Gamma dx_2,\ dx_2 + \frac{\delta v}{\delta x_2}\, dx_2\right).$$

A treatment without rotation (deformation) transforms

$$(dx_1, 0) \quad \text{into} \quad \left(dx_1 + \frac{\delta u}{\delta x_1}\, dx_1,\ \Gamma dx_1\right)$$

and

$$(0, dx_2) \quad \text{into} \quad \left(\Gamma dx_2,\ dx_2 + \frac{\delta v}{\delta x_2}\, dx_2\right).$$

The matrix of this transformation is found through substitution of these two transformations in

$$x_1' = ax_1 + bx_2$$
$$x_2' = cx_1 + dx_2$$

yielding

$$dx_1 + \frac{\delta u}{\delta x_1}\, dx_1 = a\, dx_1 + 0\,, \quad \text{hence,} \quad a = 1 + \frac{\delta u}{\delta x_1}$$

$$\Gamma dx_1 = c\, dx_1 + 0\,, \quad \text{hence,} \quad c = \Gamma$$

$$\Gamma dx_2 = 0 + b\, dx_2\,, \quad \text{hence,} \quad b = \Gamma$$

$$dx_2 + \frac{\delta v}{\delta x_2}\, dx_2 = 0 + d\, dx_2\,, \quad \text{hence,} \quad d = 1 + \frac{\delta v}{\delta x_2}.$$

The matrix of deformation is, therefore,

$$Z = \begin{pmatrix} 1 + \dfrac{\delta u}{\delta x_1} & \Gamma \\ \Gamma & 1 + \dfrac{\delta v}{\delta x_2} \end{pmatrix}$$

$$\text{or because} \quad \Gamma = \frac{1}{2}\left(\frac{\delta v}{\delta x_1} + \frac{\delta u}{\delta x_2}\right),$$

$$Z = \begin{bmatrix} 1 + \dfrac{\delta u}{\delta x_1} & \dfrac{1}{2}\left(\dfrac{\delta v}{\delta x_1} + \dfrac{\delta u}{\delta x_2}\right) \\ \dfrac{1}{2}\left(\dfrac{\delta v}{\delta x_1} + \dfrac{\delta u}{\delta x_2}\right) & 1 + \dfrac{\delta v}{\delta x_2} \end{bmatrix}$$

$$= \begin{bmatrix} 1 & 0 \\ 0 & 1 \end{bmatrix} + \begin{bmatrix} \dfrac{\delta u}{\delta x_1} & \dfrac{1}{2}\left(\dfrac{\delta v}{\delta x_1} + \dfrac{\delta u}{\delta x_2}\right) \\ \dfrac{1}{2}\left(\dfrac{\delta v}{\delta x_1} + \dfrac{\delta u}{\delta x_2}\right) & \dfrac{\delta v}{\delta x_2} \end{bmatrix}.$$

Hence, an infinitely small deformation of a vector $\boldsymbol{x}$ can be represented by the linear transformation

$$x' = Zx = (Z_1 + Z_2)x = Z_1x + Z_2x$$

where Z_1 and Z_2 are the two components of Z given above. This is pictured in Fig. A.3b. Because Z_1 is the identity transformation $Z_1x = x$, $v = Zx - Z_1x = Z_2x$. Thus, the transformation Z_2 of a vector x is the vector that should be added to vector x to obtain vector x'. For a given Z_2 the length of v is proportional to the length of x. By considering x to be a unit vector, it is easily understood that the eigenvalues of Z_2 are equal to the normal strains in the directions where v has the same direction as x. Therefore, eigenvalues of Z_2 are principal strains, eigenvectors of Z_2 are principal directions. To relate this matrix to the state of stress, no rotation is needed because the rotation is so small that its influence on the position of the stress reference planes is negligible. Note that Z_2 is the matrix of the strain tensor presented in Sect. 2.1.

Finite, Small Strain. What was derived for infinitely small strain is a reasonable approximation for finite, very small strain. If we measure in such a case

$$\frac{\delta u}{\delta x_1}, \frac{\delta v}{\delta x_2}, \frac{\delta v}{\delta x_1}, \frac{\delta u}{\delta x_2},$$

we may substitute these values in

$$\begin{bmatrix} \dfrac{\delta u}{\delta x_1} & \dfrac{1}{2}\left(\dfrac{\delta v}{\delta x_1} + \dfrac{\delta u}{\delta x_2}\right) \\ \dfrac{1}{2}\left(\dfrac{\delta v}{\delta x_1} + \dfrac{\delta u}{\delta x_2}\right) & \dfrac{\delta v}{\delta x_2} \end{bmatrix}$$

and calculate the principal strains and principal directions. Generally, rotation is so small that the principal directions before and after rotation are approximately the same. In integral problems rotation may be relatively large and deformation small. Then rotation should be taken into account. This is easy because in this case $l = m$, if $\alpha = \beta =$ rotation (see Fig. A.3c).

References

Allison LE (1956) Soil and Plant responses to VAMA and HPAN soil conditioners in the presence of high exchangeable sodium. Soil Sci Soc Am Proc 20:147 – 151

Arndt W (1965) The impedance of soil seals and the forces of emerging seedlings. Aust J Soil Res 3:55 – 68

Atkinson JH, Bransby PL (1977) The mechanics of soils. An introduction to critical state soil mechanics. McGraw-Hill, London

Baganz K (1963/64) Spannungs- und Verdichtungsmessungen im Boden bei verschiedenen Fahrgeschwindigkeiten. Arch Landtechnik 4(1):35 – 45

Baganz K, Kunath L (1963) Einige Spannungs- und Verdichtungsmessungen unter Schlepperlaufwerken. Agrartechnik 13:180 – 182

Bailey AC, VandenBerg GE (1968) Yielding by compaction and shear in unsaturated soil. Trans ASAE 11:307 – 311, 317

Bailey AC, Weber JA (1965) Comparison of methods of measuring soil shear strength using artificial soils. Trans ASAE 8:153 – 156, 160

Bakhtin PU, Kirtbaya KYu, Nikolaeva, IN, Volotskaya, VI (1968) Resistance of soils in the USSR to deformation and ploughing. Trans 9th Int Congr Soil Sci 1:781 – 792

Basak P, Brahma SP (1974) Stress-strain response for sand. Soil Sci 118:358 – 364

Bekker MG (1956) Theory of land locomotion. Univ Michigan Press, Ann Arbor

Bekker MG (1960) Off-the-road locomotion. Univ Michigan Press, Ann Arbor

Bekker MG (1969) Introduction to terrain-vehicle systems. Univ Michigan Press, Ann Arbor

Bernacki H (1963) Ergebnisse der Untersuchung an Schnellpflugkörpern. Deutsche Agrartech 13:493 – 494

Bernacki H, Haman J (1973) Grundlagen der Bodenbearbeitung und Pflugbau. VEB Technik, Berlin

Bernstein R (1913) Probleme zur experimentellen Motorpflugmechanik. Der Motorwagen, vol 16

Bertilsson G (1971) Topsoil reaction to mechanical pressure. Swed J Agric Res 1:179 – 189

Blight DP (1970 – 71) A summary of published experiments with oscillating tines. J Inst Agric Eng 25(4):173 – 178, 180

Boekel P (1978) De werkbaarheid van de grond in het voorjaar in verband met de ontwatering en de samenstelling van de grond. Symp Werkbaarheid en Bedrijf Wageningen 1977, Imag rapport 1:14 – 23

Boels D, Davies DB, Johnston AE (1982) Soil degradation. Balkema, Rotterdam

Boguslawski E von, Lenz KO (1958) Untersuchungen über mechanische Widerstandsmessungen mit einer Rammsonde auf Ackerböden. Z Acker Pflanzenb 106:245 – 256

Butterfield R, Andrawes KZ (1972a) An investigation of a plane strain continuous penetration problem. Geotechnique 22:597 – 617

Butterfield R, Andrawes KZ (1972b) On the angles of friction between sand and plane surfaces. J Terramech 8(4):15 – 23

Butterfield R, Andrawes KZ (1972c) A consistent analysis of a soil cutting problem. Proc 4th ISTVS conf. Vol 2, Stockholm 3 – 20

Camp CR, Lund ZF (1968) Effect of mechanical impedance on cotton root growth. Trans ASAE 11:188 – 190

Campbell DJ (1975) Liquid limit determination of arable topsoils using a drop-cone penetrometer. J Soil Sci 26:234 – 241

Chancellor WJ (1976) Compaction of soil by agricultural equipment. Univ Calif Div Agric Sci Bull 1881

Chancellor WJ, Korayem AY (1965) Mechanical energy balance for a volume element of soil during strain. Trans ASAE 8:426 – 430, 436

Chancellor WJ, Schmidt RH (1962) Soil deformation beneath surface loads. Trans ASAE 5:240 – 246, 249

Chase LW (1942) A study of subsurface tiller blades. Agric Engin 23:43 – 45, 50

Cho SW, Schwanghard H, Sybel H von (1969) The spacing effect of track shoes on loose soils. J Terramech 6(3):21 – 45

Coleman GE, Perumpral JV (1974) The finite element analysis of soil compaction. Trans ASAE 17:856 – 860

Cook PER, Reece AR (1966) Theory of bulldozer action in friable soil. 2nd Int Conf ISTVS, Quebec

Costes NC, Cohron GT, Moss DC (1971) Cone penetration resistance test – an approach to evaluating in-place strength and packing characteristics of lunar soils. Proc 2nd Lunar Science Conf, Vol 3:1973 – 1987, MIT Press

Dalleinne E, Billot JF (1975) Evolution des matériels classiques de travail du sol. Procédé's nouveaux de travail du sol, Tome 1. Bull Tech Inf 302 – 303:521 – 537

Dam JGC van, Hulshof JA (1967) De penetrometer als instrument voor het onderzoek naar de geschiktheid van de grond voor aspergeteelt. Med Dir Tuinb 30(5):186 – 190

Davis B, Eagle D, Finney B (1972) Soil management. Farming Press, Ipswich

Dexter AR, Tanner DW (1973) The response of unsaturated soils to isotropic stress. J Soil Sci 24:491 – 502

Dransfield P, Willatt ST, Willis AH (1964) Soil-to-implement reaction experienced with simple tines at various angles of attack. J Agric Eng Res 9:220 – 225

Drees G (1956) Untersuchungen über das Kräftespiel an Flachbagger-Schnittwerkzeugen im Mittelsand und schwach bindigem, sandigem Schluff unter besonderer Berücksichtigung der Planierschilde und ebenen Schürfkübelschneiden. Dissertation, TH Aachen

Drucker DC (1967) Introduction to mechanics of deformable solids. McGraw-Hill, New York

Dunlap WH, VandenBerg GE, Hendrick JG (1966) Comparison of soil shear values obtained with devices of different geometrical shapes. Trans ASAE 9:896 – 900

Dunlap WH, Weber JA (1971) Compaction of an unsaturated soil under a general state of stress. Trans ASAE 14:601 – 607

Dwyer MJ (1973) Relating tyre performance to soil mechanical properties. Silsoe, NIAE 7

Dwyer MJ, Comely DR, Evernden DW (1974) Handbook of agricultural tyre performance. Silsoe, NIAE

Dwyer MJ, McAllister M, Evernden DW (1977) Comparison of the tractive performance of a tractor driving wheel during its first and second passes in the same track. J Terramech 14(1):1 – 10

El-Domiaty AM, Chancellor WJ (1970) Stress-strain characteristics of a saturated clay soil at various rates of strain. Trans ASAE 13:685 – 690

Elijah DL, Weber JA (1968) Soil failure and pressure patterns for flat cutting blades. ASAE paper 68 – 655, St. Joseph

Eggenmüller A (1958) Untersuchungen an schwingenden Bodenbearbeitungswerkzeugen. Grundl Landtechnik 10:55 – 95, 143 – 150

Farrell DA, Greacen EL, Larson WE (1967) The effect of water content on axial strain in a loam under tension and compression. Soil Sci Soc Am Proc 31:445 – 450

Florescu CI, Canarache A (1973) Draft requirement and soil physical properties as related to planning of mechanised agriculture. 6th Int Conf Soil Tillage, Wageningen

Ford H (1963) Advanced mechanics of materials. Longman, London

Fountaine ER, Payne PCJ (1954) Causes of non-scouring in soil working implements. 5th Int Cong Soil Sci Trans, Leopoldville, vol 2, pp 35 – 45

Freitag DR (1968) Penetration tests for soil measurements. Trans ASAE 11:750 – 753

Freitag DR, Smith ME (1966) Centre-line deflection of pneumatic tires moving in dry sand. J Terramech 3(1):31 – 46

Freitag DR, Schafer RL, Wismer RD (1970) Similitude studies of soil machine systems. Trans ASAE 13:201 – 213

Gerard CJ (1965) The influence of soil moisture, soil texture, drying conditions, and exchangeable cations on soil strength. Soil Sci Soc Am Proc 29:641 – 645

Gerlach A (1953) Physikalische Untersuchungen über die zwischen den Bodenteilchen wirkenden Kräfte. Grundl Landtechnik 5:81 – 86

Ghavami M, Keller J, Dunn IS (1974) Predicting soil density following irrigation. Trans ASAE 17:166 – 171

Gill WR (1968) Influence of compaction hardening of soil on penetration resistance. Trans ASAE 11:741 – 745
Gill WR (1969) Soil deformation by simple tools. Trans ASAE 12:234 – 239
Gill WR, Reaves CA (1956) Compaction patterns of smooth rubber tires. Agric Eng 37:677 – 680
Gill WR, VandenBerg GE (1967) Soil dynamics in tillage and traction. Agric Handbook 316, Washington
Gliemeroth G (1953) Untersuchungen über Verfestigungs- und Verlagerungsvorgänge im Ackerboden unter Rad- und Raupenfahrzeugen. Z Acker Pflanzenb 96:219 – 234
Godwin RJ, Spoor G (1977) Soil failure with narrow tines. J Agric Eng Res 22:213 – 228
Griffith AA (1920) The phenomenon of rupture and flow in solids. Philos Trans R Soc Lond A 221:163 – 198
Gupta CP, Pandya AC (1966) Rheological behavior of soil under static loading. Trans ASAE 9:718 – 724
Hajela RB, Bhatnagar JM (1972) Application of rheologic measurements to determine liquid limit of soils. Soil Sci 114:122 – 130
Håkansson I (1973) The sensitivity of different crops to soil compaction. 6th Int Conf Soil Tillage, Wageningen, pp 141 – 144
Hanks RJ, Thorp FC (1957) Seedling emergence of wheat, grain sorghum, and soybeans as influenced by soil crust strength and moisture content. Soil Sci Soc Am Proc 21:357 – 359
Harr ME (1966) Foundations of theoretical soil mechanics. McGraw-Hill, New York
Harrison WL (1972) Soil failure under inclined loads I. J Terramech 9(4):41 – 63
Harrison WL (1973) Soil failure under inclined loads II. J Terramech 10(1):11 – 50
Hawkins JC (1957) The design of potato harvesters. J Agric Eng Res 2:14 – 24
Hegedus E (1965) Pressure distribution under rigid wheels. Trans ASAE 8:305 – 308, 311
Hendrick JG, Gill WR (1973) Soil reaction to high speed cutting. Trans ASAE 16:401 – 403
Hénin S, Gras R, Monnier G (1969) Le profil cultural. Masson, Paris
Hettiaratchi DRP, O'Callaghan JR (1980) Mechanical behaviour of agricultural soils. J Agric Eng Res 25:239 – 259
Hettiaratchi DRP, Reece AR (1967) Symmetrical 3-dimensional soil failure. J Terramech 4:45 – 67
Hettiaratchi DRP, Witney BB, Reece AR (1966) The calculation of passive pressure in 2-dimensional soil failure. J Agric Eng Res 11:89 – 107
Holm IC (1969) Das Verhalten von Reifen beim mehrmaligen Überfahren einer Spur. Proc 3rd Conf ISTVS, Essen, vol II, pp 96 – 123
Houben JMMTh (1970) Bewortelingsmogelijkheden in zandprofielen. De Buffer 16(4):53 – 58
Ikeda I, Persson SPE (1968) A track shoe for soft soil. Trans ASAE 11:746 – 749, 753
Jamison VC (1954) The effect of some soil conditioners on friability and compactibility of soils. Soil Sci Soc Am Proc 18:391 – 396
Janosi Z (1962) Theoretical analysis of the performance of tracks and wheels operating on deformable soil. Trans ASAE 5:133 – 134, 146
Jaworski J, Mierzwicki A, Tyro G (1978) Vergleichsuntersuchungen der Kraftübertragung zwischen Raupenketten und Boden. Proc 6th Int Conf ISTVS, Vienna, vol III, pp 879 – 886
Karafiath LL, Nowatzki EA (1978) Soil mechanics for off-road vehicle engineering. Trans Tech Publ, Rockport, Mass
Kawamura N (1952) Study of the plow shape (3). Study on soil cutting and pulversation (1). Translated from J Soc Agric Mach, Japan 14:3 – 4
Kawamura N, Umeda S (1958) Dynamic behaviour of soil (1). High speed compression test. Translated from J Soc Agric Mach, Japan 20(1)
Kermis L (1968) Basisgegevens bij de studie der samendrukbaarheid van niet gesatureerde landbouwgronden. Meded Rijksfac Landbouwwet Gent 32(2):201 – 225
Kirkham D, de Boodt MF, de Leenheer L (1959) Modulus of rupture determination on undisturbed soil core samples. Soil Sci 87:141 – 144
Knight SJ, Freitag DR (1962) Measurement of soil trafficability characteristics. Trans ASAE 5:121 – 124, 132
Koenigs FFR (1961) The mechanical stability of clay soils as influenced by the moisture conditions and some other factors. VLO 67.7, Wageningen
Koenigs FFR (1972) Practical aspects of structure deterioration due to air explosion. Meded Rijksfac Landbouwwet Gent 37:1086 – 1093

Koenigs FFR, Mann MAM, Ghazalli MZ (1976) The mechanical stability of clay soil II. Development of shear strength in clays in dependence of moisture content and suction. Desorption of slurried and condensed aggreagates. Meded Rijksfac Landbouwwet Gent 41(1):117 – 133

Kogure K, Sugiyama N (1975) A study of soil thrust exerted by a tracked vehicle. J Terramech 12(3 + 4):225 – 238

Komandi G (1966) Bestimmung der physikalischen Bodenkennwerte auf Grund der Zusammenhänge zwischen Scherdiagrammen und Zugkraftcharakteristik. Landtechn Forschung 16(4): 115 – 123

Koolen AJ (1974) A method for soil compactibility determination. J Agric Eng Res 19:271 – 278

Koolen AJ (1976) Mechanical properties of precompacted soil as affected by the moisture content at precompaction. 7th Conf Int Soil Tillage Res Organ, Sweden, paper 20

Koolen AJ (1977) Soil loosening processes in tillage. Analysis, systematics and predictability. Meded Landbouwhogesch Wageningen 77 – 17

Koolen AJ (1978) The influence of a soil compaction process on subsequent soil tillage processes. A new research method. Neth J Agric Sci 26:191 – 199

Kondner RL (1963) Hyperbolic stress-strain response: cohesive soils. J Soil Mech and Found Div Proc Am Soc Civ Eng 89: SMI part 1, 115 – 143

Kop LG (1960) Het meten van de draagkracht van grasland met een penetrometer. Intern Rapport 281, PAW Wageningen

Kouwenhoven JK (1979) Herschikking van stortgoederen door tanden van grondbewerkingswerktuigen. Meded Landbouwhogesch Wageningen 79 – 7

Knight SJ, Freitag DR (1962) Measurements of soil trafficability characteristics. Trans ASAE 5:121 – 124, 132

Krause R, Lorenz F (1979) Bodenbearbeitung in den Tropen und Subtropen. GTZ, Eschborn

Krick G (1969) Druck- und Schubverteilung unter Rädern und Reifen auf nachgiebigem Boden unter Berücksichtigung der Reifendeformation. Proc 3rd Int Conf ISTVS, Essen, vol 2, pp 50 – 75

Kuether DO, Reed IF (1964) Effect of track shoe design upon traction. ASAE paper 64 – 117 St Joseph, Mich

Kuipers H (1959a) Confined compression tests on soil aggregate samples. Meded. Landbouwhogesch Opzoekingsstn Staat Gent 24(1):349 – 357

Kuipers H (1959b) Some remarks on pore space and pressure on marine clay soils. Meded Landbouwhogesch Opzoekingsstn Staat Gent 24(1):392 – 397

Kuipers H (1970) Entgegengesetzte Effekte von Reifen und Bodenbearbeitungen. Ber Intern Symp Warna, Sofia, pp 59 – 65

Kuipers H, Van Ouwerkerk C (1963) Total pore space estimations in freshly plowed soil. Neth J Agric Sci 11:45 – 53

Kumar L, Weber JA (1974) Compaction of unsaturated soil by different stress paths. Trans ASAE 17:1064 – 1069, 1072

Kurtay R, Reece AR (1970) Plasticity theory and critical state soil mechanics. J Terramech 7(3 + 4):23 – 56

Lee IK, Donald IB (1968) Pore pressures in soils and rocks. Effective stress law for saturated and unsaturated soils and rocks. In: Leed IK (ed) Soil mechanics, selected topics. Butterworth, London

Lucius J (1971) Bestimmung des Einflusses der Verformungsgeschwindigkeit auf die Bruchspannung im Boden. Agrartechnik 21:526 – 528

Marchant JA (1980) An incremental stress/strain law for cohesionless granular materials. J Agric Eng Res 25:421 – 444

Masuda S, Tanaka T, Oida A (1969) Soil deformation under model shoe and its reaction evaluated from stress-strain characteristics. Proc 3rd Int Conf ISTVS, Essen, vol II, pp 25 – 49

Maurer ER, Withey MO (1940) Strength of materials. Wiley and Sons, New York; Chapman and Hall, London

McKibben EG, Green RL (1940) Transport wheels for agricultural machinery VII. Relative effects of steel wheels and pneumatic tires on agricultural soils. Agric Eng 21:183 – 185

McMurdie JL (1963) Some characteristics of the soil deformation process. Soil Sci Soc Am Proc 27:251 – 254

Melzer KJ (1970) Measuring relative density by means of a cone penetrometer. Working Conf 3rd Sect CIGR, Wageningen, pp 172 – 188

Melzer KJ, Knight SJ (1973) Dual-wheel performance in sand. Trans ASAE 16:204 – 207

Minkin MB, Kalmykow AG, Buravchuk NI (1972) Study of soil plasticity over a wide range of soil moisture contents. Translated from Pochvovedeniye 10:121 – 125
Murphy G (1950) Similitude in engineering, Ronald, New York
Nadai A (1950) Theory of flow and fracture of solids, vol I. McGraw-Hill, New York
Nichols HL (1976) Moving the earth. The workbook of excavation, 3rd ed. North Castle Books, Greenwich, Connecticut
Nichols ML (1931) The dynamic properties of soil. II. Soil and metal friction. Agric Eng 12:259 – 264
Nichols ML, Reaves CA (1958) Soil reaction: to subsoiling equipment. Agric Eng 39:340 – 343
Nichols ML, Reed IF (1934) Soil dynamics, VI. Physical reactions of soils to moldboard surfaces. Agric Eng 15:187 – 190
Nichols ML, Reed IF, Reaves CA (1958) Soil reaction: to plow share design. Agric Eng 39:336 – 339
NN (1969) Effects of temperature and heat on engineering behavior of soils. Highway Res Board, Spec Rep 103
NN (1971) Soiltest. Inc Gen catalog, vol 2a. Evanston
NN (1976) Fundamentals of machine operation. Tillage. Deere and Co, Moline, Ill
NN (1978) Leistungsvergleich beim Pflügen. Top Agrar 1978 (12):68 – 71
NN (1981) ASAE Yearbook 1981. St Joseph
O'Callaghan JR (1967) Der Bruchmechanismus des Bodens bei der Bodenbearbeitung. Grundl Landtech 17:92 – 95
O'Callaghan JR, Farrelly KM (1964) Cleavage of soil by tined implements. J Agric Eng Res 9:259 – 269
O'Callaghan JR, McCullen PJ (1965) Cleavage of soil by inclined wedge-shaped tines. J Agric Eng Res 10:248 – 254
Oida A (1975) Analysis of tractive performance of track-laying tractor. Techn Rep 4, Farm Power Mach Lab, Kyoto Univ, pp 121 – 136
Olson DJ, Weber JA (1966) Effect of speed on soil failure patterns in front of model tillage tools. Trans Soc Automot Eng 74:298 – 310
Ometto DA (1970) Influence of humidity on the coefficient of resistance in soils when being plowed. Working Conf 3rd Sect. CIGR, Wageningen, pp 136 – 137
Onafeko O, Reece AR (1967) Soil stresses and deformations beneath rigid wheels. J Terramech 4(1): 59 – 80
Osman MS (1964) The mechanics of soil cutting blades. J Agric Eng Res 9:313 – 328
Pandey KP, Ojha TP (1978) Effect of design parameters on the performance of rigid traction wheels on saturated soils. J Terramech 15(3):145 – 156
Paul B (1968) Macroscopic criteria for plastic flow and brittle fracture. Fracture vol II. Academic Press, London, New York
Payne PCJ (1956) The relationship between the mechanical properties of soil and the performance of simple cultivation implements. J Agric Eng Res 1:23 – 50
Payne PCJ, Fountaine ER (1952) A field method of measuring the shear strength of soils. J Soil Sci 3:136 – 144
Payne PCJ, Tanner DW (1959) The relationship between rake angle and the performance of simple cultivation implements. J Agric Res 4:312 – 325
Perdok UD, van de Werken G (1982) Power and labour requirements in soil tillage. Int Congr 12th Agric mach exhib. Landbouw RAI 1982, Amsterdam, pp 55 – 70
Poesse GJ, van Ouwerkerk C (1967) Ristervorm en ploegsnelheid. ILR Wageningen publik 102
Raghavan GSV, McKyes E, Chassé M (1976) Soil compaction patterns caused by off-road vehicles in eastern Canadian agricultural soils. J Terramech 13(2):107 – 115
Raghavan GSV, McKyes E, Beaulieu B (1977) Prediction of clay soil compaction. J Terramech 14(1):31 – 38
Rao VNM, Hammerle JR (1973) Some viscoelastic properties of Hickory clay – Ottawa Sand. J Agric Eng Res 18:253 – 259
Reaves CA, Cooper AW (1960) Stress distribution in soils under tractor loads. Agric Eng 41:20 – 21, 31
Reece AR (1965) The fundamental equation of earth-moving mechanics. Symp Earth-moving Mach, Auto Div Instn Mech Eng
Reece AR, Adams J (1966) One aspect of tracklayer performance. Trans ASAE 9:6 – 9, 13
Reiner M (1960) Lectures on theoretical rheology. Elsevier North-Holland, Amsterdam

Roscoe KH (1970) The influence of strains in soil mechanics. Geotechnique 20:129 – 170
Roscoe KH, Poorooshasb HB (1963) A theoretical and experimental study of strains in tri-axial compression tests on normally consolidated clays. Geotechnique 13:12 – 38
Rowe PW (1962) The stress-dilatancy relation for static equilibrium of an assembly of particles in contact. Proc R Soc Lond A 269:500 – 527
Rowe PW (1971) Theoretical meaning and observed values of deformation parameters for soil. Proc Roscoe Mem Symp, Cambridge, pp 143 – 194
Rowland D (1972) Tracked vehicle ground pressure and its effect on soft ground performance. Proc 4th Int Conf ISTVS, Stockholm, pp 353 – 384
Sanglerat G (1972) The penetrometer and soil exploration. Elsevier, Amsterdam
Schaffer G (1960) Eine Methode der Abscherwiderstandsmessung bei Ackerböden zur Beurteilung ihrer Strukturfestigkeit im Felde. Landwirtsch Forsch 13:24 – 33
Schüring D (1968) Zur Theorie des Geländerads. VDI Forsch Ing Wes 34(6):165 – 200
Schothorst CJ (1963) Beweidingsverliezen op diverse graslandgronden. Landbouwkd Tijdschr 75:869 – 878
Schothorst CJ (1974) De meting van indringweerstanden in het terrein. Intern Rapport, ICW Wageningen
Seed HB, Chan CK (1957) Thixotropic characteristics of compacted clays. J Soil Mech and Found Div Proc Am Soc Civ Eng SM 4:1 – 35
Sela AD (1964) The shear stress-deformation relationship of soils. J Terramech 1(1):31 – 37
Sela AD, Ehrlich IR (1971) Load support capability of flat plates of various shapes in soils. Proc Autom Eng Congr, Detroit Jan 11 – 15
Selig ET, Nelson RD (1964) Observations of soil cutting with blades. J Terramech 1(3):32 – 53
Shames IH (1962) Mechanics of fluids. McGraw-Hill, New York
Siemens JC, Weber JA, Thornburn TH (1965) Mechanics of soil as influenced by model tillage tools. Trans ASAE 8:1 – 7
Sitkei G (1969) Die Kennzahlen von AS-Reifen und die Probleme der Bereifung. Proc 3rd Int Conf ISTVS, Essen, vol III, pp 23 – 43
Sitkei G (1972) Die viskoelastischen Eigenschaften von Ackerboden und deren Einfluß auf die Boden-Rad-Wechselwirkung. Proc 4th Conf ISTVS, Stockholm, vol 1, pp 284 – 300
Smits FP (1973) Boundary value problems in soil mechanics as related to soil cutting. Soil Mech Lab, Delft
Söhne W (1952) Die Verformbarkeit des Ackerbodens. Grundl Landtechnik 3:51 – 59
Söhne W (1953 a) Druckverteilung im Boden und Bodenverformung unter Schlepperreifen. Grundl Landtechnik 5:49 – 63
Söhne W (1953 b) Reibung und Kohäsion bei Ackerboden. Grundl Landtechnik 5:64 – 80
Söhne W (1955) Die Verdichtbarkeit des Ackerbodens unter Berücksichtigung des Einflusses organischer Bestandteile. Z Pflanzenernaehr Dueng Bodenk 114:116 – 125
Söhne W (1956) Einige Grundlagen für eine Landtechnische Bodenmechanik. Grundl Landtechnik 7:11 – 27
Söhne W (1958) Fundamentals of pressure distribution and soil compaction under tractor tires. Agric Eng 39:276 – 281, 290
Söhne W (1960) Anpassung der Pflugkörperform an höhere Fahrgeschwindigkeiten. Grundl Landtechnik 12:51 – 62
Söhne W, Möller R (1962) Über den Entwurf von Streichblechformen unter besonderer Berücksichtigung von Streichblechen für höhere Geschwindigkeit. Grundl Landtechnik 15:15 – 27
Soltynski A (1968) Mechanics of the terrain-vehicle systems. Translation from Polish. Foreign Techn Off, AMSTA-RR DFI, TACOM, Warren, Michigan
Sommer C, Stoinev K, Altemüller HJ (1972) Das Verhalten vier verschiedener Modellböden unter vertikaler Belastung. Landbauforsch Voelkenrode 22:45 – 56
Spoor G (1969) Design of soil engaging implements. Farm Machine Design Eng Sept, Dec
Spoor G, Godwin RJ (1978) An experimental investigation into the deep loosening of soil by rigid tines. J Agric Eng Res 23:243 – 258
Sprinkle LW, Langston TD, Weber JA, Sharon NM (1970) A similitude study with static and dynamic parameters in an artificial soil. Trans ASAE 13:580 – 586
Stafford JV (1979) The performance of a rigid tine in relation to soil properties and speed. J Agric Eng Res 24:41 – 56

Stippes M, Wempner GA, Stern M, Beckett RE (1961) An introduction to the mechanics of deformable bodies. Merrill, Columbus
Tanner DW (1960) Further work on the relationship between rake angle and the performance of simple cultivation implements. J Agric Eng Res 5:307 – 315
Taylor JH (1973) Lug angle effect on traction performance of pneumatic tractor tires. Trans ASAE 16:16 – 18
Taylor HM, Burnett E (1964) Influence of soil strength on the rootgrowth habits of plants. Soil Sci 98:174 – 180
Taylor HM, Gardner R (1963) Penetration of cotton seedling toproots as influenced by bulk density, moisture content and strength of the soil. Soil Sci 96:153 – 156
Taylor JH, Burt EC, Bailey AC (1976) Radial tire performance in firm and soft soils. Trans ASAE 19:1062 – 1064
Telischi B, McColly HF, Erickson E (1956) Draft measurements for tillage tools. Agric Eng 37:605 – 608
Timoshenko S, Goodier JN (1951) Theory of elasticity. McGraw-Hill, New York
Towner GD, Childs EC (1972) The mechanical strength of unsaturated porous granular material. J Soil Sci 23:481 – 498
Trabbic GW, Lask KV, Buchele WF (1959) Measurement of soil-tire interface pressures. Agric Eng 40:678 – 681
Tschebotarioff GP (1951) Soil mechanics, foundation and earth structures. McGraw-Hill, New York
Turnage GW (1972) Tire selection and performance prediction for off-road wheeled-vehicle operations. Proc 4th Int Conf ISTVS Stockholm, vol I, pp 61 – 82
Tijink FGJ, den Haan WP (1981) Wielslip tijdens ploegen. Landbouwmechanisatie 32: 961 – 964
VandenBerg GE (1966) Triaxial measurements of shearing strain and compaction in unsaturated soil. Trans ASAE 9:460 – 467
VandenBerg GE, Gill WR (1962) Pressure distribution between a smooth tire and the soil. Trans ASAE 5:105 – 107
VandenBerg GE, Reed IF (1962) Tractive performance of radial ply and conventional tractor tires. Trans ASAE 5:126 – 129, 132
Verma BP (1971) Oscillating soil tools. A review. Trans ASAE 14:1107 – 1115, 1121
Vermeer PA (1980) Formulation and analysis of sand deformation problems. Report 195 Geotechn Lab, Delft Univ Techn
Vermeer PA (1981) Formulation and prediction of sand behaviour. 10th Int Congr Soil Mech Found Eng, Stockholm
Vornkahl W (1967) Dynamik gezogener Bodenwerkzeuge im Modellversuch. Fortsch Ber VDI-Z Reihe 14, 7
Willatt ST, Willis AH (1965a) A study of the through formed by the passage of tines through soil. J Agric Eng Res 10:1 – 4
Willatt ST, Willis AH (1965b) Soil compaction in front of simple tillage tools. J Agric Eng Res 10:109 – 113
Williford JF, Larson LW (1968) A study of soil strength values included in cone index readings. ASAE paper 68 – 666
Wills BMD (1960) Horizontal shear in soil vehicle mechanics. US Army Tank Automotive Center, Techn Rept 9560, Res Rep 6:21 – 45
Wills BMD (1966) The load sinkage equation in theory and practice. Proc 2nd Int Conf ISTVS, Quebec, pp 200 – 246
Wismer RD, Luth HJ (1972) Performance of plane cutting blades in clay. Trans ASAE 15:211 – 216
Wismer RD, Luth HJ (1973) Off-road traction prediction for wheeled vehicles. J Terramech 10(2):49 – 61
Wismer RD, Freitag DR, Schafer RL (1976) Application of similitude to soil-machine systems. J Terramech 13(3):153 – 182
Witney BD (1968) The determination of soil particle movement in two-dimensional failure. J Terramech 5(1):39 – 52
Witney BD, Hettiaratchi DRP, Reece AR (1966) The basis of soil failure theory. Proc 2nd Int Conf ISTVS, Stockholm, pp 353 – 366
Wong J-Y (1967) Behaviour of soil beneath rigid wheels. J Agric Eng Res 12:257 – 269

Wong, J-Y (1970) The effect of vibrations on the performance of terrain-vehicle systems. J Terramech 7(3 + 4):11 – 21

Wong J-Y (1978) Prediction of multiple-pass performance of tires. A review. 6th Int Conf ISTVS, Vienna, vol II, pp 541 – 553

Wong J-Y, Reece AR (1967) Prediction of rigid wheel performance based on the analysis of soil-wheel stresses. Part I. Performance of driven rigid wheels. J Terramech 4(1):81 – 98

Wu TH (1971) Soil dynamics. Allyn and Bacon, Boston

Wijk ALM van, Beuving J (1975) Relation between playability and some soil physical aspects of the toplayer of grass sportfields. Rasen Turf Gazon 3:77 – 83

Yong RN (1969) Energy dissipation and drawbar pull prediction in soil-wheel interactions. Proc 3rd Int Conf ISTVS, Essen, vol I, pp 93 – 142

Yong RN (1973) Analytical predictive requirements for physical performance of mobility. J Terramech 10(4):47 – 60

Zoz FM (1974) Factors affecting the width and speed for least cost tillage. Agric Eng 29(3):75 – 79

Subject Index

Advanced Series in Agricultural Sciences

Volume 1
A. P. A. Vink
Land Use in Advancing Agriculture
1975. 94 figures, 115 tables. X, 394 pages
ISBN 3-540-07091-5

Volume 2
H. Wheeler
Plant Pathogenesis
1975. 19 figures, 5 tables. X, 106 pages
ISBN 3-540-07358-2

Volume 3
R. A. Robinson
Plant Pathosystems
1976. 15 figures, 2 tables. X, 184 pages
ISBN 3-540-07712-X

Volume 4
H. C. Coppel, J. W. Mertins
Biological Insect Pest Suppression
1977. 46 figures, 1 table. XIII, 314 pages
ISBN 3-540-07931-9

"... *Another* book on biological control? Yes and no. The title of this book gives the clue that the authors have a somewhat different viewpoint regarding "biological control." The authors restricted their discussion to those cases in which insect pests are suppressed through human intervention... it appears to be most suitable for a general course in insect pest suppression that excludes the use of pesticides;... As an introductory level textbook it has its virtues - among them its compactness. The book has **1199 references,** of which a number are as recent as 1976. The book is **attractively printed** and should be a useful introduction for students of the various alternatives to chemical insect pest suppression."

The Quarterly Review of Biology

Volume 5
J. J. Hanan, W. D. Holley, K. L. Goldsberry
Greenhouse Management
1978. 283 figures, 117 tables. XIV, 530 pages
ISBN 3-540-08478-9

"... *Greenhouse Management* strongly emphasizes the mechanical and engineering information backgrounding our greenhouse construction and management practices. It is especially strong in its descriptions and discussions of the equipment needed for greenhouse environmental control. ...The Table of Contents is unusually detailed and will be invaluable to the reader trying to locate specific information. ... The abundant illustrative material used includes **many photographs of excellent quality.** ... We truly believe that most readers will appreciate the monumental task that has been accomplished in gathering together and organizing such a large mass of data and information not previously available to the general greenhouse manager, floriculture student, or research specialist. It will surely serve as **an excellent sourcebook for a long time to come...**"

Journal of Hort. Science

Volume 6
J. E. Vanderplank
Genetic and Molecular Basis of Plant Pathogenesis
1978. 3 figures, 36 tables. XI, 167 pages
ISBN 3-540-08788-5

"This book is an extended essay in which **a distinguished plant pathologist puts forward a new molecular hypothesis** for disease resistance in plants... The book is well written throughout. ... The effort is well worth while and I would like to recommend it to all plant biochemists working on aspects of plant resistance to disease." *Phytochemistry*

Volume 7
J. K. Matsushima
Feeding Beef Cattle
1979. 31 figures, 23 tables. IX, 128 pages
ISBN 3-540-09198-X

" ... The book is written as a practical handbook on a theoretically qualified basis ... It is systematically composed, richly provided with tables and practical directions, and written in an intelligible language - without excessive use of difficult technical words and complicated explanations. In a simple way, Matsushima's little handbook explains the character of many feed items and their suitability in various ratios in compound feeds and for different cattle groups. ... The relevant reference may be found quickly and the necessary, practical knowledge may easily be acquired. Although written for the American feed-lot farmer, this book has a message for several groups other than the large-scale beef producers. It will be **an excellent tool for the trained cattle husbandry researcher,** wherever he might be, and it will also be **a good handbook** for new beef cattle systems in technical poor or undeveloped countries. No matter the feed items are different or the technology missing, Matsushima's book may be useful. ..."

Animal Feed Sci. and Technol.

Springer-Verlag Berlin Heidelberg New York Tokyo

Advanced Series in Agricultural Sciences

Volume 8
R. J. Hanks, G. L. Ashcroft
Applied Soil Physics
Soil Water and Temperature Applications
1980. 55 figures, 19 tables. VI, 159 pages
ISBN 3-540-09457-1

" ... This short volume is a scholarly analysis of soil water and heat flow in relation to climate and plant growth. The book is divided into 5 sections dealing with water quantities, water potential, water flow, soilplant-atmosphere relations, and soil heat flow and temperature. The writing is lucid, to the point, and essentially free of mechanical errors. The volume not only clearly describes basic concepts but also is liberally interlaced with specific problems, together with computations and solutions. It is recommended highly for mathematically oriented students interested in effects of water and temperature on crop yields ..."
The Quarterly Review of Biology

Volume 9
J. Palti
Cultural Practices and Infectious Crop Diseases
1981. 43 figures. XVI, 243 pages
ISBN 3-540-11047-X

Cultural Practices and Infectious Crop Diseases is the first monograph to deal comprehensively with the effects of agricultural practices on plant health. Following the effects of background factors (climate, soil, stress, and crop age), the author desribes the impact of the major farming operations on the development of crop diseases, among them crop planning and alternation, multiple cropping, tillage, fertilitzation, moisture management, sowing, harvesting, and sanitation. The author concludes with a consideration of integrated disease control combining agricultural practices, resistance breeding and the use of chemical agents.
This volume will prove an invaluable aid to agriultural advisors, growers, researchers, students a teachers in appreciating the importance of approbriate practices management in the prevention of crop disease.

Volume 10
E. Bresler, B. L. McNeal, D. L. Carter
Saline and Sodic Soils
Principles - Dynamcis - Modeling
1982. 78 figures. X, 236 pages. ISBN 3-540-11120-4

Saline and Sodic Soils a comprehensive exposition of the principles and processes involved in the genesis, formation and reclamation of saline and sodic soils. The coverage includes critical interpretations of models characterizing the physical and chemical behavior of salt concentration and composition and their effects on soils and plants, as well as practical suggestions for the control of soil salinity to improve economic potential.
Each topic in this volume is clearly explained and readily acessible for all students and professionals in the agricultural and environmental sciences with a general background in mathematics, physics, chemistry and biology.

Volume 11
J. R. Parks
A Theory of Feeding and Growth of Animals
1982. 123 figures. XVI, 322 pages. ISBN 3-540-11122-0

The subject of this volume is the search fot the deterministic elements in animal feeding and growth patterns that could form the basis of a testable theory, making this book a valuable guide to laying a scientific foundation for any undertaking in animal management and production technology.

Volume 12
J. Hagin, B. Tucker
Fertilization of Dryland and Irrigated Soils
1982. 64 figures. VII, 188 pages. ISBN 3-540-11121-2

This book is a treatment of the proper and judicious use of fertilizers with emphasis for semi-arid regions of the world. Enough background information is given on soil chemical processes and plant nutritaion to provide the reader with an understanding of the rates of plant food neeeded and allows for the proper selection of fertilizer materials and methods of applications. The book is most complete on those subjects important to low or erratic rainfall areas. Conciseness has, however, been achieved by eliminating soil fertility considerations which are not pertinent to arid and semi-arid regions.

Springer-Verlag Berlin Heidelberg New York Tokyo